UAB

Universitat Autònoma de Barcelona

Higgs Phenomenology and The Hamiltonian Truncation Method

Doctorand:
Marc Montull Garcia

Directors de tesi:
Dr. Alex Pomarol, Dr. Francesco Riva

Memòria de recerca presentada per a l'obtenció del títol de Doctor en Física

Institut de Física d'Altes Energies
Grup de Física Teòrica
Departament de Física – Facultat de Ciències
Universitat Autònoma de Barcelona

September 22, 2016

Abstract

This thesis is based on the publications done as a PhD student at IFAE during the periods 2012-2013 and 2015 [1–4]. These include two separate topics, Higgs phenomenology at the LHC within the frameworks of Composite Higgs and Supersymmetry [1–3], and the improvement of the Renormalized Hamiltonian Truncation Method (RHTM) [4].

The first part of this thesis was motivated by the Naturalness problem in the Standard Model (SM), which was triggered by the discovery in 2012 of a scalar particle with a mass of 125 GeV and signal strengths compatible with the SM Higgs. The aim of these projects [1–3] was to asses the impact of the measured mass and signal strengths on two of the best motivated frameworks that tackle the Naturalness problem; Composite Higgs and Supersymmetric extensions of the SM. This part of the thesis is organised as follows.

In Chapter 1 we give an overview to the SM its shortcomings and motivate the need to go beyond the Standard Model (BSM). Brief introductions to Spontaneous Symmetry Breaking (SSB) and the CCWZ [5, 6] are also included due to their importance in the understanding of the SM and their pivotal role in the study of BSM physics .

In Chapter 2 we study the implications of the Higgs discovery for different Composite Higgs models. This is done by using the signal strengths given by the experiments right after the Higgs discovery in 2012, which allow to greatly constrain the parameter space of some of these models.

Chapter 3 is focused on the study of the Higgs couplings in Composite Higgs models based on the $SO(5)/SO(4)$ coset. We show that the Higgs couplings to gluons and photons are insensitive to light fermionic resonances assuming that they preserve CP. Also, we find that at leading order in the mixings, the Higgs couplings to tops and gluons, when normalized to the Standard Model (SM), are equal.

In Chapter 4 we study the relation between the Higgs couplings and the Higgs mass in Supersymmetric models while finding that the measured 125 GeV Higgs and the signal strengths can be competitive with direct searches in excluding some parts of the parameter space in the Higgs sector. We focus on the MSSM with heavy stops, and possible extensions that alleviate the small hierarchy problem.

The second part of this thesis was motivated by two papers by Rychkov et al. [7, 8] where they present a promising new method to solve strongly coupled systems. The method consist in improving the already known Hamiltonian Truncation Method used to numerically solve strongly coupled systems. The improvement comes from analytically integrating out the high energy modes which results in a considerable improvement to the numerical result, and allows to reduce computational power needed to solve any given system. Our work, presented in Ch. 5, improves the method by finding the general expressions needed in the procedure to integrating out the high energy modes, and solves some of the issues left open in [7, 8].

Acknowledgements

Contents

Chapter 1

Introduction

1.1 The Standard Model

The Standard Model of particle physics (SM) represents our state of the art understanding of how elementary particles interact via the electromagnetic, weak and strong forces. Its construction is a long journey that started with the discovery of the electron and the electromagnetic force and closed the last chapter with the discovery of the Higgs in 2012. With a huge number of experiments agreeing with the SM predictions, the SM seems to be the theory that governs the interactions of elementary particles at least up to the center of mass energies allowed by today's colliders (unless there are some very weakly interacting particles that we haven't been able to detect yet). The standard model though, is certainly an effective theory due to the presence of gravity which is not accounted for in its construction. At low energies ($E_{CM} \ll M_P$, with M_P the quantum gravity scale), any putative theory of quantum gravity could in principle be written as an effective theory in powers of fields and derivatives over M_P, and with it describe the interactions between ordinary matter and gravity [1]. However, this implies that when $E \gtrsim M_P$ one needs a more fundamental theory to consistently describe particles' interactions with gravity, making the SM an effective theory of this more fundamental one.

Whether other new physics may appear before the Planck scale is an interesting question which we discuss later in Sec. 1.2. First, let us make a brief review on the SM in its current closed form as a renormalizable QFT without gravity, and from here see what shortcomings it may have and how to modify it. The SM is built imposing that it must be invariant under global Poincaré space-time transformations,

$$SO^+(3,1) \rtimes R^{3,1} \tag{1.1}$$

and under the local gauge group

$$SU(3)_c \times SU(2)_L \times U(1)_Y \, . \tag{1.2}$$

---

[1]This is achieved adding to the gravity action the SM Lagrangian with its global Poincaré symmetry gauged.

Fields with the appropriate charges are introduced to accommodate the 61 elementary particles (and antiparticles) observed as of today. The SM, as a renormalisable QFT introduces fields with the Lorentz quantum numbers of the particles observed, and organises them in different linear representations of the gauge group. Its field content is then,

	$SO(3,1)$	$SU(3)$	$SU(2)$	$U(1)$
$Q_L^{ij} = \begin{pmatrix} u_L^{ij} \\ d_L^{ij} \end{pmatrix}$	$(\frac{1}{2},0)$	□	□	$\frac{1}{6}$
u_R^{ij}	$(0,\frac{1}{2})$	□	-	$\frac{2}{3}$
d_R^{ij}	$(0,\frac{1}{2})$	□	-	$-\frac{1}{3}$
$\ell_L^i = \begin{pmatrix} \nu_L^i \\ e_L^i \end{pmatrix}$	$(\frac{1}{2},0)$	-	□	$-\frac{1}{2}$
e_R^i	$(0,\frac{1}{2})$	-	-	-1
$H = \begin{pmatrix} \phi^+ \\ \phi^0 \end{pmatrix}$	$(\frac{1}{2},0)$	-	□	$\frac{1}{2}$
G_μ^a	$(\frac{1}{2},\frac{1}{2})$	Adj	-	-
W_μ^b	$(\frac{1}{2},\frac{1}{2})$	-	Adj	-
B_μ	$(\frac{1}{2},\frac{1}{2})$	-	-	Adj

where $i = 1, 2, 3$ is an index for families, and $j = 1, 2, 3$ denote colour and the Higgs doublet H is composed by two ϕ^0 and ϕ^+ complex fields. The vector fields appear in the Lagrangian as the connections associated to gauge transformations, therefore they transform in the adjoint representation of their gauge group. The defining principles of the SM are the imposed local symmetries and renormalizability (meaning here the absence of irrelevant interactions); the most general Lagrangian that fulfils these properties is unique and can be written as

$$\mathcal{L}_{SM} = \mathcal{L}_{gauge}^{kin} + \mathcal{L}_{fermions}^{kin} + \mathcal{L}_{scalars}^{kin} + \mathcal{L}^{Yukawa} + V . \tag{1.3}$$

As a matter of fact, the principle is so stringent that the resulting particles, except the Higgs, are massless unless there is spontaneous symmetry breaking. We review this in detail and discuss each term in Eq. (1.3) individually.

Higgs potental

The potential for the scalar fields is,

$$V = -\mu^2 |H|^2 + \lambda |H|^4 , \tag{1.4}$$

and depends only on the modulus of H. In the SM, $\mu^2 > 0$, therefore the minimum of this potential is at $|\bar{H}| = \mu/\sqrt{2\,\lambda} \equiv v/\sqrt{2}$ which signals SSB. Notice that one can always go to a basis where

$$\langle H \rangle = \begin{pmatrix} 0 \\ v/\sqrt{2} \end{pmatrix} . \tag{1.5}$$

In this case the only unbroken generator is $Q \equiv T_3 + Y$, and the braking is given by $SU(2)_L \times U(1)_Y \to U(1)_Q$. [2] To get rid of the NGB's in H from hereonafter we fix the gauge in the unitary gauge. Also, it is convenient for perturbation theory to redefine the field h as $h \to h + v/\sqrt{2}$ such that $\langle h \rangle_{tree} = 0$. With these changes $H = \left(\begin{smallmatrix} 0 \\ h+v/\sqrt{2} \end{smallmatrix} \right)$. Then, the kinetic term in Eq. (1.9) is canonically normalized if h is redefined as $h \to h/\sqrt{2}$. After this choice of gauge and field redefinitions H is given by

$$H = \frac{1}{\sqrt{2}} \begin{pmatrix} 0 \\ h + v \end{pmatrix}, \tag{1.6}$$

where h stands for the physical Higgs boson. In this form, the potential is

$$V = -\frac{\mu^2}{2} (h + v)^2 + \frac{\lambda}{4} (h + v)^4. \tag{1.7}$$

The potential V contains the self interactions of the Higgs and its mass term, which at tree level is

$$m_h = \frac{\mu}{\sqrt{2}} = v \sqrt{2\lambda}. \tag{1.8}$$

Higgs kinetic term

Continuing with our analysis, the scalars' kinetic term is,

$$\mathcal{L}_{scalars}^{kin} = |D_\mu H|^2, \tag{1.9}$$

with $D_\mu = \partial_\mu - i\, g\, W_\mu^a\, T^a - ig'\, B_\mu$. Going to the unitary gauge Eq. (1.6), the Higgs kinetic term is

$$\mathcal{L}_{scalars}^{kin} = \frac{1}{2}(\partial_\mu h)^2 + (h + v)^2 \big(g^2 (W_1^2 + W_2^2 + W_3^2 + B^2) - 2gg'W_\mu^3 B^\mu \big). \tag{1.10}$$

In this gauge, one can read from the Lagrangian the tree level mass terms for the electroweak gauge bosons and their interactions with the Higgs. The mass matrix for the gauge bosons (W_1, W_2, W_3, B) can be written as

$$M_{gauge}^2 = \begin{pmatrix} g^2 & 0 & 0 & 0 \\ 0 & g^2 & 0 & 0 \\ 0 & 0 & g^2 & -gg' \\ 0 & 0 & -gg' & g^2 \end{pmatrix}. \tag{1.11}$$

Upon diagonalizing the (W_3, B) entries,

$$\begin{pmatrix} Z_\mu \\ \gamma_\mu \end{pmatrix} = \begin{pmatrix} \cos\theta_W & -\sin\theta_W \\ \sin\theta_W & \cos\theta_W \end{pmatrix} \begin{pmatrix} W_\mu^3 \\ B_\mu \end{pmatrix}, \qquad \tan\theta_W \equiv g'/g, \tag{1.12}$$

---

[2] $(i\,T_k)$ are the generators of $SU(2)_L$, with $T_k = \sigma_k/2$, and σ_k the Pauli matrices. Y is the charge of the $U(1)_Y$.

we find that at tree level the following fields create mass eigenstates,

$$Z_\mu = \frac{1}{\sqrt{g^2 + g'^2}}(gW_\mu^3 - g'B_\mu) \qquad \text{with} \qquad m_Z = v\,\frac{\sqrt{g^2 + g'^2}}{2}\,, \qquad (1.13)$$

$$\gamma_\mu = \frac{1}{\sqrt{g^2 + g'^2}}(g'W_\mu^3 + gB_\mu) \qquad \text{with} \qquad m_\gamma = 0\,,$$

while W_μ^1, W_μ^2 have masses of $m_{W^1} = m_{W^2} = v\,g/2$. As explained later in Sec. 1.3, it is useful to work with representations of the unbroken group, which in this case is the $U(1)_Q$. Checking how Z and γ transform under $U(1)_Q$ one sees that they are singlets, so $Q_Z = Q_\gamma = 0$. On the other hand, W^1 and W^2 are not representations of $U(1)_Q$, but we can perform the following change of variables

$$W_\mu^\pm = \frac{W_\mu^1 \mp i\,W_\mu^2}{\sqrt{2}}, \qquad\qquad m_{W^\pm} = v\,\frac{g}{2}, \qquad (1.14)$$

making now $W^\pm$ covariant under $U(1)_Q$ with $Q_{W^\pm} = \pm e = \pm\frac{gg'}{\sqrt{g^2 + g'^2}}$.

Yukawa terms

We next study the Yukawa terms,

$$\mathcal{L}^{Yukawa} = Y_u^{ij}\bar{Q}_L^i\tilde{H}u_R^j + Y_d^{ij}\bar{Q}_L^iHd_R^j + Y_e^{ij}\bar{\ell}_L^iHe_R^j + h.c.\,, \qquad (1.15)$$

where Y_u^{ij}, Y_d^{ij}, Y_e^{ij} are arbitrary 6×6 Hermitian matrices, $\tilde{H} \equiv i\,\sigma_2 H$ and the indices $i,\,j = 1,2,3$ stand for the generation of fermions, i.e. $\{(u,d),\,(c,s),\,(t,b)\}$ for quarks and $\{(e,\nu_e),\,(\mu,\nu_\mu),\,(\tau,\nu_\tau)\}$ for leptons. Going to the unitary gauge the Yukawa term is

$$\mathcal{L}^{Yukawa} = \frac{(h+v)}{\sqrt{2}}\left(Y_u^{ij}\,\bar{u}_L^iu_R^j + Y_d^{ij}\,\bar{d}_L^id_R^j + Y_e^{ij}\,\bar{e}_L^ie_R^j + h.c.\right)\,, \qquad (1.16)$$

which contains the mass terms for the fermions and their interactions with the Higgs. Notice that the neutrinos don't get a mass due to not having introduced a right handed neutrino in the original Lagrangian.[3]

To get the fermion masses, we must diagonalize the Yukawa matrices Y_u^{ij}, Y_d^{ij}, Y_e^{ij}. To do so, one uses the property that a general complex matrix can be diagonalized by a biunitary transformation (i.e. using two different unitary matrices). Let us see how it is done. Given a generic complex 3×3 matrix Y, then $(Y\,Y^\dagger)$ is hermitian, and therefore can be diagonalised by a unitary matrix U_L,

$$U_L^\dagger\,(Y\,Y^\dagger)\,U_L = Y_D^2 \qquad \text{with} \qquad Y_D^2 = \begin{pmatrix} y_1^2 & 0 & 0 \\ 0 & y_2^2 & 0 \\ 0 & 0 & y_3^2 \end{pmatrix}\,, \qquad (1.17)$$

---

[3]Neutrinos seem to have mass. Introducing a right handed neutrino, neutral under all gauge interactions, allows to introduce a Dirac mass term for the neutrinos. If lepton number is not imposed as a fundamental symmetry of the Lagrangian, a Majorana mass term for the right-handed neutrinos is also allowed. Until being sure of wether neutrinos have a Dirac, Majorana or both mass terms we leave them in the realm of BSM physics. A hint of Majorana mass term would be the observation of a neutrinoless double β-decay.

and U_L is fixed up to a multiplication by a matrix $F = diag\{e^{i\phi_1}, e^{i\phi_2}, e^{i\phi_3}\}$ because $F\,Y_D^2\,F^\dagger = Y_D^2$. Therefore $(U_L F)$ also diagonalizes $(Y\,Y^\dagger)$, i.e. $(U_L F)^\dagger\,(Y\,Y^\dagger)\,(U_L F) = Y_D^2$. One can now define the hermitian matrix $N \equiv U_L\,Y_D\,U_L^\dagger$ and the unitary matrix $\tilde{U} \equiv N^\dagger Y$, and use them to write down the following relations

$$U_L^\dagger\,N\,U_L = U_L^\dagger\,(Y\,\tilde{U})\,U_L = U_L^\dagger\,(U_L\,Y_D\,U_L^\dagger)U_L = Y_D \qquad (1.18)$$

which imply that $U_L^\dagger\,Y(\tilde{U}\,U_L) = Y_D$, or in other words, that U_L and $U_R \equiv \tilde{U}U_L$ are two unitary matrices that diagonalize Y,

$$U_L^\dagger\,Y\,U_R = Y_D\,. \qquad (1.19)$$

With this, we find that the Yukawa matrices Y_u, Y_d, Y_e can be diagonalised by a change of variables $\psi_L \rightarrow \psi_L' \equiv U_L\,\psi_L$ and $\psi_R \rightarrow \psi_R' \equiv U_R\,\psi_R$, where U_L and U_R are $U(3)$ transformations that act on the family indices (which we have omitted for clarity). One can ensure that Y_D has positive eigenvalues by making use of the F matrices, which are equivalent to performing a $U(1)$ transformation to each left field $\psi_L^j \rightarrow e^{i\phi_j}\psi_L^j$ with $j = 1, 2, 3$. After this redefinition of fields, the matrices are diagonalised and the fermion masses are directly given by their multiplication with $v/\sqrt{2}$, i.e.

$$m_\psi^i = v\,\frac{y_\psi^i}{\sqrt{2}}, \qquad (1.20)$$

where $\psi = \{u, d, e\}$, $i = 1, 2, 3$ and y_ψ^i are the entries of each diagonalised matrix Y_{uD}, Y_{dD} and Y_{eD}. Even though the redefinition performed on the fermion fields doesn't change the S-matrix, the $U(3)$ or $U(1)$ transformations on the fermions are not symmetries of our theory, and therefore they don't leave the Lagrangian invariant, i.e. other terms in the Lagrangian where fermions appear can in principle be modified by these transformations. [4] Let us see it in the following section.

Fermions' kinetic terms

The fermions' kinetic terms are given by,

$$\mathcal{L}_{fermions}^{kin} = i\bar{Q}^i{}_L\slashed{D}Q_L^i + i\bar{u}^i{}_R\slashed{D}u_R^i + i\bar{d}^i{}_R\slashed{D}d_R^i + i\bar{\ell}^i{}_L\slashed{D}\ell_L^i + i\bar{e}^i{}_R\slashed{D}e_R^i\,, \qquad (1.21)$$

with $\slashed{D} = \slashed{\partial} - i\,g'\,\slashed{B}Y - i\delta_2\,g\slashed{W}^a T^a - i\delta_3\,g_s\slashed{G}^b\lambda^b$, where iT^a and $i\lambda^b$ are the generators of $SU(2)_L$ and $SU(3)_c$ respectively, while δ_2, δ_3 are 0 or 1 depending on wether the fields on which $\slashed{D}$ acts are charged under $SU(2)_L$ and $SU(3)_c$ or not. To find the fermion interactions with the gauge fields one has to take into account the changes of variables done to diagonalise the Yukawa matrices. Since these are done performing a different $U(3)$ transformation of

---

[4]At the quantum level these field redefinitions may also induce anomalous terms through the measure of the path integral.

the form $\psi_L \rightarrow \psi'_L \equiv U_L \psi_L$ and $\psi_R \rightarrow \psi'_R \equiv U_R \psi_R$ to each $u_L, u_R, d_L, d_R, e_L, e_R$, field, only terms that have interactions that are diagonal in $SU(2)$ indices will remain invariant. [5] These are the strong interactions, the $U(1)_Y$ interactions and the ones with $W^3_\mu T^3$ which don't mix different components of the doublet. Let us focus then on the terms that contain $W^1_\mu T^1$, $W^2_\mu T^2$, which are $i\bar{Q}^i_L \slashed{D} Q^i_L$ and $i\bar{\ell}^i_L \slashed{D} \ell^i_L$. For $i\bar{Q}^i_L \slashed{D} Q^i_L$ we find that after the field redefinitions to diagonalize Y_u and Y_d the interactions with $W^\pm$ are

$$
\begin{aligned}
i\bar{Q}'^i_L \slashed{D} Q'^i_L \;\supset\; & i\frac{g}{\sqrt{2}} \begin{pmatrix} \bar{u}'^i_L & \bar{d}'^i_L \end{pmatrix} \begin{pmatrix} 0 & \slashed{W}^+ \\ \slashed{W}^- & 0 \end{pmatrix} \begin{pmatrix} u'^i_L \\ d'^i_L \end{pmatrix} \\
=\; & i\frac{g}{\sqrt{2}} \left(\bar{u}'^i_L d'^i_L \slashed{W}^+ + \bar{d}'^i_L u'^i_L \slashed{W}^- \right) \\
=\; & i\frac{g}{\sqrt{2}} \left(\bar{u}^i_L U^{\dagger\,ij}_{uL} U^{jk}_{dL} d^k_L \slashed{W}^+ + \bar{d}^i_L U^{\dagger\,ij}_{dL} U^{jk}_{uL} u^k_L \slashed{W}^- \right) \\
=\; & i\frac{g}{\sqrt{2}} \left(V^{ij}_{CKM} \bar{u}^i_L d^j_L \slashed{W}^+ + V^{\dagger\,ij}_{CKM} \bar{d}^i_L u^j_L \slashed{W}^- \right),
\end{aligned}
\tag{1.22}
$$

where $V_{CKM} \equiv U^\dagger_{uL} U_{dL}$ is a unitary matrix which is not diagonal a priori. As any 3×3 unitary matrix, it can be parametrized with 3 rotation angles and 6 phases. Here one can use the freedom still left after having diagonalized the Y_u, Y_d, Y_e matrix to rotate each pair of L, R quarks together (to not spoil the phases in the Yukawa matrices) with a different phase for each flavor, i.e. one can perform a vectorial rotation by a $U(1)^6$. With this, 5 of the 6 phases in the CKM can be removed without modifying the S-matrix. After performing these rotations the CKM matrix can be written as,

$$
V_{CKM} = \begin{pmatrix} c_{12}c_{23} & s_{12}c_{23} & s_{13}e^{i\delta_{13}} \\ -s_{12}c_{23} - c_{12}s_{23}s_{13}e^{i\delta_{13}} & c_{12}c_{23} - s_{12}s_{23}s_{13}e^{i\delta_{13}} & s_{23}c_{13} \\ s_{12}s_{23} - c_{12}c_{23}s_{13}e^{i\delta_{13}} & -c_{12}s_{23} - s_{12}c_{23}s_{13}e^{i\delta_{13}} & c_{23}c_{13} \end{pmatrix}
\tag{1.23}
$$

with $c_{xy} \equiv \cos(\theta_{xy})$ and $s_{xy} \equiv \sin(\theta_{xy})$. The angles $\theta_{12}, \theta_{23}, \theta_{13}$ and the phase δ_{13} are not predictions in the SM and have to be measured. This shows that due to the diagonalization of the quark fields in mass eigenstates, we have now interactions mediated by the $W^\pm$ gauge bosons that can mix different families of quarks with strengths proportional to the V_{CKM} entries. Surprisingly it is experimentally found that V_{CKM} is almost diagonal,

$$
|V_{ckm}| \sim \begin{pmatrix} 1 & \lambda & \lambda^3 \\ \lambda & 1 & \lambda^2 \\ \lambda^3 & \lambda^2 & 1 \end{pmatrix},
\tag{1.24}
$$

with $\lambda \ll 1$. One could think that the term $i\bar{\ell}^i_L \slashed{D} \ell^i_L$ would also have a CKM-like matrix $\tilde{V} = U^\dagger_{eL} U_{\nu L}$. This is not the case if the neutrinos are massless because one has always the

---

[5]Since only then the unitary matrices get contracted in a way to "cancel out" as $U^{\dagger\,ij}_\alpha U^{jk}_\alpha = \delta^{ik}$, where α labels the fields that need to be redefined to diagonalize the Yukawas in Eq. (1.16), i.e. $u_L, u_R, d_L, d_R, e_L, e_R$.

freedom to redefine the neutrino field $\nu_L \to \nu'_L = U_{eL}\nu_L$ with the same unitary matrix U_{eL} as the one used to redefine e_L when diagonalizing Y_e, and therefore $\tilde{V} = \mathbb{1}$. [6]

From this discussion we learn that the only term in the SM where different generations interact is in interactions between two quarks and $W^\pm$ with a strength proportional to the V_{CKM}. Even more, it predicts that there should not be interactions between leptons of different families at tree level, nor tree level flavour changing neutral currents. A very important aspect to notice, is that the interactions in the CKM matrix containing a phase are not CP invariant. Under $C : \psi \to -i\gamma_2\psi^*$ and $C : W_\mu^\pm \to -W_\mu^\mp$, while under $P : \psi \to \gamma_0\psi$ and $P : W^\pm \to W^\pm$. Therefore under CP the term containing W^+ turns into the term with W^- and viceversa, e.g.

$$
\begin{aligned}
\mathcal{L}_{fermions}^{kin} &\supset i\frac{g}{\sqrt{2}}\left(V_{CKM}^{ij}\,\bar{u}_L^{\,i}\,W^+ d_L^j\right) \\
&= i\frac{g}{\sqrt{2}}\left(V_{CKM}^{ij}\,\bar{u}^{\,i}\,W^+\left(\frac{1-\gamma_5}{2}\right)d^j\right) \\
&\overset{CP}{\to} i\frac{g}{\sqrt{2}}\left(V_{CKM}^{ij}\,\bar{d}^{\,j}\,W^-\left(\frac{1-\gamma_5}{2}\right)u^i\right).
\end{aligned}
\tag{1.25}
$$

For CP to be conserved we must match this term with the one in $\mathcal{L}_{fermions}^{kin}$ containing W^-, and therefore we should have that $V_{CKM}^{ji} = V_{CKM}^{\dagger\,ij}$, or more concretely $V_{CKM}^{ij} = V_{CKM}^{*\,ij}$. Since this is not the case due to the $e^{i\delta_{13}}$ phase appearing in several entries, the SM has several processes that are CP-violating (see [49]).

Gauge kinetic terms

We end our discussion by focusing on $\mathcal{L}_{gauge}^{kin}$ which is given by

$$
\begin{aligned}
\mathcal{L}_{gauge}^{kin} =&\; -\frac{1}{4}B^{\mu\nu}B_{\mu\nu} - \frac{1}{4}W^{a\,\mu\nu}W_{\mu\nu}^a - \frac{1}{4}G^{b\,\mu\nu}G_{\mu\nu}^b \\
&- \theta_{QCD}\,\tilde{G}^{b\,\mu\nu}G_{\mu\nu}^b - \theta_W\,\widetilde{W}^{a\,\mu\nu}W_{\mu\nu}^a - \theta_Y\,\tilde{B}^{\mu\nu}B_{\mu\nu}\,,
\end{aligned}
\tag{1.26}
$$

where we defined

$$
\begin{aligned}
B_{\mu\nu} &\equiv \partial_\mu B_\nu - \partial_\nu B_\mu\,, \\
W_{\mu\nu}^a &\equiv D_\mu W_\nu^a - D_\nu W_\mu^a\,, & D_\mu W_\nu^a &\equiv \partial_\mu W_\nu^a + g\,\epsilon^{abc}W_\mu^b W_\nu^c\,, \\
G_{\mu\nu}^a &\equiv D_\mu G_\nu^a - D_\nu G_\mu^a\,, & D_\mu G_\nu^a &\equiv \partial_\mu G_\nu^a + g_s\,f^{abc}G_\mu^b G_\nu^c\,, \\
\tilde{F}^{\mu\nu} &\equiv \epsilon^{\mu\nu\rho\sigma}\,F_{\rho\sigma} \quad \text{with} \quad F = G,\,W,\,B\,.
\end{aligned}
\tag{1.27}
$$

---

[6]If one modifies the SM to give masses to the neutrinos, pegging the rotation of ν_L to the one of e_L is not allowed and one has a CKM-like matrix for the leptons (called Pontecorvo-Maki-Nakagawa-Sakata (PMNS) matrix [48]) which has the same form and number of free parameters as the CKM matrix if the neutrinos have only Dirac masses. If a Majorana mass is also added, two extra phases need to be added by multiplying the PMNS matrix by diag$(1,\,e^{i\alpha_{12}/2},\,e^{i\alpha_{23}/2})$.

With these definitions we find that the terms in the first line of Eq. (1.26) yield the kinetic terms and self interactions of the gauge bosons. To have a better picture of the interactions let us rewrite the electroweak part in terms of fields creating mass and electric charge eigenstates,

$$
\begin{aligned}
- &\ \frac{1}{4}\, F^{\mu\nu} F_{\mu\nu} - \frac{1}{4}\, Z^{\mu\nu} Z_{\mu\nu} - D^{\dagger\,\mu} W^{-\,\nu} D_\mu W_\nu^+ + D^{\dagger\,\mu} W^{-\,\nu} D_\nu W_\mu^+ &\text{(1.28)}\\
+ &\ ie(F^{\mu\nu} + \cot\theta_w Z^{\mu\nu}) W_\mu^+ W_\nu^- \\
- &\ \frac{1}{2}(e^2/\sin^2\theta_w)(W^{+\,\mu} W_\mu^- W^{+\,\nu} W_\nu^- - W^{+\,\mu} W_\mu^+ W^{-\,\nu} W_\nu^-)\,,
\end{aligned}
$$

where $D_\mu = \partial_\mu - ie(A_\mu + \cot\theta_w Z_\mu)$, $F_{\mu\nu} = \partial_\mu A_\nu - \partial_\nu A_\mu$ and $Z_{\mu\nu} = \partial_\mu Z_\nu - \partial_\nu Z_\mu$. The terms in Eq. (1.28) give the SM prediction for triple and quartic gauge couplings and are uniquely fixed from the requirement of Poincare symmetry, gauge invariance and renormalizability.

Let us now discuss the terms in the second line of Eq. (1.26). The Feynman rules for these terms give trivial zeros so they don't contribute in perturbation theory [50]. Therefore only non-perturbative effects due to non-trivial solutions to the classical equations of motion may contribute to the path integral (i.e. other local minima or saddle points of the action). Whether such configurations exist depends on the specific gauge group and boundary conditions imposed. Imposing that A_μ is pure gauge at infinity (i.e. $A_\mu = 0$ up to gauge transformations), so the classical action is finite, one finds that only the gauge fields for $SU(2)$ and $SU(3)$ have solutions to the equations of motion where $F_{\mu\nu}$, $\tilde{F}_{\mu\nu} \neq 0$ meaning that $\int \tilde{F}F \neq 0$. This is not the case for the $U(1)$ gauge field, and therefore $\int B\tilde{B} = 0$, making θ_B a non-physical parameter.

One the other hand, θ_{QCD}, θ_W can be physical, but since they shift under certain fermion field redefinitions they are not physical by themselves. For the case of θ_{QCD} on sees that the rotations used to diagonalise the Yukawa matrices, i.e. $\psi_L^i \to U_L^{ij}\,\psi_L^j$, $\psi_R^i \to U_R^{ij}\psi_R^j$ induce a change in the measure given by

$$
\int D\psi\, D\bar\psi \to \int D\psi\, D\bar\psi\ e^{i\int d^4x\,\delta\theta\,\frac{g_s^2}{32\pi^2}\,G_{\mu\nu}^a G^{a\,\mu\nu}+\cdots}\,, \tag{1.29}
$$

where

$$
\delta\theta = \arg\left(\det(U_R^\dagger)\det(U_L)\right)\,, \tag{1.30}
$$

U_R, U_L are rotation matrices belonging to $U(N)$ that mix one or more flavours, and the dots appearing in Eq. (1.29) stand for other terms proportional to $\tilde{W}W$ and $\tilde{B}B$ that don't shift θ_{QCD}. Interestingly, working on the basis where the Yukawa matrices are diagonal and real, (which as seen previously can be achieved by rotating with a $U(3)$ up and down type quarks independently) we have that

$$
\begin{aligned}
\delta\theta &= \arg\left(\det(U_{u\,R}^\dagger)\det(U_{u\,L})\right) + \arg\left(\det(U_{d\,R}^\dagger)\det(U_{d\,L})\right) &\text{(1.31)}\\
&= \arg\left(\det(U_{u\,R}^\dagger)\det(Y_{u\,D})\det(U_{u\,L})\right) + \arg\left(\det(U_{d\,R}^\dagger)\det(Y_{u\,D})\det(U_{d\,L})\right) \\
&= \arg\left(\det(Y_u)\right) + \arg\left(\det(Y_d)\right)\,,
\end{aligned}
$$

where Y_u, Y_d are the original Yukawa matrices, and $Y_{u\,D}$, $Y_{d\,D}$ the diagonalised ones. Therefore

$$\bar{\theta} \equiv \theta_{QCD} + \arg\left(\det(Y_u)\right) + \arg\left(\det(Y_d)\right), \tag{1.32}$$

is a physical quantity since it doesn't depend on the choice of basis for the phases of quarks and can be found by the requirement of the quark mass matrices to be real. This quantity appears in the calculation of the neutron electric dipole moment (d_e) and can be estimated to be $d_e \sim 10^{-15}\,\bar{\theta}$ in units of $e \cdot cm$ (see for instance [51]); with bounds on this quantity given by $d_e \lesssim 10^{-25}\,e\,cm$ [52], the parameter $\bar{\theta}$ is bounded to be

$$\bar{\theta} \lesssim 10^{-10}\,. \tag{1.33}$$

The unexplainable smallness of this parameters, result of the sum of θ_{QCD} plus some phases in the Yukawa matrices is called the *strong CP problem.*

Moving to the term with θ_W, let us notice that one can decompose the elements of $U(N)$ as $U(N) = U(1) \otimes SU(N)$, and therefore

$$U_R = e^{i\varphi_R}\bar{U}_R\,, \qquad U_L = e^{i\varphi_L}\bar{U}_L\,, \tag{1.34}$$

where $\bar{U}_R$, $\bar{U}_L \in SU(N)$ and they have det= 1. With this we learn that the shifts on the θ parameters under a $U(N)$ rotation induces a change in Eq. (1.29) with $\delta\theta$

$$\delta\theta = \arg\left(\det(\bar{U}_R^\dagger)\det(e^{-i\varphi_R}\mathbb{1})\det(e^{i\varphi_L}\mathbb{1})\det(\bar{U}_L)\right) = 2N(\varphi_L - \varphi_R)\,, \tag{1.35}$$

and therefore the angle $\delta\theta$ only depends on the $U(1)$ part of the rotation. This property is important when trying to get rid of redundant parameters like θ_W, because one can then rotate the left and right components of a field by the same angle φ in the $U(1)$ of a $U(N)$ without inducing any change in the $G\tilde{G}$ term, but inducing a change in the θ_W since only the left-handed quarks are charged under $SU(2)_L$. One can get rid of anything in front of $W\tilde{W}$ though, by performing a $U(1)$ vector rotation to all the quarks with the same angle for all the flavours [7]. Since only the left quarks are charged under $SU(2)$ this vectorial rotation can be used to eliminate everything in front of $W\tilde{W}$ passing all the information in front of $B\tilde{B}$, which as illustrated above is unphysical. Therefore making θ_W an unphysical parameter.

Summary of the SM

After eliminating all the redundancies, one finds that the SM Lagrangian has 19 parameters that can't be computed and need to be fitted from experiments. Let us present the values of these parameters just to have an idea of what their values are at the energies were they have been measured, see [49] for more details. These 19 parameters then can be chosen to be: 6

---

[7]To not spoil the CKM nor the phases in the Yukawa matrices

masses for the quarks $m_u, m_d, m_c, m_s, m_t, m_b$, 3 masses for the leptons m_e, m_μ, m_τ, and the Higgs mass m_h,

$$
\begin{array}{c|cccccc|ccc|c}
 & m_u & m_d & m_c & m_s & m_t & m_b & m_e & m_\mu & m_\tau & m_h \\
\hline
\text{GeV} & 0.002 & 0.005 & 1 & 0.1 & 173 & 4 & 0.0005 & 0.1 & 2 & 125
\end{array}
\tag{1.36}
$$

3 dimensionless gauge couplings g', g, g_s, 4 parameters coming from the CKM matrix, the Higgs vev and the dimensionless parameter $\bar\theta$:

$$
\begin{array}{ccc}
g' & g & g_s \\
\hline
0.36 & 0.65 & 1.2
\end{array}
\qquad
\begin{array}{cccc}
\theta_{12} & \theta_{23} & \theta_{13} & \delta_{13} \\
\hline
13^o & 2.4^o & 0.2^o & 57^o
\end{array}
\qquad
\begin{array}{c}
v\,(\text{GeV}) \\
\hline
245
\end{array}
\qquad
\begin{array}{c}
\bar\theta \\
\hline
\leqslant 10^{-10}
\end{array}
\tag{1.37}
$$

where the gauge couplings are measured at $\mu_{\overline{MS}} = m_Z \simeq 91$ GeV, and the rest of couplings at different scales depending on the experiment (see [49] for details).

As final remarks, it is interesting to notice that all the masses in the SM are given by a coupling $g, g', \sqrt{\lambda}, y_\psi$ times the higgs vev, and therefore for couplings $\mathcal{O}(1)$ implies that all the particles will have masses $\mathcal{O}(v)$, i.e. the EW scale. This is true for the weak gauge bosons, the Higgs and the top quark. On the other hand, besides the top quark, all other fermions are much lighter than the EW scale due to the Yukawa couplings being $y_\psi \ll 1$. It is also important to notice that all the CP violating effects in the SM are due to the complex phase in the V_{CKM} matrix and the term $\bar\theta\, G\tilde{G}$.

1.2   Is new physics around the corner?

As mentioned in the previous chapter, the SM restricted to operators of dimension $d \leqslant 4$ is most certainly an effective theory due to its inability to describe gravitational interactions at arbitrary high energies. Besides this fact though, there are also experimental observations that can't be explained using only the the SM (with operators of $d \leqslant 4$), and therefore require its modification. These experimental observations are:

- Neutrinos have mass: Various experiments with solar, accelerator, atmospheric and reactor neutrinos provide compelling results indicating that neutrinos oscillate from one flavour state into another during flight, meaning that flavour states are non trivial superpositions of mass eigenstates (so they must have mass). See [9, 10] and references therein.

- Dark matter: There are various experimental observations (e.g. rotation speed of galaxies, model of galaxy formation, bullet cluster) and theoretical motives (the experimental agreement with the ΛCDM model) which indicate that about $80 - 85\%$ of the matter in the universe is non luminous and non-baryonic. Furthermore there are strong constrains which indicate that this matter must be neutral under colour and electrical charges, leaving the neutrino as the only candidate in the SM. Even if massless neutrinos were not

disfavoured by direct experiments, they are disfavoured as DM candidates by large scale structure formation models and the Tremain-Gunn bound. On the other hand, massive neutrinos or other neutral colour and charge particles not included in the SM like axions or neutralinos may be possible candidates, indicating that new physics are required to explain a large piece of the Universe's composition. See [11, 12] and references therein.

- Matter antimatter asymmetry in the universe: The SM doesn't provide an explanation to account for the asymmetry of matter and antimatter if one assumes that at the beginning of the Universe they were equal in amount.

- Cosmological inflation: The Friedmann-Robertson-Walker cosmological model of our Universe's expansion suffers from various initial conditions problems. For example, the fact that causally disconnected parts of the Universe (as seen in the CMB) have the same temperature. See [13] and references therein for details.

As of now though, these observations have not been corroborated by direct experimental evidence (colliders/DM direct detection) pushing upwards the scale of new physics Λ_{NP} with every new experiment. Hence to know if we'll be able to see this effects we have to find compelling theoretical models beyond the SM that can accommodate these observations. In the theoretical side, the current situation is as follows: all the experimental evidence that requires going beyond the SM can be explained with new physics around the Planck scale (e.g. neutrino's mass with Seesaw mechanism and $m_{\nu_R} \sim 10^{15}$ GeV, for coefficients of order one). Also the SM doesn't have any theoretical inconsistencies up to M_P (e.g. no problems with vacuum stability [14] or problems with anomaly cancellation that could predict new families). This is quite different from the situation before the Higgs discovery, where the inconsistency of an incomplete SM guaranteed the need of new physics at low energies [8] or problems with anomaly cancellation that could predict new families). Even more, the accidental (exact or approximate) symmetries that the $d \leqslant 4$ operators in the SM have, and that one would expect to not be fulfilled in the full theory (so not fulfilled by $d > 4$ operators), haven't yield any new discoveries, e.g. the $d = 6$ operator that would produce proton decay is bounded to have $\Lambda_{NP} \gtrsim 10^{16}$ (for a coefficient of order one).

Given this situation, where the SM is consistent up to the Planck scale and no experimental inconsistencies have been found in direct experiments, we may try to find new insight of any underlying theory by trying to understand the values of the parameters of our current theory. Historically this approach has been successful in predicting new physics. In the SM, we would like to better understand the following:

- The Naturalness problem of the Higgs' mass: this is in some sense an aesthetic problem that stems from having a fundamental scalar with a mass m_H, not protected by any symmetry, that receives radiative corrections from particles with masses $M \gg m_H$, and

---

[8]These predicted a discovery at the electroweak scale to unitarize the $W_L W_L \to W_L W_L$ scattering.

requires in general that the fundamental parameters of the theory be precisely fine tuned to predict such small mass if M is large.

Is Nature actually fine tuned or is there an alternative explanation? If it isn't, should we expect new physics around the EW scale or instead nature is realised by models that can solve the fine-tuning problem without the need of new physics at low energies?

- Gauge coupling unification: if one extrapolates the strength of the weak, electromagnetic and strong forces at high energies, one finds that for interactions with Center of Mass energy of about $10^{13} - 10^{15}$ the three forces have about the same strength (crossing each other at different points).

Is there a more fundamental theory where the three forces are unified at some high energy scale? This could bring light into understanding the values of these forces at the low energies where we are proving them today?

- The strong CP problem: We would like to know if there is some fundamental reason as of why the $\bar{\theta}$ parameter in the SM is so small (see Eq. (1.32) and following discussion).

- CKM and Yukawa matrices: The values of the diagonalised Yukawa matrices span several orders of magnitudes, while the CKM matrix which in principle could have any form, is almost diagonal with a small value in the CP violating entries. Is there any underlying reason for the particular form of the CKM matrix and the hierarchies seen in the fermion masses?

- Number of families: Who ordered that? Why are there 3 families? Is there a fundamental reason that explains why there are three families both for quarks and leptons?

- Charge quantisation: Even though the hypercharges of the different particles in the SM have no theoretical constrain to be what they are, surprisingly they all have values that yield for each particle an electric charge that is a fraction of the electron charge. Is there a reason for that? (e.g. Grand Unification models predict this for example).

- The Cosmological constant: The measured value of the Cosmological constant is of order $\Lambda_{cosmo} \sim 10^{-47}$ GeV^4. On the other hand, if one naively estimates its value using the SM one finds that the prediction is off by more than 10^{100} GeV^4 orders of magnitude; a problem similar in spirit to the Naturalness problem mentioned above. What are we missing?

In this thesis we focus on models that tackle the Naturalness problem of the Higgs' mass, since many of them require the appearance of new physics at low energies which modify some of the SM predictions, like the couplings to the Higgs boson or the appearance of new particles around the EW scale. Given the recent discovery of the Higgs, trying to learn what its couplings are telling us in the framework of BSM physics is a sensible thing to do. Due to its central importance in motivating the models at study, in the next section we explain in a bit more detail the Naturalness problem, and sketch how Composite Higgs models solve it.

1.2.1 The Naturalness problem

The clearest example in which the Naturalness problem arises is in condensed matter systems where the theory has a physical cutoff Λ given by the inverse of the lattice spacing of the material. [9] In a generic QFT the mass of a scalar particle is given by $m_{phys}^2 = m_{bare}^2 + \delta m^2$, where m_{bare}^2 is the mass parameter in the Lagrangian and δm^2 accounts for the radiative corrections. Notice that in systems without a physical cutoff one must use different renormalisation schemes to make sense of the infinite radiative corrections, which in turn may obscure the impact of high energy modes to the different physical values of the theory; on the other hand, systems with a physical cutoff have finite radiative corrections which depend on the physical cutoff Λ, which allows to explicitly see the dependence of the physical parameters like m_{phys}^2 to the high energy behaviour of the theory. The dependence of the mass terms of any particle to the cutoff Λ is highly dependent on the details of the theory. For a simple theory with a generic elementary scalar [10] one finds that $\delta m^2 \propto \Lambda^2$. The Naturalness problem arises if one finds a scalar particle with $m_{phys}^2 \ll \Lambda^2$, since this implies that there is a huge cancellation between $m_{bare}^2 \sim \Lambda^2$ and $\delta m^2 \sim \Lambda^2$ such that their sum is $m_{phys}^2 \ll \Lambda^2$. If one finds a system with these types of cancellations taking place, one may suspect that the calculation is not being done "properly", in other words, that there is a more fundamental theory in which the calculation of m_{phys}^2 yields an expression that doesn't require such big cancelations to take place. In principle, it could be possible to have systems where by chance one would have these types of "unlikely" cancellations. So far though, in generic condensed matter systems, every time one has found a fundamental scalar not protected by any symmetry or any other external mechanism, it has been found to have a mass of order Λ. [11]

In the SM, where we have by construction a fundamental scalar particle, it is then fair to ask if this implies that there is some cutoff scale close to the Higgs' mass where new physics appears (as it happens with scalars in condensed matter systems). Since in the SM there isn't any physical cutoff akin to the lattice spacing, let us explain in a bit more detail how the Naturalness problem arises in this case (we follow the discussion in [17]). As explained in the previous chapter, the SM is an effective theory, so we can imagine how the Higgs mass is computed in the underlying more fundamental theory. We assume that the Higgs mass will be computed from the more fundamental parameters of the underlying theory, and can be schematically written as

$$m_h^2 = (\delta m_h^2)_{E<\Lambda} + (\delta m_h^2)_{E\geqslant\Lambda} , \tag{1.38}$$

where Λ represents the scale below which the SM is a good approximation to the full theory, and we have separated the contributions to the Higgs mass between energies below and above

---

[9]In theories with a physical cutoff, the cutoff itself is a parameter of the theory like any other.

[10]Here elementary means that it is very insensitive to form factors for energies much smaller than the physical cutoff Λ.

[11]For example, in systems with SSB one has that the mass depends on the temperature, and $m(T) \ll \Lambda$ only when T is very close to the critical temperature T_c, or if one fine tunes the amount of doping in the material.

Λ. Notice that δm_h^2 can have both radiative and tree level contributions to the Higgs mass (as it is the case in supersymmetric and GUT theories). Given that for energies below Λ the SM is a good approximation, we can calculate low energy contributions to the Higgs. This yields

$$(\delta m_h^2)_{E<\Lambda} = \frac{3}{8\pi^2 v^2} \left(4m_t^2 - 2m_W^2 - m_Z^2 - m_h^2\right) \Lambda^2 \,, \tag{1.39}$$

meaning that $(\delta m^2)_{E<\Lambda} \sim \Lambda^2 \gg m_h^2$; therefore, in order to have a small Higgs mass, one must have that the low energy and high energy contributions cancel each other to a very good precision, i.e. $(\delta m_h^2)_{E<\Lambda} \simeq -(\delta m_h^2)_{E\geqslant\Lambda}$. One can estimate the cancellation needed to achieve the observed Higgs mass as follows

$$\Delta \geqslant \frac{(\delta m_h^2)_{E<\Lambda}}{m_h^2} \simeq \frac{3\,m_t^2}{2\pi^2 v^2}\frac{\Lambda^2}{m_h^2} \simeq \left(\frac{\Lambda}{450\,\mathrm{GeV}}\right)^2 \,, \tag{1.40}$$

which can be taken as a measure of the fine-tuning of the theory. Summarising, if the SM is valid up to very large energies, the underlying theory will have to explain why the low and high energy contributions to the Higgs mass cancel up to a very small fraction. It is important to notice that when constructing models beyond the SM that reduce the fine-tuning Δ, one may find new sources of fine-tuning if gravity is not being taken into account, and therefore a new source of fine-tuning may appear in the terms that contribute to $(\delta m_h^2)_{E\geqslant\Lambda}$, since naively these can be of order $\Lambda_{Planck} \gg \Lambda$. There are many ways to solve both Naturalness problems, some predict new physics around the EW scale, and some don't. Even though it could be that Nature is fine-tuned, or that the underlying theory has a mechanism to explain these cancellations without the need of lowering Λ (no new physics at the EW scale), as researchers we should explore all avenues, so in this thesis we have studied two of the most compelling constructions that solve both Naturalness problems and predict new physics at the EW scale. These are Composite Higgs models, where the Higgs is a Pseudo Nambu Goldstone boson (PNGB), and Supersymmetric models. In the next section we give a brief overview on the motivation and general features of Composite Higgs models. Further details on Composite Higgs and Supersymmetric models can be found in the subsequent chapters of the thesis.

1.2.2 Composite Higgs as a solution

At low energies, we know that QCD, a theory of quarks and gluons, creates bound states with different spins, in particular spin zero; nonetheless, the scalars in the low energy effective theory don't have Naturalness problem in the sense of the previous section, nor does QCD have a Naturalness problem with respect to the Planck scale. For example, the mass of a generic resonance like $K_0^*(1430)$ has two contributions $\delta m_h^2 = (\delta m_h^2)_{E<\Lambda} + (\delta m_h^2)_{E\geqslant\Lambda}$ where here $\Lambda \sim 1$ GeV is the QCD confinement scale. In the low energy effective theory $(\delta m_h^2)_{E<\Lambda}$ is estimated to be of order Λ^2. The interesting thing for composite particles is that we expect the contribution of $(\delta m_h^2)_{E\geqslant\Lambda}$ to be very small due to having form factors that go to zero at energies above the confinement scale Λ (which makes any composite particle insensitive to physics above Λ). Following this line of reasoning yields a "naive" prediction for the scalar

resonance's mass to be of order Λ. This is exactly what we see for scalar resonances in QCD (e.g. $m_{K_0^*(1430)} \sim 1$ GeV), and therefore we don't have a Naturalness problem. If we had found that the mass of these resonances was much smaller than Λ we would try to find the reason behind it.

Regarding the Naturalness problem with the Planck scale, since QCD is a theory with only quarks and gluons, these are protected by the chiral and gauge symmetries and therefore don't have a Naturalness problem. [12]

Since the only scalars that we have seen in Nature are composite, and since they can avoid the Naturalness problem, it is compelling to think that the Higgs is not an elementary particle that has a Naturalness problem, but instead a Composite particle that behaves similarly to the ones we have already seen. The challenge of Composite Higgs models is to build viable phenomenologically models that agree with the plethora of data in agreement with the SM. Some of the most relevant for model building are electroweak precision tests, and not having seen any evidence of a strong sector (no resonances found close to the Higgs), indicate that new physics may be well above the Higgs mass. For this reason, within models where the Higgs is Composite, those where it is a PNGB of some strong sector have gained attention, since they can naturally explain this apparent separation of scales. This phenomenon is already realised in nature, e.g. the pions (which can be thought of PNGB's of $SU(2)_L \times SU(2)_R \to SU(2)_{L+R}$) are much lighter than the other resonances. Their lightness with respect to the confinement scale Λ is explained by the protection they have from the shift symmetry that the theory would have if they were exact Nambu Goldstone Bosons.

Therefore, composite Higgs models rely on the idea that the Higgs be a composite particle and that, moreover, the whole Higgs doublet is a (Pseudo) NGB of a global symmetry spontaneously broken by strong dynamics. In the following sections we shall describe the details of SSB and the PNGB interactions at small energies; here we will briefly summarize the main generic ingredients that characterize composite Higgs models (CH), while more model-dependent aspect will be discussed in the dedicated chapters throughout the thesis.

CH models are characterized by a sector with strong dynamics which, similarly to QCD, confines at a scale $\Lambda \sim$ TeV. In addition, this sector is associated with a global symmetry (the analog of $SU(2)_L \times SU(2)_R$ for pions) and this is spontaneously broken to a subgroup, in such a way that a number of naturally massless degrees of freedom are delivered according to Goldstone theorem [21]; these are the NGB's, and as we explain in the Sec. 1.3, they parametrize the coset space G/H if there is a SSB of $G \to H$. In CH models then, in

---

[12]We say that a mass term is protected by a symmetry if setting it to zero make the theory gain a new symmetry. For example, if one sets to zero the mass term of a fermion, the theory gains a new symmetry (chiral symmetry) given by the transformation $\psi_L \to e^{i\theta}\psi_L$ and $\psi_R \to e^{-i\theta}\psi_R$ (with $\psi = \psi_L + \psi_R$). This implies that any radiative correction to the fermion mass must be proportional to the mass term since when the symmetry is restored any radiative correction has to go to zero (since any contribution to the mass would violate the chiral symmetry). Using dimensional analysis one finds that the radiative corrections can only depend on the cutoff Λ_{Planck} through logarithms (making them much less sensitive to it) thus avoiding the need for big cancellations.

order to have the complete Higgs doublet as PNGB's, the coset will need to contain at least 4 degrees of freedom (d.o.f.); additional phenomenological requirements (in particular the presence of custodial symmetry $SO(4)$ in order to ovoid large strong-sector contributions to the T-parameter) limit the possibility to just a few. The minimal possibility follows the $SO(5)/SO(4)$ symmetry breaking pattern [27, 55] and reproduces just the necessary degrees of freedom for the Higgs, but more extended coset solutions have also been discussed in the literature.

This strong sector represents the core of CH models, but in order for this scenarios to be realistic, it must include fermions and gauge boson interactions at small energies. Generically these are assumed to be elementary, but coupled to the strong sector through mixings to strong sector resonances. These mixings necessarily break the global symmetry ($SO(5)$ for the minimal model) and therefore introduce departures from the Higgs as a NGB. In particular, the Lagrangian describing this system will include a strong sector part $\mathcal{L}_{strong}$ (this will be carefully described in the following sections), an elementary part $\mathcal{L}_{elem}$ (this corresponds to the SM kinetic Lagrangian discussed above) and the linear mixing $\mathcal{L}_{mix}$ of the form (for fermions)

$$\mathcal{L}_{mix} = y^{I,\alpha} \psi_{\alpha}^{elem} \mathcal{O}_{I}^{compo}, \tag{1.41}$$

where ψ_{α}^{elem} is an elementary fermion with SM indices α while $\mathcal{O}_{I}^{compo}$ is instead a composite field operator from the strong sector with index I belonging to, e.g. $SO(5)$.[13] Eq. (1.41) makes it clear that the coupling between the elementary and composite sector $y^{I,\alpha}$ explicitly breaks the $SO(5)$ symmetry. It is assumed in CH models that this represents the only source of breaking for this symmetry, so that the explicit contributions to the Higgs potential (departures from the $V = 0$ NGB limit) will be proportional to powers of y and will be in particular sensitive to the top quark interaction with the strong sector (similarly the gauge coupling g also breaks the symmetry, but the effects it induces are subdominant with respect to the ones involving the top quark Yukawa). An explicit construction of the effective potential will be presented in Sec. 3 , while in the next section we provide the tools to describe and construct $\mathcal{L}_{strong}$.

1.3   Spontaneous Symmetry Breaking and the CCWZ

In this chapter, we do a brief review of SSB and the CCWZ construction [5, 6], which are both of key importance when studying the phenomenology of Composite Higgs models. We start by defining SSB and studying the general properties of theories that present it; then we proceed to explain the CCWZ formalism and why it is useful when constructing effective theories where there is SSB.

---

[13]The linear mixing of Eq. (1.41) is referred to as Partial compositeness; other possibilities, in which composite operators interact with SM bilinears have also been proposed in the literature but are disfavored phenomenologically (see however the recent [18]).

Global transformation

A theory is symmetric under the transformation $|i\rangle \to |j\rangle = \hat{g}|i\rangle$ if

$$|\langle i |i'\rangle| = |\langle i| \hat{g}^\dagger \hat{g} |i'\rangle|, \tag{1.42}$$

for any two states $|i\rangle$, $|i'\rangle$. If the vacuum state of the theory is not invariant under the symmetry transformation

$$\hat{g}|\Omega\rangle = |\Omega'\rangle \neq |\Omega\rangle, \tag{1.43}$$

we say that the symmetry is spontaneously broken (even though the symmetry is still fulfilled like in Eq. (1.42)). [14,] Wether the vacuum is invariant or not under the symmetry has some general repercussions on the spectrum of the theory. Since in most cases we deal with SSB of compact Lie Groups, we restrict our discussion to the general features of SSB under those. We start studying the case of global symmetry group G, which being a Lie Group has a quantum representation given by

$$\hat{g}(\alpha) = e^{i\alpha_a \hat{Q}_a}, \tag{1.44}$$

where $\hat{Q}_a$ are the generators of the group and α_a a set of continuous real parameters defining the element of the group.

To learn about the spectrum of the theory we can look at the states created by operators $\hat{\phi}_i(x)$ (which create 1-particle states that can be elementary or composite),

$$|i\rangle \equiv |i(x)\rangle = \hat{\phi}_i(x)\,|\Omega\rangle. \tag{1.45}$$

Let's start by the case where the vacuum is invariant under the symmetry transformation,

$$\hat{g}(\alpha)|\Omega\rangle = |\Omega\rangle. \tag{1.46}$$

The point here is that if the Lagrangian depends on operators that transform as linear irreducible representations $\mathcal{D}_{ij}(\alpha)$ of G, i.e.

$$\hat{g}(\alpha)\,\hat{\phi}_i(x)\,\hat{g}(\alpha)^\dagger = \mathcal{D}_{ij}(\alpha)\,\hat{\phi}_j(x), \tag{1.47}$$

(an assumption that we will make throughout this chapter), then the states $|i\rangle$ created by any $\hat{\phi}_i(x)$ have all the same mass. This is seen by first showing that the states $|i\rangle$ transform in the same linear representation $\mathcal{D}_{ij}(\alpha)$ as the operators $\hat{\phi}_i(x)$,

$$\hat{g}(\alpha)\,|i\rangle = \hat{g}(\alpha)\,\hat{\phi}_i(x)\,|\Omega\rangle = \hat{g}(\alpha)\,\hat{\phi}_i(x)\hat{g}(\alpha)^\dagger\,\hat{g}(\alpha)\,|\Omega\rangle = \hat{g}(\alpha)\,\hat{\phi}_i(x)\hat{g}(\alpha)^\dagger\,|\Omega\rangle. \tag{1.48}$$

Then, using Eq. (1.47) we get

$$\hat{g}(\alpha)\,|i\rangle = \mathcal{D}_{ij}(\alpha)\,|j\rangle, \tag{1.49}$$

---

[14]In all this discussion we have assumed that the vacuum state of the theory can't be a superposition of the lowest energy states of the theory. This is valid when the volume of the space is infinite.

and in particular since we can write $|i\rangle = \hat{\phi}_i(x)|\Omega\rangle$ as a linear superposition of $\hat{P}^\mu$ eigenstates $|p^\mu, i\rangle$, all with the same mass, each of these will transform under $\hat{g}(\alpha)$ with $\mathcal{D}_{ij}(\alpha)$. Using that $[\hat{H}, \hat{Q}_a] = 0$, and focusing on the states with $\vec{p} = 0$ for simplify, we find that

$$\sum_j \mathcal{D}_{ij}(\alpha)\, m_j\, |m_j, j\rangle = \hat{H} \sum_j \mathcal{D}_{ij}(\alpha)\, |m_j, j\rangle = \hat{H}\left(\hat{g}(\alpha)\,|m_i, i\rangle\right) \tag{1.50}$$
$$= \hat{g}(\alpha)\,\hat{H}\,|m_i, i\rangle = m_i \sum_j \mathcal{D}_{ij}(\alpha)\,|m_j, j\rangle,$$

so $m_j = m_i$ and therefore all the physical states created by any $\hat{\phi}_i$ in a given multiplet of G will all have the same mass. Having a clear connection between how the fields and states transform simplifies the way of thinking about theories (e.g. all three quark fields in the triplet of $SU(3)_c$ create states with equal masses). This way in which physical states and fields transform linearly under a symmetry is known as the Wigner-Weyl realization and is the general way of writing Lagrangians when we don't have SSB.

When the vacuum state is not invariant $\hat{g}(\alpha)|\Omega\rangle = |\alpha\rangle \neq |\Omega\rangle$ things are a bit different. We see that the last equality in Eq. (1.48) is not fulfilled, and it seems to indicate that states transform very differently from the fields when these transform linearly under G. From here there doesn't seem to be an easy way to infer wether the masses of the states created by fields in a multiplet of G are all equal or not. Nontheless one can still learn some things by separating the transformations of G between those that leave the vacuum invariant and those that don't

$$\hat{h}(\alpha)\,|\Omega\rangle = |\Omega\rangle \qquad \text{with} \qquad \hat{h}(\alpha) = e^{i\alpha_a \hat{Y}_a} \tag{1.51}$$
$$\hat{g^*}(\alpha)\,|\Omega\rangle = |\alpha\rangle \neq |\Omega\rangle \qquad \text{with} \qquad \hat{g^*}(\alpha) = e^{i\alpha_a \hat{X}_a},$$

where we defined $\hat{Y}$, $\hat{X}$ to be the unbroken and broken generators respectively. The elements $\hat{h}(\alpha)$ form a subgroup $H \subset G$ and since $\hat{h}(\alpha)|\Omega\rangle = |\Omega\rangle$ we can follow the logic of Eqs. (1.46)-(1.48) to see that the states $|i\rangle = \hat{\phi}_i(x)|\Omega\rangle$ transform in the same linear representation under H as the fields ϕ_i,

$$\hat{h}(\alpha)\,\hat{\phi}_i(x)\,\hat{h}(\alpha)^\dagger = \mathcal{D}_{ij}^h(\alpha)\,\hat{\phi}_j(x) \qquad \Rightarrow \qquad \hat{h}(\alpha)\,|i\rangle = \mathcal{D}_{ij}^h(\alpha)\,|j\rangle. \tag{1.52}$$

If $D_{ij}^h(\alpha)$ is irreducible, following the same reasoning as in Eq. (1.50), we see that all the states $|i\rangle$ must have the same mass. For the case where $D_{ij}^h(\alpha)$ is reducible we have that,

$$\hat{h}(\alpha)\left(|i\rangle \oplus |i'\rangle\right) = \left(\begin{array}{c|c} \hat{h}_1(\alpha) & 0 \\ \hline 0 & \hat{h}_2(\alpha) \end{array}\right)\left(\begin{array}{c} |i\rangle \\ \hline |i'\rangle \end{array}\right) = \mathcal{D}_{ij}^{h_1}(\alpha)\,|j\rangle \oplus \mathcal{D}_{i'j'}^{h_2}(\alpha)\,|j'\rangle, \tag{1.53}$$

and only states in the same irreducible representation of H will have the same mass. [15] Therefore, when working with theories with SSB it can be useful to separate the irreducible

---

[15] Each irrep will have an analog of Eqs. 1.50 with possible different m_i and $m_{i'}$.

representations of G in irreducible representations of H (especially when we don't have knowledge of the full theory, like in low energy QCD or Composite Higgs models).

Another key aspect of SSB (for global symmetries) is that $n = \dim(G) - \dim(H)$ massless $spin = 0$ particles appear in the spectrum of the theory. This can be seen by finding the number of poles at $p^2 = 0$ in the connected 2-point function $\Delta(x, y) = \int d^4p\, D(p)\, e^{-ip(x-y)} = \langle \phi(x)\phi(y)\rangle_{conn}^{J=0}$, or by finding the zero eigenvalues of its inverse,

$$\Delta^0(x, y)_{ij}^{-1} = \left.\frac{\delta\Gamma(\bar{\phi})}{\delta\phi_i\delta\phi_j}\right|_{\partial\phi^\mu=0}, \tag{1.54}$$

where the zero above $\Delta^0(x, y)^{-1}$ denotes that $\partial\phi^\mu = 0$ (i.e. $\Delta^0(x, y) = \int d^4p\, D(0)\, e^{-ip(x-y)}$), and $\Gamma(\bar{\phi}) = \Gamma(\phi)|_{\phi=\bar{\phi}}$ is the 1-PI effective action evaluated at $J = 0$, so it fulfills that

$$\left.\frac{\delta\Gamma(\phi)}{\delta\phi(x)}\right|_{\phi=\bar{\phi}} = 0 \qquad \text{for} \qquad \bar{\phi} = \langle\Omega|\hat{\phi}(x)|\Omega\rangle_{conn}^{J=0}. \tag{1.55}$$

Since we want to evaluate $\Gamma(\phi)$ at $\partial\phi^\mu = 0$ we work with the effective potential

$$V_{eff}(\phi) = -\frac{\Gamma(\phi)}{\mathcal{V}}\Big|_{\partial\phi^\mu=0} \qquad \text{where} \qquad \mathcal{V} \equiv \int d^4x. \tag{1.56}$$

We focus here on the case where the symmetry transformation is linearly realized. In this case, the Slavnov-Taylor relations, tell us that if the Lagrangian in the path integral is invariant under some linear symmetry transformation, $\phi \to \phi + \delta\phi$, the effective action will also be invariant under the same transformation $\phi_c \to \phi_c + \delta\phi_c$. Hence, the effective action satisfies

$$\frac{\delta V_{eff}(\phi)}{\delta\phi_i}(\delta\phi)_i = 0 = \frac{\delta V_{eff}(\phi)}{\delta\phi_i}Q_{ij}^a\phi_j \qquad \text{(for any } \phi\text{)}, \tag{1.57}$$

where Q_{ij}^a is any of the conserved Noether charges (in the classical Lagrangian of $Z[J]$). Deriving this expression with respect to ϕ_i and evaluating it at $\phi(x) = \bar{\phi}$ we get

$$\frac{\delta^2 V_{eff}(\bar{\phi})}{\delta\phi_l\delta\phi_i}Q_{ij}^a\bar{\phi}_j = 0 = \frac{1}{\mathcal{V}}\Delta^0(x, y)_{li}^{-1}Q_{ij}^a\bar{\phi}_j. \tag{1.58}$$

This equation is non-trivial only if $\bar{\phi} \neq 0$. For a linearly realised symmetry this is equivalent to say that there is SSB. Performing this transformation on the operator $\hat{\phi}$ we get,

$$\begin{aligned}
\bar{\phi}_i(x) \equiv \langle\Omega|\hat{\phi}_i(x)|\Omega\rangle \quad &\to \quad \langle\Omega|\hat{g}(\alpha)\hat{\phi}_i(x)\hat{g}^\dagger(\alpha)|\Omega\rangle = \langle\Omega'|\hat{\phi}_i(x)|\Omega'\rangle \\
&= \quad \mathcal{D}_{ij}(\alpha)\langle\Omega|\hat{\phi}_j(x)|\Omega\rangle = \mathcal{D}_{ij}\bar{\phi}_j.
\end{aligned} \tag{1.59}$$

From the Slavnov-Taylor relations, we know that $\bar{\phi}_i$ transforms with the same linear representation $\mathcal{D}_{ij}$ as $\hat{\phi}$. Then, if $\hat{\phi}$ is not a singlet under the symmetry transformation, neither is $\bar{\phi}$. This implies that $\mathcal{D}_{ij}\bar{\phi}_j \neq \bar{\phi}_i$ when $\bar{\phi}_i \neq 0$. In this case, we find that

$$\langle\Omega|\hat{\phi}_i(x)|\Omega\rangle = \bar{\phi}_i \neq \mathcal{D}_{ij}\bar{\phi}_j = \langle\Omega'|\hat{\phi}_i(x)|\Omega'\rangle \qquad \Rightarrow \qquad |\Omega\rangle \neq \hat{g}^\dagger|\Omega\rangle = |\Omega'\rangle, \tag{1.60}$$

which signals SSB as defined in Eq. (1.43). In the case where there is SSB, we find that taking Eq. (1.58) with Q_{ij} equal to the unbroken generators is trivially zero since $Y_{ij}^a \bar{\phi}_j = Y_{ij}^a \langle \Omega | \hat{\phi} | \Omega \rangle \propto \langle \Omega | \hat{Y} \hat{\phi} \hat{Y} | \Omega \rangle_{ij} = 0$ so no constrains are imposed on $\Delta^0(x,y)_{ij}^{-1}$. On the other hand if we take the broken generators where $X_{ij}^a \bar{\phi}_j \neq 0$ we have that

$$\Delta^0(x,y)_{li}^{-1} X_{ij}^a \bar{\phi}_j = 0 \,, \tag{1.61}$$

and then the sum $X_{ij}^a \bar{\phi}_j$ is an eigenvector of $\Delta^0(x,y)_{li}^{-1}$ with eigenvalue zero. This means that the propagator $D(p)$ appearing in $\Delta^0(x,y) = \int d^4p \, D^{-1}(0) \, e^{-ip(x-y)}$ has a pole at $p^2 = 0$ for each broken generator X^a, and therefore there are $\dim(G) - \dim(H)$ massless particles in the theory. If we want to work in a theory where the Poincare symmetry is not spontaneously broken $\bar{\phi}$ must be a singlet under Poincaré (see Eq. (1.60)), thus the only operators $\hat{\phi}$ that can have a vacuum expectation value different than zero must be scalars. We find then that if Poincaré is not broken, SSB implies that the spectrum of the theory will have $n = \dim(G) - \dim(H)$ massless *spin = 0* particles, which are the Nambu-Goldstone bosons (NGB's). This result is nice because it shows that NGB's are massless even when taking all the quantum corrections into account.

An important property of NBGs is that they always couple through derivatives. This can be easily shown in the case where a field ϕ_i has a vacuum expectation value different than zero. Here on can perform the following change of variables

$$\phi_i(x) = \varphi_{ij}(x) \, \phi_j'(x) \,, \tag{1.62}$$

which puts all de NGB's degrees of freedom into $\varphi_{ij}(x)$ and leaves $\phi_j'(x)$ without any of them. This is seen by noting that $\varphi_{ij}(x)$ is orthogonal to the vacuum expectation value of ϕ_i (like the linear combinations of fields that are eigenvectors of $(\Delta^0)^{-1}$ with eigenvalue zero, see [47]). Now, one can show show that $\varphi(x)$ is a local linear representation of a G which can span all the possible transformations that get $\phi_j'(x)$ rid of the NGB with just the representatives of G belonging to the coset G/H. Since any element of G can be written in some neighbourhood of the identity as,

$$g = e^{\alpha^a(x)X^a} \, e^{u^a(x)Y^a} \,. \tag{1.63}$$

It is convenient to standardise the form of φ_{ij} as an element of G/H and write it as

$$e^{i\,\alpha^a(x)\,X^a} \,. \tag{1.64}$$

One can check that the transformation in Eq. (1.62) is just a change of variables which modifies the form of the Lagrangian $\mathcal{L}(\phi) \neq \mathcal{L}'(\phi')$ but doesn't change the S-matrix, since its Jacobian is equal to one when $\phi(x) = \bar{\phi}$ (see [5,6]). On the other hand, when $\alpha^a(x)$ is constant we have that the form of the Lagrangian doesn't change $\mathcal{L}(\phi) = \mathcal{L}'(\phi')$ (since $\mathcal{L}$ is invariant under global G). For this to happen we must have that the fields $\varphi(x)$ appear in each term of $\mathcal{L}'$ with at least one derivative, so any term containing the fields $\alpha^a(x)$ must also contain at least one derivative. A consistency check to ensure that $\alpha^a(x)$ contain the Goldstone degrees of

freedom is by noticing that there there their number a is equal to the number of broken generators and that they are massless, since they only appear in terms with derivatives.

Another way to connect the $\alpha^a(x)\hat{X}^a$ fields with the Goldstone bosons is by noticing from Eq. (1.51) that when $\alpha^a(x)$ are constant, $\alpha^a \hat{X}^a$ act as creation operators on the vacuum, i.e.

$$\alpha^a \hat{X}^a \left| \Omega \right\rangle = \left| \alpha^a \right\rangle \neq 0 \qquad \text{for each fixed } a \,, \tag{1.65}$$

creating states with the same energy as the vacuum,

$$\hat{H} \left| \alpha^a \right\rangle = \hat{H} \alpha^a \, \hat{X}^a \left| \Omega \right\rangle = \alpha^a \, \hat{X}^a \hat{H} \left| \Omega \right\rangle = E_0 \left| \alpha_a \right\rangle \,, \tag{1.66}$$

where E_0 is the vacuum energy defined as $\hat{H} \left| \Omega \right\rangle = E_0 \left| \Omega \right\rangle$, and we used that $[H, X^a] = 0$. These states $\left| \alpha_a \right\rangle$ are therefore massless and describe a particle with $\vec{p} \to 0$.

Local transformation

Now we turn to SSB when we have a local symmetry. Most of the statements presented for the global case are the same, with the only difference that now if G is local one doesn't expect to have massless states in the theory. A simple way to see it is by performing the change of variables in Eq. (1.62) (recall that this transformation makes the field $\phi'(x)$ not contain any NGB). As previously pointed out, $\varphi(x)$ is an element of the local symmetry group G, therefore this change of variables is in effect just a local symmetry transformation and therefore $\mathcal{L}'(\phi') = \mathcal{L}(\phi)$. Since we know that after the transformation the scalar multiplet getting a vacuum expectation value $\phi'(x)$ doesn't contain any NGB's one can naively say that there aren't any massless degrees of theory in the theory. The choice of $\phi'(x)$ such that it doesn't contain NGB's is just a choice of gauge. [16] Another way to see that there aren't any massless NGB's is by fixing the gauge with a general R_ξ gauge. In perturbation theory one can see that the masses of the would be NGB's are not zero and depend on the ξ parameter, meaning that they are not a meaningful physical quantity in our theory. Moreover one sees that in computations of e.g. scattering processes, the combination of the propagator of these NGB with the gauge bosons associated with the broken symmetries leads to a gauge invariant propagator which is equivalent to the one corresponding to massive particles transforming as vectors under Lorentz, with the NGB providing the term corresponding to the helicity zero (longitudinal) component. [17]Combining these degrees of freedom therefore we have massive vector bosons. In concrete examples one can see that their masses are proportional to the coupling related to the broken symmetries and the vev that breaks it. For example for a theory with a scalar field and a $SU(N)$ local symmetry the kinetic term is given by

$$\mathcal{L}_{kin} = \frac{1}{2} \left| D_\mu \phi_i(x) \right|^2 = \frac{1}{2} \left(\partial_\mu \phi_i(x) - ig\, Q_{ij}^a \, A^a(x)_\mu \, \phi_j(x) \right)^2 \,, \tag{1.67}$$

---

[16]This choice is called unitary gauge and in the R_ξ gauge is given by $\xi \to \infty$.

[17]For a simple example see Peskin chapter 21.1.

given that $\phi(x)$ acquires a vev, we can state that we are in the unitary gauge which means that $\phi(x)$ doesn't contain any would be NGB's. The masses of the gauge bosons at tree level can be found by looking at the quadratic terms of V_{eff} evaluated at its minimum,

$$\frac{\delta^2 V_{eff}^{tree}(v)}{\delta A_\mu^a \, \delta A^{b\,\mu}} = \frac{1}{2} \, g^2 \, (Q_{ij}^a \, \bar\phi_j \, Q_{ik}^b \, \bar\phi_k) \, A^a(x)_\mu A^{b\,\mu}(x) \,. \tag{1.68}$$

Recalling that when $Q = T$ we have that $T_{ij}^a \, \bar\phi_j = 0$, only those terms with broken generators will be different than zero. One can see [47] that the number of gauge bosons acquiring a mass are given by the number of broken generators X^a, and that their their squared masses are proportional to g^2 and some combination of $\bar\phi_i \bar\phi_j$. This effect where massless goldstone bosons acquire a mass due to SSB of a local symmetry, is called the Higgs mechanism.

The CCWZ

The CCWZ is a general method to build effective low energy Lagrangians for theories that have SSB of $G \to H$ where G is a (compact, connected, semisimple) Lie Group and H is a continuous subgroup of G. The method has two parts, one where the general framework and some theorems are demonstrated, and another one where the method to build Lagrangians (where G is non linearly realised) is presented.

Framework

The CCWZ interprets the fields appearing in the Lagrangian of the path integral as coordinates $\phi = (\phi_1, ..., \phi_n)$ of some manifold M. The coordinates $(\phi_1, ...\phi_n)$ may represent the components of fields each having different transformation properties under G, e.g. $\phi = (\vec\xi, \vec\psi, \vec\sigma, ...)$. There are three main assumptions in the CCWZ, the first one is that if there is SSB $G \to H$ there is a point

$$\phi_0 = (0, 0, 0...) \,, \tag{1.69}$$

called the origin, which is invariant under the action of $h \in H$. The second assumption is that the coordinates ϕ are in some neighbourhood of ϕ_0 (so they can be Taylor expanded). The third one is that only transformations of G near the identity are studied (hence excluding "large" transformations); since G is a connected Lie Group its local properties can be studied near the identity, and its elements written as

$$g = e^{i\,\alpha^a\,X^a} \, e^{i\,u^a\,Y^a} \,, \tag{1.70}$$

with X, Y the broken and unbroken generators respectively. As shown in Eq. (1.64) the elements of G/H are given by $U = e^{i\,\alpha^a\,X^a}$, while the elements of H are given by $h = e^{i\,u^a\,Y^a}$.

Three theorems provide the CCWZ with its generality and usefulness. First, the S-matrix of a Lagrangian $\mathcal{L}(\phi, \partial_\mu\phi)$ is invariant under the change of variables $\phi \to \phi' = \phi F(\phi)$ if the origin ϕ_0 is unchanged by this transformation (i.e. the Jacobian is one at ϕ_0); notice that

this is ensured by Eq. (1.69). Second, if the point ϕ_0 is invariant under H, there exist some coordinates $\phi' = (\phi'_1, ..., \phi'_n)$ that transform linearly under $h \in H$ (in some neighbourhood of ϕ_0). Third, all sets of coordinates $\{\phi, \phi', ...\}$ that transform non-linearly under G but linearly under $H \subset G$ produce the same S-matrix. Thanks to these theorems, one can choose the most convenient set of coordinates to get the S-matrix, as long as they have the origin at $\phi_0 = (0, 0, 0...)$ and transform linearly under H.

Choice of coordinates

A convenient set of coordinates to build invariants under G is given by $\phi = (\vec{\xi}, \vec{\psi})$. Define the submanifold $\mathcal{N} \subset \mathcal{M}$ given by all the points result of applying transformations of the coset $U = e^{i\xi^a X^a}$ on the origin, $\phi_0 = (\vec{0}, \vec{0}) \xrightarrow{U} (\vec{\xi}, \vec{0})$. All the points in $\mathcal{N}$ are then characterised by $\vec{\xi}$, making these a suitable set of coordinates for $\mathcal{N}$. Define the rest of coordinates on $\mathcal{M}$ as $\psi_i \equiv \mathcal{D}(U^{-1})_{ij} \Psi_j$, where Ψ transforms linearly under G, and $\mathcal{D}$ is a linear representation of elements in G/H.

$\vec{\xi}, \vec{\psi}$ transformation properties

Let us check that $\phi = (\vec{\xi}, \vec{\psi})$ transform non-linearly under G and linearly under H as required for them to be a good choice of coordinates. The transformation properties of ξ and ψ are derived from the transformation of $U \xrightarrow{g} U'$. Since $U \in G/H \subset G$, then $gU = g' \in G$ so $g\, U = g' = e^{i\xi' X} e^{iuY} = U' h$, which yields

$$U \xrightarrow{g} U' = g\, U h^{-1}\,. \tag{1.71}$$

From this transformation is readily seen that the coordinates $\phi = (\vec{\xi}, \vec{\psi})$ transform non-linearly under G and linearly under H. First, ψ always transforms with an element of H, i.e.

$$\psi = \mathcal{D}(U^{-1})\Psi \xrightarrow{g} \psi' = \mathcal{D}(hU^{-1}g^{-1})\mathcal{D}(g)\Psi = \mathcal{D}(h)\mathcal{D}(U^{-1})\Psi = \mathcal{D}(h)\psi\,, \tag{1.72}$$

so it transforms non-linearly with $g \in G$, and linearly with $g \in H$. If $\mathcal{D}(h)$ is a reducible representation, then one can do the same exercise for each. Notice that one can always rewrite an irreducible representation as tensors with each index transforming under the fundamental. Then, if U transforms with g and h in the fundamental of G, one has for example,

$$\psi_i = U_{ij}^{-1}\Psi_j \quad \xrightarrow{g} \quad \psi'_i = h_{i\alpha}\,\psi_\alpha\,, \tag{1.73}$$

$$\psi_{ij} = U_{ij}^{-1} U_{i'j'}^{-1}\Psi_{jj'} \quad \xrightarrow{g} \quad \psi'_{ij} = h_{i\alpha} h_{j_\beta}\,\psi_{\alpha\beta}\,.$$

Next, to see that ξ transform non-linearly with G one can check how U transforms under $g_c = e^{i\alpha X} \in G/H \subset G$. Then, $U \xrightarrow{g_c} U' = g_c U h^{-1}$ yields

$$\xi^a \rightarrow \xi'^a = \xi^a + \alpha^a + \mathcal{O}(\alpha\,\xi^2)\,, \tag{1.74}$$

which is non-linear. Instead when $g = h \in H$ we have that

$$hU = hUh^{-1}h = U'h \quad \Rightarrow \quad U \xrightarrow{h} U' = hUh^{-1} = he^{i\xi X}h^{-1} = e^{i\xi hXh^{-1}}\,. \tag{1.75}$$

Using that $[Y^a, X^{\hat{a}}] = i f^{a\hat{a}}{}_{\hat{b}} X^{\hat{b}}$, and $h = e^{iuY}$ one finds that for u small

$$X^{\hat{a}} \xrightarrow{h} X'^{\hat{a}} = \left(X^{\hat{a}} + i u^a (f^a)_{\hat{a}\hat{b}} X^{\hat{b}} \right), \tag{1.76}$$

and therefore $\xi^a X^a \xrightarrow{h} \xi^a X'^a = \xi^a e^{iu^b f^b}_{ab} X_b = \hat{\mathcal{D}}(h)_{ab} X_b$, so one can equivalently write that X^a doesn't transform with G but instead

$$\xi^a \to \xi'^a = \mathcal{D}(h)_{ab} \xi^a = \left(\mathcal{D}(h)_{ba} \right)^T \xi^a, \tag{1.77}$$

which is a linear representation of $h \in H$.

Building the Lagrangian

To build a low energy Lagrangian first want to find all possible G-invariants made out of ξ and ψ. The invariants containing only ξ can be obtained by combining the coefficients of the Maurer-Cartan form $\omega \equiv U^{-1}\partial_\mu U$. The Maurer-Cartan is a 1-form that maps the tangent space of any element in G into the algebra of G, and is used in the study of homogeneous subspaces to find G-invariants made out of the coordinates of G/H. For $U = e^{i\xi X} \in G/H$,

$$\omega = e^{-i\xi X} \partial_\mu e^{i\xi X} = d_\mu^a X^a + e_\mu^b Y^b, \tag{1.78}$$

and the coefficients d_μ^a and e_μ^b can be computed explicitly by taylor-expanding U,

$$d_\mu^a = \partial_\mu \xi^a + \cdots, \qquad e_\mu^A = -\frac{i}{4} f^{Aab} \xi^a \overleftrightarrow{\partial}_\mu \xi^b + \cdots. \tag{1.79}$$

Using that $U \xrightarrow{g} g U h_x$ we find how $d_\mu \equiv d_\mu^a X^a$ and $e_\mu^b \equiv e_\mu^b Y^b$ transform:

$$\begin{aligned} U^{-1}\partial_\mu U \xrightarrow{g} U'^{-1}\partial_\mu U' &= d'_\mu + e'_\mu = h_x U^{-1}\partial_\mu (U h_x^{-1}) \\ &= h_x d_\mu h_x^{-1} + h_x e_\mu h_x^{-1} + h_x (\partial_\mu h_x^{-1}), \end{aligned} \tag{1.80}$$

so

$$d_\mu \xrightarrow{g} h_x d_\mu h_x^{-1}, \qquad e_\mu \xrightarrow{g} e'_\mu = h_x e_\mu h_x^{-1} + h_x (\partial_\mu h_x^{-1}). \tag{1.81}$$

Since e_μ transforms like a connection, one can use it to build a covariant derivative, $D_\mu \equiv (\partial_\mu + e_\mu)$, for anything transforming with h_x under G. The claim of the CCWZ is that using d_μ and D_μ allows to build all invariants under G containing only the ξ fields. The fact that d_μ and e_μ only contain derivatives of ξ makes it impossible to build any mass term for ξ. Together with the fact that it parametrises the G/H, we can identify them as the NGB's fields. At low energies the Lagrangian describing the NGB's is given by $\mathcal{L}_{eff} = \mathcal{L}(d_\mu, D_\mu)$, with the terms having less derivatives dominating. The leading contribution is given by the first term in

$$\mathcal{L} = f^2 \operatorname{Tr}\left[d_\mu^\dagger d^\mu \right] = d_\mu^{a\dagger} d^{b\mu} \operatorname{Tr}[X^a X^b] = d_\mu^{a\dagger} d^{a\mu}, \tag{1.82}$$

which contains two derivatives and is the kinetic term for the NGB's. [18,19]

One can add the rest of fields ψ to $\mathcal{L}_{eff}$ by building the usual invariants under local H and using the covariant derivatives $D_\mu \psi$.

Local symmetries

If instead of having a global G transformation we have a local one we notice that all the derivations done for the global case hold as well in the local one if we just replace the derivative for the covariant one, $\partial_\mu \to (\partial_\mu + ig A_\mu)$. Then, $\phi \equiv U^\dagger \Phi$ is not affected, and now the objects d_μ and e_μ are replaced by $\bar{d}_\mu$ and $\bar{e}_\mu$ derived from

$$U^\dagger (\partial_\mu + ig A_\mu) U = \bar{d}_\mu^a X^a + \bar{e}_\mu^a Y^a . \tag{1.84}$$

where now $\bar{d}_\mu$ and $\bar{e}_\mu$ will depend on both ξ and A_μ. The explicit expressions are given by

$$\bar{d}_\mu^i = \frac{\sqrt{2}}{f} D_\mu \Pi^i + \dots , \quad \bar{e}_\mu^a = -g A_\mu^a + \dots . \tag{1.85}$$

For more details on how to construct all possible invariants in the case of having local symmetries, and how to avoid including redundant terms, see [17].

---

[18]For it to be canonically normalized we have to redefine the fields $\pi \to \sqrt{2}\,\pi/f$.

[19]The term $\mathrm{Tr}[D_\mu d^\mu]$ could seem to also contain two derivatives but it is trivially zero

$$\mathrm{Tr}[D_\mu d^\mu] = \partial_\mu d^{a\,\mu} \mathrm{Tr}[X^a] + e_\mu^b d^{a\,\mu} \mathrm{Tr}[Y^a X^b] = 0 , \tag{1.83}$$

since $\mathrm{Tr}[X^a] = 0$ because the generators are traceless, and $\mathrm{Tr}[Y^a X^b] = 0$ since the two generators are never equal for any a, b.

Chapter 2

Higgs discovery, first reaction to the data

2.1 Introduction

A particle consistent with the SM Higgs boson has been discovered: 5σ deviations have been observed both by CMS [53] and ATLAS [54], in the combination of $\gamma\gamma$ and ZZ channels. Whether this is the beginning or the end of an era of investigation of natural realizations of the electroweak scale, it is not yet clear.

In this note we perform a global analysis of how compatible this excesses are with the SM expectation of a Higgs boson at $m_h \approx 125\,\mathrm{GeV}$, using the most recent data from ATLAS, CMS and Tevatron. It is then interesting to analyze different natural theories beyond the standard model (SM), to see whether they would be preferred or disfavored by the present trend of data, and to understand towards which direction the parameter space of such theories is more likely to shrink. We first turn our attention to a large variety of composite Higgs models [55], highlighting which features in these models tend to improve/worsen the fit to the data. In section 2.4, we begin with the minimal composite Higgs models (MCHMs), with coset structure SO(5)/SO(4), but with generic structures of fermion couplings to the strong sector (and hence to the Higgs boson) [55–57].

Larger coset structures can have a different phenomenology. For instance the coset structure $SO(6)/SO(4) \times SO(2)$ delivers an effective two Higgs doublets model (THDM) at low energy [119]. We compare the predictions of this composite version of the THDM with that of the MSSM in section 2.5.

Finally we also study the possibility of the Higgs mixing with other scalars, which raises the question of whether it will be possible at the LHC to understand if the particle we observe is really the one whose VEV gives mass to the gauge bosons; we try to answer this question by singling out the exclusive channels (the ones with vector boson fusion (VBF) and associated production cuts) that carry mostly this information.

Global fits of Higgs data in the context of composite Higgs models, but limited to the

MCHM4 [55] and MCHM5 [56] models, have already appeared in Refs. [60–64].

2.2   The Data

We assume the existence of a unique Higgs-like state with couplings to the SM-gauge bosons and fermions

$$c_t \equiv \frac{y_t}{y_t^{SM}}, \ c_b \equiv \frac{y_b}{y_b^{SM}}, \ c_\tau \equiv \frac{y_t}{y_\tau^{SM}}, \ a \equiv \frac{g_{hVV}}{g_{hVV}^{SM}}, \tag{2.1}$$

where we use the SM couplings as reference values and assume $g_{hVV} \equiv g_{hWW} = g_{hZZ}$. We take that the probability density functions (PDFs) provided by the experiments can be approximated by Gaussian distributions, and we use the theoretical prediction for the ratio [62],

$$\mu^i = \frac{\sum_p \sigma_p(a, c_t, c_b, c_\tau)\zeta_p^i}{\sum_p \sigma_p^{SM}\zeta_p^i} \frac{BR_i(a, c_t, c_b, c_\tau)}{BR_i^{SM}}, \tag{2.2}$$

for each channel i with production crossections σ_p and cut efficiencies ζ_p^i (which we take to be independent from the parameters a and $c_{t,b,\tau}$; the values of ζ_p^i are discussed in the Appendix). We sum theoretical [65] and experimental errors in quadrature (both errors are first symmetrized by average in quadrature and when negative error bars are not provided by the experimental collaborations, we have assumed symmetric distributions around the mean value). We summarize the data used in table 4.1.[1]

ATLAS finds that the peak of the combined signal strength's best fit is at $m_h = 126.5$ GeV, which is within experimental error from $m_h = 125.3$ GeV, where the peak of CMS occurs, so one can assume them to belong to the same resonance. We perform the statistical analysis taking the values at $m_h = 125$ GeV for CMS and Tevatron and $m_h = 126.5$ GeV for ATLAS. For comparison we also study the case where $m_h = 125$ GeV is assumed for all experiments, this appears in the plots as dashed lines.

Taking the ATLAS data at 126.5(125) GeV we obtain for the SM

$$\chi_{SM}^2 = 26.36(23.9), \tag{2.3}$$

which for $N = 33$ independent channels corresponds to $\chi^2/N \approx 0.8(0.7)$. For the parameters mentioned above, in the case with $c \equiv c_t = c_b = c_\tau$, the best fit ($\chi^2$=19.4(19.9) which, for 33 channels and 2 variables, $N = 33 - 2 = 31$ corresponds to $\chi^2/N \approx 0.6$) occurs in

$$c = -0.69(-0.61), \ a = 0.86(0.83), \tag{2.4}$$

while another local probability maximum (χ^2= 22.7(20.7), $\chi^2/N \approx 0.7$) occurs for positive c at

$$c = 0.69(0.68), \ a = 1.02(0.98). \tag{2.5}$$

---

[1]When data has been provided only in the combination of the 7 TeV and 8 TeV runs, we extract the information about the 8 TeV run assuming that the PDFs corresponding to the combined data can be written as the product of uncorrelated PDFs i.e. PDF$_{7+8}$=PDF$_7$PDF$_8$.

In fig. 2.1 we show the 68%,95% and 99% C.L. contours for the parameters a and c from a global fit of data from ATLAS and CMS. C.L. regions are found by finding the isocontour of $P(x,y) = $ const such that $\int dx\, dy\, P(x,y)\pi(x,y) = 0.99, 0.95, 0.68$, where x, y are any of the parameters a, c_t, c_b, c_τ shown in the specific plot, $\pi(x,y)$ is a flat prior and $P(x,y) = \prod_i \mathrm{PDF_i(x,y)}$ (product over all the channels where PDFs are given).
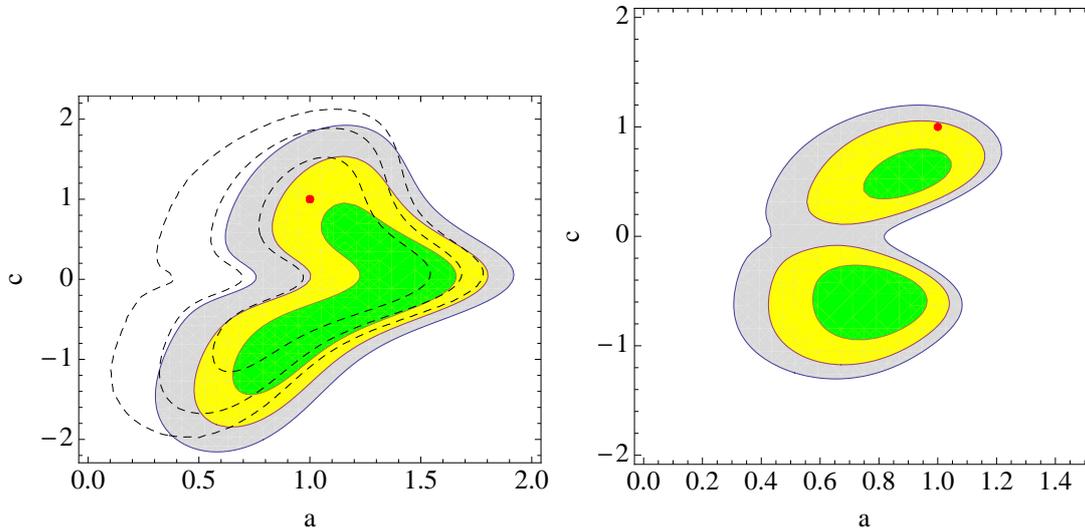
Figure 2.1: *In green, yellow and gray, the 68%,95%,99% C.L. contours for the parameters a and c with the most recent data (table 4.1). Upper plot: ATLAS with data taken at $m_h = 126.5$ GeV (dashed contours correspond to data taken at $m_h = 125\,GeV$). Lower plot:CMS with data taken at $m_h = 125\,GeV$. A flat prior $a \in [0,3]$, $c \in [-3,3]$ is used.*

2.3 Composite Higgs Models

As shown above, the best fits occur for modified couplings of the Higgs boson to the SM fermions and gauge bosons. This is a typical features of Composite Higgs models [71]: for instance, due to the Pseudo Nambu-Goldstone boson (PNGB) nature of the Higgs, the couplings between h and the W, Z gauge bosons are modified as

$$a = \sqrt{1 - \xi}, \tag{2.6}$$

where $\xi \equiv v^2/f^2$, f being the analogue of the pion decay constant and $v = 246$ GeV is the vacuum expectation value (VEV) of the Higgs field. Interestingly, on the one hand $\xi \ll 1$ from constraints coming from electroweak precision data (EWPD); on the other hand ξ is a measure of fine-tuning in these models[2] and is expected to be sizable.

---

[2] The loop-induced potential for the PNGB's is a function of $\sin v/f$ and, without any fine-tuned cancellation, would naturally induce $v \approx f$ or $v = 0$.

2.4 SO(5)/SO(4) and different fermion couplings

While the strong sector alone is SO(5) symmetric, the couplings of elementary fermions to the strong sector break this symmetry, since the SM fermions do not fill complete SO(5) multiplets. We can parametrize these couplings as spurions which transform both under the SM-gauge group and under some representation $\mathbf{r}$ of SO(5) (the well known minimal models MCHM4 [55] and MCHM5 [56] correspond to $\mathbf{r} = 4$ and $\mathbf{r} = 5$, respectively). Depending on the size of $\mathbf{r}$, the coupling of h to fermions f might deviate from the SM as [57]:

$$c_f = \frac{1 + 2m - (1 + 2m + n)\xi}{\sqrt{1 - \xi}} , \qquad (2.7)$$

where m, n are positive integers which depend on $\mathbf{r}$. The specific cases with $m = n = 0$ or $m = 0$, $n = 1$ correspond to the MCHM4 (with $c = \sqrt{1 - \xi}$) and MCHM5 (with $c = (1 - 2\xi)/\sqrt{1 - \xi}$), where all fermions share the same coupling structure. Models with $m \neq 0$ have deviations w.r.t. the SM of order unity (in the direction $c > 1$), even in the limit $\xi \to 0$ and we shall not consider them any further.

In the specific case with $c \equiv c_t = c_b = c_\tau$, the effects of Eq. (2.6) and Eq. (2.7) can be well described in the (a, c) plane. We compare this theoretical expectation, for $m = 0$ and $n = 0, ..., 5$, with the best fit from the combined results of ATLAS (at $m_h = 126.5$ GeV) and CMS ($m_h = 125$ GeV), for the parameters (a, c) in fig. 2.2 (the dashed contours show the same fit taking the ATLAS data at $m_h = 125$ GeV). We assume that no states, beside the SM ones, contribute via loop-effects to the hgg and $h\gamma\gamma$ vertices.
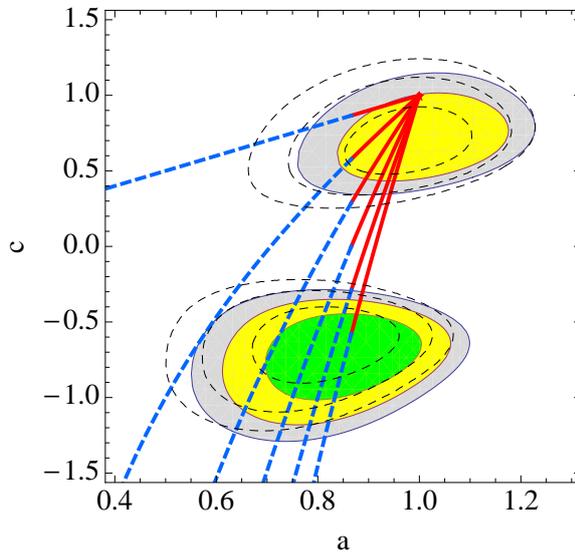
Figure 2.2: *Global fit for the parameters a and c, obtained combining CMS and Tevatron for $m_h = 125$ GeV and ATLAS for $m_h = 126.5$ (dashed circles use ATLAS at $m_h = 125$ GeV); colors and priors as in fig. 1. The lines denote predictions of a generic MCHM; different curves correspond to different values of $n = 0, ..., 5$ in Eq. (2.7) (m = 0), going downwards (n = 0, 1 correspond to the MCHM4 and MCHM5). The red part of the curves is for $0 < \xi < 0.25$ and the blue dashed for $0.25 < \xi < 1$.*

Interestingly, representations leading to large $n \gtrsim 4$ can fit well the data also in the region with $c < 0$, where the rate $h \to \gamma\gamma$ is enhanced, due to a positive interference between W and t loops in the $h\gamma\gamma$ vertex (the fact that it is possible to have order 1 changes in this coupling, from modification of order $O(v^2/f^2) \ll 1$ is due to the large $n \gtrsim 4$ enhancement). To our knowledge, explicit models of this type do not exist yet in the literature ($n = 4$ would appear in models where the spurions connecting SM fields and the strong sector transform as an irreducible representation $\mathbf{r} \in 5 \otimes 5 \otimes 5 \otimes 5$ of SO(5)) and it would be interesting to see if realistic models can be built.

As a final example, we consider the possibility of coupling top and down-type (b and τ) fermions in different ways to the strong sector (models of this type have been proposed, for instance, in refs. [72, 119]). We show examples of this as dots in the $c_t, |c_b|$ plane in fig. 2.3 with $c_t = \sqrt{1 - \xi}$ and $c_b = c_\tau = (1 - 2\xi)/\sqrt{1 - \xi}$ (black dot) and with $c_t = (1 - 2\xi)/\sqrt{1 - \xi}$ and $c_b = c_\tau = \sqrt{1 - \xi}$ (gray dot). Fig. 2.3 shows slices of constant a: for this reason these models, which map into a curve in the 3D (a, c_b, c_t)-space, appear as dots in the figure. The asymmetric couplings do not improve the fit to the data, which shows a preference for the region $c_b \approx c_t$.

2.5 $SO(6)/SO(4) \times SO(2)$ **and natural two Higgs doublets models**

The $SO(6)/SO(4) \times SO(2)$ coset delivers at low energy 8 PNGB's that can be identified with an effective THDM [119]. Large contributions to the $\hat{T}$-parameter can be avoided thanks to the symmetry $C_2 : (H_1, H_2) \to (H_1, -H_2)$, which also allows us to differentiate three cases:

i) If C_2 is exact, the model is a Type I THDM. The second doublet is heavy and inert [81] and there is no mixing between the CP-even states; this model resembles the SO(5)/SO(4) models of section 2.4.[3]

ii) If C_2 is spontaneously broken, an effective Type II THDM is realized at low energy, but only at the price of large fine-tuning (both Higgs VEVs have to be tuned much smaller than f). The couplings of a Type II THDM are [82]

$$\frac{y_t^{THDM}}{y_t} = \frac{\cos\alpha}{\sin\beta}, \quad \frac{y_b^{THDM}}{y_b} = -\frac{\sin\alpha}{\cos\beta}, \tag{2.8}$$

where $\tan\beta = v_1/v_2$ is the ratio between VEVs, and α is the mixing angle (the analog of Eq. (**??**) but for two doublets); the coupling of the lightest Higgs to the vectors is reduced, in comparison with the case of only one Higgs doublet, by $\sin(\beta - \alpha)$. On top of mixing, also higher dimension operators reduce the couplings between h and the SM

---

[3]A similar h_0 phenomenology is realized in the *almost inert* model of Ref. [119], where the C_2 symmetry is unbroken by the top-quark couplings and is broken only by the smaller Yukawas.

vectors and fermions f (as in all composite Higgs models) and for small ξ we obtain

$$
\begin{aligned}
a &= (1 - \xi/2)\sin(\beta - \alpha), \\
c_t &= (1 - \xi/2)\frac{\cos\alpha}{\sin\beta}, \\
c_{b,\tau} &= -(1 - \xi/2)\frac{\sin\alpha}{\cos\beta}.
\end{aligned}
\tag{2.9}
$$

We compare this model with the tree-level MSSM[4] in fig. 2.3 in the (c_t, c_b)-plane with $c_b = c_\tau$ and for different slices of $a = 0.8, 0.9$ (see ref. [145] for an approach with a marginalized). The black line shows the prediction for the MSSM varying β (α is fixed by the slice choice $a = 0.8, 0.9$); the thin part of the line is unaccessible to the tree-level MSSM due to the peculiar relation between the quartic couplings in the potential [82]. The composite THDM is drawn in red.

iii) If C_2 is explicitly broken, then a small VEV $\langle H_2 \rangle \neq 0$, leading to $\tan\beta \approx \xi^{-1}$, and a small mixing $\tan\alpha \lesssim \xi$ is generated [119]. In this case a Type III THDM originates, in which both H_1 and H_2 couple to each SM fermion f,

$$
\frac{y_f}{\sqrt{2}}\bar{f}f(H_1 + a_f H_2) = \frac{y_f}{\sqrt{2}}\bar{f}f(\cos\alpha + a_f \sin\alpha)h_1^0 + \cdots ,
\tag{2.10}
$$

where we have retained only the interactions of the lightest CP-even state h_1^0, and where $y_f = (1 - \xi/2)y_f^{SM}$, as discussed above. For FCNC to be suppressed, the Yukawas for $H_{1,2}$ must be aligned [82]. In fig. 2.3, red dashed line, we show the situation with $a_t = a_{b,\tau} \approx 1$, varying $-\xi \lesssim \alpha \lesssim \xi$.

---

[4]Notice that if some superpartners (such as staus [85] or other states [87, 144]) are light, the rate $h \to \gamma\gamma$ can be enhanced and the MSSM fit might change considerably; other loop-effects that contribute to the Higgs quartic, can also change this prediction [145].
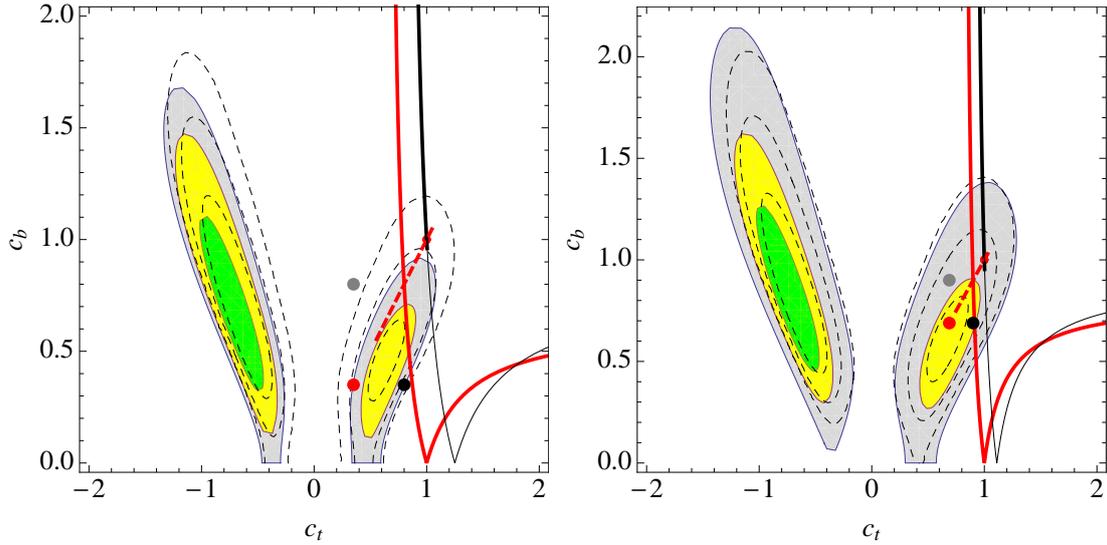
Figure 2.3: *C.L. contours (colors as fig. 1) in the (c_t,|c_b|)-plane for $c_b = c_\tau$ and fixed values of a=0.8, 0.9 (upper and lower plot respectively). The black line corresponds to the couplings of the elementary (composite) THDM Eq. (2.8), once fixed a=0.8, 0.9; the thick part is accessible to the tree-level MSSM. Red lines are for the composite THDM Type II (solid) and Type III (red dashed, varying $-\xi \lesssim \alpha \lesssim \xi$). Shown are also two points (black and gray) corresponding to the SO(5)/SO(4) coset, with $c_t = \sqrt{1-\xi}$ and $c_b = (1-2\xi)/\sqrt{1-\xi}$ and vice versa; the red point is the MCHM5 for comparison. A flat prior $c_t \in [-4, 4]$ and $c_b \in [0, 4]$ is used.*

As shown in fig. 2.3, the preferred region is along the direction $c_t \approx -c_b = -c_\tau$ or, with less significance, along $c_t \approx c_b = c_\tau$. Despite the different possibilities realized in composite THDMs, none touches the first preferred region, and the models that are preferred by the data are those closer to the line $c_t \approx c_\tau \approx c_b = c$, which are more similar, in terms of h phenomenology, to the MCHM with $SO(5)/SO(4)$.

2.6   Higgs impostors?

Independently from the composite Higgs realization, it could be that h can mix with other states that do not necessarily participate in the breaking of the electroweak symmetry (an analog example is the two Higgs doublet model just discussed). This raises the question of whether the state observed at the LHC is or is not the one whose VEV generates m_W and m_Z. This can be done by measuring the parameter a independently: while the Higgs field can have trilinear renormalizable couplings to WW and $a = 1$, impostors will have to couple to WW via loops (also the dilaton would couple to matter as m/f and could reproduce the observed excesses [64, 78]; it is however unlikely that, if $f \approx v$, there would have not been other observable deviations from the SM [79]). Therefore $a < 1$ might imply that the state we observe is not *the* Higgs, or that it is a Higgs that mixes with another state.

One possibility to answer this question, is to marginalize over all parameters except a. Since we don't know whether some of the Higgs couplings have large deviations from the SM values, another possibility is to isolate some channels that are mostly sensible to a and are

sensible to the least number of other parameters. In particular we choose the exclusive VBF channels $pp \to hjj \to WWjj$ measured by CMS [181], which scales roughly as $\sim a^4/c_b^2$ and the exclusive associated production $pp \to Vh \to V\bar{b}b$ measured both at Tevatron [188], CMS and ATLAS, which scales roughly as $\sim a^2$. These channels are mostly insensitive to c_t and c_τ and allow a study of a with c_b as the only other parameter. Fig. 2.4 shows that, unless $c_b \ll 1$, values close to $a \approx 1$ are preferred by data (we have checked that the influence of the other parameters is negligible).
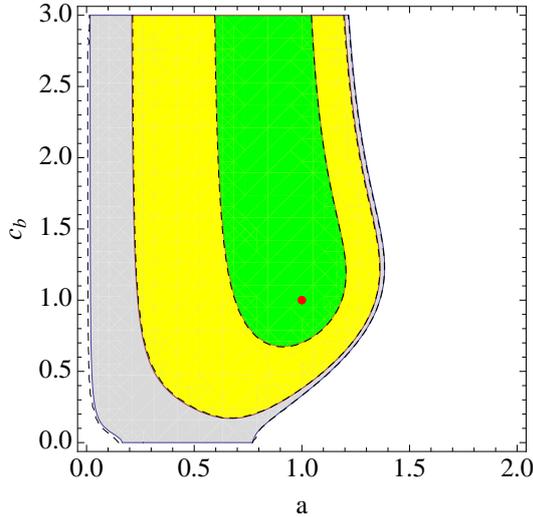
Figure 2.4: *Preferred regions in the plane* (a, c_b) *using only the exclusive channels with associated production (CMS and Tevatron) and VBF cuts (CMS). Colors as in fig. 1. A flat prior is assumed for* $a \in [0,3]$ *and* $c_b \in [0,3]$ *(this choice for the upper limit in* c_b *leads to the most conservative conclusions).*

2.7 Conclusions

Using global fits with the most recent data provided by ATLAS, CMS and Tevatron, we have analyzed the parameter space given by couplings of the Higgs to top and bottom quarks, taus and vector bosons. We have shown that the hypothesis of a SM Higgs with $m_h \approx 125$ GeV agrees well with the data.

We have then studied different models, in particular in the context of composite Higgs, to see what features could improve/worsen the situation of these scenarios when more data is available. In particular, we have shown that, depending on the coupling structure of elementary fermions to the strong sector, the couplings of h to the SM fields can change considerably w.r.t. the SM case. Some composite models, such as the MCHM4, seem to point towards the disfavored direction. Other models, however, follow better the trend of data: the MCHM5, for instance, reduces the couplings of h to fermions, c, more than the one to vectors, a, and for small ξ crosses the best fit region with $c > 0$. Models with $n \gtrsim 4$ in Eq. (2.7) have an even better trend, as the best fit region with $c_t < 0$ lies within their parameter space even for $f \gtrsim 500$ GeV. Different couplings of top and bottom quarks to the
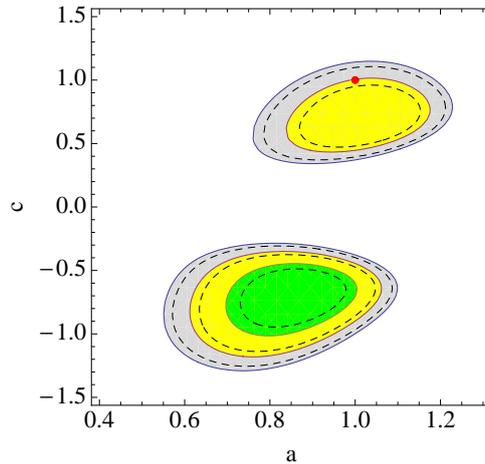
Figure 2.5: *Comparison between data analyses based on Bayesian interval (as used throughout this work) and isocontours of constant $\chi^2 = \chi^2_{min} + 2.3, 5.99, 9.21$ (the dashed ones).*

strong sector, on the other hand do not seems to ameliorate much the fit, although more drastic possibilities could be considered, that reproduce the preferred region $c_t = -c_b = -c_\tau$, shown in fig. 2.3.

We have also studied larger coset structures such as $SO(6)/SO(4) \times SO(2)$ which, in some cases reduce to a composite model with an inert doublet (Type I THDM) and the light Higgs phenomenology is not much affected, thus resembling to the SO(5)/SO(4) coset. If more fine-tuning is allowed, a version of a Type II THDM is possible; compared with the MSSM this has the advantage of having less constrained quartics, which allows the model to have both $c_b > 1$ and $c_b < 1$, thus covering a larger region of parameter space [145]. Despite this, present data show a mild preference for the composite THDM only for sizable deviations from $a = 1$ (upper plot of fig. 2.3). If FCNC can be kept under control, a version of Type III THDM is also possible. In this case the couplings of the second Higgs doublet to fermions enter as new parameters in the theory; despite this freedom, the greatest overlap with the best fit regions occur along $c_t \approx c_{b,\tau}$ which is the region also touched by the minimal model. In summary, the composite THDM provides its best fit to the data when the parameter space is such that its phenomenology resembles much that of the minimal composite Higgs model $SO(5)/SO(4)$.

Finally, we studied if the found Higgs particle is responsible for giving mass to the W boson. We find that with the data at hand, for values of $c_b \gtrsim 1$, the region where the Higgs is fully responsible for the W mass is favoured, making it consistent with the SM prediction.

Note: While this work was in preparation, refs. [80, 88, 89] appeared, also discussing deviations of Higgs couplings from its SM values.

2.8 Appendix

Bayesian interval versus χ^2 analyses
In fig. 2.5 we compare the effects of using analyses based on χ^2 (where the point χ^2_{min} is

first found and then the 68%,95%,99%C.L. intervals are found as isocontours with, in the case two fitting parameters, $\chi^2 = \chi^2_{min} + 2.3, 5.99, 9.21$), versus analyses that use Bayesian intervals [90] (as done throughout this work). If μ is just a parameter and not a function depending on a, c_t, c_b, c_τ, the methods do not differ; however, when $\mu = \mu(a, c_t, c_b, c_\tau)$ is a function of the parameters $a, c_{t,b,\tau}$ as in Eq. (4.52), then the probability density function is no longer Gaussian in $a, c_{t,b,\tau}$ and the two methods differ. As shown in fig. 2.5, however, the small differences do not alter the qualitative conclusions.

Cut efficiencies ζ_p^i

The production cross-section for channel i receives contributions from gluon fusion (G), vector boson fusion (VBF) associated production with a vector boson (A) and associated $t\bar{t}$ production (tth),

$$\frac{\sum_p \sigma_p \zeta_p^i}{\sum_p \sigma_p^{SM} \zeta_p^i} = \frac{c_t^2(\sigma_G \zeta_G^i + \sigma_{tth}\zeta_{tth}^i) + a^2(\sigma_{VBF}\zeta_{VBF}^i + \sigma_A \zeta_A^i)}{\sigma_G \zeta_G^i + \sigma_{VBF}\zeta_{VBF}^i + \sigma_A \zeta_A^i + \sigma_{tth}\zeta_{tth}^i},$$

where the cut efficiencies ζ_p^i for each production mode p corresponding to channel i from table 4.1 are as follows: when only G, VBF or A is indicated, we have assumed no contamination from other production channels; inclusive channels correspond to $\zeta_G^i = \zeta_{VBF}^i = \zeta_A^i = \zeta_{tth}^i = 1$; other channels, denoted $\gamma\gamma_X$ in table 4.1, are reported below, where the numbers in brackets denote efficiencies at 8 TeV, the others at 7 TeV [179],

i	ζ_G^i	ζ_{VBF}^i	ζ_A^i	ζ_{tth}^i
$\gamma\gamma_0$	0.28(0.45)	1(1)	1.52(1.91)	2.33(4)
$\gamma\gamma_1$	1.16(1.2)	1(1)	1.36(1.4)	0(0)
$\gamma\gamma_2$	1.82(1.84)	1(1)	1.36(1.4)	0(0)
$\gamma\gamma_3$	1.82(1.84)	1(1)	1.36(1.4)	0(0)
$\gamma\gamma_{jj}$	0.029	1	0.01	0
$\gamma\gamma_{jj}$ (T)	(0.024)	(1)	(0)	(0)
$\gamma\gamma_{jj}$(L)	(0.094)	(1)	(0.063)	(0)

and the overall normalization in each line factorizes.

Table 2.1: *CMS, ATLAS and Tevatron data for the most sensitive channels. The cuts are classified as inclusive (I), associated production (A), vector boson fusion (VBF) or else ($\gamma\gamma_X$), see Appendix. $\hat{\mu}^{1.96,7,8}$ denote the best fits for the 1.96 TeV Tevatron, and the 7,8,7+8 TeV LHC data.*

CMS	Cuts	$\hat{\mu}^7$	$\hat{\mu}^8$	$\hat{\mu}^{7+8}$
$\gamma\gamma_0$ [179]	$\gamma\gamma_X$	$3.1^{+1.9}_{-1.8}$	$1.5^{+1.3}_{-1.3}$	-
$\gamma\gamma_1$ [179]	$\gamma\gamma_X$	$0.6^{+1.0}_{-0.9}$	$1.5^{+1.1}_{-1.1}$	-
$\gamma\gamma_2$ [179]	$\gamma\gamma_X$	$0.7^{+1.2}_{-1.2}$	$1.0^{+1.2}_{-1.2}$	-
$\gamma\gamma_3$ [179]	$\gamma\gamma_X$	$1.5^{+1.6}_{-1.6}$	$3.8^{+1.8}_{-1.8}$	-
$\gamma\gamma_{jj}$ [179]	$\gamma\gamma_X$	4.2^{+2}_{-2}	$L:\ -0.6^{+2.0}_{-2.0}$ $T:\ \ \ 1.3^{+1.6}_{-1.6}$	-
$\tau\tau$ [53, 181]	I	$0.6^{+1.1}_{-1.3}$	-	$-0.2^{+0.7}_{-0.7}$
bb [53, 181]	A	$1.2^{+2.1}_{-1.9}$	-	$0.1^{+0.8}_{-0.7}$
WW_{0j} [53]	G	$0.1^{+0.6}_{-0.6}$	$1.3^{+0.8}_{-0.6}$	-
WW_{1j} [53]	G	$1.7^{+1.2}_{-1.0}$	$0.0^{+0.8}_{-0.8}$	-
WW_{2j} [53]	VBF	$0.0^{+1.3}_{-1.3}$	$1.3^{+1.7}_{-1.3}$	-
ZZ [53, 181]	I	$0.6^{+1.0}_{-0.6}$	-	$0.7^{+0.5}_{-0.4}$
ATLAS 125 GeV	Cuts	$\hat{\mu}^7$	$\hat{\mu}^8$	$\hat{\mu}^{7+8}$
$\gamma\gamma$ [138, 182]	I	$1.6^{+0.8}_{-0.7}$	$0.9^{+0.5}_{-0.7}$	-
$\tau\tau$ [138]	I	$0.2^{+1.7}_{-1.8}$	-	-
bb [138]	A	$0.5^{+2.1}_{-2.0}$	-	-
WW [138]	I	$0.6^{+0.7}_{-0.7}$	-	-
ZZ [54, 138]	I	$1.4^{+1.3}_{-0.8}$	-	$1.3^{+0.6}_{-0.6}$
CDF/D0	Cuts	$\hat{\mu}^{1.96}$	-	-
$\gamma\gamma$ [188]	I	$3.6^{+3.0}_{-2.5}$	-	-
bb [188]	A	$2.0^{+0.7}_{-0.6}$	-	-
WW [188]	I	$0.3^{+1.2}_{-0.3}$	-	-
ATLAS 126.5 GeV	Cuts	$\hat{\mu}^7$	$\hat{\mu}^8$	$\hat{\mu}^{7+8}$
$\gamma\gamma$ [138, 182]	I	$2.0^{+0.8}_{-0.7}$	$1.7^{+0.7}_{-0.6}$	-
$\tau\tau$ [138]	I	$0.3^{+1.7}_{-1.8}$	-	-
bb [138]	A	$0.5^{+2.2}_{-2.2}$	-	-
WW [138]	I	$0.5^{+0.6}_{-0.6}$	-	-
ZZ [54, 138]	I	$1.1^{+1.0}_{-0.7}$	-	$1.0^{+0.6}_{-0.5}$

Chapter 3

Higgs Couplings in Composite Models

3.1 Introduction

Models in which the Higgs boson arises as a composite resonance from a strongly coupled sector can provide a natural explanation of the small value of the electroweak (EW) scale. If in addition the Higgs is a pseudo-Nambu-Goldstone Boson (pNGB) associated to a spontaneously broken global symmetry, then the small value observed for its mass, compared to the mass of the other yet unobserved resonances, can be naturally explained. The minimal realization of this idea, known as Minimal Composite Higgs Model (MCHM), is based on the coset structure $SO(5)/SO(4)$ [91, 92].

The most promising signatures of these models are provided by the fermionic resonances, which are tightly connected to the EW scale because they are responsible for cutting off divergent contributions to the Higgs potential [93–98]. The bounds on heavy vector-like quarks from LHC direct searches are approaching the TeV [99, 100]. These resonances are also expected to modify the couplings of the Higgs to Standard Model (SM) particles and in particular the loop-induced couplings to gluons and photons. Information extracted from experimental analyses of Higgs couplings [101, 102] can usefully complement the one coming from direct searches in constraining the natural parameter space of these models [103, 104]. Generically, the pNGB nature of the Higgs implies that the resonance contributions to the loop induced couplings, related to operators of the form $H^\dagger H F_{\mu\nu}F^{\mu\nu}$ that explicitly break the shift symmetry, are suppressed by powers of g_{SM}/g_ρ, where g_ρ is a characteristic strong coupling [105, 106]. The question then is whether or not this suppression disappears in the limit in which some of the resonances Ψ are lighter than the others, $g_\Psi \ll g_\rho$. Surprisingly, this is not the case for a broad class of composite Higgs models, where light fermionic resonances do not contribute to the hgg and $h\gamma\gamma$ couplings as the consequence of an exact cancellation between corrections to the $ht\bar{t}$ coupling and loops of resonances [107–109]. In a two-site realization of the MCHM, this cancellation was shown to hold when only one Left-Right (LR) $SO(4)$ invariant is present [109]. In this paper we show that in the MCHM the cancellation, and therefore the insensitivity to light resonances, follows automatically from the pNGB nature of the Higgs and the assumption of partial compositeness, while it is independent of the

number of LR $SO(4)$ invariants and of the particular realization of the elementary-composite couplings. Moreover, we find that under the further assumption of CP conservation, derivative interactions of the Higgs to the resonances do not contribute to the hgg and $h\gamma\gamma$ couplings. We show that the $ht\bar{t}$ and hgg couplings are both fixed uniquely by the top mass, and coincide for small elementary/composite mixings. We also discuss how, in models where more than one LR $SO(4)$ invariant is present, these couplings are sensitive to the details of the UV physics [109], even in the case where all resonances are heavy and possibly out of the direct reach of the LHC.

This chapter is organized as follows. In Section 3.2 we present the general approach to the Higgs couplings in composite models based on the Callan-Coleman-Wess-Zumino (CCWZ) construction [5,6]. In Section 3.3 we describe an explicit realization based on a two-site version of the MCHM$_{14}$ [96–98] where the general features discussed in Section 3.2 are exemplified. We also comment on an alternative approach based on the Weinberg Sum Rules (WSR) [95, 96]. Finally, in 3.4 we draw our conclusions. Appendices 3.5 and 3.6 contain a summary of our notations and details on our fit to Higgs data, respectively.

3.2 General Composite Higgs Models

The scalar sector of minimal pNGB Higgs models, based on the $SO(5)/SO(4)$ coset structure[1], is described by the Goldstone matrix

$$U(\Pi) = \exp\left(i\frac{\sqrt{2}\Pi^i T^i}{f}\right). \tag{3.1}$$

where T^i are the broken generators, Π^i the Goldstone bosons and f the corresponding decay constant (see Sec. 3.5 for the notation).

We assume that the SM fermions obtain their masses through *partial compositeness* [110], by mixing with operators of the strong sector $\mathcal{O}^{I,\cdots,J}$, with capital letters I, J denoting $SO(5)$ indices. This mixing is conveniently described by formally promoting the elementary fermions to full representations of the $SO(5)$ group, the *embeddings*. The embeddings for the $SU(2)_L$ doublet q_L and for the singlet q_R are denoted by $\mathcal{Q}_L^{I,\cdots,J}$, $\mathcal{Q}_R^{I,\cdots,J}$, respectively. Then the Lagrangian for partial compositeness takes the form

$$\mathcal{Q}_{L,R}^{I\cdots J}\mathcal{O}_{I\cdots J}. \tag{3.2}$$

At low energy, in the broken phase, this implies mixing terms between elementary fermions and resonances of the strong sector Ψ_r, which, up to small splittings proportional to the EW symmetry breaking VEV, can be taken as full multiplets **r** of the unbroken $SO(4)$. A convenient way to write these low-energy interactions, while keeping track of the underlying $SO(5)$ symmetry, exploits the transformation properties of the Goldstone matrix $U \to g\, U\, \hat{h}(g, \Pi)^{-1}$

---

[1] An extra unbroken $U(1)_X$ is always understood in the coset structure, in order to reproduce the correct hypercharge of the SM fermions. Our normalization is such that $Y = T_R^3 + X$.

with $g \in SO(5)$, $\hat{h} \in SO(4)$ [5, 6]. In fact, the Goldstone matrix U can be used to 'convert' irreducible representations of $SO(5)$ into reducible representations of $SO(4)$. Then one can write interactions between the embeddings, transforming under $SO(5)$, and the resonances in representations of $SO(4)$:

$$
\begin{aligned}
\mathcal{L}_{\text{mix}} \quad = \quad & \left(F_r^L \overline{\mathcal{Q}}_L^{I \dots J} U_{Ii} \dots U_{Jj} \Psi_r^{i \dots j} + \cdots \right. \\
& \left. + F_1^L \overline{\mathcal{Q}}_L^{I \dots J} U_{I5} \dots U_{J5} \Psi_1 + \text{h.c} \right) + (L \to R) \ ,
\end{aligned}
\tag{3.3}
$$

where the dots stand for couplings with resonances in other $SO(4)$ representations. The simplest example of Eq. (3.3) is the MCHM$_5$ [92]: in this case Eq. (3.2) implies the existence of resonances in a $\mathbf{5} = \mathbf{4} \oplus \mathbf{1}$ of $SO(4)$, and Eq. (3.3) reads $F_4^L \overline{\mathcal{Q}}_L^I U_{Ii} \Psi_4^i + F_1^L \overline{\mathcal{Q}}_L^I U_{I5} \Psi_1 +$ h.c. $+ (L \to R)$.

We further assume that some of the fermionic resonances are lighter than the typical scale of the other resonances. This assumption is motivated by the tension between the necessary scale of bosonic resonances which, to account for the smallness of the S parameter, are expected to be in the multi-TeV range, and the need for light fermionic resonances as necessary to reproduce the smallness of the observed Higgs mass [93–98]. In this limit we can keep some of the resonances in our effective description, while decoupling the heavy ones. The Lagrangian describing this setup contains, in addition to Eq. (3.3), a part describing the strong sector alone, which can be written, again, with the $SO(5)$ symmetry non-linearly realized [5, 6],

$$
\begin{aligned}
\mathcal{L}_{\text{strong}} \quad = \quad & (\text{kin. term for } \Psi_r) - M_r \overline{\Psi}_r \Psi_r + \cdots \\
& + i c_L \, \overline{\Psi}_{rL}^{i \dots jk} \gamma^\mu d_\mu^k \Psi_{r'L}^{i \dots j} + \cdots + \text{h.c.} + (L \to R),
\end{aligned}
\tag{3.4}
$$

where at leading order in the chiral expansion and in the unitary gauge $d_\mu^k \simeq (\sqrt{2}/f)\delta_\mu h \, \delta^{k4}$ (see Appendix 3.5 for details) and the dots stand for different representations. We have denoted by $\mathbf{r}$ and $\mathbf{r'}$ two representations that differ by one $SO(4)$ index, in order to allow for the first term in parentheses. In the example of the MCHM$_5$, the second line of Eq. (3.4) reads $i c_L \overline{\Psi}_{4L}^k \gamma^\mu d_\mu^k \Psi_{1L} + \text{h.c.} + (L \to R)$.

Notice that a number $n_r > 1$ of copies of each $SO(4)$ multiplet could be present in the low-energy theory. In this case, mass mixing terms between the $\Psi_r^{(i)}$, $(i = 1, \dots, n_r)$ are allowed by the global symmetry. However, these mass mixings can always be eliminated with a suitable field redefinition, so the masses in the strong sector can be taken diagonal without loss of generality. In Eq. (3.4) we have neglected higher derivative interactions: beside being suppressed by the strong sector scale, these interactions do not affect the couplings of a single Higgs with a pair of gauge bosons.

The terms in the second line of Eq. (3.4) couple h with two resonances and can potentially give sizeable corrections to the hgg coupling. However, as we now show, if a further assumption is made on the theory, namely CP conservation, then the contribution to the hgg coupling of these operators exactly vanishes. Indeed, if the coefficient c_L is real then the Higgs derivative

interactions contained in Eq. (3.4) can be written as

$$i\sqrt{2}c_L\frac{\partial_\mu h}{f}\left(\overline{\Psi}_{rL}^{i...j4}\gamma^\mu\Psi_{r'L}^{i...j} - \overline{\Psi}_{r'L}^{i...j}\gamma^\mu\Psi_{rL}^{i...j4}\right).\tag{3.5}$$

The interactions in Eq. (3.5) are manifestly *antisymmetric*[2] in the fermion fields (notice that because d_μ transforms as a **4** of $SO(4)$, Eq. (3.4) does not generate Higgs derivative interactions that are bilinear in the same fermion field). Equation (3.5) is written in the gauge eigenstate basis for fermions. Now, if the parameters that appear in the fermion mass matrix, namely the masses M_r and the linear mixings $F_r^{L,R}$, are also real, then the unitary transformations that diagonalize the mass Lagrangian are orthogonal, and the Higgs derivative couplings are antisymmetric in the mass eigenstate basis as well. Because the gluon only has diagonal couplings, however, vertices involving the Higgs and two distinct fermions do not contribute to the triangle one-loop diagrams for hgg. Thus we conclude that under the hypothesis that the Lagrangian preserves a CP symmetry, the operators in Eq. (3.4) do not contribute to single Higgs production.[3] Alternatively, if CP is not preserved a contribution to the hgg coupling generically arises, proportional to $G_{\mu\nu}^A\widetilde{G}^{\mu\nu\,A}$. A completely analogous argument holds for the $h\gamma\gamma$ coupling.

As an example, let us consider the top sector of the MCHM$_5$. Assuming that all the parameters in Eq. (3.4) are real but allowing for complex linear mixings in Eq. (3.3), the Higgs derivative interactions that contribute to the hgg coupling, obtained transforming Eq. (3.5) into the mass eigenstate basis, read

$$c_L\frac{\delta_\mu h}{f}\sum_{a=1}^{4}k_L^a\,\overline{\psi}_L^a\gamma^\mu\psi_L^a,\tag{3.6}$$

where ψ^a are the mass eigenstate fermions (that is, the physical top quark and its partners) and the leading contributions to the coefficients k_L^a scale as

$$\frac{\text{Im}(F_4^{L,R\,*}F_1^{L,R})}{M_1 M_4}\sqrt{\xi}.\tag{3.7}$$

For simplicity, since in this paper we focus on the top sector, from here on we assume that all the parameters in the Lagrangian can be made real by redefining the fermion fields. Under this assumption, therefore, we conclude that the terms in Eq. (3.4) have no impact on the couplings between the Higgs and massless gauge bosons. Of course, when all the SM fermions are included, a source of CP violation must be present to reproduce the Cabibbo-Kobayashi-Maskawa phase. In this case the strong constraints on CP-odd observables from flavor physics [112–115] should be taken into account.

---

[2]In the argument that follows we neglect, without loss of generality, the phases that appear in the definitions of the composite multiplets (see for example Eq. (3.51)).

[3]The situation is different in the double Higgs production process, $gg \to hh$, because couplings of the Higgs to two distinct fermions can enter in box diagrams [111].

From the above discussion we conclude that the *hgg* coupling is determined by Higgs interactions at zero momentum. In this limit, the coupling of the Higgs to gluons mediated by loops of a particle with mass $M \gg m_h$ can be derived from the contribution of the heavy particle to the QCD β function, by means of the Higgs low-energy theorem [116, 117]. Therefore, neglecting the contribution of the light SM fermions we simply have (for each SM particle x we define $c_x \equiv g_{hxx}/g_{hxx}^{\rm SM}$)

$$c_g = \frac{v}{2}\left[\frac{\partial}{\partial h}\log\det\mathcal{M}_t^\dagger\mathcal{M}_t(h) + \sum_i \frac{\partial}{\partial h}\log M_{f,i}^2(h)\right]_{\langle h\rangle}, \qquad (3.8)$$

where $\mathcal{M}_t(h)$ is the mass matrix in the top sector, and we have also included the contribution from the partners of the light SM fermions, with squared masses $M_{f,i}^2(h)$. Fermions with 'exotic' electric charges (such as for example $Q_{el} = 5/3$ or $8/3$, which are present in composite Higgs models) do not contribute to the *hgg* coupling, because since they do not mix with the elementary fermions, they do not feel any explicit breaking of the $SO(5)$ symmetry; as a consequence, loops involving only the exotic states cannot generate any effects that break the shift symmetry, including a $hG_{\mu\nu}^A G^{\mu\nu\,A}$ coupling.

Let us focus on the contribution arising from the top sector.[4] Assuming the presence of n top partners in the theory, the mass Lagrangian in the top sector can be written in full generality as

$$-\left(\begin{array}{c|c}\bar{t}_L & \overline{\mathbf{C}}_L\end{array}\right)\mathcal{M}_t(h)\left(\begin{array}{c}t_R\\\hline\mathbf{C}_R\end{array}\right) + \text{h.c.} \qquad (3.9)$$

with

$$\mathcal{M}_t(h) = \left(\begin{array}{c|c}0 & \mathbf{F}_L^T(h)\\\hline\mathbf{F}_R(h) & \mathbf{M}_c\end{array}\right), \qquad (3.10)$$

where $\mathbf{C}$ is a n-dimensional vector collecting all the top partners, and $\mathbf{F}_{L,R}(h)$ are n-dimensional vectors containing the elementary-composite mixing terms. Since, by assumption, the only breaking of the global symmetry under which the Higgs shifts is contained in the mixings with elementary states, the strong sector alone can only generate derivative interactions of h and the $n \times n$ mass matrix in the composite sector $\mathbf{M}_c$ is independent of the Higgs field. Thus the structure in Eq. (3.9) follows from the assumption of partial compositeness. From the properties of block matrices we find

$$\det\mathcal{M}_t(h) = m_t^0(h) \times \det\mathbf{M}_c, \qquad (3.11)$$

---

[4]The partners of a light SM fermion f give a contribution to $c_g - 1$ that scales like $\sim \epsilon_{f\,L,R}^2\xi$, where $\epsilon_{f\,L,R}$ measure the degree of compositeness of $f_{L,R}$, and is thus competitive with the $\sim \xi$ contribution of the top sector only in the limit of full compositeness for one of the chiralities of f [109, 118]. Therefore, for a generic point in parameter space, the contribution of the partners of the light SM fermions is expected to be subleading. See for example Eq. (3.35) in the following.

which implies that the contribution to the *hgg* coupling from the top sector is

$$c_g^{(t)} = v \left[\frac{\partial}{\partial h} \log m_t^0(h) \right]_{\langle h \rangle} . \tag{3.12}$$

Here $m_t^0(h) = -\mathbf{F}_L^T(h) \mathbf{M}_c^{-1} \mathbf{F}_R(h)$ is the top mass at quadratic order in the mixings $F_r^{L,R}$, which can be readily obtained from Eq. (3.9) by integrating out the composite states:

$$\mathcal{L}_{\text{eff}} = -m_t^0(h) \bar{t}_L t_R + \text{h.c.} + i Z_{t_L}(h) \bar{t}_L \slashed{\partial} t_L + i Z_{t_R}(h) \bar{t}_R \slashed{\partial} t_R , \tag{3.13}$$

where we have also included the renormalizations to the wavefunctions of $t_{L,R}$. From Eq. (3.13) we derive the coupling of the Higgs to the top

$$c_t = v \left[\frac{\partial}{\partial h} \log m_t(h) \right]_{\langle h \rangle} , \quad m_t(h) = \frac{m_t^0(h)}{\sqrt{Z_{t_L}(h) Z_{t_R}(h)}} . \tag{3.14}$$

In the limit where the breaking of the global symmetry is small, $\epsilon_{L,R}^2 \sim (F_r^{L,R}/M_\Psi)^2 \ll 1$ (where M_Ψ generically denotes the composite masses), one finds $Z_{t_{L,R}}(h) \sim 1 + \epsilon_{L,R}^2 f_{L,R}(h)$, where $f_{L,R}(h)$ are periodic functions of h, and we neglected terms of higher order in $\epsilon_{L,R}^2$. Thus the top contribution to the *hgg* amplitude, Eq. (3.12), is tightly correlated with the $ht\bar{t}$ coupling in Eq. (3.14), and the two can differ sizably only if $\epsilon_{L,R} \sim 1$, that is if one of the chiralities of the top is mostly composite. Furthermore and importantly, while the $ht\bar{t}$ coupling receives corrections at all orders in $\epsilon_{L,R}^2$, from Eq. (3.12) we read that the *hgg* coupling is formally of zeroth-order in this expansion. This implies that the terms of higher order in $\epsilon_{L,R}^2$ in the top loop contribution to the *hgg* amplitude are exactly canceled by those coming from loops of resonances. This cancellation was found to take place in several models where the Higgs is a pseudo-Goldstone boson [107–109], and implies that the presence of light fermionic resonances would not affect the production rate of the Higgs via gluon fusion, nor its decay width into photons. Our analysis shows that, in the context of pNGB Higgs models, this result follows automatically from the assumption of partial compositeness, and is not dependent on the choice of the embedding for the elementary fermions nor on the specific realization of the model. Indeed, our analysis was performed by applying the general CCWZ approach.

Let us now inspect more closely the structure of the *hgg* coupling. According to Eq. (3.12), its expression is determined by the LR $SO(4)$ invariants that can be built out of the embeddings $\mathcal{Q}_{L,R}$ and that contribute to the top mass m_t^0. The latter has the form

$$m_t^0(h) = \sum_{n=1}^{N} \left(\sum_r c_r^{(n)} y_r \right) \times I_{LR}^{(n)} \left(\frac{h}{f} \right) , \tag{3.15}$$

where $I_{LR}^{(n)}$ indicates the $N \geqslant 1$ $SO(4)$ invariants. The coefficient of each invariant is given by a linear combination of the quantities

$$y_r \equiv \sum_{i=1}^{n_r} \frac{F_{r(i)}^L F_{r(i)}^R}{M_{r(i)}} , \tag{3.16}$$

with coefficients $c_r^{(n)}$. This was expected, since y_r is simply the leading contribution of the **r**-plets to the top Yukawa coupling. From Eq. (3.15) we readily obtain

$$c_g^{(t)} = 1 - \Delta_g^{(t)}(y_r/y_{r'}) \, \xi + \mathcal{O}(\xi^2) \,, \tag{3.17}$$

where $\Delta_g^{(t)}$ is a function with values of $\mathcal{O}(1)$ and $y_r/y_{r'}$ schematically denotes all the different ratios of y_r that can be built in the chosen model. While this is indeed the most general form of the *hgg* coupling, its expression further simplifies if only one LR invariant can be built out of the embeddings $\mathcal{Q}_{L,R}$, *i.e.* if $N = 1$ in Eq. (3.15). In this case, when taking $\partial \log m_t^0/\partial h$ in Eq. (3.12), the dependence on the y_r drops and the *hgg* coupling turns out to be a simple 'trigonometric' rescaling of the SM expression. In other words, if $N = 1$ then $\Delta_g^{(t)} = $ constant in Eq. (3.17). This was already noticed in Ref. [109], where a two-site setup was considered. For example, in the popular MCHM$_5$ and MCHM$_{10}$ [92] there is only one LR invariant: [5]

$$\mathbf{5}_{L,R}: \quad U_{Ii}(\hat{Q}_{t_L}^\dagger)_I(\hat{Q}_{t_R})_J U_{Ji} = \frac{1}{2\sqrt{2}} \, s_{2h} \,,$$

$$\mathbf{10}_{L,R}: \quad U_{Ii}(\hat{Q}_{t_L}^\dagger)_{IJ}(\hat{Q}_{t_R})_{JK} U_{Ki} = -\frac{1}{8} \, s_{2h} \tag{3.18}$$

where $s_{nh} \equiv \sin(nh/f)$ and we defined $\mathcal{Q}_L \equiv t_L \hat{Q}_{t_L} + b_L \hat{Q}_{b_L}$ and $\mathcal{Q}_R \equiv t_R \hat{Q}_{t_R}$. In both cases $I_{LR}^{(1)} = s_{2h}$, leading to

$$\mathbf{5}_{L,R} \,, \quad \mathbf{10}_{L,R}: \quad c_g^{(t)} = \frac{1 - 2\xi}{\sqrt{1 - \xi}} \quad \Rightarrow \quad \Delta_g^{(t)} = \frac{3}{2} \,. \tag{3.19}$$

On the other hand, two independent LR invariants are present for example in MCHM$_{14}$:

$$U_{I5}(\hat{Q}_{t_L}^\dagger)_{IJ}U_{J5}U_{K5}(\hat{Q}_{t_R})_{KL}U_{L5} = \tfrac{1}{16\sqrt{5}}(-6\,s_{2h} - 5\,s_{4h}),$$

$$U_{Ii}(\hat{Q}_{t_L}^\dagger)_{IJ}U_{Jj}U_{Ki}(\hat{Q}_{t_R})_{KL}U_{Lj} = \tfrac{1}{16\sqrt{5}}(6\,s_{2h} - 5\,s_{4h}) \,. \tag{3.20}$$

It follows that the dependence on the y_r does not drop out of the *hgg* coupling, which takes the general form in Eq. (3.17). By explicit computation we find

$$\mathbf{14}_{L,R}: \quad \Delta_g^{(t)} = \frac{11}{2}\left(\frac{1 - \frac{64}{55}\frac{y_1}{y_4} - \frac{6}{11}\frac{y_9}{y_4}}{1 - \frac{8}{5}\frac{y_1}{y_4}}\right). \tag{3.21}$$

Contrarily to the models with only one invariant, where a single universal function of ξ appears (see for example Eq. (3.19)), when $N > 1$ a continuum of possible couplings to photons and gluons is allowed by the symmetry structure. Furthermore, while the 'trigonometric' rescaling of models with a single invariant always suppresses the Higgs production rate, in models with

---

[5]Naively, in each of the products $\mathbf{5}_L \times \mathbf{5}_R$ and $\mathbf{10}_L \times \mathbf{10}_R$ *two SO*(4) invariants appear. However, whenever q_L and t_R are embedded in the same $SO(5)$ representation **r**, one invariant does not depend on the Higgs and can be written as $\overline{\mathcal{Q}}_L \mathcal{Q}_R$, which vanishes when the embeddings are set to their physical values. Thus the number of invariants is lowered by one unit [119].

$\mathcal{Q}_L \backslash \mathcal{Q}_R$	1	5	10	14
5	$1/2$	$3/2$	$1/2$	$\dfrac{5}{2}\dfrac{1-\frac{24}{25}\frac{y_1}{y_4}}{1-\frac{4}{5}\frac{y_1}{y_4}}$
10	$\times$	$1/2$	$3/2$	$3/2$
14	$3/2$	$\dfrac{9}{2}\dfrac{1-\frac{10}{9}\frac{y_1}{y_4}}{1-2\frac{y_1}{y_4}}$	$3/2$	$\dfrac{11}{2}\dfrac{1-\frac{64}{55}\frac{y_1}{y_4}-\frac{6}{11}\frac{y_9}{y_4}}{1-\frac{8}{5}\frac{y_1}{y_4}}$

Table 3.1: Summary table showing the value of $\Delta_g^{(t)}$, defined by Eq. (3.17), for different choices of the embeddings of elementary fermions. The y_r were defined in Eq. (3.16). The points at which $\Delta_g^{(t)}$ formally diverges (for example, $y_4 = 8y_1/5$ for $\mathbf{14}_L + \mathbf{14}_R$) correspond to the nonviable situation where $m_t^0 \propto s_h^3 c_h$ and thus $c_t \to 3$ for $\xi \to 0$, *i.e.* the SM top Yukawa is not recovered in the limit $\xi \to 0$. In the case $\mathcal{Q}_L \sim \mathbf{10}$, $\mathcal{Q}_R \sim \mathbf{1}$, there is no invariant that can generate the top mass.

more than one invariant $\Delta_g^{(t)}$ can take both signs depending on the values of the ratios $y_r/y_{r'}$, thus an enhancement of the rate is in principle also possible. However, notice that from Eq. (3.21), taking the limit where one $\mathbf{1}$ ($\mathbf{4}$) is much lighter than all the other resonances,[6] we find $\Delta_g^{(t)} = 4$ ($\Delta_g^{(t)} = 11/2$): in both cases the rate is actually strongly suppressed, suggesting that in most of the parameter space of the MCHM$_{14}$ we should expect $c_g^{(t)} < 1$.[7] This will be confirmed by the detailed analysis contained in Section 3.3. In Table 3.1 we report the values of $\Delta_g^{(t)}$ for the lowest-dimensional embeddings compatible with the custodial symmetry that protects the Z-b-$\bar{b}$ coupling [120]. Notice that the results in the column corresponding to $\mathcal{Q}_R \sim \mathbf{1}$ hold even if the t_R is assumed to be a fully composite chiral state, rather than an elementary field mixed with a strong sector operator. In fact, if t_R is fully composite the structure of the mass matrix differs from that in Eq. (3.10), but Eq. (3.12) still holds. Therefore, independently of whether t_R is a partially or fully composite singlet of $SO(5)$, the hgg coupling is determined by the $SO(4)$ invariants that can be built out of $\mathcal{Q}_L$ and the Goldstone matrix, and are linear in the former.

As first pointed out in Ref. [109], in models which feature more than one LR invariant, such as MCHM$_{14}$, the Higgs production rate is sensitive to the resonance spectrum, implying that the analysis of Higgs couplings can usefully complement the information coming from direct searches for heavy fermions. We note that because of the dependence on the ratios $y_r/y_{r'}$, the Higgs coupling to gluons is insensitive to the absolute scale of the resonances. Therefore one can envisage a finely-tuned scenario where all the top partners are relatively heavy and thus out of the direct reach of the LHC [97], but the imprint they leave on Higgs

---

[6]When one $\mathbf{9}$ is much lighter than the other resonances one finds $m_t^0(h) \propto s_h^3 c_h$ and therefore $c_g^{(t)} \simeq 3 - 5\xi/2$. Similarly, the $ht\bar{t}$ coupling is equal to 3 times its SM value in the limit $\xi \to 0$. Thus we do not regard this possibility as viable.

[7]We expect the typical value of $\Delta_g^{(t)}$ to increase with the dimension of the $SO(5)$ representation. Therefore, for large enough representations negative values of $c_g^{(t)}$ might be possible.

rates still carries some information about UV physics. In this 'split' version of the composite Higgs setup, the Higgs couplings would be the primary source of information about the strong sector.

It is important to observe that when the light generations are included in the theory, the presence of multiple $SO(4)$ invariants in the LR sector gives rise to Higgs-mediated FCNC at tree level [119, 121]. These flavor-changing Higgs couplings are suppressed only by ξ, which is generically not enough to comply with bounds from flavor physics, such as Kaon mixing. This issue is relaxed if the underlying flavour structure realizes Minimal Flavor Violation (MFV) [113]. This would imply in particular a sizable degree of compositeness for one of the chiralities (either left or right) of all SM fermions, making the contribution of the partners of light quarks to the hgg and $h\gamma\gamma$ couplings potentially sizable [118].

3.3 An explicit construction: MCHM$_{14}$

In this section we describe in detail one explicit model where the Higgs couplings to gluons and photons can take a continuum of values depending on the spectrum of resonances, as in Eq. (3.17). As we discussed, this happens when the top mass arises from at least two independent $SO(4)$ invariants. Here we focus on the realization of the MCHM where both q_L and t_R are embedded into a **14** with X charge equal to $2/3$:

$$
\mathcal{Q}_L = \frac{1}{2}\begin{pmatrix} & & & & ib_L \\ & & & & b_L \\ & & & & it_L \\ & & & & -t_L \\ ib_L & b_L & it_L & -t_L & \end{pmatrix},
$$
$$
\mathcal{Q}_R = \frac{1}{2\sqrt{5}} t_R \operatorname{diag}\left(-1,-1,-1,-1,4\right). \tag{3.22}
$$

We recall that $\mathbf{14} = \mathbf{9} \oplus \mathbf{4} \oplus \mathbf{1}$ under $SO(4)$. Including for simplicity only one copy of each composite multiplet $\Psi_{9,4,1}$, the Lagrangian for the top sector can be written in the form

$$
\begin{aligned}
\mathcal{L}_t =\ & i\bar{q}_L \slashed{D} q_L + i\bar{t}_R \slashed{D} t_R + i\overline{\Psi}_1 \slashed{D}\Psi_1 \\
& + i\overline{\Psi}_4(\slashed{D} + i\slashed{e})\Psi_4 + i\mathrm{Tr}[\overline{\Psi}_9(\slashed{D}\Psi_9 + i[\slashed{e},\Psi_9])] \\
& - M_1\,\overline{\Psi}_1\Psi_1 - M_4\,\overline{\Psi}_4\Psi_4 - M_9\mathrm{Tr}[\overline{\Psi}_9\Psi_9] \\
& + \Big(F_9^L\mathrm{Tr}[(U^T\overline{\mathcal{Q}}_L U)\Psi_{9R}] + F_9^R\mathrm{Tr}[\overline{\Psi}_{9L}(U^T\mathcal{Q}_R U)] \\
& + \sqrt{2}F_4^L(U^T\overline{\mathcal{Q}}_L U)_{5i}(\Psi_{4R})_i + \sqrt{2}F_4^R(\overline{\Psi}_{4L})_i(U^T\mathcal{Q}_R U)_{i5} \\
& + \frac{\sqrt{5}}{2}F_1^L(U^T\overline{\mathcal{Q}}_L U)_{55}\,\Psi_{1R} + \frac{\sqrt{5}}{2}F_1^R\,\overline{\Psi}_{1L}\,(U^T\mathcal{Q}_R U)_{55} \\
& + \mathrm{h.c.}\Big),
\end{aligned} \tag{3.23}
$$

where $D^\mu \Psi_r \equiv (\partial^\mu - ig'XB^\mu - ig_sG^\mu)\Psi_r$. Notice that we adopted here a different normalization of the mixing terms with respect to Eq. (3.3). In Eq. (3.23) we have neglected derivative interactions:[8] these do not contribute to the potential nor affect the Higgs couplings (as discussed in the previous section), as long as all the parameters of the Lagrangian are real. In what follows we take the composite masses $M_{1,4,9}$ and linear mixings $F_r^{L,R}$ real.

Integrating out the heavy fermions in the Lagrangian (3.23), one obtains

$$
\begin{aligned}
\mathcal{L}_{\text{eff}}^t &= \bar{b}_L \not{p}\, \Pi_{b_L}(p)b_L + \bar{t}_L \not{p}\, \Pi_{t_L}(p)t_L + \bar{t}_R \not{p}\, \Pi_{t_R}(p)t_R \\
&\quad + \bar{t}_L t_R\, \Pi_{t_L t_R}(p) + \text{h.c.} ,
\end{aligned}
\tag{3.24}
$$

where the momentum-dependent form factors are

$$
\begin{aligned}
\Pi_{b_L} &= \Pi_0^{b_L} + \frac{1}{2}c_h^2\Pi_2^{b_L} , \\
\Pi_{t_L} &= \Pi_0^{t_L} + \frac{1}{4}(1 + c_h^2)\Pi_2^{t_L} + s_h^2 c_h^2 \Pi_4^{t_L} , \\
\Pi_{t_R} &= \Pi_0^{t_R} + \left(\frac{4}{5} - \frac{3}{4}s_h^2\right)\Pi_2^{t_R} + \frac{1}{20}\left(4 - 5s_h^2\right)^2 \Pi_4^{t_R} , \\
\Pi_{t_L t_R} &= \frac{3}{4\sqrt{5}}M_1 s_h c_h + \frac{1}{2\sqrt{5}}M_2 s_h c_h \left(4 - 5s_h^2\right) ,
\end{aligned}
\tag{3.25}
$$

with $s_h = \sin h/f$, $c_h = \cos h/f$ and

$$
\begin{aligned}
\Pi_0^{b_L,t_L,t_R} &= 1 + \frac{|F_9^{L,R}|^2}{p^2 + M_9^2} , \\
\Pi_2^{b_L,t_L,t_R} &= 2\frac{|F_4^{L,R}|^2}{p^2 + M_4^2} - 2\frac{|F_9^{L,R}|^2}{p^2 + M_9^2} , \\
\Pi_4^{t_{L,R}} &= \frac{5}{4}\frac{|F_1^{L,R}|^2}{p^2 + M_1^2} - 2\frac{|F_4^{L,R}|^2}{p^2 + M_4^2} + \frac{3}{4}\frac{|F_9^{L,R}|^2}{p^2 + M_9^2} , \\
M_1 &= 2\left(\frac{F_4^{L*}F_4^R M_4}{p^2 + M_4^2} - \frac{F_9^{L*}F_9^R M_9}{p^2 + M_9^2}\right) , \\
M_2 &= \left(\frac{5F_1^{L*}F_1^R M_1}{4(p^2 + M_1^2)} - \frac{2F_4^{L*}F_4^R M_4}{p^2 + M_4^2} + \frac{3F_9^{L*}F_9^R M_9}{4(p^2 + M_9^2)}\right) .
\end{aligned}
\tag{3.26}
$$

Integrating the path integral corresponding to the effective Lagrangian (3.24) over the fermionic degrees of freedom, we can write the effective Coleman-Weinberg potential as

$$
V_f(h) = -2N_c \int \frac{d^4p}{(2\pi)^4}\left[\log \Pi_{b_L} + \log\left(p^2\Pi_{t_L}\Pi_{t_R} + |\Pi_{t_L t_R}|^2\right)\right],
\tag{3.27}
$$

where p is the Euclidean momentum and $N_c = 3$ is the number of colors.

---

[8]Derivative interactions can have a strong impact on the collider phenomenology of top partners [122, 123] as well as on EWPT [124].

It is often convenient to expand the Higgs potential $V_f(h)$ in powers of $\epsilon \sim F/M_\Psi$, where F is a generic dimensionful linear mixing and M_Ψ is some linear combination of the masses of the resonances. This expansion, however, breaks down for large compositeness, $\epsilon \sim 1$, which might be relevant for the top quark. Thus a more robust choice is to expand the potential in powers of s_h^2. Upon EWSB one has $s_{\langle h \rangle}^2 = \xi$ and since $\xi \ll 1$ is required by EWPT, the expansion remains reliable even for $\epsilon \sim 1$. This expansion leads to

$$V_f(h) \simeq a s_h^2 + b s_h^4 \,. \tag{3.28}$$

From the potential of Eq. (3.28) we extract the values of the Higgs mass and VEV

$$\frac{v^2}{f^2} = -\frac{a}{2b} \,, \qquad m_h^2 = \left(\frac{\partial^2 V}{\partial h^2} \right)_{\langle h \rangle} = \frac{8b}{f^2} \xi (1 - \xi) \,. \tag{3.29}$$

It is important to note that the Higgs potential is quadratically divergent, unless the form-factors in Eq. (3.3) fall off sufficiently fast at large Euclidean momenta. In what follows we propose two simple constructions where this is the case and the degree of divergence of the potential is reduced.

3.3.1 Two-Site Model

One possibility to increase the calculability of the potential is to consider a two-site construction [125] (see also Ref. [126]). There, an unbroken $SO(5)$ global symmetry forces the relations $F_1^L = F_9^L = -F_4^L \equiv F_L$ and $F_1^R = F_9^R = -F_4^R \equiv -F_R$, and the quadratic divergences cancel. In this limit, the elementary/composite mixing terms in Eq. (3.23) can be written as

$$- F_L \mathrm{Tr}[\overline{\mathcal{Q}}_L U^T \Psi_R U] - F_R \mathrm{Tr}[\overline{\Psi}_L U \mathcal{Q}_R U^T] + \text{h.c.}, \tag{3.30}$$

where Ψ is a complete $\mathbf{14}_{2/3}$ of composite fermions, see Eq. (3.50). In the two-site construction, both a and b are *logarithmically* divergent. We recall that we are expanding the potential in powers of s_h^2.[9] One more layer of resonances, corresponding to a three-site model, would be necessary to make the potential finite and therefore fully calculable. Instead, for illustrative purposes we regulate the potential by a cut-off Λ. This simple procedure allows us to estimate the value of the parameters in the potential and make qualitative predictions on the Higgs couplings and the corresponding spectrum of the resonances. The cut-off can be seen as roughly representing the mass scale of the third site (*i.e.* of the second layer of resonances), but it is important to keep in mind that in our approach the logarithmic divergence also encodes finite terms, which can only be computed in a complete setup. For example, in a 5-dimensional realization of the model we can expect $\Lambda \sim M_{KK}^{(2)} \sim 2 M_{KK}^{(1)}$, where the KK modes are numbered with $1, 2, \dots$. Since $M_{KK}^{(1)}$ is constrained from the S parameter to be heavier than $\frac{2}{3}$ TeV (the precise bound depending on the value of the T parameter), we expect the cut-off scale Λ to lie roughly between 5 and 10 TeV.

---

[9]Notice that within this expansion one contribution to b in Eq. (3.28) is infrared divergent. We regulate this divergence with the top mass.

In order to perform a numerical study of the Higgs potential we fix $f = 800$ GeV, $m_t (\mu = 1 \text{ TeV}) = 152$ GeV and $v = 246$ GeV and scan over the region of parameters[10]

$$
\begin{aligned}
M_1, \ M_4 &\in & [-8, 8] \text{ TeV}\,, \\
M_9 &\in & [0, 8] \text{ TeV}\,, \\
\Lambda &\in & [\max(|M_1|, |M_4|, M_9), 10] \text{ TeV}\,, \\
F_L &\in & [0.1, 6] f\,.
\end{aligned}
\tag{3.31}
$$

Notice that we do not scan over F_R, which is determined by the requirement that m_t takes its experimental value. We require

$$
\begin{aligned}
\xi &\in & [0.95, 1.05] \ v^2/f^2\,, \\
m_h &< & 160 \text{ GeV}\,, \\
\Lambda &> & \max(M_{\tilde{T}}, M_Q, M_\psi)\,, \\
\min(M_{\tilde{T}}, M_X, M_\psi) &> & 500 \text{ GeV}\,.
\end{aligned}
\tag{3.32}
$$

The broad range of m_h that we consider is motivated by the need of a sufficient statistics, but we expect that restricting the scan close to the measured value $m_h \simeq 125$ GeV would not qualitatively change our results. The masses that appear in Eq. (3.32) are given by

$$
\begin{aligned}
M_{\tilde{T}} = \sqrt{M_1^2 + F_R^2}\,, \quad M_\psi = |M_9|\,, \\
M_X = |M_4|\,, \quad M_Q = \sqrt{M_4^2 + F_L^2}\,.
\end{aligned}
\tag{3.33}
$$

Neglecting EWSB effects, $M_{\tilde{T}}$ is the physical mass of the **1**, whereas M_ψ is the mass of the degenerate **9**, which contains ψ, an $SU(2)_L$ triplet with $Y = 5/3$ whose top component $\psi_{8/3}$ has electric charge 8/3 (see Table 3.2). On the other hand, the **4** is split into two $SU(2)_L$ doublets: X with $Y = 7/6$ and mass M_X, containing in particular $X_{5/3}$, a state with electric charge equal to $5/3$, and Q with $Y = 1/6$, which mixes with the elementary q_L and thus has mass M_Q. As a preliminary estimate of the bounds from direct searches for vector-like quarks at the LHC, in our scan we require that all resonances are heavier than 500 GeV, see the last line of Eq. (3.32). The actual LHC constraints obtained from 8 TeV data are however stronger: the mass of the X doublet is bounded to $M_X > 770$ GeV by a dedicated CMS search for the $X_{5/3}$ [99], whereas a CMS search for the singlet $\tilde{T}$ gives the bound $M_{\tilde{T}} \gtrsim 700$ GeV [100]. The constraint on the $\psi_{8/3}$ and thus on the **9** is even stronger, $M_\psi > 1$ TeV [98, 123].

The spectrum of fermionic resonances as obtained from the scan is shown in Fig. 3.1, together with the most up-to-date LHC constraints. The figure shows the values of (M_X, M_ψ) for the points that satisfy all the requirements in Eq. (3.32), with a color code dependent on the mass of the singlet. The preferred spectrum is $M_X \sim M_\psi < M_{\tilde{T}}$, corresponding to the red points. Notice that in most of the viable parameter space the splitting between M_X and M_ψ

---

[10]Notice that we assume $M_9 > 0$. Provided M_1, M_4 can have both signs, the sign of M_9 can always be fixed without loss of generality.
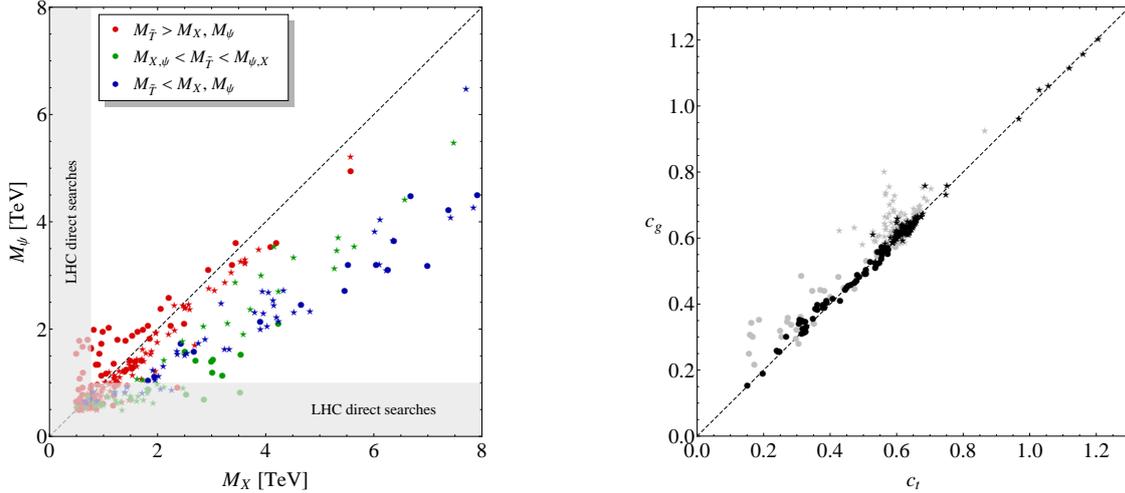
Figure 3.1: *Left panel:* distribution of the physical masses (neglecting EWSB corrections) of the X doublet and of the degenerate **9**. The current bounds from LHC direct searches are also displayed (there are no points ruled out only by the bound on the singlet $\tilde{T}$). The coloring of the points depends on the physical mass of the singlet. The points marked by a star are the ones for which the Higgs couplings c_g and c_γ are within the 95% CL region of the fit to Higgs data, see Fig. 3.3. *Right panel:* Higgs coupling to gluons c_g versus the Higgs coupling to the top quark c_t. Light gray points are excluded by LHC direct searches, while black points are currently allowed. The dashed line corresponds to the relation $c_g = c_t$, which holds for small mixings, $\epsilon^2 \ll 1$. The meaning of the star shape for the points is the same as in the left panel.

is rather mild. This can be traced back to the expression the form factors in Eq. (3.3) take in the two-site model: recalling that $M_{X,\psi} = |M_{4,9}|$, we see that for $M_X = M_\psi$ the form factors $\Pi_2^{b_L, t_L, t_R}$ exactly vanish. Thus for $M_X \sim M_\psi$ the overall size of the potential is suppressed, and a light Higgs is more likely obtained. In fact, in MCHM$_{14}$ two distinct invariants appear in the $O(\epsilon^2)$ potential. This implies that only a tuning of order ξ is necessary to obtain a realistic EWSB, as opposed for example to MCHM$_5$, where the tuning scales like $\epsilon^2 \xi$. On the other hand, the potential in MCHM$_{14}$ is generically too large and yields a too heavy Higgs, unless some additional suppression mechanism is in play [96–98]. From our study of the two-site realization, we identify three main mechanisms that help in reducing the size of the Higgs mass. The first one is the already mentioned relation $M_X \sim M_\psi$. The second can be read from the expression of the Higgs mass at $\mathcal{O}(\epsilon^2)$:

$$
\begin{aligned}
m_h^2 &\simeq \frac{2N_c}{\pi^2 f^2} \xi \int dp\, p^3 \left(\Pi_4^{t_L} - \frac{5}{4}\Pi_4^{t_R} \right) \\
&\simeq \frac{2N_c}{\pi^2 f^2} \xi \left(|F_L|^2 - \frac{5}{4}|F_R|^2 \right) M_\Psi^2 \,,
\end{aligned}
\tag{3.34}
$$

where M_Ψ parameterizes the overall scale of the resonances. Thus for $|F_L| \sim \sqrt{5}\,|F_R|/2$ the leading contribution to the Higgs mass is suppressed. This relation is mildly satisfied in most

of the viable parameter space. The last possibility is, of course, to lower the overall scale of the resonances M_Ψ. A combination of all three mechanisms is in play in our scan. The first two lead to extra tuning in addition to the one required for the Higgs VEV. This extra tuning cannot be quantified from the scan, since we restrict ourselves to small regions around the realistic Higgs VEV and mass. Nevertheless, as shown in Fig. 3.2, the relations $M_X \sim M_\psi$ and $|F_L| \sim \sqrt{5}\,|F_R|/2$ are satisfied in a very mild sense, therefore we do not expect the consequent increase of the tuning to be dramatic.
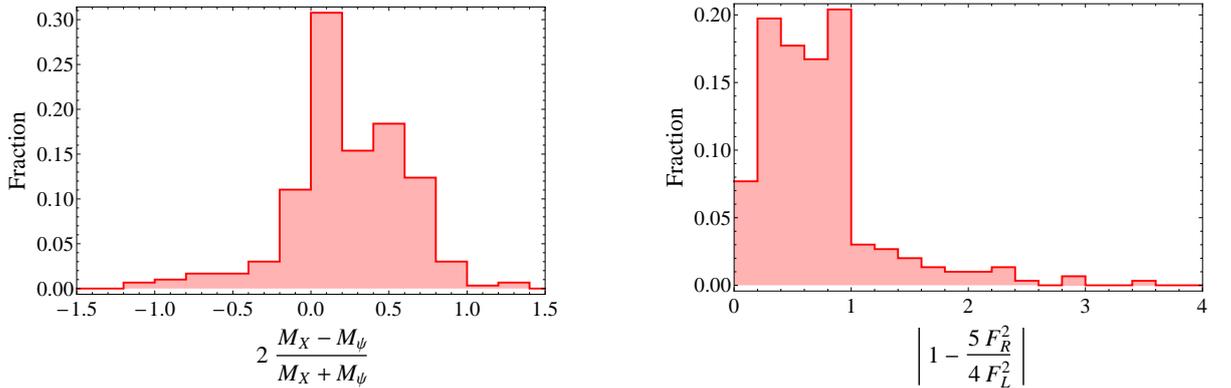

Figure 3.2: Distributions quantifying the tuning between $M_X = |M_4|$ and $M_\psi = |M_9|$ (left panel), and between $|F_L|$ and $\sqrt{5}|F_R|/2$ (right panel), as obtained from the numerical scan.

The right panel of Fig. 3.1 shows the correlation between the Higgs coupling to gluons c_g and the Higgs coupling to the top quark c_t. The former is computed from Eq. (3.8) and reads at first order in ξ

$$c_g = 1 - \Delta_g^{(t)}\,\xi + \left(\frac{M_4^2}{M_9^2} - 1\right)\sin^2\phi_L\,\xi\,, \tag{3.35}$$

where

$$\Delta_g^{(t)} = \frac{11}{2}\,\frac{1 - \frac{8}{11}\frac{M_4}{M_1} - \frac{3}{11}\frac{M_4}{M_9}}{1 - \frac{M_4}{M_1}} \tag{3.36}$$

encodes the contribution of the top sector, whereas the last term is the contribution of the heavy b-like states. The angle $\phi_L \equiv \arctan(F_L/M_4)$ measures the degree of compositeness of q_L. Notice that $\Delta_g^{(t)}$ only depends on ratios of the masses of the composite multiplets. The coupling of the Higgs to the top is obtained instead from Eq. (3.14) with the identifications

$$m_t^0 = -\Pi_{t_L t_R}(p = 0)\,, \quad Z_{t_{L,R}} = \Pi_{t_{L,R}}(p = 0)\,. \tag{3.37}$$

As discussed in the general analysis of Sec. 3.2, the hgg and $ht\bar{t}$ couplings are tightly correlated, and significant deviations from the equality $c_g = c_t$ can occur only for large values of the mixing parameters ϵ. This is clearly visible in the right panel of Fig. 3.1: sizeable deviations from $c_g = c_t$ take place only for points that have already been excluded by direct searches at the LHC, displayed in light gray. For these points at least one of the masses $|M_r|$ is small, which typically implies that one of the mixings is large. For example, a small $|M_4|$ leads to

large compositeness of t_L. In addition, we find that the corrections due to the wavefunction renormalization of the top are almost always negative, yielding $c_t \lesssim c_g$.

In Fig. 3.3 we compare the Higgs couplings (c_γ, c_g) obtained from the scan (considering only points not excluded by LHC direct searches) to the region preferred by a fit to current Higgs data. If only the contribution of fermions with electric charge $Q_t = 2/3$ is considered, the points lie on the line

$$c_g = \left(1 - \frac{7A_V(\tau_W)}{4Q_t^2}\right) c_\gamma + \frac{7A_V(\tau_W)}{4Q_t^2} c_W, \tag{3.38}$$

where $\tau_W = m_h^2/(4m_W^2)$ and $A_V(\tau_W) \simeq 1.19$ parameterizes the W loop [104], while $c_W = \sqrt{1-\xi}$ is the rescaling of the hWW coupling in the MCHM. The loops of heavy b-like fermions generate only small deviations from this expectation.[11] Although a continuum of couplings is possible, Fig. 3.3 shows that there is a clear preference for $c_g \ll 1$, and as a consequence $c_\gamma > 1$. Because we did not include the b_R in our simple model, we cannot describe the $h b\bar{b}$ coupling, which plays an important role in the fit to data. Taking a model independent approach we remain agnostic on the sector that gives mass to the bottom quark, ignore the b contribution to the hgg and $h\gamma\gamma$ couplings and marginalize over the $h b\bar{b}$ coupling in the fit to Higgs data, see Appendix 3.6 for details.

3.3.2 Weinberg Sum Rules

Another possibility to obtain a finite Higgs potential, is to impose high-energy conditions on the form-factors $\Pi_2^{t_{L,R}}$ and $\Pi_4^{t_{L,R}}$ of Eq. (3.3),

$$\begin{aligned}
\lim_{p^2 \to \infty} \Pi_{2,4}^{t_{L,R}}(p) &= 0, \\
\lim_{p^2 \to \infty} p^2 \Pi_{2,4}^{t_{L,R}}(p) &= 0, \\
\lim_{p^2 \to \infty} p^4 \Pi_{2,4}^{t_{L,R}}(p) &= 0,
\end{aligned} \tag{3.39}$$

such that they fall-off rapidly at high momenta and the potential Eq. (3.28) is convergent [95, 96]. The QCD analog of the conditions (3.39) are known as Weinberg Sum Rules (WSR) [127]. Notice that in this approach we are expanding the potential in powers of ϵ^2. Considering three resonance multiplets, as in Eq. (3.23), the conditions (3.39) cannot be satisfied simultaneously, but we can at least require that the Higgs mass be finite [96]. This can be done by imposing the conditions (3.39) only for $\Pi_4^{t_{L,R}}$ which, as shown in Eq. (3.34), control the Higgs mass. Then, the WSR translate into relations between the couplings $F_{L,R}^{1,4,9}$ and the model is completely determined by the resonance masses and one combination of the couplings, which we chose to be F_L^1 (another combination, F_R^1 can be fixed by the top mass, $m_t \sim \langle s_h c_h \rangle F_L^1 F_R^1 / M_\Psi$).

The general arguments given in section 3.2 of course apply and in particular the coupling

---

[11]Subleading corrections also arise due to the slightly different value of ξ for each point.
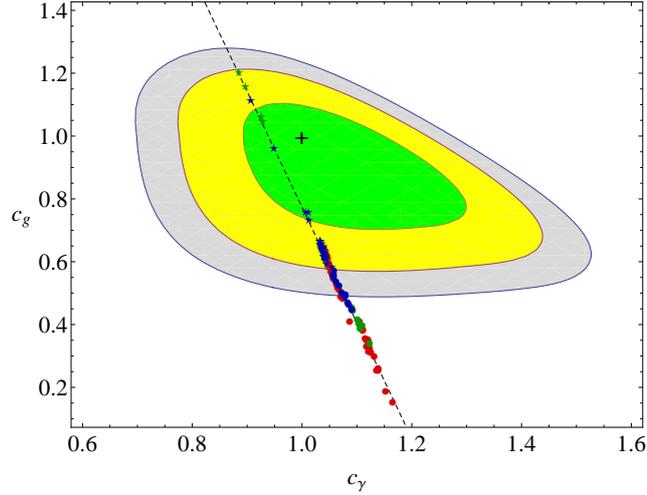
Figure 3.3: Distribution of the couplings (c_γ, c_g) as obtained from the scan, compared to the region preferred by a fit to current Higgs data. Only points not excluded by LHC searches for heavy vector-like quarks are displayed. The dashed line corresponds to the prediction of Eq. (3.38). The green, yellow and gray regions correspond to the $68.27, 95$ and 99% CL, respectively. As in Fig. 3.1, the points marked by a star are those that fall within the 95% CL region of the fit. Details on the fit can be found in Appendix 3.6.

to gluons is independent of the mixing parameter F_L^1. We find

$$c_g^{(t)} = 1 - \left[4 - \frac{M_1^3}{M_9^3} \frac{40 M_4 \left(1 - \frac{M_4^2}{M_1^2}\right) - 15 M_9 \left(1 - \frac{M_9^2}{M_1^2}\right)}{16 M_4 \left(1 - \frac{M_4^2}{M_9^2}\right) - 10 M_1 \left(1 - \frac{M_1^2}{M_9^2}\right)} \right] \xi \,, \tag{3.40}$$

which reproduces the limits discussed below Eq. (3.21). Moreover, when any two resonances become degenerate, this expression simplifies to $c_g^{(t)} = 1 - 3\xi/2$, so that $c_g^{(t)} < 1$ holds in most of the parameter space. The coupling to tops c_t differs from c_g by terms proportional to $\epsilon_{L,R}^2 \equiv (F_{L,R}^1/M_\Psi)^2$ which can in principle become sizable. Indeed, while the product $F_L^1 F_R^1$ is fixed by m_t, the Higgs mass is sensitive to another combination of the mixings,[12]

$$m_h^2 \simeq \frac{5 N_c}{4\pi^2 f^2} \xi \left(|F_L^1|^2 - \frac{5}{4} |F_R^1|^2 \right) \times \left[M_1^2 \log\left(\frac{M_1^2}{M_9^2}\right) + \frac{M_4^2 (M_9^2 - M_1^2)}{M_9^2 - M_4^2} \log\left(\frac{M_9^2}{M_4^2}\right) \right] \,.$$

This expression highlights how the Higgs mass can become small in this model; similarly to what discussed for the two-site construction, m_h can be small if either *i)* the overall scale of the resonances M_Ψ is small or *ii)* there is a tuning $|F_L^1| \sim \sqrt{5}\, |F_R^1|/2$ or *iii)* a tuning between the masses $M_1 \sim M_4$ or $M_1 \sim M_9$. In the tuned cases *ii)* and *iii)* it is easy to see that the Higgs mass does not constrain the size of the $O(\epsilon_{L,R}^2)$ corrections to c_t, and we can have a situation where c_g and c_t differ sizably. In the more natural case *i)*, on the other hand, the $O(\epsilon_{L,R}^2)$ corrections are typically small and $c_g \approx c_t$ holds.

---

[12]Gluon partner contributions can modify this expression [128].

3.4 Conclusions

In composite Higgs models, the paradigm of partial compositeness implies that a number of colored fermionic resonances couple strongly to the Higgs sector. Moreover, some of these resonances need to be relatively light to naturally reproduce the observed Higgs mass. Thus one naively expects that these states contribute sizably to the radiative hgg and $h\gamma\gamma$ couplings. However, it is well known that in some minimal models this is not the case and light fermionic resonances do not contribute to the hgg and $h\gamma\gamma$ couplings, due to an exact cancellation between corrections to the $ht\bar{t}$ coupling and loops of resonances. Indeed the hgg coupling is the leading term of the $ht\bar{t}$ one in an $\epsilon^2 \ll 1$ expansion.

In this paper we have shown that these are general features of the MCHM, following only from the Goldstone symmetry and from partial compositeness. Furthermore we found that under the assumption of CP invariance the radiative Higgs couplings are insensitive to derivative interactions of the Higgs with resonances.[13] Of particular interest for this generalization, are models where the top mass arises from more than one $SO(4)$ invariant. Such models, although disfavoured by the smallness of the Higgs mass, are particularly well-motivated by naturalness arguments.[14] In this case, naively, the presence of multiple operators can spoil the delicate cancellation that takes place in the simplest models. However, we found that this is not the case and the loop-induced Higgs couplings are insensitive to light fermionic resonances.

In the simplest models the hgg coupling is reduced with respect to the SM value by a simple trigonometric factor (*e.g.* $\cos(2\langle h\rangle/f)/\cos(\langle h\rangle/f)$ in the MCHM$_{5,10}$). On the contrary, in models with two or more invariants this coupling depends on the masses of the resonances and on their mixings with elementary fermions. In particular, it can become larger than the SM value and, for very special combinations of the parameters, it can differ from the SM value also in limit $v/f \to 0$. Furthermore the coupling is insensitive to the overall scale of the resonances and only depends on ratios of their masses. Therefore one can imagine a situation where all the resonances are rather heavy and thus no signals show up in direct searches, but deviations are observed in the precision measurement of the Higgs couplings.

As an example, we have studied in detail a prototype model where both q_L and t_R are embedded in a **14** of $SO(5)$. We have built a two-site realization that enables the dominant part of the potential to be estimated, and used it to find a relation between the Higgs mass and VEV, and the masses of the lightest resonances of the strong sector. In this simplified model, we have verified that $O(\epsilon)$ effects are small in the region of phenomenological interest. This confirms the tight connection between the $ht\bar{t}$ and the hgg couplings. Moreover we find that these couplings are typically suppressed, leading also to a slight increase of the $h\gamma\gamma$ coupling.

---

[13]In models based on larger cosets the results of this paper would be modified, due to the presence of additional scalars that can mix with the Higgs [119, 129, 130].

[14]More precisely, naturalness arguments prefer models in which more than one Left-Left (LL) or Right-Right (RR) invariant can be built, independently of the number of LR invariants. Nevertheless, the simplest models with more than one LR invariant, also feature more than one LL/RR invariants.

Similar qualitative conclusions have also been obtained by applying the WSR approach. The future direct measurement of the $ht\bar{t}$ coupling will provide a further test of these results.

3.5 Appendix: Notations

3.5.1 Sigma model

The generators of the fundamental representation of $SO(5)$ read

$$
T_{IJ}^{a\,L,R} = -\frac{i}{2}\left[\frac{1}{2}\epsilon^{abc}(\delta_I^b\delta_J^c - \delta_J^b\delta_I^c) \pm (\delta_I^a\delta_J^4 - \delta_J^a\delta_I^4)\right],
$$

$$
T_{IJ}^i = -\frac{i}{\sqrt{2}}(\delta_I^i\delta_J^5 - \delta_J^i\delta_I^5), \tag{3.41}
$$

where $I, J = 1, \ldots, 5$, $i = 1, \ldots, 4$, $a = 1, 2, 3$. $T^{a\,L,R}$ are the generators of the unbroken $SO(4) \sim SU(2)_L \times SU(2)_R$, whereas T^i are the generators of $SO(5)/SO(4)$. We will also use the equivalent notation T^a, $a = 1, \ldots, 6$ for the unbroken generators. The Goldstone bosons appear through the matrix $U(\Pi)$ defined by

$$
U(\Pi) = \exp\left(i\frac{\sqrt{2}\Pi^i T^i}{f}\right). \tag{3.42}
$$

Notice that $U(\Pi)$ is an orthogonal matrix transforming as

$$
U(\Pi) \to g\, U(\Pi)\, \hat{h}(g,\Pi)^{-1}, \qquad g \in SO(5),\ \hat{h} \in SO(4). \tag{3.43}
$$

The quantities d_μ and e_μ are defined as the projections of the object $-U^T(A_\mu + i\partial_\mu)U$ onto the broken and unbroken generators respectively, such that d_μ transforms linearly as a 4-plet, while e_μ shifts under the unbroken $SO(4)$. At lowest order in the chiral expansion, we have

$$
d_\mu^i = \frac{\sqrt{2}}{f}\nabla_\mu\Pi^i + \ldots, \quad e_\mu^a = -gA_\mu^a + \ldots \tag{3.44}
$$

with $\nabla_\mu\Pi^i = \partial_\mu\Pi^i - iA_\mu^a(T^a)^i{}_j\,\Pi^j$. A_μ^a contains the vector fields associated to the gauged generators T_L^a and T_R^3 in the unbroken $SO(4)$. See for example Ref. [122] for the complete expressions. At the two-derivative level the Goldstone Lagrangian reads

$$
\mathcal{L} = \frac{f^2}{4}d_\mu^i d^{i\mu}. \tag{3.45}
$$

In the unitary gauge where $\Pi^1 = \Pi^2 = \Pi^3 = 0$ and $\Pi^4 = h$, we have simply

$$
U = \left(\begin{array}{c|cc} \mathbb{1}_3 & & \\ \hline & c_h & s_h \\ & -s_h & c_h \end{array}\right), \tag{3.46}
$$

where we defined $s_h \equiv \sin(h/f)$ and $c_h \equiv \cos(h/f)$. The two-derivative Lagrangian (3.45) can now be written as

$$\mathcal{L} = \frac{1}{2}\partial_\mu h \partial^\mu h + \frac{g^2 f^2}{4} s_h^2 \left[W_\mu^+ W^{-\,\mu} + \frac{1}{2\cos^2\theta_w} Z_\mu Z^\mu \right], \qquad (3.47)$$

which fixes, once we identify the W mass,

$$\xi \equiv \frac{v^2}{f^2} = \sin^2 \frac{\langle h \rangle}{f} . \qquad (3.48)$$

3.5.2 Fermion representations

$\mathbf{1}_{2/3}$	T_3^L	T_3^R	Y	Q
$\tilde{T}$	0	0	$\frac{2}{3}$	$\frac{2}{3}$

$\mathbf{4}_{2/3}$	T_3^L	T_3^R	Y	Q
$\color{red}{T}$	$+\frac{1}{2}$	$-\frac{1}{2}$	$\frac{1}{6}$	$\frac{2}{3}$
$\color{red}{B}$	$-\frac{1}{2}$	$-\frac{1}{2}$	$\frac{1}{6}$	$-\frac{1}{3}$
$X_{5/3}$	$+\frac{1}{2}$	$+\frac{1}{2}$	$\frac{7}{6}$	$\frac{5}{3}$
$X_{2/3}$	$-\frac{1}{2}$	$+\frac{1}{2}$	$\frac{7}{6}$	$\frac{2}{3}$

$\mathbf{6}_{2/3}$	T_3^L	T_3^R	Y	Q
χ_1	$+1$	0	$\frac{2}{3}$	$\frac{5}{3}$
T_1	0	0	$\frac{2}{3}$	$\frac{2}{3}$
B_1	-1	0	$\frac{2}{3}$	$-\frac{1}{3}$
χ_2	0	$+1$	$\frac{5}{3}$	$\frac{5}{3}$
$\color{blue}{T_2}$	0	0	$\frac{2}{3}$	$\frac{2}{3}$
$\color{magenta}{B_2}$	0	-1	$-\frac{1}{3}$	$-\frac{1}{3}$

$\mathbf{9}_{2/3}$	T_3^L	T_3^R	Y	Q
$\psi_{8/3}$	$+1$	$+1$	$\frac{5}{3}$	$\frac{8}{3}$
χ_3	0	$+1$	$\frac{5}{3}$	$\frac{5}{3}$
T_3	-1	$+1$	$\frac{5}{3}$	$\frac{2}{3}$
χ_4	$+1$	0	$\frac{2}{3}$	$\frac{5}{3}$
T_4	0	0	$\frac{2}{3}$	$\frac{2}{3}$
B_3	-1	0	$\frac{2}{3}$	$-\frac{1}{3}$
T_5	$+1$	-1	$-\frac{1}{3}$	$\frac{2}{3}$
B_4	0	-1	$-\frac{1}{3}$	$-\frac{1}{3}$
$\psi_{-4/3}$	-1	-1	$-\frac{1}{3}$	$-\frac{4}{3}$

Table 3.2: Electroweak quantum numbers of the fermion fields in the $\mathbf{1}_{2/3}$, $\mathbf{4}_{2/3}$, $\mathbf{6}_{2/3}$, $\mathbf{9}_{2/3}$ representations of $SO(4) \times U(1)_X$. In red, blue and fuchsia we indicate the states with the SM quantum numbers of the q_L, t_R and b_R.

We report here for convenience the decomposition of the $SO(5)$ representations used in this paper in terms of $SO(4)$ multiplets. We have

$$\Psi_{\mathbf{5}} = \begin{pmatrix} \Psi_4 \\ \hline \Psi_1 \end{pmatrix}, \quad \Psi_{\mathbf{10}} = \left(\begin{array}{c|c} \Psi_6 & \Psi_4/\sqrt{2} \\ \hline -\Psi_4^T/\sqrt{2} & 0 \end{array} \right) \tag{3.49}$$

and

$$\Psi_{\mathbf{14}} = \left(\begin{array}{c|c} \Psi_9 - \Psi_1 \mathbb{I}_4/(2\sqrt{5}) & \Psi_4/\sqrt{2} \\ \hline -\Psi_4^T/\sqrt{2} & 2\Psi_1/\sqrt{5} \end{array} \right), \tag{3.50}$$

where Ψ_r are $SO(4)$ multiplets. For the case $X = 2/3$, the singlet and 4-plet can be written as

$$\Psi_{1\frac{2}{3}} = \tilde{T}, \qquad \Psi_{4\frac{2}{3}} = \frac{1}{\sqrt{2}} \begin{pmatrix} iB - iX_{5/3} \\ B + X_{5/3} \\ iT - X_{2/3} \\ iX_{2/3} - T \end{pmatrix}, \tag{3.51}$$

while for the antisymmetric tensor we have

$$\Psi_{6\frac{2}{3}} = \frac{1}{2} \begin{pmatrix} 0 & \mathcal{T}_{12}^+ & i(\mathcal{B}_{12}^+ - \mathcal{X}_{12}^+) & \mathcal{B}_{12}^- + \mathcal{X}_{12}^- \\ & 0 & \mathcal{B}_{12}^+ + \mathcal{X}_{12}^+ & i(-\mathcal{B}_{12}^- + \mathcal{X}_{12}^-) \\ & & 0 & -i\mathcal{T}_{12}^- \\ & & & 0 \end{pmatrix}, \tag{3.52}$$

with $\mathcal{T}_{12}^\pm \equiv T_1 \pm T_2$, $\mathcal{B}_{12}^\pm \equiv (B_1 \pm B_2)/\sqrt{2}$ and $\chi_{12}^\pm \equiv (\chi_1 \pm \chi_2)/\sqrt{2}$, and for the symmetric traceless tensor

$$\Psi_{9\frac{2}{3}} = \frac{1}{2} \begin{pmatrix} \mathcal{P}^+ - T_4 & i\mathcal{P}_- & \mathcal{B}_{34}^+ + \mathcal{X}_{34}^+ & -i\mathcal{B}_{34}^- + i\mathcal{X}_{34}^- \\ & -\mathcal{P}^+ - T_4 & -i\mathcal{B}_{34}^+ + i\mathcal{X}_{34}^+ & -\mathcal{B}_{34}^- - \mathcal{X}_{34}^- \\ & & T_4 - \mathcal{T}_{35}^- & i\mathcal{T}_{35}^+ \\ & & & T_4 + \mathcal{T}_{35}^- \end{pmatrix}, \tag{3.53}$$

where $\mathcal{P}^\pm \equiv \psi_{8/3} \pm i\psi_{-4/3}$, $\mathcal{B}_{34}^\pm \equiv (B_3 \pm iB_4)/\sqrt{2}$, $\chi_{34}^\pm \equiv (\chi_4 \pm i\chi_3)/\sqrt{2}$ and $\mathcal{T}_{35}^\pm \equiv T_3 \pm T_5$. The decomposition of the $SO(4)$ multiplets in terms of fermions with definite electroweak quantum numbers is given in Table 3.2.

3.6   Appendix: Details of the experimental fit

The best option to compare these models with experiments, as we do in Fig. 3.3, is to present the data as extracted assuming modified couplings between the Higgs and the SM states.

In composite Higgs models the Higgs couplings to $V = W, Z$ are shifted by $\delta c_V \simeq -\xi/2$, which we fix in our analysis assuming $f = 800 \,\text{GeV}$, and hence $\xi \approx 0.1$. Higgs couplings to bottom quarks, on the other hand can vary considerably in general models (they can have a parametric form similar to $h\bar{t}t$ couplings, approximately corresponding to Eq. (3.19) or Eq. (3.21)) but typically are smaller than one (in units of the SM coupling). For this reason we parametrize our theoretical ignorance by marginalizing over the $h\bar{b}b$ coupling in the region $c_b \in [0.5, 1]$. Fig. 3.3 is then obtained by letting the effective hgg and $h\gamma\gamma$ couplings vary (the $h\bar{t}t$ coupling, independently from its contribution to hgg and $h\gamma\gamma$, is not yet measured with enough accuracy to change this picture considerably).

The statistical analysis is performed using the latest signal strenght data given by the Tevatron experiments and by ATLAS and CMS at Moriond 2013 and soon after; a summary of the signal strengths in the individual channels can be found in Refs. [103, 104]. The signal strengths are assumed to follow a Gaussian distribution and we fit the data by minimizing a χ^2 as described in detail in Chapter 2 of this thesis and in Ref. [1]. We sum statistical and theoretical errors in quadrature and neglect possible correlation effects, which we find to be a reasonable approximation.

Chapter 4

Higgs mass and couplings in SUSY

4.1 Motivation

The quest for SUSY has taken an unexpected turn with the Higgs discovery at 125 GeV [131]. Indeed, it is well known that the supersymmetric contribution to the Higgs mass is at most $(m_h^{tree})^2 \lesssim m_Z^2$, implying that a large portion of the Higgs mass $\Delta m_h^2 \gtrsim 86^2 \, \text{GeV}^2$ must originate from symmetry breaking effects. Within the MSSM, for large stop masses, top/stop loops provide this necessary contribution, but only at the expense of naturalness, as the large loop effects needed to increase the Higgs mass also destabilize the EW scale. Experiments are therefore telling us that, if SUSY exists, it is either tuned, or it doesn't fulfill Occam's principle and that more complicated models, with additional contributions to the Higgs quartic, have to be considered.

Still, a common feature of most SUSY models[1], is the Higgs sector, containing at least a particular version of a two Higgs doublets model (2HDM). Mixings in this extended Higgs sector, lead to modified tree-level couplings between the lightest CP-even Higgs and the SM gauge bosons and fermions, and provides a distinctive signature of SUSY, complementary to direct searches. While the latter remain the most favorable strategy for SUSY searches (in particular in the most natural SUSY realizations, where states associated with the stabilization of the electroweak (EW) scale are expected to be light), modified couplings could be the strongest evidence for SUSY in particular regions of parameter space, such as those with compressed spectra.

Interestingly, in 2HDMs, a correlation exists between the Higgs mass and its tree-level couplings to SM fields. Indeed, any contribution to the Higgs quartic potential, necessary in SUSY models to increase the Higgs mass from its tree-level value up to the observed value of approximately 125 GeV, also changes the relation between mass and hypercharge eigenstates and modifies the couplings of the lightest CP-even Higgs. In this article we investigate this correlation in detail, showing how different models that accommodate the observed Higgs

---

[1]An exception is the model of Ref. [132] where the Higgs is the neutrino superpartner and there are no extra Higgs doublets. Ref. [133] also proposes a model with one doublet only while in Refs. [134, 135] additional doublets have been studied.

mass also modify their Higgs couplings. We then confront these expectations with the most recent LHC data [138]- [142], which we use to extract limits on the parameter space of such theories (in particular on m_A and $\tan\beta$).

We first show, with a simple and intuitive analytical approximation, how Higgs mass and couplings are correlated in SUSY models (or 2HDMs in general) (section 4.2). Then we study, in turn, the MSSM with heavy stops (section 4.3), the MSSM with extra non-decoupling D-terms (section 4.4), and the F-term contributions of NMSSM-like models (section 4.5), where we also discuss a general class of models beyond the MSSM (BMSSM). In section 4.6 we comment on how these conclusions are modified in the presence of sizable loop-effects due to light SUSY partners and we leave for Appendix 4.8 the details related to our global fits and for Appendix 4.9 a summary of the formulas used in our plots.

4.2 The Higgs Mass/Couplings Connection

Supersymmetry requires the existence of two Higgs doublets, $H_{1,2}$ giving mass to leptons and down-type/up-type quarks. Limiting our discussion to the third family fermions, which have the strongest couplings to the Higgs sector, we consider

$$\mathcal{L} \supset -Y_b H_1 \bar{q} b - Y_t H_2 \bar{q} t - Y_\tau H_1 \bar{l} \tau . \tag{4.1}$$

Only a linear combination of H_1 and H_2 obtains a vacuum expectation value (vev) $v \equiv 174\,\text{GeV}$; its couplings to SM fermions and vectors equal those of a SM Higgs. Any quartic contribution to the scalar potential for H_1 and H_2 introduces, in general, a misalignment between this linear combination and the mass eigenstates: this misalignment is responsible for a modification in the Higgs couplings. The best way to see this is in the basis h, H, where only one state (h) has a vev. The angle β denotes the angle between these states and the neutral CP-even components of the gauge eigenstates H_1, H_2:

$$\begin{aligned}
h_1^0 &= \cos\beta h + \sin\beta H \\
h_2^0 &= \sin\beta h - \cos\beta H.
\end{aligned} \tag{4.2}$$

In this basis, the couplings Eq. (4.1) of h and H to fermions are,

$$-\cos\beta Y_b(h + \tan\beta H)\bar{b}b, \quad -\sin\beta Y_t(h - \cot\beta H)\bar{t}t, \tag{4.3}$$

where couplings to charged leptons have the same form as for down-type quarks. Now, consider a general contribution to the quartic of the Higgs potential written in terms of h, H,

$$\Delta V(H_1, H_2) = +\delta_\lambda h^4 + \delta h^3 H + \delta_2 h^2 H^2 + \delta_3 h H^3 + \delta_4 H^4, \tag{4.4}$$

where the δ's are given dimensionless couplings. The first term contributes to the lightest CP-even Higgs mass as

$$\Delta m_h^2 = 16\delta_\lambda v^2; \tag{4.5}$$

in order to account for the observed value $m_h^2 \approx 125\,\text{GeV}$,

$$\Delta m_h^2 = m_h^{obs\,2} - m_Z^2 (\cos 2\beta)^2 \gtrsim (86\,\text{GeV})^2 \tag{4.6}$$

is needed. Interestingly, the same physics that is responsible for δ_λ, also generates a mixing between h and H, via the term $\delta h^3 H$, that leads to a modification of the Higgs couplings, as illustrated in Fig. 4.1. We can quantify these modifications, in the limit where H is heavy,
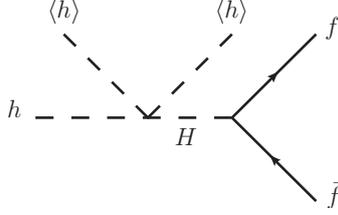

Figure 4.1: *The mixing between h and H, induced by the quartic interaction $\delta h^3 H$, modifies the couplings of h to the fermions w.r.t to its SM value.*

by integrating out the heaviest eigenstate from the relevant part of the Lagrangian

$$\mathcal{L} \supset -\delta h^3 H - \sum_{f=t,b,\tau} Y_f^H \bar{f} f H - \frac{m_H^2}{2} H^2, \tag{4.7}$$

where Y_f^H, the coupling of H to fermion $f = t, b, \tau$, can be read from Eq. (4.3). For large m_H we can solve the equations of motion of H, giving $H \approx \delta h^3 Y_f^H \bar{f} f / m_H^2$, and obtain the effective interaction

$$\mathcal{L}_{eff} \supset \delta \sum_{f=t,b,\tau} Y_f^H h \bar{f} f \frac{h^2}{m_H^2}. \tag{4.8}$$

Now, notice that the equations of motion for H imply a small vev $\langle H \rangle \approx 2\sqrt{2}\delta(v^3/m_H^2)$, so that the expression for the fermion mass is modified accordingly and we can write the coupling of the physical Higgs $\tilde{h} = h - \sqrt{2}\,v$, normalized with its SM value $y_f^{SM} = m_f/v$, as

$$c_f \equiv \frac{y_f}{m_f/v} \approx \frac{Y_f^h - 6Y_f^H \delta \frac{v^2}{m_H^2}}{Y_f^h - 2Y_f^H \delta \frac{v^2}{m_H^2}} \approx 1 - 4\delta \frac{Y_f^H}{Y_f^h} \frac{v^2}{m_H^2}. \tag{4.9}$$

Using Eq. (4.3) to read $Y_f^{h,H}$, we finally obtain

$$\begin{aligned} c_{b,\tau} &\approx 1 - 4\tan\beta\,\delta \frac{v^2}{m_H^2}, \\ c_t &\approx 1 + 4\cot\beta\,\delta \frac{v^2}{m_H^2}. \end{aligned} \tag{4.10}$$

This simple, yet important, expression summarizes the goal of this work: any new physics that is responsible for the large Higgs mass Eq. (4.5) also affects the Higgs couplings to fermions.

This approximate formula allows us to understand qualitatively how this connection works and predicts whether a given contribution to the Higgs mass results in an increase or decrease of the couplings to tops and bottoms/taus (similar methods have been used in Refs. [143–145] to study Higgs couplings modifications). Nevertheless, notice that in our plots we always use the exact expressions listed in Appendix 4.9, rather than Eq. (4.10).

Deviations in the Higgs couplings to vectors can be studied in a similar way, giving

$$c_V = 1 - \mathcal{O}\left(\delta^2 \frac{v^4}{m_H^4}\right) \tag{4.11}$$

which is generally suppressed w.r.t. deviations in the couplings to fermions (we have checked that in the region preferred by data this statement holds at better then the 2 % level and deviations in c_V can be ignored).

In principle, complete analyses of Higgs couplings in a SUSY context should take into account possible modifications of the tree-level couplings to up-type quarks, to down-type quarks (and leptons) and to vectors; at the loop level extra contributions from light SUSY partners to the couplings to gluons and photons could be present, and in total generality also the possibility of an invisible decay width should be considered (see Ref. [132] for a motivated scenario were the Higgs can decay invisibly in a SUSY context): a total of six parameters (see Refs. [146, 147] for a list of recent analyses of this type). Nevertheless, ignoring the last possibility, Eq. (4.11) tells us that in the simplest SUSY models, couplings to vectors are not expected to deviate much from the SM ones (this is not true when the Higgs sector is extended to include extra states in different $SU(2)_L$ representations that can mix with the Higgs, as we shall discuss in section 4.5.1). Furthermore, the null results of direct SUSY searches suggest that SUSY partners should have masses of a few hundreds GeV and that their loop contributions to the effective hgg and $h\gamma\gamma$ couplings might be small (we comment about this in section 4.6). For these reasons, in what follows, we orient our analysis mostly to the Higgs couplings to tops and to bottoms/taus and compare theoretical expectations with data through an intuitive simplified scenario where only c_t, c_b are free to vary, and all other couplings are fixed to their SM values.

4.3 The Minimal Supersymmetric Standard Model

The technique of the previous section can be applied also to the tree-level contribution of the Minimal Supersymmetric Standard Model (MSSM)[2]. The only contribution to the quartic potential comes from the D-term which, for the $SU(2)_L \times U(1)_Y$ MSSM gauge group, reads

$$\Delta V_{MSSM} = \frac{g^2 + g'^2}{8}\left(|H_1^0|^2 - |H_2^0|^2\right)^2 = \frac{g^2 + g'^2}{32}\left((c_\beta^2 - s_\beta^2)^2 h^4 + 8(c_\beta^2 - s_\beta^2)s_\beta c_\beta h^3 H + \cdots\right) \tag{4.12}$$

---

[2]In this case, h and H can be thought of as the eigenstate of the mass matrix before electroweak symmetry breaking.

with $c_\beta \equiv \cos\beta$ and $s_\beta \equiv \sin\beta$ and in what follows we shall also use $t_\beta \equiv \tan\beta$. This defines

$$\delta_\lambda \quad = \quad \frac{m_Z^2}{16v^2}(c_\beta^2 - s_\beta^2)^2, \tag{4.13}$$

$$\delta \quad = \quad \frac{m_Z^2}{2v^2}s_\beta c_\beta(c_\beta^2 - s_\beta^2). \tag{4.14}$$

From Eq. (4.10), this gives

$$c_b \quad \approx \quad 1 - \frac{m_Z^2}{2m_H^2}\sin 4\beta \tan\beta \tag{4.15}$$

$$c_t \quad \approx \quad 1 + \frac{m_Z^2}{2m_H^2}\sin 4\beta \cot\beta. \tag{4.16}$$

which coincides with the usual decoupling limit of the MSSM [148] with the identification $m_H \approx m_A$ (which is accurate for $m_{A,H} \gg m_Z$ or in the large $\tan\beta$ limit), and we will use in what follows in the comparison between exact and approximate results. At the same time, Eq. (4.13) provides the well known contribution to the Higgs mass $m_h^2 = m_Z^2 \cos^2 2\beta$; this tree-level result is modified by loop effects, in particular from top quarks/squarks, which we consider in what follows.

4.3.1   Top Squarks with no mixing

We begin with the case of top squarks with no mixing (realized in popular SUSY breaking mechanisms such as gauge mediation and gaugino mediation where a small trilinear coupling is expected [149]). The dominant loop contribution to the scalar effective potential is [148, 150],

$$\Delta V_{stop} = \frac{\lambda_2}{2}|H_2|^4, \tag{4.17}$$

where,

$$\lambda_2 \approx \frac{3y_t^4}{8\pi^2}\log[m_{\tilde{t}_1}m_{\tilde{t}_2}/M_t^2] \tag{4.18}$$

(a more accurate expression can be found in Appendix 4.9). After rotating into the basis of Eq. (4.2) one identifies

$$\delta_\lambda \quad = \quad s_\beta^4 \frac{\lambda_2}{8} \tag{4.19}$$

$$\delta \quad = \quad -4s_\beta^3 c_\beta \frac{\lambda_2}{8}. \tag{4.20}$$

From Eq. (4.18) and from Eq. (4.19) it follows that, in order to obtain a Higgs mass compatible with experiment, multi-TeV stop masses are required. Such heavy stops also destabilize the EW scale through loop effects and push the MSSM into fine-tuning territory [151]. Ignoring for a moment this tension, we can assume these loop contributions to be uniquely responsible
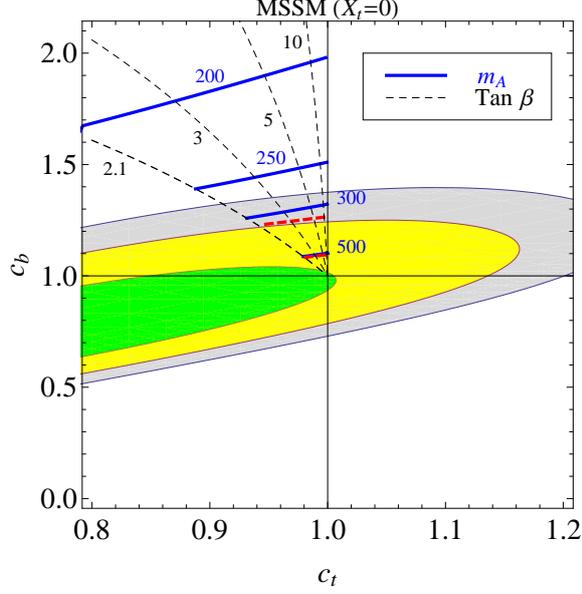
Figure 4.2: *Theoretical expectation for Higgs couplings deviations for the MSSM with heavy stops and no mixing, taking $m_h = 125\,\text{GeV}$, showing contours of constant m_A (solid blue) and $\tan\beta$ (dashed), obtained from the exact expressions of Eqs. (4.68,4.69) of Appendix 4.9. Also shown are the 68% (green), 95%(yellow) and 99%(grey) C.L. regions obtained by a global fit of the most recent LHC Higgs data, as explained in Appendix 4.8, neglecting loop contributions to the hgg and $h\gamma\gamma$ couplings. The dashed red lines show the approximate results of Eq. (4.21) for $m_H = 300, 500\,\text{GeV}$.*

for the large value of the Higgs mass, and write the deviations of $c_{b,t}$ induced by loop effects Eq. (4.20) together with the ones from the tree-level potential Eq. (4.14), as

$$
\begin{aligned}
c_b &\approx 1 + \frac{m_h^2 - m_Z^2 \cos 2\beta}{m_H^2}\,, \\
c_t &\approx 1 - (\cot\beta)^2 \frac{m_h^2 - m_Z^2 \cos 2\beta}{m_H^2}.
\end{aligned}
\tag{4.21}
$$

This shows that, in the MSSM with no stops mixing and for $\tan\beta > 1$, the deviations in c_b (c_t) are always positive (negative), as already observed in Ref. [145]. For large $\tan\beta$ the deviations in c_t are suppressed, while

$$
(c_b - 1) \approx \left(\frac{154\,\text{GeV}}{m_H} \right)^2.
\tag{4.22}
$$

We can compare these results with the exact ones of Fig. 4.2, which shows the intuitive (c_b, c_t)-plane mentioned above, and compares these theoretical expectations with the most recent data [138]- [142], using the methods described in Appendix 4.8. We assume a heavy sparticle spectrum, that does not affect the Higgs couplings to gluons and photons, other
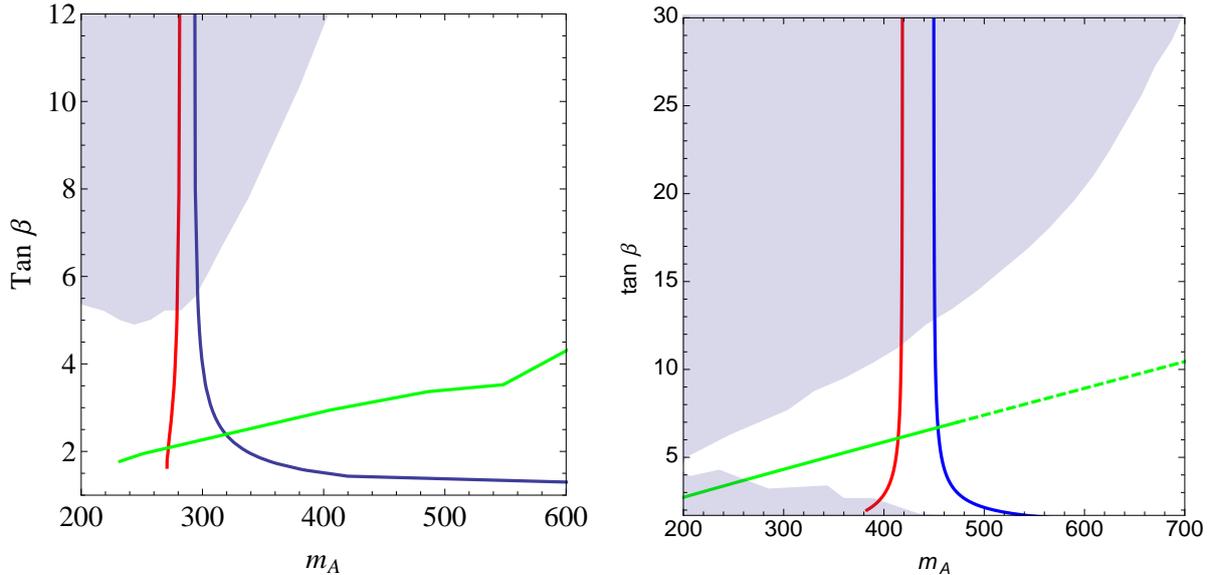
Figure 4.3: *Exclusion plot in the $m_A, \tan\beta$ plane for the MSSM with heavy stops (red), for models with additional non-decoupling D-terms (blue) and F-terms (green); regions to the left of the lines are excluded. The shaded region corresponds to bounds from direct searches [189]. Left: present data; right: longterm projection based on [169] assuming no deviations from the SM, shaded region from Ref. [170] (the dashed part of the line corresponds to a region where λ_S is bigger than 2 and non reaches the non-perturbative regime below approximately 10 TeV [151, 153]).*

than through Eq. (4.21) (this is motivated by the fact that in this example, we are assuming multi-TeV stops). Masses $m_H \lesssim 250$ GeV can be excluded, almost independently of $\tan\beta$, as suggested already by Eq. (4.22) for a sensitivity to the $h\bar{b}b$ coupling of about 50%. In Fig. 4.3 we also show the CMS bounds on the traditional MSSM $m_A, \tan\beta$ plane (for a recent analysis see Ref. [152]) from direct searches of the heavy Higgs decaying into τ pairs, as performed by CMS [189]. As can be appreciated, analyses of the light Higgs couplings offer a complementary search strategy in the intermediate $\tan\beta$ region.

4.3.2 Top Squarks with mixing

In the presence of sizable A-terms, L and R top squarks can mix, inducing additional contributions to the Higgs effective potential [150, 155],

$$\Delta V^{mix} = \frac{\lambda_2}{2}|H_2|^4 + (\frac{\lambda_5}{2}|H_1 H_2|^2 + \lambda_7|H_2|^2 H_1 H_2 + c.c), \qquad (4.23)$$

where the values of λ_2, λ_5 and λ_7 depend in particular on the parameter μ and the trilinear A_t and their expression, at the one loop level, can be found in Appendix 4.9. In the point of 'maximal mixing', when the trilinear term is $|A_t - \mu \cot\beta| = \sqrt{6}m_{\tilde{t}}$ (where $m_{\tilde{t}}$ is the geometric

mean of the lightest stop masses), the contribution to the Higgs mass proportional to λ_2 is maximized, while $\lambda_7 = 0$. Recasting the potential in the h, H basis gives,

$$\delta_\lambda = s_\beta^4 \left(\frac{\lambda_2}{8} + \frac{\lambda_5}{4\,t_\beta^2} + \frac{\lambda_7}{2\,t_\beta} \right), \tag{4.24}$$

$$\delta = s_\beta^3 c_\beta \left(\frac{\lambda_2}{2} + \frac{\lambda_5}{2} \left(1 - \frac{1}{t_\beta^2} \right) + \frac{\lambda_7}{2} \frac{t_\beta^2 - 3}{\sqrt{t_\beta^2 + 1}} \right), \tag{4.25}$$

where it can be seen that for large $\tan\beta$ (which is necessary in the MSSM to maximize the tree-level mass), the dominant contribution to the Higgs mass still comes from the first term λ_2, similarly to the case with no mixing discussed in the previous paragraph. As mentioned above, this term is maximized by large mixing, with drastic effects and the stop mass can be as low as 550 GeV in this case. Nevertheless, a fine-tuning at the percent level persists due to the fact that large A_t terms also contribute to the Higgs mass-parameter [151].

Unfortunately, for a generic choice of μ and A_t, the multitude of parameters introduced by mixing weakens the Higgs mass/coupling connection as shown by Eq. (4.25) where sizable $\lambda_{5,7}$ can affect the Higgs couplings without contributing to the Higgs mass. We show this effect in Fig. 4.4 where we consider small deviations from maximal mixing: departures from $\lambda_7 = \lambda_7^{MaxMix} = 0$ are enhanced at large $\tan\beta \gtrsim 20$ and the contribution to δ and to our predictions can be seizable. Nevertheless such large values of $\tan\beta$ are already in tension with rare B processes, such as $B_s \to \mu^+\mu^-$ [156], and with direct searches for $H/A \to \bar{\tau}\tau$ [189], so that we do not expect our results to change significantly in the intermediate $\tan\beta$ region, where our bounds are more competitive, see Fig. 4.3.

4.4 Extra D-Terms

As discussed above, a 125 GeV Higgs in the MSSM is generally associated with fine-tuning. This suggests that the principle of SUSY, if realized at low energy in a natural way, extends beyond the MSSM, with new tree-level effects contributing to the Higgs quartic. The first possibility is to envisage additional gauge symmetries that contribute to the Higgs quartic, similarly to the MSSM gauge group [149,153,157]. In this section we study the example of an additional abelian gauge group under which H_1 and H_2 have opposite charges (as compatible with the μ-term). Then, the extra contribution to the Higgs sector quartic[3]

$$\Delta V = \kappa \left(|H_1^0|^2 - |H_2^0|^2 \right)^2 \tag{4.26}$$

where,

$$\kappa = \frac{g_X^2}{8\left(1 + \frac{M_{Z'}^2}{2m_\phi^2}\right)}. \tag{4.27}$$

---

[3]The form of the potential in Eq. (4.26) holds also for the non-abelian extension considered in Refs [153,157].
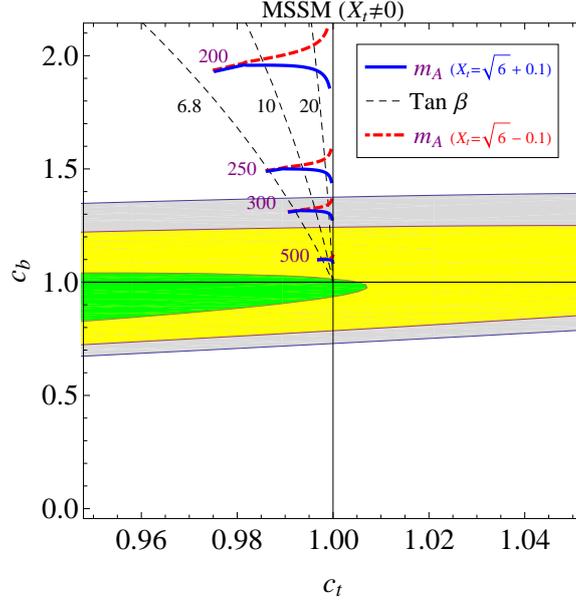
Figure 4.4: *Same as Fig.4.2, but for near maximal mixing and, again, we adjust $\sqrt{m_{\tilde{t}_1} m_{\tilde{t}_2}} \in$ [550, 2000] GeV in order to obtain the observed Higgs mass. We take $x_t = \sqrt{6} \pm 0.1$ for the blue/red curve in order to show the influence, for large $\tan\beta$, of small deviations from maximal mixing; $\mu = 400$ GeV.*

Here m_ϕ is the soft SUSY breaking mass of the MSSM singlets that breaks the $U(1)_X$ group (with gauge coupling g_X) and $M_{Z'}$ the SUSY-preserving mass of the gauge boson. Eq. (4.27) shows that, in the limit $M_{Z'} \gg m_\phi$, the Z' can be supersymmetrically integrated out and the D-term contribution of the $U(1)_X$ group decouples: non-decoupling D-terms require a large soft mass $m_\phi \sim M_{Z'}$ and result in an effective hard breaking in the Higgs sector.

The contributions to δ_λ and δ are similar to Eqs. (4.13,4.14), with the substitution $m_Z^2/v^2 \to 4\kappa$. In the absence of other effects that affect the Higgs mass (we assume the loop effects of Eqs. (4.20,4.24) to be subdominant), we can fix κ in order to obtain the observed Higgs mass [4], we can then write

$$c_b \approx 1 + 2\frac{m_h^2}{m_H^2}\frac{t_\beta^2}{t_\beta^2 - 1} \tag{4.28}$$

$$c_t \approx 1 - 2\frac{m_h^2}{m_H^2}\frac{1}{t_\beta^2 - 1}. \tag{4.29}$$

meaning that, for $\tan\beta > 1$, positive (negative) deviations are expected in c_b (c_t). For large $\tan\beta$ the modifications in c_t vanish, as usual, while those on c_b asymptote to $c_b - 1 \approx (176\,\text{GeV}/m_H)^2$. This is shown, using the exact expressions from Appendix 4.9, in Fig. 4.5.

---

[4]Notice that as $\tan\beta \to 1$, all contributions to the Higgs mass from D-terms vanish; hence these expressions have to be trusted only away from this singular point: in Fig. 4.5 we show curves of constant g_X (in the limit of large $m_\phi \gg M_{Z'}$) to show that in the region of interest the parameters are under control.
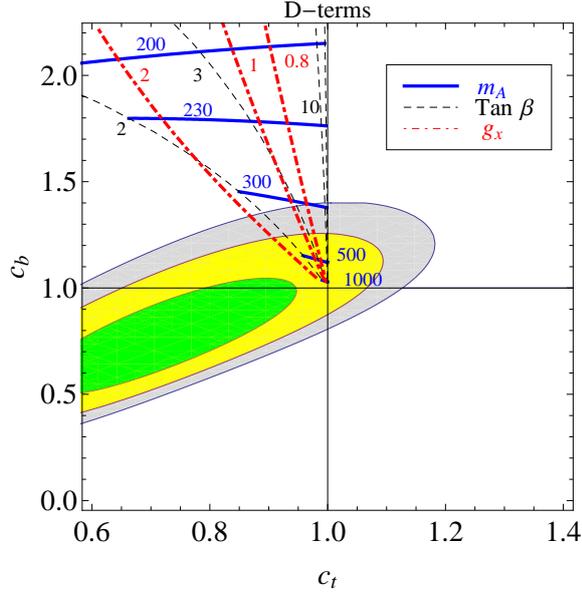
Figure 4.5: *Higgs couplings deviations in the MSSM with additional non-decoupling D-terms to raise the Higgs mass to 125 GeV (on top of the effect of light stops $m_{\tilde{t}} = 500\,\mathrm{GeV}$). The global fit (Colors as in Fig. 4.2) includes the effect of a 500 GeV stop (to be compared with Fig. 4.2 where the effects of stops on the fit are vanishingly small).*

Differently from Fig. 4.2, the global fit of Fig. 4.5 includes the effect of a light stop at 500 GeV (as opposed to the previous section, where heavy stops were necessary to increase the Higgs mass, here this is taken care by the additional D-terms, and the stops can be naturally light, see also Section 4.6). Masses $m_H \lesssim 300\,\mathrm{GeV}$ can already be excluded, with better results in the small $\tan\beta$ region (see also Fig. 4.3).

In principle we could relax the assumption that H_1 and H_2 carry equal and opposite $U(1)_X$ charges. In this case, however, additional structure is needed in order to generate a μ-term. For example an extra SM singlet, charged under $U(1)_X$ can generate this term by aquiring a non-vanishing vev. This extension, however, implies additional contributions to the quartic potential from F-terms which, as we comment in the next-section, are expected to dominate.

4.5   F-Terms, the NMSSM and the BMSSM

It is tempting to parametrize these new effects using an effective field theory approach with an expansion in powers of the scale of physics beyond the MSSM (in the example of the previous section, this would be the mass of the new gauge bosons $M_{Z'}$). The most general such parametrization, however, lacks any predictive power (peculiar directions in parameter space can be found where an increase in the Higgs quartic coupling doesn't imply modifications of the couplings [158]). Nevertheless, as shown in Ref. [159], the leading order effects in such an

expansion have a very specific form[5]:

$$\mathcal{L}_5 = \int d^2\theta \left(\frac{\lambda_1}{M} (H_1 H_2)^2 + \mathcal{Z} \frac{\lambda_2}{M} (H_1 H_2)^2 \right) \tag{4.30}$$

where $\mathcal{Z} = \theta^2 m_{SUSY}$ is a dimensionless spurion that parametrizes SUSY breaking. This leads to additional contributions to the scalar potential,

$$\Delta V_5 = 2\epsilon_1 H_1 H_2 (H_1^\dagger H_1 + H_2^\dagger H_2) + \epsilon_2 (H_1 H_2)^2 + c.c \tag{4.31}$$

with $\epsilon_1 = \lambda_1 \mu^*/M$ and $\epsilon_2 = -\lambda_2 m_{SUSY}/M$. We obtain

$$\begin{aligned}
\delta_\lambda &= \frac{\epsilon_1}{4} \sin 2\beta + \frac{\epsilon_2}{16} \sin^2 2\beta \\
\delta &= -\frac{\epsilon_1}{2} \cos 2\beta - \frac{\epsilon_2}{8} \sin 4\beta.
\end{aligned} \tag{4.32}$$

By construction $\beta \in [0, \pi/2]$ and for the first term to contribute positively to the Higgs mass, a positive ϵ_1 is necessary, implying an enhancement of c_b and a decrease in c_t, similarly to the case studied in the previous section. The term proportional to ϵ_2, on the other hand, reduces for $\tan \beta > 1$ the $h\bar{b}b$ coupling while increasing the coupling to top quarks, oppositely to the effects of D-terms. This is an interesting case that corresponds to the non-decoupling F-term contribution of an extra singlet, interacting with the Higgs sector via the superpotential term $W = \lambda_S S H_1 H_2$, as in the NMSSM. Indeed, in the limit where the mass of the singlet is large, its contribution is given by the second term of Eq. (4.30), where $M = M_S$ ($m_{SUSY} = m_S$) is the supersymmetric (SUSY breaking) mass of the singlet, and $\lambda_2 = \lambda_S^2$ (notice that the singlet also gives a generally subdominant contribution to the first term of Eq. (4.30) with $\epsilon_1 = -\mu^* \lambda_S^2/(2M_S)$, which we ignore for the time being).

If the largeness of the Higgs mass is due to a combination of the MSSM D-terms effects of Eq. (4.12) and the present contribution from F-terms due to the singlet (i.e. with negligible contributions from loop-effects), then the Higgs couplings to fermions are modified as

$$c_b \approx 1 - \frac{t_\beta^2 - 1}{2} \frac{m_h^2 - m_Z^2}{m_H^2} \tag{4.33}$$

$$c_t \approx 1 + \frac{t_\beta^2 - 1}{2t_\beta^2} \frac{m_h^2 - m_Z^2}{m_H^2}, \tag{4.34}$$

which, for large $\tan \beta$, gives deviations in the $h\bar{t}t$ coupling of order $\Delta c_t \approx (60\,\text{GeV}/m_H)^2$, and in the couplings to bottom quarks $\Delta c_b \approx t_\beta^2 (60\,\text{GeV}/m_H)^2$. We show the exact coupling deviations in Fig. 4.6 (we assume, again, the presence of 500 GeV stops, see section 4.6) where we also emphasize curves of constant λ_S: values below $\lambda_S \lesssim 0.7$ are perturbative up to the GUT scale, while for values $0.7 \lesssim \lambda_S \lesssim 2$ the non-perturbative regime is reached above a scale of 10 TeV [151, 160]. The bounds on m_H that can be extracted from this analysis are very much dependent on $\tan \beta$, as can be seen in Fig. 4.3.

---

[5]For large $\tan \beta$ interactions at higher order in the expansion could be enhanced and dominate.
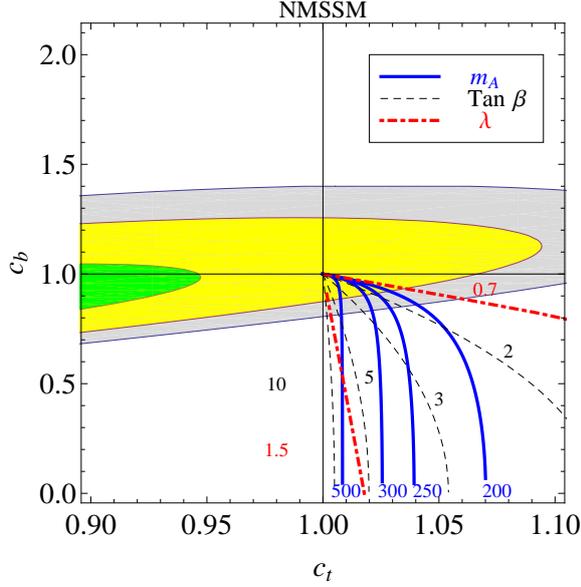
Figure 4.6: *Coupling deviations in the NMSSM assuming a Higgs mass of 125 GeV in the limit where the singlet is heavy and it doesn't mix with the Higgs, but its contributions do not decouple. Global fit as in Fig. 4.5.*

While the approach of Eq. (4.30) encompasses large classes of models, its applicability is limited to cases with widely separated scales, such as the NMSSM where the singlet has both a large SUSY preserving and SUSY breaking mass [6]. In the opposite case, however, its interactions with the Higgs sector can induce mixings with the lightest CP-even Higgs and the analysis changes completely, as we now discuss.

4.5.1 Doublet-singlet mixing

When the singlet is not much heavier than the EW scale, the above analysis ceases to be valid; moreover singlet-Higgs mixing can affect our discussion of section 4.2 (see also Ref. [161] for other LHC bounds on this possibility). Indeed, in this case, the potential Eq. (4.4) includes in particular the term $\Delta V(H_1, H_2, S) \supset \delta_S s h^2/2$. Once h gets a vev, this term leads to a mixing between h and S so that h becomes a linear combination of the three gauge eigenstates:

---

[6] Triplets with hypercharge $Y \pm 1$ and superpotential $W = \lambda_T T H_2 H_2 + \lambda_{\bar{T}} \bar{T} H_1 H_1$ have also been considered in the literature: in the non-decoupling limit, their contribution to the potential is

$$\Delta V = |\lambda_T|^2 H_2^4 + |\lambda_{\bar{T}}|^2 H_1^4 \tag{4.35}$$

and

$$\delta_\lambda = \frac{|\lambda_{\bar{T}}|^2}{4} c_\beta^4 + \frac{|\lambda_T|^2}{4} s_\beta^4, \quad \delta = |\lambda_{\bar{T}}|^2 c_\beta^3 s_\beta + |\lambda_T|^2 s_\beta^3 c_\beta. \tag{4.36}$$

For large $\tan\beta$ only the H_2^4 term is important and the results coincide with those of section Ê4.3.1.

Figure 4.7: *Feynman diagrams illustrating modifications in the couplings between the Higgs and the fermions (or vectors) due to mixings with the singlet S.*

Eq. (4.2) now must include

$$h = \cos\theta(\sin\beta h_2^0 - \cos\beta h_1^0) + \sin\theta s. \tag{4.37}$$

The mixing θ can be estimated by using the techniques of section 4.2: the term $(\delta_S/2)h^2s$ corrects the h-propagator when s is integrated out and two of the h legs are replaced by vevs, as illustrated in the first diagram of Fig.4.7. This correction, beside modifying the quartic structure δ and δ_λ as discussed so far, it also universally affects all h couplings by shifting the kinetic term to

$$\mathcal{L}_{eff} \supset (1 + 2\frac{\delta_S^2\, v^2}{m_S^4})\frac{1}{2}\partial_\mu h \partial^\mu h \ . \tag{4.38}$$

Indeed, making this kinetic term canonical leads to a universal suppression of all h couplings by the factor

$$\cos\theta \approx 1 - \frac{\delta_S^2 v^2}{m_S^4} \ , \tag{4.39}$$

where θ is defined by Eq. (4.37) and the coupling of Eqs. (4.10, 4.11) become,

$$c_b \approx 1 - 4\tan\beta\delta\frac{v^2}{m_H^2} - \frac{\delta_S^2 v^2}{m_S^4} \tag{4.40}$$

$$c_t \approx 1 + 4\cot\beta\delta\frac{v^2}{m_H^2} - \frac{\delta_S^2 v^2}{m_S^4} \tag{4.41}$$

$$c_V \approx 1 - \frac{\delta_S^2 v^2}{m_S^4}. \tag{4.42}$$

Notice that in this case, if the singlet is light or if its couplings to the Higgs sector are large, sizable modifications of the hZZ and hWW vertices can be produced. In principle, it is still possible to exploit the Higgs mass/coupling connection to fix δ and then a simultaneous measurement of c_V and $c_{b,t}$ would allow to extract information about m_H and about the mixing with the singlet. In practice, however, models of this type introduce many new contributions to the Higgs quartic potential and the Higgs mass/coupling connection looses most of its predictive power. We show this in the example of the NMSSM [162], where the superpotential $W = \lambda S H_1 H_2 + \kappa S^3/3$ generates the following relevant terms in the potential

(which add to the usual MSSM D-terms Eq. (4.12)),

$$\Delta V_{NMSSM}(H_1, H_2, S) \supset m_S^2 S^2 + \lambda^2 \left(|H_1 H_2|^2 + S^2 |H_1|^2 + S^2 |H_2|^2 \right) - (\lambda A_\lambda S H_1 H_2 + \lambda \kappa H_1 H_2 S^{*2} + h.c.)$$
(4.43)

where we assume real coefficients for simplicity (m_S, A_λ are soft SUSY breaking terms [162]). After the singlet obtains a vev $\langle S \rangle \equiv v_S$, we can integrate out its real part, with mass m_S, and obtain the effective quartic potential

$$\Delta V_{NMSSM}^{eff}(H_1, H_2) \supset \lambda^2 |H_1 H_2|^2 - \frac{\mu_1^2}{m_S^2} \text{Re}(H_1 H_2)^2 - \frac{\mu_2^2}{4m_S^2}(|H_1|^2 + |H_2|^2)^2 + \frac{\mu_1 \mu_2}{m_S^2}\text{Re}(H_1 H_2)(|H_1|^2 + |H_2|^2)$$
(4.44)

(where we have neglected higher order terms in the couplings) and the mixing term

$$\delta_S = \frac{(\mu_2 - \mu_1 \sin 2\beta)}{\sqrt{2}},$$
(4.45)

with $\mu_1 \equiv \lambda A_\lambda + 2\lambda \kappa v_S$, and $\mu_2 \equiv 2\lambda^2 v_S$. In this procedure, also contributions from the second diagram of Fig. 4.7 are taken into account. As usual the quartic potential can be written in terms of h, H and we find,

$$\delta_\lambda = \frac{\lambda^2}{16}\sin^2 2\beta - \frac{1}{8}\frac{\delta_S^2}{m_S^2}$$
(4.46)

$$\delta = -\frac{\lambda^2}{8}\sin 4\beta - \frac{\mu_1 \delta_S}{m_S^2}\frac{\cos 2\beta}{2\sqrt{2}}$$
(4.47)

As it could have been foreseen, the multitude of parameters that characterize this model breaks the connection between δ and δ_λ and it becomes possible to raise the Higgs mass independently of a modification of its couplings. Even for small m_H a conspiracy between the MSSM D-term and these additional F-terms could allow for a large Higgs mass without any observable effect in the Higgs couplings (a similar example in the context of D-terms is discussed in Ref. [158]).

Nevertheless, perturbativity up to the GUT scale (up to 10 TeV) limits the size of $\lambda \lesssim 0.7(2)$ and the necessity of a positive contribution to the Higgs mass from Eq. (4.46), imposes an upper bound on the negative contribution proportional to δ_S^2/m_S^2, as we show in the left panel of Fig. 4.8. Since the latter governs the coupling modification due to mixing through Eqs. (4.40-4.42), we see that in the perturbative NMSSM only small deviations are expected due to mixing, $\Delta c_V \lesssim 5\%$ for $m_S \gtrsim v$. Deviations in the couplings $c_{b,t}$ are still proportional to the parameter δ which, as mentioned above, is now independent of the Higgs mass and would allow only to constrain the ratio μ_1/m_H, which is not particularly interesting.

In λSUSY [163], on the other hand, deviations can easily be of order unity. In particular, if δ in Eq. (4.47) is positive (notice that for $\tan \beta > 1$, both $\sin 4\beta$ and $\cos 2\beta$ are negative) we have $c_t \gtrsim c_V > c_b$, which enhances the rate of both $h \to \gamma\gamma$ and $h \to VV$. Notice that if we consider only deviations in the tree-level couplings, an enhancement of $h \to \gamma\gamma$ only, would require $c_V \gtrsim c_t \gtrsim c_b$, a region which is not touched by this model.
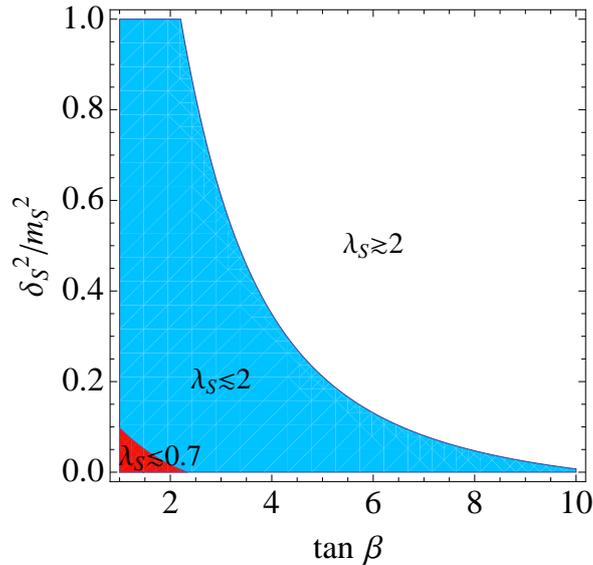
Figure 4.8: *Upper bound on δ_S^2/m_S^2 as a function of $\tan\beta$ requiring perturbativity of the coupling λ_S up to the GUT scale ($\lambda_S \lesssim 0.7$) or only up to 10 TeV ($\lambda_S \lesssim 2$), as in λSUSY; the contribution of a 500 GeV stop is also included. The parameter δ_S^2/m_S^2 enters the modifications of couplings to fermions and gauge bosons Eqs. (4.40-4.42) via the combination $\delta_S^2 v^2/m_S^4$.*

4.6 Light SUSY Partners

So far we have studied modifications of the direct couplings between Higgs and fermions, restricting our attention to the 2HDM structure of the Higgs sector. When comparing with data, however, the presence of light sparticles can introduce additional nuisances, as they contribute via loop-effects to the hgg and $h\gamma\gamma$ effective vertices. Naturalness suggests that only the partners of third family fermions be light (other bounds on natural SUSY have been studied in Refs. [164–166]); these have also the strongest couplings to the Higgs sector and have potentially a bigger impact than other sparticles. While staus and sbottoms have a negligible effect, light stops can change the analysis considerably [144]. We show this in Fig. 4.9, where we compare 99%C.L. contours, assuming that a stop has been found, with mass $m_{\tilde{t}} = 160, 500\,\mathrm{GeV}$ (dotted, dashed), with the contours without taking this effect into account (solid)[7]. Since c_t itself affects Higgs physics mostly through a modification of the Higgs-gluon effective vertex[8], the leading effect of light stops, which themselves affect the hgg

---

[7]Recall that in our plots of the MSSM Figs. 4.2-4.4, since heavy stops are needed to increase the Higgs mass, we have assumed heavy stops in the fit too, with no seizable loop contributions to hgg and $h\gamma\gamma$; in Figs. 4.5-4.8, on the other hand, where a natural spectrum is allowed thanks to the D-term/F-term contributions to the Higgs mass, we assumed $m_{\tilde{t}} = 500\,\mathrm{GeV}$.

[8]c_t enters also directly through a contribution of a few percent of the $\bar{t}th$ associated production channel to the total production crossection and through the exclusive $pp \to h t \bar{t} \to \bar{b} b \bar{t} t$ channel, which is however badly measured at present.
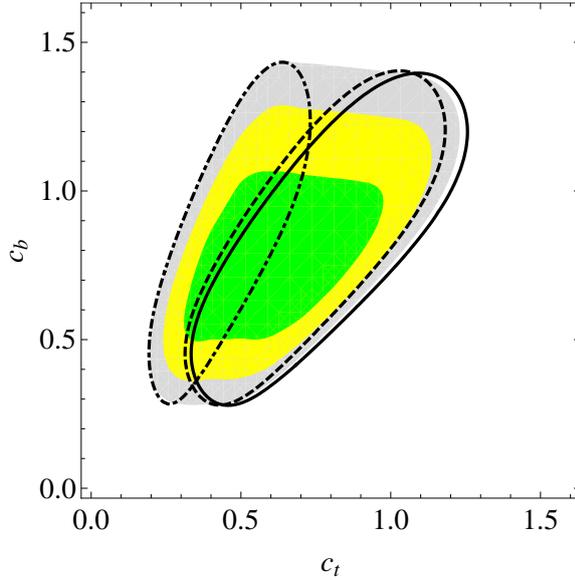
Figure 4.9: *99% C.L. contours from a global fit to the parameters c_b and c_t, taking into account the loop effects due to a stop quark with $m_{\tilde{t}} = 160, 500$, GeV (dot-dashed,dashed); in the solid line this effect is not taken into account, while in the colored contours stops (color coding as in Fig. 4.2) are treated as a nuisance and their contribution is marginalized assuming $m_{\tilde{t}} > 160\,\mathrm{GeV}$.*

effective coupling, results in a shift along the direction of c_t. As it can be seen, stops heavier than about 500 GeV have negligible influence on the fit. Nevertheless, in Fig. 4.9 we also show the global fit treating the stop contribution as nuisance and marginalizing over it: this is useful to take into account the possibility that a very light stop lies in a region inaccessible to direct searches.

The mass of charginos is also directly related to the EW scale if the chargino is mostly Higgsino: then , In principle light charginos introduce an additional unknown through their contribution to the $h\gamma\gamma$ coupling. However, for this to have any impact, small $\tan\beta \lesssim 5$ [144], very light charginos $m_{\chi^\pm} \ll 250\,\mathrm{GeV}$ [167] and large wino-chargino mixing (which is typically suppressed by inverse powers of the wino mass m_W^2/M_2^2 [168]) are necessary. We consider this a peculiar, rather than representative, point in parameter space and we assume these effects to be small in our analysis.

4.7   Conclusions and Outlook

In the MSSM, the tree-level Higgs mass is too small to account for the observed value of ≈ 125 GeV. We have shown, using a simple analytical method based on an expansion in inverse powers of the heavy Higgs mass, how the physics that contributes to increase the light Higgs mass, also modifies the couplings of the lightest CP-even Higgs with fermions and

gauge bosons. In the simplest examples (MSSM with no mixing between top squarks, MSSM with extra non-decoupling D-terms/F-terms) this connection provides distinctive predictions for the Higgs couplings, which allow us to extract bounds on the parameters m_A and $\tan\beta$, competitive with bounds from direct searches [189]. Deviations in the couplings hZZ and hWW are expected to be small in 2HDMs and we could use the intuitive c_b, c_t plane to show our results. In this way we could extract bounds on the heavy Higgs mass m_H, depending on the model and on the size of $\tan\beta$, as we summarized in Fig. 4.3.

Models that include extra gauge singlets that mix with the Higgs sector, can in principle be studied in a similar way. In the most popular realizations, such as the NMSSM, however, the large number of parameters of the model weakens the Higgs mass/coupling connection and predictability is compromised. Yet, theoretical consistency of the model, based for instance on the requirement of perturbativity, can strongly constrain the size of the expected effects.

As long as the uncertainty in measuring Higgs couplings is dominated by statistical errors, more data will lead to better measurments. In the long term, with an integrated luminosity $\sim 300\text{fb}^{-1}$, the sensitivity to the Higgs couplings to bottom/top quarks is expected to reach 15% [169, 170] and, as we show in the right panel of Fig. 4.3, some deviations from the SM are expected if $m_{H,A} \lesssim 400\,\text{GeV}$. At the same time, direct searches would have probed a much larger region of parameter space, but the bounds from Higgs couplings will remain competitive in the intermediate $\tan\beta$ region (better results can be achieved by considering ratios of couplings [171]).

Let us conclude with a comment regarding bounds from flavour physics. The cross-section for $B_s \to \mu^+\mu^-$ processes is proportional to $\tan^6\beta$ and therefore this measurement practically excludes the region $\tan\beta \gtrsim 30$ (depending on other parameters of the model [156]) while it has a relatively small impact for intermediate and small $\tan\beta$; in this regime the bounds discussed in this paper can be considered complementary. Constraints from $b \to s\gamma$ can be more important [176], but a fair comparison is difficult, as the amplitude for this process depends as much on the details of the sparticle sector as it depends on the parameters of the Higgs sector, which we consider here (in regions where the former are small, bounds on Type II 2HDMs exclude $m_{H^\pm} \lesssim 300$ GeV, independently of $\tan\beta$ Ê [178]). In any case, while the $b \to s\gamma$ bounds are competitive with the Higgs coupling bounds at present[9], the latter are expected to become stronger as the integrated luminosity increases.

---

[9]An interesting contribution to $b \to s\gamma$, which we have neglected throughout this work, comes from loop-effects involving squark-charginos or sbottom-gluino, which do not decouple when the mass of the superpartners is large and induce a coupling of H_2 to down-type quarks, $y_b(H_1^0 b\bar{b} + \epsilon_b H_2^0 b\bar{b})$ that can be enhanced at large $\tan\beta$ (which is interesting for the MSSM and for the D-term case of section 4.4). This can strengthen (weaken) the bounds from $b \to s\gamma$ for negative (positive) ϵ_b [175]. At the same time, however, it can affect the hbb coupling [144],

$$\Delta c_b \approx -\epsilon_b \tan\beta \frac{m_h^2}{m_H^2}, \tag{4.48}$$

which, for the MSSM or for the D-terms of Eq. (4.28), goes also towards strengthening (weakening) our bounds. Thus in the MSSM (also with additional D-terms) stronger constraints from Higgs coupling data are correlated with stronger $b \to s\gamma$ constraints and vice-versa [177].

Note Added: While this work was being finalized (see [173]), Ref. [174] appeared, which also considers modifications of Higgs couplings in SUSY models with additional, non-decouplings F-terms or D-terms.

4.8   Appendix I: Details of experimental fit

To perform the statistical analysis of the data we take the following reescaled couplings of the higgs to the SM particles

$$c_t \equiv \frac{y_t}{y_t^{SM}}, \ c_b = c_\tau \equiv \frac{y_b}{y_b^{SM}}, \ c_V \equiv \frac{g_{hVV}}{g_{hVV}^{SM}}, \tag{4.49}$$

but fixing $c_V = 1$ the reason of which is explained before in the text.

We also take into account the stop loop effects which appear in the $gg \to h$, $h \to \gamma\gamma$, $h \to gg$ production and decay modes. The main contributions to these effects [185–187] are given by the following expressions:

$$\frac{\sigma(gg \to h)}{\sigma(gg \to h)_{SM}} \approx \frac{\Gamma(h \to gg)}{\Gamma(h \to gg)_{SM}} \approx \left| \frac{A_t^{gg} + A_{\tilde{t}_1}^{gg} + A_{\tilde{t}_2}^{gg}}{A_{t,SM}^{gg}} \right|^2 \tag{4.50}$$

$$\approx c_t^2 \left| 1 + \frac{m_t^2}{4m_{\tilde{t}_1}} + \frac{m_t^2}{4m_{\tilde{t}_2}} - \frac{m_t^2 X_t^2}{4m_{\tilde{t}_1} m_{\tilde{t}_2}} \right|^2 \tag{4.51}$$

$$\frac{\Gamma(h \to \gamma\gamma)}{\Gamma(h \to \gamma\gamma)_{SM}} \approx \left| \frac{A_w^{\gamma\gamma} + A_t^{\gamma\gamma} + A_{\tilde{t}_1}^{\gamma\gamma} + A_{\tilde{t}_2}^{\gamma\gamma}}{A_{w,SM}^{\gamma\gamma} + A_{t,SM}^{\gamma\gamma}} \right|^2 \tag{4.52}$$

$$\approx \left| 1.28\, a - 0.28\, c_t \left(\frac{m_t^2}{4m_{\tilde{t}_1}} + \frac{m_t^2}{4m_{\tilde{t}_2}} - \frac{m_t^2 X_t^2}{4m_{\tilde{t}_1} m_{\tilde{t}_2}} \right) \right|^2 \tag{4.53}$$

The statistical analysis is performed using the latest signal strenght data given by Tevatron and ATLAS, and the one given by CMS at ICHEP. We didn't take the latest CMS data due to the fact that only a combination of 7 and 8 TeV is given in the signal strenghts at a higgs mass different than the one of ICHEP which doesn't allow us to extract them separatedly [10].

The signal strengths are assumed to follow a Gaussian distribution and we fit the data by minimizing a χ^2 with the theoretical prediction for the signal strenght:

$$\mu^i = \frac{\sum_p \sigma_p(a, c_t, c_b, c_\tau) \zeta_p^i}{\sum_p \sigma_p^{SM} \zeta_p^i} \frac{BR_i(a, c_t, c_b, c_\tau)}{BR_i^{SM}}, \tag{4.54}$$

In the few cases where the given signal strenght errors are not symmetric we symmetrize them in quadrature. Statistical and theoretical errors are summed in quadrature without taking into account possible correlations, this approach is reasonable since at the moment the effect of this correlations is still small and can be neglected. In the other hand when

---

[10]An alternative approach can be found in [147]

comparing our fits using ICHEP data for both CMS and ATLAS we find an agreement of better than %10 between our figure and the one provided by them (we find this agreement to become better depending on the assumed cuts in the channels where they are not completely specified).

The data used can be found in table 4.1 where all the channels taken into account are specified. In this table we see that for each channel a particular set of cuts is defined. These refer to the values of ζ_p^i found in equation 4.54 which are the cuts for each higgs production mode: gluon fusion (G), vector boson fusion (VBF), associated production with a vector boson (A) and associated $t\bar{t}$ (tth). Expanded this can be seen as:

$$\frac{\sum_p \sigma_p \zeta_p^i}{\sum_p \sigma_p^{SM} \zeta_p^i} = \frac{c_t^2(\sigma_G \zeta_G^i + \sigma_{ttH}\zeta_{ttH}^i) + a^2(\sigma_{VBF}\zeta_{VBF}^i + \sigma_{WH}\zeta_{WH}^i + \sigma_{ZH}\zeta_{ZH}^i)}{\sigma_G \zeta_G^i + \sigma_{VBF}\zeta_{VBF}^i + \sigma_{WH}\zeta_{WH}^i + \sigma_{ZH}\zeta_{ZH}^i + \sigma_{ttH}\zeta_{ttH}^i},$$

where the cut efficiencies ζ_p^i for each production mode p corresponding to each channel i are reported below in table 4.2.

4.9 Appendix II: Details of the exact theory computation

The most general two Higgs doublet model (2HDM) potential for the neutral components of the doublet is,

$$\Delta V = m_1^2 H_1^2 + m_2^2 H_2^2 - (m_{12}^2 H_1 H_2 + c.c.) + \frac{\lambda_1}{2}|H_1|^4 + \frac{\lambda_2}{2}|H_2|^4 + \lambda_3|H_1|^2|H_2|^2 + \lambda_4(H_1 H_2)^\dagger(H_1 H_2)$$
$$+ (\frac{\lambda_5}{2}|H_1 H_2|^2 + \lambda_6|H_1|^2 H_1 H_2 + \lambda_7|H_2|^2 H_1 H_2 + c.c) \qquad (4.55)$$

We have used the convention of Ref. Ê [150, 155]. We can rewrite this potential in the h-H basis to obtain,

$$\delta = \frac{\lambda_1}{2}c_\beta^3 s_\beta + \frac{\lambda_2}{2}s_\beta^3 c_\beta + \frac{1}{2}(\lambda_3 + \lambda_4 + \lambda_5)s_\beta c_\beta(s_\beta^2 - c_\beta^2) + \frac{\lambda_6}{2}(c_\beta^2(s_\beta^2 - c_\beta^2) + 2s_\beta^2 c_\beta^2) + \frac{\lambda_7}{2}(s_\beta^2(s_\beta^2 - c_\beta^2) - 2s$$
$$\delta_\lambda = \frac{\lambda_1}{8}c_\beta^4 + \frac{\lambda_2}{8}s_\beta^4 + \frac{1}{4}(\lambda_3 + \lambda_4 + \lambda_5)s_\beta^2 c_\beta^2 + \frac{\lambda_6}{2}(c_\beta^3 s_\beta) + \frac{\lambda_7}{2}(s_\beta^3 c_\beta) \qquad (4$$

We will now give the values of λ_1-λ_5 in the different models we have considered. In the MSSM we have,

$$\lambda_1 = \frac{m_Z^2}{2v^2} \qquad \lambda_2 = \frac{m_Z^2}{2v^2} \qquad \lambda_3 = -\frac{m_Z^2}{2v^2} \qquad (4.57)$$

Table 4.1: *CMS, ATLAS and Tevatron data for the most sensitive channels. The cuts are classified as inclusive (I), associated production (A), vector boson fusion (VBF) or else ($\gamma\gamma_X$), see Appendix for details. $\hat{\mu}^{1.96,7,8}$ denote the best fits for the 1.96 TeV Tevatron, and the 7,8 TeV LHC data.*

CMS 125 GeV	Cuts	$\hat{\mu}^7$	$\hat{\mu}^8$
$\gamma\gamma_0$ [179]	$\gamma\gamma_X$	$3.1^{+1.9}_{-1.8}$	$1.5^{+1.3}_{-1.3}$
$\gamma\gamma_1$ [179]	$\gamma\gamma_X$	$0.6^{+1.0}_{-0.9}$	$1.5^{+1.1}_{-1.1}$
$\gamma\gamma_2$ [179]	$\gamma\gamma_X$	$0.7^{+1.2}_{-1.2}$	$1.0^{+1.2}_{-1.2}$
$\gamma\gamma_3$ [179]	$\gamma\gamma_X$	$1.5^{+1.6}_{-1.6}$	$3.8^{+1.8}_{-1.8}$
$\gamma\gamma_{jj}$ [179]	$\gamma\gamma_X$	4.2^{+2}_{-2}	$L:\ -0.6^{+2.0}_{-2.0}$ $T:\ 1.3^{+1.6}_{-1.6}$
$\tau\tau_{0/1j}$ [180]	I	$1.0^{+1.5}_{-1.4}$	$2.1^{+1.5}_{-1.6}$
$\tau\tau_{VBF}$ [180]	VBF	$-1.8^{+1.4}_{-1.2}$	$-1.8^{+1.4}_{-1.3}$
$\tau\tau_{VH}$ [180]	A	$0.6^{+4.2}_{-3.1}$	-
bb_{VH} [180]	A	$0.6^{+1.3}_{-1.2}$	$0.4^{+1.2}_{-0.9}$
bb_{ttH} [180]	ttH	$-0.8^{+2.1}_{-1.8}$	-
WW_{0j} [131]	I	$0.1^{+0.6}_{-0.6}$	$1.3^{+0.8}_{-0.6}$
WW_{1j} [131]	I	$1.7^{+1.2}_{-1.0}$	$0.0^{+0.8}_{-0.8}$
WW_{2j} [131]	VBF	$0.0^{+1.3}_{-1.3}$	$1.3^{+1.7}_{-1.3}$
ZZ [180]	I	$0.6^{+0.8}_{-0.5}$	$0.8^{+0.7}_{-0.5}$

CDF/D0 125 GeV	Cuts	$\hat{\mu}^{1.96}$	-
$\gamma\gamma$ [188]	I	$3.6^{+3.0}_{-2.5}$	-
bb [188]	A	$2.0^{+0.7}_{-0.6}$	-
WW [188]	I	$0.3^{+1.2}_{-0.3}$	-

ATLAS 126.5 GeV	Cuts	$\hat{\mu}^7$
$\gamma\gamma_{UnCeLPTt}$ [141, 142]	$\gamma\gamma_X$	$0.5^{+1.4}_{-1.4}$
$\gamma\gamma_{UnCeHPTt}$ [141, 142]	$\gamma\gamma_X$	$0.2^{+2.0}_{-1.9}$
$\gamma\gamma_{UnReLPTt}$ [141, 142]	$\gamma\gamma_X$	$2.5^{+1.7}_{-1.7}$
$\gamma\gamma_{UnReHPTt}$ [141, 142]	$\gamma\gamma_X$	$10.4^{+3.7}_{-3.7}$
$\gamma\gamma_{CoCeLPTt}$ [141, 142]	$\gamma\gamma_X$	$6.1^{+2.7}_{-2.7}$
$\gamma\gamma_{CoCeHPTt}$ [141, 142]	$\gamma\gamma_X$	$-4.4^{+1.8}_{-1.8}$
$\gamma\gamma_{CoReLPTt}$ [141, 142]	$\gamma\gamma_X$	$2.7^{+2.0}_{-2.0}$
$\gamma\gamma_{CoReHPTt}$ [141, 142]	$\gamma\gamma_X$	$-1.6^{+2.9}_{-2.9}$
$\gamma\gamma_{CoTr}$ [141, 142]	$\gamma\gamma_X$	$0.3^{+3.6}_{-3.6}$
$\gamma\gamma_{2j}$ [141, 142]	$\gamma\gamma_X$	$2.7^{+1.9}_{-1.9}$
$\gamma\gamma_{LepTag}$ [142]	$\gamma\gamma_X$	-
$\tau\tau$ [138, 140]	I	$0.3^{+1.7}_{-1.8}$
bb [137, 138]	A	$-2.7^{+1.6}_{-1.6}$
WW [138, 140]	I	$0.5^{+0.6}_{-0.6}$
ZZ [131, 138]	I	$1.1^{+1.0}_{-0.7}$

At the one loop level we get the following additional contributions to the effective potential from top squark loops,

$$\Delta\lambda_2 = \frac{y_t^4}{32\pi^2}(6(2 + c_{21}l_s)l_s + (1 + c_{21}l_s)x_t a_t y_t^4(12 - x_t a_t))$$

$$\Delta\lambda_5 = -\frac{y_t^4}{32\pi^2}(1 + c_{11}l_s)(\tilde{\mu})^2 x_t^2 y_t^4$$

$$\Delta\lambda_7 = -\tilde{\mu}\frac{y_t^4}{32\pi^2}x_t(6 - x_t a_t)(1 + c_{31}l_s)$$

$$(4.58)$$

Table 4.2: Cut efficiencies for production modes [141, 142, 179] of the channels of table 4.1. Numbers in brackets give the efficiencies at 8 TeV, the others at 7 TeV and the overall normalization in each line factorizes.

i	ζ_G^i	ζ_{VBF}^i	ζ_{WH}^i	ζ_{ZH}^i	ζ_{ttH}^i
$\gamma\gamma_0$	0.28(0.45)	1(1)	1.52(1.91)	1.52(1.91)	2.37(4.00)
$\gamma\gamma_1$	1.16(1.17)	1(1)	1.36(1.43)	1.36(1.43)	2.24(2.00)
$\gamma\gamma_2$	1.80(1.84)	1(1)	1.36(1.07)	1.36(1.07)	0(0)
$\gamma\gamma_3$	1.80(1.84)	1(1)	1.36(1.43)	1.36(1.43)	0(0)
$\gamma\gamma_{jj}$	0.029	1	0.019	0.019	0
$\gamma\gamma_{jj}$ (T)	(0.024)	(1)	(0)	(0)	(0)
$\gamma\gamma_{jj}$(L)	(0.094)	(1)	(0.064)	(0.064)	(0)
$\gamma\gamma_{UnCeLPTt}$	1.85 (1.78)	1 (1)	0.97 (0.77)	0.99 (0.87)	0.74 (0.58)
$\gamma\gamma_{UnCeHPTt}$	0.34 (0.41)	1 (1)	1.36 (0.59)	1.44 (0.77)	2.27 (1.37)
$\gamma\gamma_{UnReLPTt}$	1.90 (1.79)	1 (1)	1.11 (0.93)	1.12 (1.06)	0.76 (0.58)
$\gamma\gamma_{UnReHPTt}$	0.32 (0.41)	1 (1)	1.45 (0.69)	1.50 (0.89)	1.66 (0.97)
$\gamma\gamma_{CoCeLPTt}$	1.85 (1.78)	1 (1)	1.03 (0.77)	0.99 (0.87)	0.74 (0.58)
$\gamma\gamma_{CoCeHPTt}$	0.35 (0.43)	1 (1)	1.41 (0.65)	1.48 (0.78)	2.43 (1.44)
$\gamma\gamma_{CoReLPTt}$	1.95 (1.83)	1 (1)	1.14 (0.95)	1.15 (1.09)	0.78 (0.60)
$\gamma\gamma_{CoReHPTt}$	0.33 (0.40)	1 (1)	1.49 (0.75)	1.46 (0.91)	1.67 (1.05)
$\gamma\gamma_{CoTr}$	1.37 (1.30)	1 (1)	1.37 (0.95)	1.30 (1.09)	0.86 (0.66)
$\gamma\gamma_{2j}$	0.02	1	0.01	0.01	0.02
$\gamma\gamma_{2j}$ (H)	(0.037)	(1)	(0.010)	(0.012)	(0.018)
$\gamma\gamma_{2j}$ (L)	(0.95)	(1)	(9.3)	(9.6)	(3.8)
$\gamma\gamma_{LepTag}$	(0.65)	(1)	(359.4)	(160.2)	(551.4)
I	1	1	1	1	1
A	0	0	1	1	0
VBF	0.029	1	0.019	0.019	0
ttH	0	0	0	0	1

Here,

$$
\begin{aligned}
l_s &= \log[M_s^2/m_t^2], \quad y_t = m_t(m_t)/(v\sin\beta), \\
x_t &= (A_t - \mu\cot\beta)/M_s, \quad \tilde{\mu} = \mu/M_s, \quad \hat{E}a_t = A_t/M_s \\
c_{11} &= \frac{1}{32\pi^2}(12y_t^2 - 32g_3^2(m_t)) \\
c_{21} &= \frac{1}{32\pi^2}(6y_t^2 - 32g_3^2(m_t)) \\
c_{31} &= -\frac{1}{32\pi^2}(9y_t^2 - 32g_3^2(m_t))
\end{aligned}
\tag{4.59}
$$

For the BMSSM we get,

$$\Delta\lambda_5 = 2\epsilon_1 \qquad \Delta\lambda_6 = 2\epsilon_2 \qquad \Delta\lambda_7 = 2\epsilon_2 \tag{4.60}$$

For the D-term extension we get,

$$\Delta\lambda_1 = 2\kappa \qquad \Delta\lambda_2 = 2\kappa \qquad \Delta\lambda_3 = -2\kappa \tag{4.61}$$

Finally for the NMSSM with no doublet singlet mixing we get,

$$\Delta\lambda_4 = |\lambda_S|^2 \tag{4.62}$$

The case of NMSSM with doublet singlet mixing has been dealt with in great detail in Sec. Ê4.5.1. For F-terms from triplets we get,

$$\Delta\lambda_1 = 2|\lambda_T|^2 \qquad \Delta\lambda_2 = 2|\lambda_{\bar{T}}|^2 \tag{4.63}$$

We can now write the mass matrix elements of the CP-even sector in terms of these couplings,

$$\mathcal{M}_{12} = 2v^2[(\lambda_3 + \lambda_4)s_\beta c_\beta + \lambda_6 c_\beta^2 + \lambda_7 s_\beta^2] - m_A^2\sigma c_\beta \tag{4.64}$$

$$\mathcal{M}_{12} = 2v^2[\lambda_1 c_\beta^2 + 2\lambda_6 c_\beta s_\beta + \lambda_5 s_\beta^2] + m_A^2\sigma^2 \tag{4.65}$$

$$\mathcal{M}_{22} = 2v^2[\lambda_2 s_\beta^2 + 2\lambda_7 c_\beta s_\beta + \lambda_5 c_\beta^2] + m_A^2 c_\beta^2 \tag{4.66}$$

where we have used [155],

$$m_{12}^2 = \sigma c_\beta(m_A^2 + 2\lambda_5 v^2 + \lambda_6 t_\beta^{-1} v^2 + \lambda_7 t_\beta v^2). \tag{4.67}$$

Once we know the CP-even matrix elements we can easily find the exact coupling deviations. First we demand that the light Higgs mass,

$$m_h^2 = \frac{1}{2}\left(\mathcal{M}_{11} + \mathcal{M}_{22} - \sqrt{(\mathcal{M}_{22} - \mathcal{M}_{11})^2 - 4\mathcal{M}_{12}^2}\right) \tag{4.68}$$

is equal to 125 GeV by choosing an appropriate value of the stop mass in the MSSM, an appropriate value of g_X for the D-term extension and an appropriate value of λ for the NMSSM. Now we can compute $c_b = -\sin\alpha/\cos\beta$ and $c_t = \cos\alpha/\sin\beta$, where α is extracted from

$$\tan 2\alpha = \frac{2\mathcal{M}_{12}}{\mathcal{M}_{11} - \mathcal{M}_{22}}. \tag{4.69}$$

Chapter 5

The Renormalized Hamiltonian Truncation Method

5.1   Introduction and review

An outstanding problem in theoretical physics is to solve strongly coupled Quantum Field Theories (QFT). When they are not amenable to analytic calculations one can resort to numerical approaches. The two most used numerical approaches are lattice simulations and direct diagonalization of truncated Hamiltonians. In this paper we further develop the Hamiltonian truncation method recently presented in Ref. [7,8,190], that renormalizes the truncated Hamiltonian H_T to improve the numerical accuracy.

The Hamiltonian truncation method consists in truncating the Hamiltonian H into a large finite matrix $(H_T)_{ij}$ and then diagonalizing it numerically. There is a systematic error with this approach that vanishes as the size of the truncated Hamiltonian H_T is increased. There are different versions of the Hamiltonian truncation method that mainly differ on the frame of quantization and the choice of basis in which H is truncated. Two broad categories within the Hamiltonian truncation methods are the Truncated Conformal Space Approach [191] and Discrete Light Cone Quantization [192]. A less traveled route consists in using the Fock-Space basis to truncate the Hamiltonian [7,190,193–197]. Lately there have been many advances in the Hamiltonian Truncation methods, see for instance [8,198–204].

We review the truncated Hamiltonian approach following the discussion of Ref. [7,8]. The problem we are interested in is finding the spectrum of a strongly coupled QFT. Therefore we want to solve the eigenvalue equation

$$H | \mathcal{E} \rangle = \mathcal{E} | \mathcal{E} \rangle , \tag{5.1}$$

where $H = H_0 + V$, H_0 is a solvable Hamiltonian or the free Hamiltonian and V is the potential. H_0 is diagonalized by the states $H_0 | E_n \rangle = E_n | E_n \rangle$. Suppose we are interested in studying the lowest energy states of the theory. One way to do it is separating the Hilbert space $\mathcal{H}$ into $\mathcal{H} = \mathcal{H}_l \oplus \mathcal{H}_h$, where $\mathcal{H}_l$ is of finite dimension and it is spanned by the states

$|E_n\rangle$ with $E_n \leqslant E_T$. Then, the Hilbert space $\mathcal{H}_h$ is an infinite-dimensional Hilbert space containing the rest of the states $E_n > E_T$. The states are projected as $P_l|x\rangle \equiv |x_l\rangle \in \mathcal{H}_l$ and $(\mathbb{I} - P_l)|x\rangle = P_h|x\rangle \equiv |x_h\rangle \in \mathcal{H}_h$. Then, the eigenvalue problem can be replaced by

$$H_{eff}(\mathcal{E})|\mathcal{E}_l\rangle = \mathcal{E}|\mathcal{E}_l\rangle \,, \tag{5.2}$$

where $H_{eff} \equiv H_T + \Delta H(\mathcal{E})$, the truncated Hamiltonian is $H_T = P_l H P_l$ and

$$\Delta H(\mathcal{E}) = V_{lh} \frac{1}{\mathcal{E} - H_{0\,hh} - V_{hh}} V_{hl} \,, \tag{5.3}$$

with $O_{ij} \equiv P_i O P_j$ for $i, j \in \{h, l\}$. To derive Eq. (5.2), project Eq. (5.1) into the two equations

$$H_{ll}|\mathcal{E}_l\rangle + H_{lh}|\mathcal{E}_h\rangle = \mathcal{E}|\mathcal{E}_l\rangle \,, \qquad H_{hl}|\mathcal{E}_l\rangle + H_{hh}|\mathcal{E}_h\rangle = \mathcal{E}|\mathcal{E}_h\rangle \,, \tag{5.4}$$

and then substitute $|\mathcal{E}_h\rangle = (\mathcal{E} - H_{hh})^{-1} H_{hl}|\mathcal{E}_l\rangle$ from the second equation in (5.4) into the first.

Notice that Eq. (5.2) is an exact equation and that a complete knowledge of $\Delta H(\mathcal{E})$ would render the original eigenvalue problem of Eq. (5.1) solvable by an easy numerical diagonalization. In the limit where $E_T \to \infty$ the corrections ΔH to H_T can be neglected, but it is computationally very costly to increase the size of H_T and then diagonalize it. Therefore it is interesting to calculate ΔH to improve the numerical accuracy for a given E_T. A first step to compute ΔH is to perform an expansion of Eq. (5.2) in powers of $V_{hh}(\mathcal{E} - H_0)^{-1}$,

$$\Delta H(\mathcal{E},\, E_T) = \sum_{n=0}^{\infty} \Delta H_n(\mathcal{E},\, E_T) \,, \quad \text{where} \quad \Delta H_n(\mathcal{E},\, E_T) = V_{lh} \frac{1}{\mathcal{E} - E_{hh}} \left(V_{hh} \frac{1}{\mathcal{E} - E_{hh}} \right)^n V_{hl} \,,$$

where the matrix elements of ΔH_n are given by

$$\Delta H_n(\mathcal{E})_{rs} = \sum_{j_1, \cdots, j_n - 1:\, E_{j_i} > E_T} V_{rj_1} \frac{1}{\mathcal{E} - E_{j_1}} V_{j_1 j_2} \frac{1}{\mathcal{E} - E_{j_2}} V_{j_2 j_3} \cdots V_{j_{n-2} j_{n-1}} \frac{1}{\mathcal{E} - E_{j_{n-1}}} V_{j_{n-1} s} \,, \tag{5.5}$$

in the H_0 eigenbasis and the sums run over all labels $j_1, \ldots, j_{n-1}$ of states belonging to $\mathcal{H}_h$ with r, s denoting the matrix elements (corresponding to eigenstates of H_0 with $E_s, E_r \leqslant E_T$ eigenvalues). Naively the truncation of the series in Eq. (5.5) is justified for $V_{hh}/H_{0\,hh} < 1$ which for large enough E_T and $\mathcal{E} \ll E_T$ is fulfilled, and allows to go to strong coupling. This is discussed in detail in Sec. 5.5.3. The operator ΔH depends on the exact eigenvalue and in practice the way Eq. (5.2) is solved is by diagonalizing iteratively $H_{eff}(\mathcal{E}^*)$ starting with an initial seed $\mathcal{E}^*$. It is convenient to take $\mathcal{E}^*$ close to the exact eigenvalue $\mathcal{E}$, a simple and effective choice is to take the eigenvalue obtained from diagonalizing H_T.

In Ref. [7] the ϕ^4 theory in two dimensions was studied at strong coupling using the Hamiltonian truncation method just presented in the Fock basis. There, the leading terms of ΔH_2 doing a local expansion were computed and shown to improve the results with respect to the ones found by only diagonalizing H_T. The main result of our work is to explain a way to calculate the exact corrections to ΔH at any order ΔH_n. As an example we calculate the

ΔH_2 correction and some of the ΔH_3 terms for the ϕ^4 theory in two dimensions and present various approximation schemes for a faster numerical implementation. This can be seen as an extension of the method presented in Ref. [7] which we believe to be very promising.

The paper is organized as follows. In Sec. 5.2 we introduce a general formula to compute $\Delta H_n(\mathcal{E}, E_T)$ at any order n. Then we apply the method to the ϕ^2 and ϕ^4 scalar field theories in $d = 2$ space-time dimensions which we first define in Sec. 5.3. The method is tested in Sec. 5.4 by studying the spectrum of the solvable ϕ^2 perturbation with the calculation of ΔH_2 and ΔH_3. Other numerical tests are also performed in this section. Next, in Sec. 5.5 we give the ΔH_2 correction for the ϕ^4 theory, and discuss the ΔH_3 calculation with some examples. There we also discuss the convergence of the ΔH_n expansion and compute the lowest energy levels of the theory at strong coupling. In Sec. 5.6, we conclude and outline future directions of the method that are left open. In Appendix 5.6 we introduce a simple diagrammatic representation to compute ΔH_n. Lengthy derivations and results are relegated to the Appendices 5.6 and 5.6. All the numerical calculations for this work have been done with `Mathematica`.

5.2 Calculation of ΔH at any order

In this section we present one of the main results of this paper which is the derivation of the nth-order correction ΔH_n of Eq. (5.5) to the Truncated Hamiltonian. We start by defining the operator

$$\Delta \hat{H}(\mathcal{E}) = \sum_{n=2}^{\infty} \Delta \hat{H}_n(\mathcal{E}), \quad \text{where} \quad \Delta \hat{H}_n(\mathcal{E}) = \left(V \frac{1}{\mathcal{E} - H_0} \right)^{n-1} V \tag{5.6}$$

which in the H_0 eigenbasis is given by

$$\Delta \hat{H}_n(\mathcal{E})_{rs} = \sum_{j_1, \ldots, j_{n-1}=1}^{\infty} V_{rj_1} \frac{1}{\mathcal{E} - E_{j_1}} V_{j_1 j_2} \frac{1}{\mathcal{E} - E_{j_2}} V_{j_2 j_3} \cdots V_{j_{n-2} j_{n-1}} \frac{1}{\mathcal{E} - E_{j_{n-1}}} V_{j_{n-1} s}, \tag{5.7}$$

where the indices $j_1, j_2, \ldots, j_{n-1}$ run over the states of the full Hilbert space $\mathcal{H}$. Notice that the only difference between ΔH_n and $\Delta \hat{H}_n$ is that the later receives contributions from all the eigenstates of H_0 while ΔH_n only from those with E_j energies $E_j > E_T$. This translates into the fact that each term in $\Delta H_n(\mathcal{E})$ has all the poles located at $\mathcal{E} > E_T$ as seen in Eq. (5.5).

From here the derivation of ΔH_n follows from the observation that Eq. (5.7) can be rewritten as the improper Fourier transform of the product of potentials restricted to positive times

$$\Delta \hat{H}_n(\mathcal{E})_{rs} = \lim_{\epsilon \to 0} (-i)^{n-1} \int_0^{\infty} dt_1 \cdots dt_{n-1} \, e^{i(\mathcal{E} - E_r + i\epsilon)(t_1 + \cdots t_{n-1})} \mathcal{T} \{ V(T_1) \cdots V(T_n) \}_{rs}, \tag{5.8}$$

where $T_k = \sum_{i=1}^{i=n-k} t_i$, $V(t) = e^{iH_0 t} V e^{-iH_0 t}$ and $\mathcal{T}$ denotes the time ordering operation [1].

---

[1] This can be seen by introducing the indentity $\mathbb{I} = \sum_n |E_n\rangle\langle E_n|$ between each pair of V's in Eq. (5.8) and integrating over all times $t_1, \ldots t_n$. Also notice that the time ordering operation is trivial because the V operators are time ordered in all the integration domain. The $\lim_{\epsilon \to 0}$ is taken at the end of the calculation.

Then, our method consists in applying the Wick theorem to Eq. (5.8) to calculate $\Delta \widehat{H}_n$ and obtaining ΔH_n by keeping only the terms of $\Delta \widehat{H}_n$ corresponding to states with $E_j > E_T$, i.e. by keeping only the terms of $\Delta \widehat{H}_n$ which have all poles above E_T. [2] In the following sections we show how to carry this procedure for the cases of the ϕ^2 perturbation and ϕ^4 theory.

5.3   Scalar theories

We study scalar theories in two space-time dimensions defined by the Minkowskian action $S = S_0 + S_I$ where

$$S_0 = \frac{1}{2} \int_{-\infty}^{\infty} dt \int_0^L dx \, : (\partial \phi)^2 - m^2 \phi^2 : , \tag{5.9}$$

$$S_I = - \int_{-\infty}^{\infty} dt \, V(\phi) = -g_\alpha \int_{-\infty}^{\infty} dt \int_0^L dx \, : \phi^\alpha : . \tag{5.10}$$

For simplicity we consider the cases where $\alpha = 2, 4$ and $m^2 > 0$. The symbol $::$ stands for normal ordering which for S_0 means that we set the vacuum energy to zero; while the interaction term is normal ordered with respect to S_0, which in perturbation theory is equivalent to renormalize to zero the UV divergences from closed loops with propagators starting and ending on the same vertex.

To study these theories using the Hamiltonian truncation method we begin by defining them on the cylinder $\mathbb{R} \times S_1$ where the circle corresponds to the space direction which we take to have a length $Lm \gg 1$, and $\mathbb{R}$ is the time. We impose periodic boundary conditions $\phi(t, x) = \phi(t, x + nL)$ for $n \in \mathbb{Z}$ on S_1. The compact space direction makes the spectrum of the free theory discrete and regularizes the infra-red (IR) divergences.

In canonical quantization the scalar operators can be expanded in terms of creation and annihilation operators as

$$\phi(x) = \sum_k \frac{1}{\sqrt{2L\omega_k}} \left(a_k e^{ikx} + a_k^\dagger e^{-ikx} \right) , \tag{5.11}$$

where $\omega_k = \sqrt{m^2 + k^2}$, $k = \frac{2\pi n}{L}$ with $n \in \mathbb{Z}$ and the creation and anihilation operators satisfy the commutation relations

$$\left[a_k, a_{k'}^\dagger \right] = \delta_{kk'} , \qquad \left[a_k, a_{k'} \right] = 0 . \tag{5.12}$$

The Hamiltonian then reads $H = H_0 + V$, where

$$H_0 = \sum_k \omega_k \, a_k^\dagger a_k \tag{5.13}$$

---

[2]This procedure can be formalized as follows. The first correction can be written as $\Delta H_2(\mathcal{E}) = \oint_{\mathcal{C}} \frac{dz}{2\pi i} \frac{\Delta \widehat{H}_2(z)}{\mathcal{E} - z}$, where $\mathcal{C}$ is any path than encircles only all the poles above E_T. For $\Delta H_3(\mathcal{E}) = \oint_{\mathcal{C}} \frac{dz}{2\pi i} \frac{1}{\mathcal{E} - z} \oint_{\mathcal{C}} \frac{dz'}{2\pi i} \frac{1}{\mathcal{E} - z'} \Delta \widehat{H}_3(z', z)$ where we have generalized the operator $\Delta \widehat{H}_3(z, z')_{rs} = -\lim_{\epsilon \to 0} \int_0^\infty dt_1 dt_2 \, e^{i(z - E_r + i\epsilon)t_1} e^{i(z' - E_r + i\epsilon)t_2} \mathcal{T} \left\{ V(T_1) V(T_2) V(T_3) \right\}_{rs}$. The generalization to the nth correction is straightforward.

and the potentials for a ϕ^2 and a ϕ^4 interaction are given by

$$V = g_2 \sum_{k_1 k_2} \frac{L\,\delta_{k_1+k_2,0}}{\sqrt{2L\omega_{k_1}}\sqrt{2L\omega_{k_2}}} \left(a_{k_1} a_{k_2} + a^\dagger_{-k_1} a_{k_2} \right) + h.c.\,, \tag{5.14}$$

and

$$V = g \sum_{k_1,k_2,k_3,k_4} \frac{L\,\delta_{\sum_{i=1}^4 k_i,0}}{\prod_{i=1}^4 \sqrt{2L\omega_{k_i}}} \left(a_{k_1} a_{k_2} a_{k_3} a_{k_4} + 4 a^\dagger_{-k_1} a_{k_2} a_{k_3} a_{k_4} + 3 a^\dagger_{-k_1} a^\dagger_{-k_2} a_{k_3} a_{k_4} \right) + h.c.\,, \tag{5.15}$$

respectivley, where $g \equiv g_4$ and $\delta_{k_1+k_2,0}$, $\delta_{\sum_{i=1}^4 k_i,0}$ stand for Kronecker deltas.

We implement the Hamiltonian truncation using the basis of H_0 eigenstates

$$| E_i \rangle = \frac{a^{\dagger\,n_N}_{k_N}}{\sqrt{n_N!}} \cdots \frac{a^{\dagger\,n_2}_{k_2}}{\sqrt{n_2!}} \frac{a^{\dagger\,n_1}_{k_1}}{\sqrt{n_1!}} | 0 \rangle\,. \tag{5.16}$$

which satisfy $\mathbb{I} = \sum_i | E_i \rangle\langle E_i |$, where $E_i = \sum_{s=1}^N n_s \sqrt{k_s^2 + m^2}$ and $H_0 | 0 \rangle = 0$. The Hilbert space is divided into $\mathcal{H} = \mathcal{H}_l \oplus \mathcal{H}_h$ with $\mathcal{H}_l$ spanned by the states $| E_r \rangle$ such that $E_i \leqslant E_T$ while $\mathcal{H}_h$ is spanned by the rest of the basis. Then, the truncated Hamiltonian is

$$(H_T)_{rs} = \langle E_r | H | E_s \rangle\,, \quad \text{for} \quad E_i \leqslant E_T\,. \tag{5.17}$$

In this basis, the operator ΔH is given by

$$\Delta H(\mathcal{E})_{rs} = \sum_{j,j'} V_{rj} \left(\frac{1}{\mathcal{E} - H_0 - V} \right)_{jj'} V_{j's} \tag{5.18}$$

where the labels r, s denote entries with $E_r, E_s \leqslant E_T$ and the sum over j, j' runs over all states with $E_j, E_{j'} > E_T$.

The Hamiltonian H can be diagonalized by sectors with given quantum numbers associated with operators that commute with H. These are the total momentum P, the spatial parity $\mathcal{P} : x \to -x$ and the field parity $\mathbb{Z}_2 : \phi(x) \to -\phi(x)$, which act on the H_0-eigenstates as $P| E_i \rangle = \sum_s n_s k_s | E_i \rangle$, $\mathcal{P} \prod_{i=1}^N \frac{a^{\dagger\,n_i}_{k_i}}{\sqrt{n_i!}} | 0 \rangle = \prod_{i=1}^N \frac{a^{\dagger\,n_i}_{-k_i}}{\sqrt{n_i!}} | 0 \rangle$ and $\mathbb{Z}_2 | E_i \rangle = (-1)^{\sum_s n_s} | E_i \rangle$. We work in the orthonormal basis of eigenstates of H_0, P, $\mathcal{P}$ and $\mathbb{Z}_2$ given by

$$| \widetilde{E}_i \rangle = \beta \cdot \left(| E_i \rangle + \mathcal{P} | E_i \rangle \right)\,, \tag{5.19}$$

where $\beta = 1/2,\ 1/\sqrt{2}$ for $\mathcal{P} | E_i \rangle = | E_i \rangle$ and $\mathcal{P} | E_j \rangle \neq | E_j \rangle$, respectively. As done in Ref. [7], in the whole paper we focus on the sub-sector with total momentum $P| \widetilde{E}_i \rangle = 0$, spatial parity $\mathcal{P} | \widetilde{E}_i \rangle = +| \widetilde{E}_i \rangle$ and diagonalize separately the $\mathbb{Z}_2 = \pm$ sectors. [3] In this paper we do not investigate the dependence of the spectrum as a function of the length L of the compact dimension which we leave for future work, and always consider it to be finite. [4] All the numerical calculations are done for $m = 1$ and $L = 10$.

---

[3] For the $V = \int dt : \phi^2 :$ theory, the matrix element $\langle E_i | V | E_j \rangle = 0$ with $\mathcal{P} | E_i \rangle = | E_i \rangle$ and $\mathcal{P} | E_j \rangle \neq | E_j \rangle$. Therefore, one can diagonalize the $\mathcal{P} | E_i \rangle = | E_i \rangle$ and $\mathcal{P} | E_i \rangle \neq | E_i \rangle$ sectors separately.

[4] To match the $L \to \infty$ spectrum one has to take into account the Casimir energy difference between the $L \to \infty$ and the finite L theory and inspect how various states converge as L is increased. See Refs. [205, 206] and Ref. [7] for a thorough study of the L dependence.

5.4   Case study ϕ^2 perturbation

In this section we apply the method introduced in Sec. 5.2 to the scalar theory $H = H_0 + V$ with a potential

$$V = g_2 \int_0^L dt \; : \phi^2 : \tag{5.20}$$

This is a simple theory that allows to illustrate various aspects of the calculation of $\Delta \hat{H}$ in Eq. (5.8) and its relation to ΔH. Also since the theory is solvable we can compare our procedure with the exact results. The theory is solved by using the eigenstates of H, given by

$$| \mathcal{E}_i \rangle = \frac{b_{k_N}^{\dagger \, n_N}}{\sqrt{n_N!}} \cdots \frac{b_{k_2}^{\dagger \, n_2}}{\sqrt{n_2!}} \frac{b_{k_1}^{\dagger \, n_1}}{\sqrt{n_1!}} | \Omega \rangle \, , \tag{5.21}$$

where $| \Omega \rangle = | \mathcal{E}_0 \rangle$ is the vacuum of the theory and $b^\dagger/b$ are the creation/annihilation operators so that

$$H = \sum_k b_k^\dagger b_k \Omega_k + \mathcal{E}_0 \, , \tag{5.22}$$

with $\Omega_k = \sqrt{\omega_k^2 + 2g_2}$. Then, one can relate the operators $b^\dagger/b$ to the $a^\dagger/a$ in H_0 (given in Eq. (5.13) and Eq. (5.14)) by the Bogolyubov transformation $b_k = \sinh \alpha_k \, a_{-k}^\dagger + \cosh \alpha_k \, a_k$ provided that $\Omega_k \sinh 2\alpha_k = \omega_k^{-1} g_2$, $\Omega_k \cosh 2\alpha_k = \omega_k + g_2/\omega_k$. Then, since $\langle 0 | H | 0 \rangle = 0$ we have that [7]:

$$\mathcal{E}_0(g_2) = \frac{1}{2} \sum_k \left(\sqrt{\omega_k^2 + 2g_2} - \omega_k - \frac{g_2}{\omega_k} \right) = \frac{L(m^2 + 2g_2)}{8\pi} \left[\log \left(\frac{m^2}{m^2 + 2g_2} \right) + \frac{2g_2}{m^2 + 2g_2} \right], \tag{5.23}$$

where the sum can be done by means of the Abel-Plana formula, which is the exact vacuum energy of the theory.

A brief summary of the rest of this section is the following. In Sec. 5.4.1 and Sec. 5.4.2 we calculate the 2 and 3-point corrections to the operator ΔH. In Sec. 5.4.3 we perform a numerical test to check that our expressions for ΔH are correct. Then, in Sec. 5.4.4 we discuss the numerical results and the convergence of the expansion $\Delta H(\mathcal{E}_i) = \sum_n \Delta H_n(\mathcal{E}_i)$ by comparing with the exact spectrum $\mathcal{E}_i$.

5.4.1   Two-point correction

Following the steps explained in Sec. 5.2 we begin the calculation of the two-point correction by first computing $\Delta \hat{H}_2$. From Eq. (5.8) we have that

$$\Delta \hat{H}_2(\mathcal{E})_{rs} = \sum_j V_{rj} \frac{1}{\mathcal{E} - E_j} V_{js} = \lim_{\epsilon \to 0} -i \int_0^\infty dt \, e^{i(\mathcal{E} - E_r + i\epsilon)t} \mathcal{T} \{ V(t) V(0) \}_{rs} \, . \tag{5.24}$$

Then, applying the Wick theorem to Eq. (5.24) we find

$$\lim_{\epsilon \to 0} -i g_2^2 \int_0^\infty dt \, e^{i(\mathcal{E} - E_r + i\epsilon)t} \int_{-L/2}^{L/2} dx dz \sum_{m=0}^2 s_{2-m} D_F^{2-m}(z, t) : \phi^m(x + z, t) \phi^m(x, 0) :_{rs} \, , \tag{5.25}$$

where $s_p = \binom{2}{p}^2 p!$ are the symmetry factors and $D_F(z,t)$ is the Feynman propagator with discretized momenta. Henceforth we label the terms $m = 0, 1, 2$ by $\Delta\widehat{H}_2^{\phi^{2m}}$ so that $\Delta\widehat{H}_2 = \Delta\widehat{H}_2^{\mathbb{1}} + \Delta\widehat{H}_2^{\phi^2} + \Delta\widehat{H}_2^{\phi^4}$ and similarly for ΔH_2; the labels only inform about the total number of fields in each term which do not need to be local. Due to the time integration domain, it is convenient to use *half* Feynman propagator

$$D_L(z,t) \equiv D_F(z,t)\theta(t) = \frac{1}{2L}\sum_{n=-\infty}^{n=\infty}\frac{1}{\omega_k}e^{-i\omega_k t}e^{i\frac{2\pi n z}{L}}\theta(t)\,, \tag{5.26}$$

the momentum of the propagator is discretised due to the finite extent of the space. Next, we proceed to calculate the operators in Eq. (5.25), starting with the detailed calculation of the coefficient of the identity operator $\Delta\widehat{H}_2^{\mathbb{1}}$:

$$\Delta\widehat{H}_2^{\mathbb{1}}(\mathcal{E})_{rs} = \lim_{\epsilon\to 0} -is_2 g_2^2 \int_0^\infty dt \int_{-L/2}^{L/2} dz\ e^{i(\mathcal{E}-E_r+i\epsilon)t_1}D_L^2(t,z)\,\mathbb{1}_{rs}\,, \tag{5.27}$$

where $\mathbb{1}_{rs} \equiv \delta_{rs}\int_{-L/2}^{L/2}dz$ has dimensions of $[E]^{-1}$. Then, upon inserting the propagator of Eq. (5.26) and performing the space-time integrals we find

$$\Delta\widehat{H}_2^{\mathbb{1}}(\mathcal{E})_{rs} = \frac{s_2 g_2^2}{4L}\sum_k \frac{1}{\omega_k^2}\frac{1}{\mathcal{E}-E_r-2\omega_k}\,\mathbb{1}_{rs}\,. \tag{5.28}$$

The operator in Eq. (5.28) has poles from all possible intermediate states and, as explained in Sec. 5.2, the operator $\Delta H_2^{\mathbb{1}}(\mathcal{E})$ is found by keeping only those terms with poles located at $E_r + 2\omega_k > E_T$, therefore

$$\Delta H_2^{\mathbb{1}}(\mathcal{E})_{rs} = \frac{s_2 g_2^2}{L}\sum_{k:\, E_r+2\omega_k>E_T}\frac{1}{4\,\omega_k^2}\frac{1}{\mathcal{E}-E_r-2\omega_k}\,\mathbb{1}_{rs}\,. \tag{5.29}$$

The calculations of $\Delta H_2^{\phi^2}$ is similar to the one for Eq. (5.29), we start by computing

$$\Delta\widehat{H}_2^{\phi^2}(\mathcal{E})_{rs} = \lim_{\epsilon\to 0} -is_1 g_2^2 \int_0^\infty dt \int_{-L/2}^{L/2} dxdz\ e^{i(\mathcal{E}-E_r+i\epsilon)t_1}D_L(z,t)\,:\phi(x+z,t)\phi(x,0):_{rs}\,, \tag{5.30}$$

where we expand $:\phi(x+z,t)\phi(x,0):$ in modes, as in Eq. (5.11), and do the simple space-time integrals. For the full expressions of $\Delta\widehat{H}_2^{\phi^2}$ see Appendix 5.6. Then, keeping only the terms with poles at $\mathcal{E} > E_T$ we get

$$\Delta H_2^{\phi^2}(\mathcal{E})_{rs} = s_1 g_2^2 \sum_{q:\, 2\omega_q+E_r>E_T}\frac{1}{4\,\omega_q^2}\frac{1}{\mathcal{E}-E_r-2\omega_q}(a_q^\dagger a_q)_{rs}\,. \tag{5.31}$$

The operator $\Delta H_2^{\phi^4}$ is obtained in a similar way,

$$\Delta H_2^{\phi^4}(\mathcal{E})_{rs} = s_0 g_2^2 \sum_{q_1,q_2:\, 2\omega_{q_2}+E_r>E_T}\frac{1}{4\,\omega_{q_2}\omega_{q_1}}\frac{1}{\mathcal{E}-E_r-2\omega_{q_2}}\left(a_{q_1}^\dagger a_{-q_1}^\dagger a_{q_2}a_{-q_2}\right)_{rs}\,. \tag{5.32}$$

In Appendix 5.6 we give a simple way to derive these expressions from diagrams, and for the full expressions of $\Delta \hat{H}_2^{\phi^2}$ and $\Delta \hat{H}_2^{\phi^4}$ see Appendix 5.6. Notice that the values of q_1, q_2 and q appearing in the sums of Eq. (5.31) and Eq. (5.32) can take only the momenta of the states $|E_s\rangle \in \mathcal{H}_l$ on which a and $a^\dagger$ act, and therefore are bounded. On the other hand, the values of the k's in Eq. (5.29) go all the way to infinity. Also, even though the operators in Eq. (5.31) and Eq. (5.32) may seem not hermitian due to the E_r appearing in the expressions, one can see that the operator $(\Delta H_2^{\phi^2})_{rs}$ is diagonal and therefore $E_r = E_s$, while $\Delta H_2^{\phi^4}$ is not diagonal, but one can check that $E_r + 2\omega_{q_2} = E_s + 2\omega_{q_1}$, making it hermitian as well.

We end this section by noticing that the operator of Eq. (5.29) can be rewritten as

$$(\Delta H_2^{\mathbb{1}})_{rs} = \int_{E_T}^{\infty} \frac{dE}{\mathcal{E} - E} \frac{s_2 g_2^2}{L} \sum_{k=-\infty}^{\infty} \frac{\delta(E - E_r - 2\omega_k)}{(2\omega_k)^2} \mathbb{1}_{rs} = s_2 g_2^2 \int_{E_T}^{\infty} \frac{dE}{2\pi} \frac{\Phi_2(E - E_r)}{\mathcal{E} - E} \mathbb{1}_{rs}, \tag{5.33}$$

where Φ_2 is the two-particle phase space with discretized momenta,

$$\Phi_2(E - E_r) = \sum_{k_1,k_2} \frac{L\,\delta_{k_1+k_2,0}}{(2L\omega_{k_1})(2L\omega_{k_2})} 2\pi\,\delta(E - E_r - \omega_{k_1} - \omega_{k_2}), \tag{5.34}$$

where from Eq. (5.33) one has that $E - E_r > 2m$. [5] Eq. (5.33) can be evaluated by means of the Abel-Plana formula, which for $LE_T \gg 1$ is well approximated by its continuum limit [6]. The continuum two-body phase space is given by

$$\Phi_2(E) = \int_{-\infty}^{\infty} \frac{d^2 p_1}{(2\pi)^2\, 2\omega_{p_1}} \frac{d^2 p_2}{(2\pi)^2\, 2\omega_{p_2}} (2\pi)^2\, \delta^{(2)}(P^\mu - p_1 - p_2) = \frac{1}{E\sqrt{E^2 - 4m^2}}, \tag{5.35}$$

where $P^\mu = (E, 0)$ and $E > 2m$. Therefore (for $LE_T \gg 1$) we find

$$\Delta H_2^{\mathbb{1}}(\mathcal{E})_{rs} \simeq s_2 g_2^2 \int_{E_T}^{\infty} \frac{dE}{2\pi} \frac{1}{\mathcal{E} - E} \frac{1}{E - E_r} \frac{1}{\sqrt{(E - E_r)^2 - 4m^2}} \theta(E - E_r - 2m)\, \mathbb{1}_{rs}. \tag{5.36}$$

This result is useful for numerical implementation since Eq. (5.36) can be integrated in terms of logarithmic functions. Finally, we notice that upon expanding the function $s_2/(2\pi)\Phi_2(E)$ around $m/E = 0$ we find agreement with Ref. [7] that computed it by other means (there called $\mu_{220}(E) = 1/(\pi E^2)$).

5.4.2   Three-point correction

The calculation of the three-point correction ΔH_3 also starts from the expression in Eq. (5.8)

$$\Delta \hat{H}_3(\mathcal{E})_{rs} = -\lim_{\epsilon \to 0} \int_0^{\infty} dt_1 dt_2\, e^{i(\mathcal{E} - E_r + i\epsilon)(t_1 + t_2)} \mathcal{T}\{V(T_1)V(T_2)V(T_3)\}_{rs}, \tag{5.37}$$

---

[5] The lower limit in Eq. (5.33) should be taken slightly above E_T to reproduce the lower limit $q : 2\omega_q + E_r > E_T$ in the sum of Eq. (5.28).

[6] The difference between the continuum limit and discrete result ranges from $\mathcal{O}(g^2 L^{-1} E_T^{-3})$ to $\mathcal{O}(g^2 L^{-1} E_T^{-1} m^{-2})$ depending on the matrix entry.

where $T_k = \sum_{n=1}^{3-k} t_n$. Next we apply the Wick theorem and find that the time ordered product $\mathcal{T}\{V(T_1)V(T_2)V(T_3)\}$ is given by

$$
g_2^3 \int_{-L/2}^{L/2} dx_1 dx_2 dz \sum_{m,n,v=0}^{2} s_2^{mnv} D_F^m(x_1,t_1) D_F^n(x_2,t_2) D_F^v(x_1+x_2,t_1+t_2) : \phi_{X_1,T_1}^{2-n-m} \phi_{X_2,T_2}^{2-n-v} \phi_{X_3,T_3}^{2-v-m} :
$$
(5.38)

where we have introduced the notation $X_k = z + \sum_{n=1}^{3-k} x_n$ and $\phi_{x,t} = \phi(x,t)$; while the symmetry factor is given by

$$
s_p^{mnv} = \frac{p!^3}{(p-m-n)!(p-m-v)!(p-n-v)!m!n!v!}.
$$
(5.39)

We use the same notation as in the previous section $\Delta\hat{H}_3 = \Delta\hat{H}_3^{\mathbb{1}} + \Delta\hat{H}_3^{\phi^2} + \Delta\hat{H}_3^{\phi^4} + \Delta\hat{H}_3^{\phi^6}$, and similarly for ΔH_3. Then, upon performing the space-time integrals in Eq. (5.38) and only keeping the terms with all the poles above E_T we find ΔH_3. Then, for the term $\Delta H_3^{\mathbb{1}}$ we get

$$
\Delta H_3^{\mathbb{1}}(\mathcal{E})_{rs} = s_2^{111} g_2^3 \frac{1}{L} \sum_{k:E_{rs}+2\omega_k>E_T} \frac{1}{(2\omega_k)^3} \frac{1}{(\mathcal{E}-E_r-2\omega_k)^2} \mathbb{1}_{rs}.
$$
(5.40)

The expressions for $\Delta H_3^{\phi^2}$, $\Delta H_3^{\phi^4}$ and $\Delta H_3^{\phi^6}$ are lengthy but straightforward to obtain and are relegated to Appendix 5.6.

As done in the previous section, Eq. (5.40) can be written as

$$
\Delta H_3^{\mathbb{1}}(\mathcal{E})_{rs} = s_2^{111} g_2^3 \int_{E_T}^{\infty} \frac{dE}{(\mathcal{E}-E)^2} \frac{1}{L} \sum_k \frac{1}{(2\omega_k)^3} \delta(E-E_r-2\omega_k) \mathbb{1}_{rs},
$$
(5.41)

which for $L^{-1} E_T \gg 1$ is well approximated by its continuum limit

$$
\Delta H_3^{\mathbb{1}}(\mathcal{E})_{rs} \simeq s_2^{111} \frac{g_2^3}{2\pi} \int_{E_T}^{\infty} \frac{dE}{(\mathcal{E}-E)^2} \frac{1}{(E-E_r)^2} \frac{1}{\sqrt{(E-E_r)^2-4m^2}} \mathbb{1}_{rs},
$$
(5.42)

and can be integrated in terms of logarithmic functions. This is useful for a fast numerical implementation.

5.4.3 A numerical test

We perform a numerical check to test our prescription to select the poles of $\Delta\hat{H}_n(\mathcal{E})$ to get ΔH_n, i.e. that we can select the desired intermediate states of H_0 by looking at the poles of the terms of $\Delta\hat{H}_n$. The check consists in computing $\Delta\hat{H}_2$ as explained, and then selecting only the terms with all poles at $\mathcal{E} \leqslant E_T$. We refer to the expression as ΔH_n^{ll} to differentiate it with ΔH_n that only receives corrections from terms with poles at $\mathcal{E} > E_T$. ΔH_2^{ll} is then compared with the matrix elements of $V P_l(\mathcal{E}-H_0)^{-1} P_l V$, finding an exact agreement. The same is done for $\Delta\hat{H}_3(\mathcal{E})$ by comparing it against $V P_l(\mathcal{E}-H_0)^{-1} V(\mathcal{E}-H_0)^{-1} P_l V$. This check
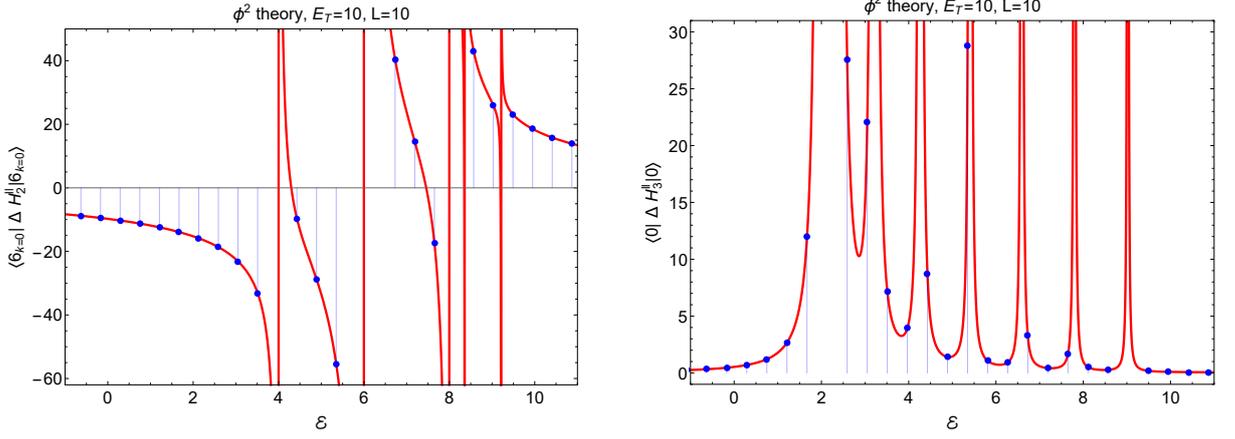
Figure 5.1: Comparison of both sides of Eqs. (5.43) and (5.44).

has been done for all the matrices used in the present work, both for ϕ^2 and ϕ^4. For brevity we only show the check for two matrix entries of the ϕ^2 theory. These are

$$\langle 6_{k=0} \,|\, V P_l \frac{1}{\mathcal{E} - H_0} P_l V \,|\, 6_{k=0} \rangle \;=\; \sum_{k:\, 2\omega_k + 6m < E_T} \frac{g_2^2}{2\,\omega_k^2} \frac{1}{\mathcal{E} - 6m - 2\omega_k}$$

$$+\; \frac{3\,g_2^2}{2m^2} \left(\frac{5}{\mathcal{E} - 4m} + \frac{24}{\mathcal{E} - 6m} + \frac{9}{\mathcal{E} - 8m} \right), \quad (5.43)$$

$$\langle 0 \,|\, V P_l \frac{1}{\mathcal{E} - H_0} V \frac{1}{\mathcal{E} - H_0} P_l V \,|\, 0 \rangle \;=\; g_2^3 \sum_{k:\, 2\omega_k < E_T} \frac{1}{\omega_k^3} \frac{1}{(\mathcal{E} - 2\omega_k)^2}. \quad (5.44)$$

In Fig. 5.1 we compare both sides of equations Eq. (5.43) and (5.44). The red curves correspond to the right hand side of Eqs. (5.43)-(5.44), which are our analytical results, and the blue dots are given by the product of the matrices in the left hand side of the equations. In the left plot, done for $\langle 6_{k=0} \,|\Delta H_2^{ll}|\, 6_{k=0} \rangle$, the first pole arises at the four-particle threshold and subsequent poles appear for higher excited states. Instead, the first pole in the right plot, done for $\langle 0 \,|\Delta H_3^{ll}|\, 0 \rangle$, occurs at $\mathcal{E} = 2m$. Notice that in both figures there are no poles for $\mathcal{E} > E_T$.

5.4.4   Spectrum and convergence

We perform a numerical study of the convergence of the energy levels as a function of the truncation energy E_T and their convergence as higher order corrections ΔH_n are calculated for a fixed E_T. We use the formulas in Eqs. (5.29)-(5.32), (5.40) and (5.6.112)-(5.6.115) to numerically compute ΔH_2 and ΔH_3. [7]

---

[7] The sums over k in Eqs. (5.29)-(5.32), (5.40) and (5.6.112)-(5.6.115) have been done with a cutoff $k = 250$. We have checked that increasing the cutoff has little impact on the results and find agreement with analytic formulas like Eq. (5.33).
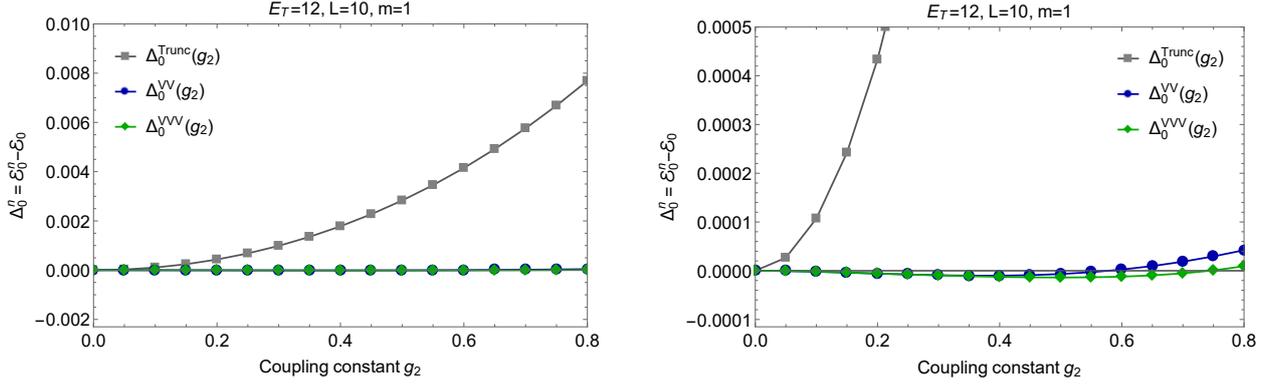
Figure 5.2: **Left:** *comparison of the exact vacuum energy with the numerical result as a function of the coupling constant g_2 (for $V = g_2 \int dx \phi^2$).* **Right:** *left plot with the y-axis zoomed in a factor $\times 20$.*

We begin by comparing the vacuum eigenstate $\mathcal{E}_0^i$ obtained by numerically diagonalizing $H_T + \sum_{n=2}^{N} \Delta H_n$ (for $N = 2$ and 3) with the exact vacuum energy $\mathcal{E}_0$. In Fig. 5.2 we show a plot of $\Delta_0^i = \mathcal{E}_0^i - \mathcal{E}_0$ as a function of the coupling constant g_2. The plot is done for a truncation energy of $E_T = 12$ and $L = 10$ (recall that we work in $m = 1$ units). For an easier comparison with previous work, these plots have been done with the same choice of parameters and normalizations as in Fig. 2 of Ref. [7]. The gray curve in Fig. 5.2 is obtained by numerically diagonalizing H_T, whose lowest eigenvalue is $\mathcal{E}_0^{\mathrm{T}}$. The blue curve is obtained by diagonalizing the renormalized hamiltonian $H_T + \Delta H_2(\mathcal{E}_0^{\mathrm{T}})$, whose lowest eigenvalue is $\mathcal{E}_0^{VV}$. Lastly, the green curve is obtained by diagonalizing $H_T + \Delta H_2(\mathcal{E}_0^{VV}) + \Delta H_3(\mathcal{E}_0^{VV})$ (we find little difference in evaluating the latter operator in $\mathcal{E}_0^{\mathrm{Trunc}}$ instead of $\mathcal{E}_0^{VV}$). The right plot of Fig. 5.2 is a zoomed in version of the left plot in order to resolve the difference between the Δ_0^{VV} and Δ_0^{VVV} curves.

The right plot shows that overall Δ_0^{VVV} performs better than Δ_0^{VV}, this indicates that the truncation of the series expansion $\Delta H = \sum_{n=2}^{\infty} \Delta H_n$ at $n = 3$ is perturbative in the studied range. The effect is more pronounced for the highest couplings $g_2 \simeq [0.6, 0.8]$. As a benchmark value $\mathcal{E}_0(g_2 = 0.8) = -0.351864$, see Eq. (5.23). Therefore the relative error at $g_2 = 0.8$ is 2%, 0.01% and 0.002% for the Truncated, the VV and the VVV corrections, respectively.

Next, we check the convergence of the energy levels as a function of the truncation energy E_T. In Fig. 5.3, in the left plot we show $\Delta_0^i = \mathcal{E}_0^i - \mathcal{E}_0$ as a function of the truncation energy E_T, for $i =$ Trunc, VV and VVV. Both the Δ_0^{VV} and Δ_0^{VVV} curves give better results than $\Delta_0^{\mathrm{Trunc}}$ for the whole range. Also, the curves Δ_0^{VV} and Δ_0^{VVV} have a better convergence behavior and, when converged, they are closer to zero than $\Delta_0^{\mathrm{Trunc}}$. The right plot is a zoomed in version to resolve the difference between Δ_0^{VV} and Δ_0^{VVV}. The plot shows that for $E_T \lesssim 15$ the curve Δ_0^{VV} gives better results than Δ_0^{VVV} while for larger E_T the behavior is reversed. This indicates that for $E_T \lesssim 15$ (and $g_2 = 1.8$) the truncation of the series $\Delta H = \sum_{n=2}^{\infty} \Delta H_n$ is not a good approximation, and adding more terms will not improve the accuracy. However,
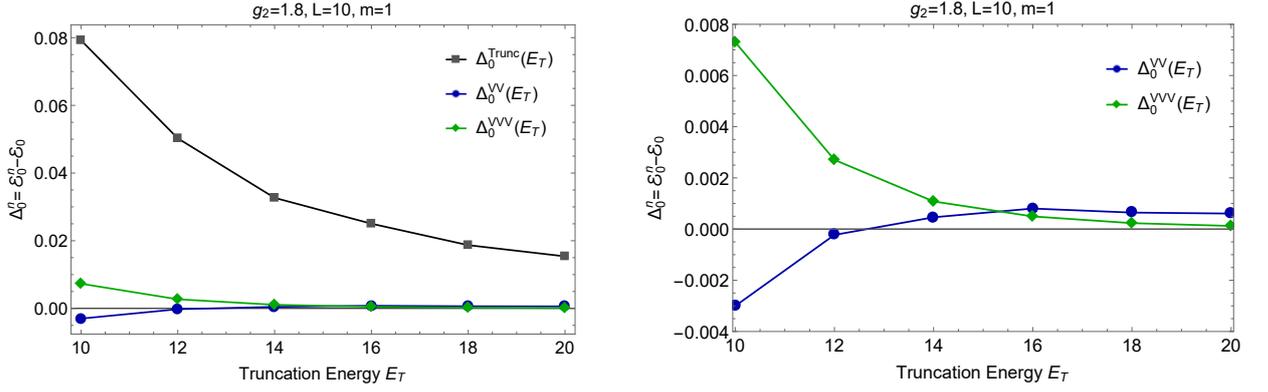
Figure 5.3: ***Left:*** *comparison of the exact vacuum energy with the numerical result as a function of the truncation energy E_T.* ***Right:*** *left plot zoomed in.*

as E_T is increased it pays off to introduce higher order corrections to get a better result. This is because Δ_0^{VVV} has a faster converge rate than Δ_0^{VV} to the real eigenvalue. The value is $\mathcal{E}_0(g_2 = 1.8) = -1.360719$, see Eq. (5.23). Therefore the relative error at $E_T = 20$ is 1%, 0.04% and 0.009% for the Truncated, the VV and the VVV corrections, respectively.
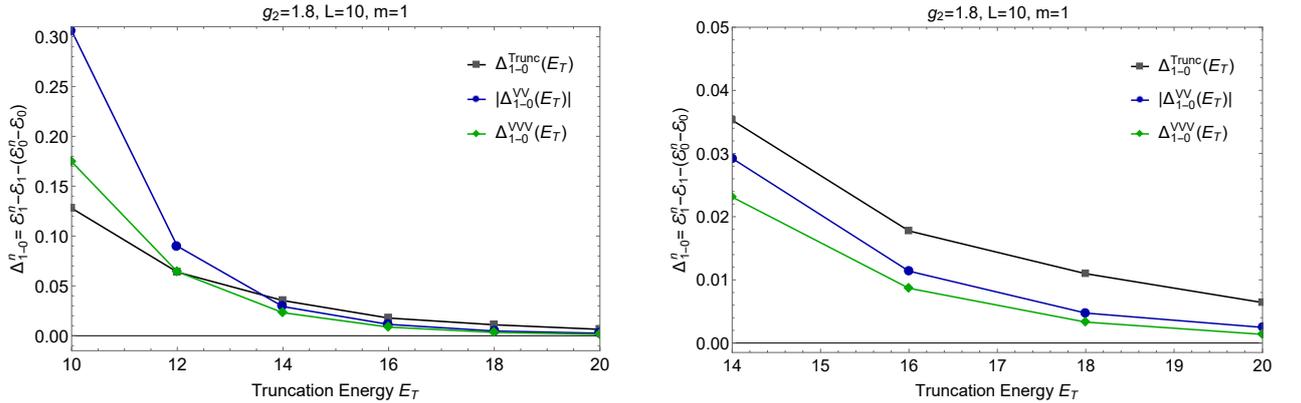

Figure 5.4: ***Left:*** *comparison of the exact energy difference $\mathcal{E}_1 - \mathcal{E}_0$ with respect the numerical result as a function of the truncation energy E_T.* ***Right:*** *left plot zoomed in. On both plots we have taken the absolute value of the curve corresponding to the VV corrections, in blue.*

In Fig. 5.4 we repeat the plots of Fig. 5.3 for the first $\mathbb{Z}_2$-even excited state but taking the absolute value of the Δ_1^{VV} curve for clarity. The plots show a similar convergence rate for the three Δ_1^i curves. However, there is a similar pattern compared to Fig. 5.3: for $E_T \lesssim 15$ introducing higher order corrections of the series $\Delta H = \sum_{n=2}^{\infty} \Delta H_n$ gives worse results, while for larger values of E_T adding higher ΔH_n corrections improves them. The value is $\mathcal{E}_1(g_2 = 1.8) = 0.784042$, hence the relative error at $E_T = 20$ is 0.8%, 0.3% and 0.17% for the Truncated, the VV and the VVV corrections, respectively.

5.5 The ϕ^4 theory

Next we apply the method presented in previous sections to the ϕ^4 theory. We start by deriving the exact expressions for ΔH_2 in detail, then we perform various useful approximations for a faster numerical implementation and discuss general aspects of the method. We also discuss the pertubativity of the ΔH_n expansion and compute the spectrum of the theory at different couplings while studying its behaviour in E_T and g using the results of ΔH_2. We end the section with some comments on future work and a discussion of the calculation of ΔH_3.

5.5.1 Two-point correction

Again, we follow Sec. 5.2 to derive ΔH by first computing $\Delta \widehat{H}$. From Eq. (5.8) we have

$$\Delta \widehat{H}_2(\mathcal{E})_{rs} = \sum_j V_{rj} \frac{1}{\mathcal{E} - E_j} V_{js} = \lim_{\epsilon \to 0} -i \int_0^\infty dt\, e^{i(\mathcal{E} - E_r + i\epsilon)t} \mathcal{T} \left\{ V(t) V(0) \right\}_{rs} . \tag{5.45}$$

It is convenient to re-write the two-point correction in the following equivalent form

$$\Delta \widehat{H}_2(\mathcal{E})_{rs} = \sum_j V_{rj} \frac{1}{\mathcal{E} - E_j} V_{js} = \lim_{\epsilon \to 0} -i \int_0^\infty dt\, e^{i(\mathcal{E} - E_{rs} + i\epsilon)t} \mathcal{T} \left\{ V(t/2) V(-t/2) \right\}_{rs} , \tag{5.46}$$

where $E_{rs} = (E_r + E_s)/2$. Applying the Wick theorem we find

$$-ig^2 \int_0^\infty dt\, e^{i(\mathcal{E} - E_{rs} + i\epsilon)t} \int_{-L/2}^{L/2} dx dz \sum_{m=0}^4 s_{4-m} D_F^{4-m}(z,t) : \phi^m(x+z, t/2) \phi^m(x, -t/2) :_{rs} , \tag{5.47}$$

where $s_p = \binom{4}{p}^2 p!$ are the symmetry factors. By integrating Eq. (5.47) and keeping only the contributions from high energy intermediate states $E_j > E_T$ we obtain the exact expression for ΔH_2. We use the shorthand notation $\Delta H_2 = \Delta H_2^{\mathbb{1}} + \Delta H_2^{\phi^2} + \Delta H_2^{\phi^4} + \Delta H_2^{\phi^6} + \Delta H_2^{\phi^8}$ for $m = 0, 1, 2, 3, 4$, and similarly for $\Delta \widehat{H}_2$. For $\Delta H_2^{\mathbb{1}}$, $\Delta H_2^{\phi^2}$ we obtain:

$$\Delta H_2^{\mathbb{1}}(\mathcal{E}, E_T) = \frac{s_4 g^2}{2^4 L^2} \sum_{k_1 k_2 k_3 k_4} \frac{1}{\omega_{k_1} \omega_{k_2} \omega_{k_3} \omega_{k_4}} F_0(k_1, k_2, k_3, k_4, \mathcal{E}, E_T) , \tag{5.48}$$

$$\Delta H_2^{\phi^2}(\mathcal{E}, E_T) = \frac{s_3 g^2}{2^4 L^2} \sum_{k_1, k_2, k_3} \sum_{q_1, q_2} \frac{1}{\omega_{k_1} \omega_{k_2} \omega_{k_3}} \frac{1}{\sqrt{\omega_{q_1} \omega_{q_2}}} F_2(k_1, k_2, k_3, q_1, q_2, \mathcal{E}, E_T) , \tag{5.49}$$

where $F_0(k_1, k_2, k_3, k_4, \mathcal{E}, E_T)$ is given by

$$F_{0\,rs} = \delta_{\Sigma_{i=1}^4 k_i, 0} \frac{\theta(\omega_{k_1} + \omega_{k_2} + \omega_{k_3} + \omega_{k_4} + E_{rs} - E_T)}{\mathcal{E} - \omega_{k_1} - \omega_{k_2} - \omega_{k_3} - \omega_{k_4} - E_{rs}} \mathbb{1}_{rs} , \tag{5.50}$$

and the operator $F_2(k_1, k_2, k_3, q_1, q_2, \mathcal{E}, E_T)$ is given by

$$
\begin{aligned}
F_{2\,rs} &= \delta_{k_1+k_2+k_3, q_1}\, \delta_{q_1, -q_2} \frac{\theta(E_{rs} + \omega_{k_1} + \omega_{k_2} + \omega_{k_3} - E_T)}{\mathcal{E} - E_{rs} - \omega_{k_1} - \omega_{k_2} - \omega_{k_3}} (a_{q_1} a_{q_2})_{rs} \\
&+ \delta_{k_1+k_2+k_3, q_1}\, \delta_{q_1, -q_2} \frac{\theta(E_{rs} + \omega_{k_1} + \omega_{k_2} + \omega_{k_3} - E_T)}{\mathcal{E} - E_{rs} - \omega_{k_1} - \omega_{k_2} - \omega_{k_3}} (a_{q_1}^\dagger a_{q_2}^\dagger)_{rs} \\
&+ \delta_{k_1+k_2+k_3, q_2}\, \delta_{q_1, q_2} \frac{\theta(E_{rs} + \omega_{k_1} + \omega_{k_2} + \omega_{k_3} + \omega_q - E_T)}{\mathcal{E} - E_{rs} - \omega_{k_1} - \omega_{k_2} - \omega_{k_3} - \omega_q} (a_{q_1}^\dagger a_{q_2})_{rs} \\
&+ \delta_{k_1+k_2+k_3, q_2}\, \delta_{q_1, q_2} \frac{\theta(E_{rs} + \omega_{k_1} + \omega_{k_2} + \omega_{k_3} - \omega_q - E_T)}{\mathcal{E} - E_{rs} - \omega_{k_1} - \omega_{k_2} - \omega_{k_3} + \omega_q} (a_{q_1}^\dagger a_{q_2})_{rs}\,.
\end{aligned}
\tag{5.51}
$$

In Eqs. (5.48)-(5.49), all q_i's are bounded from above ($q_i \leqslant q_{max}$) because they correspond to the momenta of creation/annihilation operators that act on the light states (i.e. states in $\mathcal{H}_l$). Instead the $k_i = 2\pi n_i/L$ run over all possible values $n_i \in \mathbb{Z}$. Similar expressions for $\Delta H_2^{\phi^4}$, $\Delta H_2^{\phi^6}$, $\Delta H_2^{\phi^8}$ are given in Appendix 5.6. As mentioned before, a simple way to derive these expressions from diagrams is given in Appendix 5.6. We have performed the same kind of numerical checks done in Sec. 5.4.3 for all the operators $\Delta \hat{H}_2$ in the ϕ^4 theory.

Approximations

The exact expressions for ΔH_2 are computationally demanding. Here we present different approximations that speed up the calculations and simplify their analytic structure. These basically consist in approximating the contribution from the highest energy states to ΔH in terms of a local expansion (as normally done in Effective Field Theory calculations), while keeping the contributions from lower energy states in their original non-local form. This is achieved by defining an energy E_L and then by separating ΔH_2 into two parts, ΔH_{2+} where we only sum over intermediate states with $E_j \geqslant E_L$ and ΔH_{2-} where we sum over those with $E_T < E_j < E_L$.

$$
\Delta H_{2+}(\mathcal{E}, E_L)_{rs} = \Delta H_2(\mathcal{E}, E_L)_{rs},, \tag{5.52}
$$

$$
\Delta H_{2-}(\mathcal{E}, E_T, E_L)_{rs} = \Delta H_2(\mathcal{E}, E_T)_{rs} - \Delta H_2(\mathcal{E}, E_L)_{rs}\,. \tag{5.53}
$$

We choose $E_L \gg E_T$ so that ΔH_{2+} is well approximated by local operators [8]. As an example we show how to implement this procedure for the contribution of $\Delta H_2^{\phi^2}$ given in Eq. (5.49) and Eq. (5.51). We start by examining the term $\Delta H_{2+}^{\phi^2}(\mathcal{E}, E_L) = \Delta H_2^{\phi^2}(\mathcal{E}, E_L)$, which is obtained by replacing E_T by E_L in Eq. (5.51). In this case $\sum_i \omega_{k_i} \gtrsim E_L \gg E_T \gtrsim \omega_q, E_{rs}$, and then it can be well approximated by

$$
\Delta H_{2+}^{\phi^2} \simeq c_2\, V_2 \tag{5.54}
$$

---

[8]In the cases where we are only interested in having a good approximation for the lower energy entries r, s of the matrix, then E_L can be taken to be similar to E_T.

with

$$c_2(\mathcal{E}, E_L) = \frac{s_3 g^2}{(2L)^3} \sum_{k_1,k_2,k_3} \frac{L\,\delta_{k_1+k_2+k_3,0}}{\omega_{k_1}\omega_{k_2}\omega_{k_3}} \frac{\theta(\omega_{k_1} + \omega_{k_2} + \omega_{k_3} - E_L)}{\mathcal{E} - \omega_{k_1} - \omega_{k_2} - \omega_{k_3}}\,, \tag{5.55}$$

and $V_2 = \int_0^L dx\, \phi^2(x)$ which has dimensions of $[E]^{-1}$. The approximation in Eq. (5.54) receives corrections of at most $\mathcal{O}(E_T/E_L)$. The expansion of $\Delta H_{2+}^{\phi^2}$ in terms of local operators can be obtained by expanding the term $\Delta \hat{H}_2^{\phi^2}$ in Eq. (5.47) around $t, z = 0$

$$\Delta \hat{H}_2^{\phi^2}(\mathcal{E})_{rs} = -ig^2 s_2 \int_0^\infty dt\, e^{i(\mathcal{E}-E_{rs}+i\epsilon)t} \int_{-L/2}^{L/2} dz D_F^2(z,t) \int_{-L/2}^{L/2} dx \left[:\phi^2(x,0):_{rs} + \mathcal{O}(t^2, z^2)\right], \tag{5.56}$$

and, after integrating, keeping only the contributions from those states that produce poles at $\mathcal{E} > E_L$, when E_{rs} is neglected. On the other hand $\Delta H_{2-}^{\phi^2}(\mathcal{E}, E_T, E_L) = \Delta H_2^{\phi^2}(\mathcal{E}, E_T) - \Delta H_2^{\phi^2}(\mathcal{E}, E_L)$ is given by the same expressions as in Eq. (5.49) and Eq. (5.51) but now the sums to perform are much smaller since the momenta of the intermediate states are restricted between E_T and E_L.

The same exercise done for $\Delta H_{2+}^{\phi^2}$ can be done for $\Delta H_{2+}^{\mathbb{1}}$ and $\Delta H_{2+}^{\phi^4}$ and one has that in the limit $E_L \gg E_T$

$$\Delta H_{2+}^{\mathbb{1}} \simeq c_0\, \mathbb{1}\,, \qquad \Delta H_{2+}^{\phi^2} \simeq c_2\, V_2\,, \qquad \Delta H_{2+}^{\phi^4} \simeq c_4\, V_4\,, \tag{5.57}$$

where $V_\alpha = \int_0^L dx\, \phi^\alpha(x)$ and has dimensions of $[E]^{-1}$,

$$c_0(\mathcal{E}, E_L) = \frac{s_4 g^2}{(2L)^4} \sum_{k_1,k_2,k_3,k_4} \frac{L\,\delta_{k_1+k_2+k_3+k_4,0}}{\omega_{k_1}\omega_{k_2}\omega_{k_3}\omega_{k_4}} \frac{\theta(\omega_{k_1} + \omega_{k_2} + \omega_{k_3} + \omega_{k_4} - E_L)}{\mathcal{E} - \omega_{k_1} - \omega_{k_2} - \omega_{k_3} - \omega_{k_4}}\,, \tag{5.58}$$

$$c_4(\mathcal{E}, E_L) = \frac{s_2 g^2}{(2L)^2} \sum_{k_1,k_2} \frac{L\,\delta_{k_1+k_2,0}}{\omega_{k_1}\omega_{k_2}} \frac{\theta(\omega_{k_1} + \omega_{k_2} - E_L)}{\mathcal{E} - \omega_{k_1} - \omega_{k_2}}\,, \tag{5.59}$$

and c_2 is given in Eq. (5.55). On the other hand the operators $\Delta H_2^{\phi^6}$ and $\Delta H_2^{\phi^8}$ are of the tree-level and disconnected type because they involve one and zero propagators respectively, see Eq. (5.47). Therefore the operators $\Delta H_{2+}^{\phi^6}$ and $\Delta H_{2+}^{\phi^8}$ are not well approximated by a local expansion, and we do not approximate them. For E_L sufficiently big though, $\Delta H_{2+}^{\phi^6} = \Delta H_{2+}^{\phi^8} = 0$ and all the contribution to $\Delta H_2^{\phi^6}$, $\Delta H_2^{\phi^8}$ comes from $\Delta H_{2-}^{\phi^6}$, $\Delta H_{2-}^{\phi^8}$, as can be explicitly seen from Eqs. (5.6.125)-(5.6.126). Notice that these operators only contribute to the entries of ΔH_{rs} with high values for E_r, E_s. Again, the coefficients of the local operators in Eq. (5.57) can be obtained by expanding $\Delta \hat{H}_2$ in Eq. (5.47) around $t, z = 0$

$$\Delta \hat{H}_2(\mathcal{E})_{rs} = -ig^2 \int_0^\infty dt\, e^{i(\mathcal{E}-E_{rs}+i\epsilon)t} \int_{-L/2}^{L/2} dx dz \sum_{m=0}^4 s_{4-m} D_F^{4-m}(z,t) : \phi^{2m}(x,0):_{rs} + \mathcal{O}(t,z)^2\,, \tag{5.60}$$

and, after integrating, keeping only the contributions from those states that produce poles at $\mathcal{E} > E_L$, when E_{rs} is neglected. The evaluation of the coefficients in Eq. (5.57) can still be hard to evaluate numerically. In the next section we explain an alternative and simpler derivation of the coefficients c_{2m} and further approximations to evaluate them.

5.5.2   Local expansion and the phase-space functions

From the first term in the local expansion of Eq. (5.60) the coefficients of the local operators are given by:

$$\hat{c}_{2n}(\mathcal{E}) = -ig^2 s_{4-n} \int_0^\infty dt\, e^{i(\mathcal{E}+i\epsilon)t} \int_{-\infty}^\infty dx\, D_F^{4-n}(x,t)\,, \tag{5.61}$$

where s_{4-n} is the symmetry factor and, as explained above, the common E_{rs}-shift on the eigenvalue $\mathcal{E}$ is neglected. [9] Next, applying the Kramers-Kronig dispersion relation to $c_n(\mathcal{E})$ in Eq. (5.61)

$$\hat{c}_{2n}(\mathcal{E}) = -\int_{-\infty}^\infty \frac{dE}{\pi} \frac{1}{\mathcal{E} - E + i\epsilon} \mathrm{Im}\, \hat{c}_{2n}(\mathcal{E})\,. \tag{5.62}$$

Next, we compute $\mathrm{Im}\, \hat{c}_{2n}$. First we do the space integral which, up to $g^2 s_{4-n}$, yields

$$\mathrm{Im} -i \sum_{k's} \frac{L\,\delta_{\sum_i k_i,0}}{\prod_i 2L\omega_{k_i}} \int_0^\infty dt\, e^{i(E-\sum_i \omega_{k_i}+i\epsilon)t} = -\frac{1}{2} \sum_{k's} \frac{L\,\delta_{\sum_i k_i,0}}{\prod_i 2L\omega_{k_i}} 2\pi\delta\Big(E - \sum_i \omega_{k_i}\Big)\,, \tag{5.63}$$

where we have used $D_F(t,x)\theta(t) = D(t,x)\theta(t)$ with $D(t,x) = \sum_k (2L\omega_k)^{-1} e^{ikx-i\omega_k t}$. Therefore we find [10],

$$\hat{c}_{2n}(\mathcal{E}) = \frac{g^2 s_{4-n}}{2\pi} \int_{-\infty}^\infty \frac{dE}{\mathcal{E} - E + i\epsilon} \Phi_{4-n}(E) \tag{5.64}$$

where $\Phi_m(E)$ is the m-particle phase space

$$\Phi_m(E) = \sum_{k_1,k_2,\ldots,k_m} \frac{L\,\delta_{\sum_{i=1}^m k_i,0}}{\prod_{i=1}^m 2L\omega_{k_i}} 2\pi\delta\Big(E - \sum_{i=1}^m \omega_{k_i}\Big)\,. \tag{5.65}$$

Finally, the coefficients in Eq. (5.57) are obtained by including only the contributions from poles located at $\mathcal{E} \geqslant E_L$

$$c_0(\mathcal{E}) = s_4\, g^2 \int_{E_L}^\infty \frac{dE}{2\pi} \frac{1}{\mathcal{E} - E} \Phi_4(E)\,, \tag{5.66}$$

$$c_2(\mathcal{E}) = s_3\, g^2 \int_{E_L}^\infty \frac{dE}{2\pi} \frac{1}{\mathcal{E} - E} \Phi_3(E)\,, \tag{5.67}$$

$$c_4(\mathcal{E}) = s_2\, g^2 \int_{E_L}^\infty \frac{dE}{2\pi} \frac{1}{\mathcal{E} - E} \Phi_2(E)\,. \tag{5.68}$$

It would be interesting to see if in general, higher ΔH_{n+} corrections can also be written in terms of phase space functions. In the rest of the section we explain useful approximations to evaluate Eqs. (5.66)-(5.68).

---

[9]The derivation of the coefficients $\hat{c}_{2n}(\mathcal{E})$ in Eq. (5.61) applies to any ϕ^α theory.

[10]Eq. (5.64) can also be derived from the optical theorem, with careful treatment of the symmetry factors.

Continuum and high energy limit of the phase space

We start by approximating the phase space by its continuum limit. [11] Recall that in the continuum limit the relativistic phase-space for n-particles is given by

$$\Phi_n(E) = \int \prod_{i=1}^{n} \frac{dk_i^1}{(2\pi)\,2\omega_{k_i}}\,(2\pi)^2 \delta^{(2)}\Big(P^\mu + \sum_{i=1}^{n} k_i^\mu\Big)\,, \tag{5.69}$$

where $P^\mu = (E, 0)$ and $k_i^\mu = (\omega_{k_i}, k_i)$. Then, for the 2-body phase space one has

$$\Phi_2(E) = \frac{1}{E\sqrt{E^2 - 4m^2}}\,. \tag{5.70}$$

Next, solving for the Dirac delta's in Eq. (5.69), the 3-body phase-space is given by

$$\Phi_3(E) = \frac{1}{2\pi} \int_{4m^2}^{(E-m)^2} \frac{ds_{23}}{\sqrt{s_{23}\left(s_{23} - [E+m]^2\right)\left(s_{23} - [E-m]^2\right)\left(s_{23} - 4m^2\right)}}\,, \tag{5.71}$$

with $E \geqslant 3m$. This integral can be solved by standard Elliptic integral transformations and we obtain,

$$\Phi_3(E) = \frac{g^2}{\pi}\frac{1}{(E-m)}\frac{1}{\sqrt{(E+m)^2 - 4m^2}} K(\alpha)\,, \tag{5.72}$$

where $\alpha = 1 - \frac{16Em^3}{(E-m)^3(E+3m)}$ and $K(\alpha) = \int_0^{\pi/2} \frac{d\varphi}{\sqrt{1 - \alpha \sin^2(\varphi)}}$ is an elliptic integral.

In general though, finding the exact phase space functions $\Phi_n(E)$ is difficult but can be simplified in the limit $E \gg m$. In our case, this limit is justified because the phase space functions are evaluated for $E \geqslant E_L \gg m$. Notice that to take the high energy limit of $\Phi_n(E)$ one can not expand the integrand of Eq. (5.69) because, after solving for the Dirac delta's constraints, it is of $\mathcal{O}(1)$ at the integral limits, see for instance the elliptic integral in Eq. (5.71). Instead, we use the following relation for the phase space

$$I_n(\tau) \equiv \int_{-\infty}^{\infty} dx\, D_E^n(x, \tau) = \frac{1}{2\pi} \int_0^{\infty} dE\, e^{-E\tau} \Phi_n(E) \tag{5.73}$$

where $D_E(x, \tau)$ is the euclidean propagator and $\Phi_n(E)$ is only non vanishing for $E \geqslant nm$. The Euclidean propagator in $d = 2$ is given by the special Bessel function of second kind $K_0(m\rho)$ with $\rho = \sqrt{x^2 + \tau^2}$ and $I_n(\tau) \equiv \int_{-\infty}^{\infty} dx\, K_0^n(m\rho)(2\pi)^{-n}$. At this point we can use a clever trick done in Ref. [7] to find the leading terms of the inverse Laplace transform of $I_n(\tau)$ in the limit $E \to \infty$. Since the phase space $\Phi_n(E)$ is the inverse Laplace transform of $I_n(\tau)$, the leading parts of $\Phi_n(E)$ as $E \to \infty$ come from the non-analytic parts of $I_n(\tau)$ as $\tau \to 0$. To find the non-analytics parts of $I_n(\tau)$ first one notices that

$$K_0(m\rho) = \begin{cases} -\log\left(\frac{e^\gamma m\rho}{2}\right)\left[1 + \mathcal{O}(m^2\rho^2)\right] & ,\quad \rho \ll 1/m \\ \sqrt{\frac{\pi}{2m\rho}}\, e^{-m\rho}\left[1 + \mathcal{O}(m^{-1}\rho^{-1})\right] & ,\quad \rho \gg 1/m \end{cases} \tag{5.74}$$

---

[11]This is a good approximation for $Lm \gg 1$ and we have checked it explicitly in our numerical study.

where γ is the Euler constant. Then, the contributions to $I_n(\tau) = \int_{-\infty}^{\infty} dx\, K_0^n(m\rho)(2\pi)^{-n}$ when $\tau \to 0$ are dominated by the region where $\rho \ll 1/m$ and the integrand can be approximated by $K_0(m\rho) \approx -\log\left(\frac{e^{\gamma}m\rho}{2}\right)$. [12] This approximation introduces spurious IR divergences in the region of integration $\rho \gg 1/m$ where the approximation of the integrand is not valid. These divergences can be regulated with a cutoff Λ or, equivalently, one can take derivatives with respect to the external coordinate τ to regulate the integral $I_n(\tau)$. [13] Hence, approximating $K_0(m\rho) \approx -\log\left(\frac{e^{\gamma}m\rho}{2}\right)$ and integrating over x one can find the non-analytic terms of $\partial_{\tau} I_n(\tau)$ as $\tau \to 0$. For instance, for $n = 4$

$$\partial_{\tau} I_4(\tau) = \frac{1}{4\pi^3} \log(m\tau e^{\gamma}) \left[\log(m\tau) \log(m\tau e^{2\gamma}) + \gamma^2 + \frac{\pi^2}{4} \right] + const. + \mathcal{O}(\tau), \qquad (5.75)$$

where the constant does not depend on τ. Lastly from Eq. (5.73), $\partial_{\tau} I_n(\tau)$ is related to the phase space $\Phi_n(E)$ by the Laplace transform,

$$\int_0^{\infty} dE[-E\Phi_n(E)]\, e^{-\tau E} = 2\pi\, \partial_{\tau} I_n(\tau) \qquad (5.76)$$

so that for $n = 4$ one has

$$\Phi_4(E) \quad = \quad \frac{3}{2\pi^2} \frac{1}{E^2} \left[\log^2(E/m) - \pi^2/12 \right] + \mathcal{O}\left(m^2/E^4\right). \qquad (5.77)$$

Therefore using Eq. (5.77) and expanding Eqs. (5.70), (5.72) at large E,

$$c_0(\mathcal{E}) \quad \simeq \quad s_4\, g^2 \int_{E_L}^{\infty} \frac{dE}{2\pi} \frac{1}{\mathcal{E} - E} \frac{3}{2\pi^2} \frac{1}{E^2} \left[\log^2(E/m) - \pi^2/12 \right], \qquad (5.78)$$

$$c_2(\mathcal{E}) \quad \simeq \quad s_3\, g^2 \int_{E_L}^{\infty} \frac{dE}{2\pi} \frac{1}{\mathcal{E} - E} \frac{3}{2\pi} \frac{1}{E^2} \log(E/m), \qquad (5.79)$$

$$c_4(\mathcal{E}) \quad \simeq \quad s_2\, g^2 \int_{E_L}^{\infty} \frac{dE}{2\pi} \frac{1}{\mathcal{E} - E} \frac{1}{E^2}, \qquad (5.80)$$

where the error made in the approximations is of the order $\mathcal{O}\left(m^2/E_L^2\right)$. We end this section by noticing that the leading terms of the phase space functions $\Phi_2(E)$ and $\Phi_3(E)$ in the large E expansion agree with the corresponding result of Ref. [7] (there called $\mu_{444}(E) = s_2\Phi_2(E)/(2\pi)$, $\mu_{442}(E) = s_3\Phi_3(E)/(2\pi)$). The local approximation in Eqs. (5.78)-(5.80) can be refined by taking into account the E_{rs} shift, see Ref. [7].

---

[12]This method is like the method of regions which is used to get the leading terms of multi-loop Feynman diagrams in certain kinematical limits or mass hierarchies.

[13]This is similar to the fact that the UV divergences of multi-loop Feynman diagrams are polynomial in the external momenta because taking enough derivatives with respect to the external momenta the integrals are UV finite.

5.5.3 Spectrum and convergence

Before starting with the numerical results we first discuss the series $\Delta H = \sum_{n=2} \Delta H_n$ in more detail. The truncation of the ΔH series in powers of $(V_{hh}/H_{0\,hh})^n$ is only justified for $V_{hh}/H_{0\,hh} < 1$. Notice that even for weak coupling $g \ll 1$ the series does not seem to converge. Let us consider a particular matrix entry

$$\langle E_r \left| \Delta H_n \right| E_s \rangle = \sum_{j_1,\ldots,j_{n-1}} V_{rj_1} \cdots V_{j_{i-1}j_i} \frac{1}{\mathcal{E} - E_{j_i}} \cdots \frac{1}{\mathcal{E} - E_{j_{n-1}}} V_{j_{n-1}s} , \qquad (5.81)$$

where all the terms in the sums have a definite sign depending on whether n is even or odd. For instance, consider a contribution to Eq. (5.81) from states of high occupation number but low momentum like

$$V_{j_{i-1}j_i} \frac{1}{\mathcal{E} - E_{j_i}} \rightarrow \frac{\langle N_k N_{-k} \left| V \right| N_k N_{-k} \rangle}{\mathcal{E} - 2N\omega_k} = \frac{6g}{4L\omega_k^2} \frac{(2N(N-1) + 4N^2)}{\mathcal{E} - 2N\omega_k} , \qquad (5.82)$$

where $\left| N_k N_{-k} \right\rangle$ is a Fock state with N particles of momentum k and $-k$ that satisfy $2N\omega_k > E_T$. The term of Eq. (5.82) gives a non-perturbative contribution even for small g for high enough N and becomes worse for smaller momentum $|k|$. Thus the series $(\Delta H)_{rs} = \sum(\Delta H_n)_{rs}$ seems to be non-convergent but we will assume that (when the expansion parameter is small) the first terms of the series are a good approximation to $(\Delta H)_{rs}$. Notice that the appearance of the non-perturbative contributions (like in Eq. (5.82)) can be worse for those matrix entries $(\Delta H)_{rs}$ with energies $E_{r,s}$ closer to E_T because the intermediate states in $V_{jj'}$ can have lower momentum and high occupation number for a given ΔH_n.

For the first terms of the expansion $(V_{hh}/E_h)^n$, a naive estimate of the dimensionless expansion parameter is $\alpha_{rs} \sim g/E_T \times 1/(L\mu_{rs}^2)$ where the g and L can be read off from the potential; the E_T^{-1} arises because the sums in Eq. (5.81) are dominated by the first terms, starting at $1/E_T$ (for $\mathcal{E} << E_T$); and by direct inspection of the potential $m/N \lesssim \mu_{rs} \lesssim E_T$ where N is a possibly large occupation number, depending on the matrix entry.

It can happen that entries with energies E_r, E_s close to E_T do not have a perturbative $(\Delta H)_{rs} = \sum(\Delta H_n)_{rs}$ expansion and even including the first terms of the series is a worse approximation than setting $(\Delta H)_{rs} \rightarrow 0$; these entries can induce big errors on the computed eigenvalues. Since the eigenvalues we are interested in computing are mostly affected by the lower $E_{r,s}$-energy matrix entries we will neglect the renormalization of the higher $E_{r,s}$ energy entries where the series $(\Delta H)_{rs} = \sum(\Delta H_n)_{rs}$ is not perturbative. One way to select those entries would be to keep only those that satisfy $\alpha_{rs} \sim (\Delta H_3)_{rs}/(\Delta H_2)_{rs} < 1$. However, this can be computationally expensive and instead we take a more pragmatic approach and only renormalize those matrix entries $(H_T)_{rs}$ with either E_r or E_s below some conservative cutoff E_W, below which the series is perturbative.

Up until this point the discussion has been done for $g \ll 1$. However, for those matrix entries where α_{rs} is a perturbative expansion parameter one can increase g to strong coupling [14]

[14]In the ϕ^4 theory the strong coupling can be estimated to be $g \gtrsim 1$, see Eqs. (5.83) and (5.84).
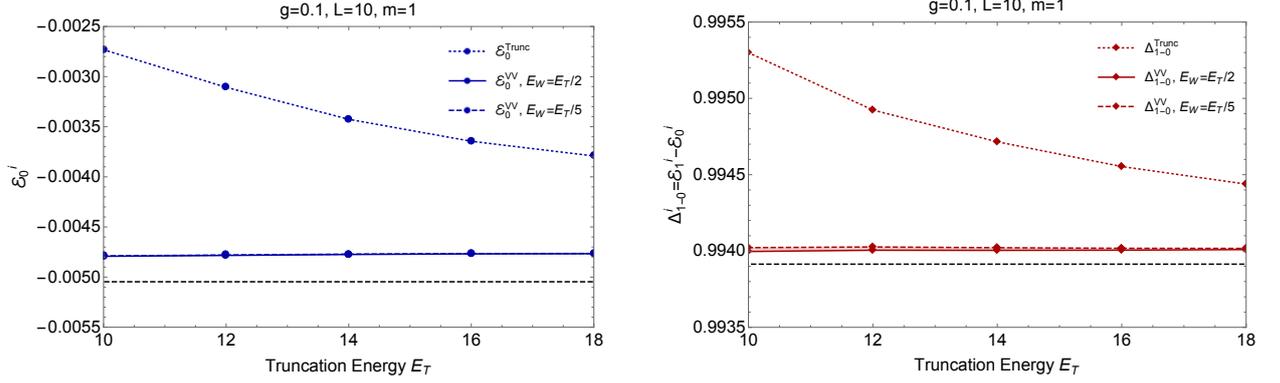
Figure 5.5: **_Left:_** _The vacuum energy_ $\mathcal{E}_0^i$ _as a function of the truncation energy_ E_T _for a coupling of_ $g = 0.1$. **_Right:_** _Energy difference between the first_ $\mathbb{Z}_2$-_odd excited state and the vacuum energy_ $\mathcal{E}_0^i$ _as a function of the truncation energy for_ $g = 0.1$. _In both plots, the dotted curves are computed with the truncated Hamiltonian while the solid and dashed curves are computed with the renormalized hamiltonian at order_ VV. _Dashed and dotted lines correspond to the cutoffs_ $E_W = E_T/2$ _and_ $E_W = E_T/5$. _We have overlaid two dashed black lines corresponding to the calculation in perturbation theory, see. Eqs. (5.83) and (5.84)._

by increasing E_T at the same time. Increasing E_T means enlarging the size of H_T and ΔH, and it can happen that the new matrix entries do not have a perturbative $(\Delta H)_{rs} = \sum(\Delta H_n)_{rs}$ expansion. As explained above, in those cases we set $(\Delta H)_{rs}$ to zero. [15]

Numerical results

In the rest of the section we perform a numerical study of the spectrum of the ϕ^4 theory. First we summarize the concrete implementation of the method. We find the spectrum of H by diagonalizing $H_{eff} = H_T + \Delta H_2(\mathcal{E}^T)$ where $\mathcal{E}^T$ is the eigenvalue of H_T. [16] As explained in Sec. 5.5.1, to calculate ΔH_2 we separate it in ΔH_{2+} and ΔH_{2-} defined in Eqs. (5.52)-(5.53) and take $E_L = 3E_T$. [17] We found little differences when iterating the diagonalization with $\mathcal{E}$. We also find that increasing E_L does not have a significant effect on the result. For $\Delta H_{2-}(\mathcal{E}, E_T, E_L)$ we use the expressions in Eqs. (5.6.122)-(5.6.126) and for $\Delta H_{2+}(\mathcal{E}, E_L)$ we use the ones in Eqs. (5.78)-(5.80). We do a conservative estimate of the expansion parameter α_{rs} and set to zero $(\Delta H_2)_{rs}$ for all those entries that are not perturbative.

First we study the lowest eigenvalues of H at weak coupling, where we can compare with standard perturbation theory. The perturbative corrections to the vacuum and the mass are

---

[15]For the ϕ^2 perturbation studied in Sec. 5.4 we find that the error in the computed eigenvalues can be decreased by increasing E_T even without introducing E_W. For the ϕ^4 we find that E_W must be introduced.

[16]The dimension of the Hilbert space $\mathcal{H}_{ll}$ for $E_T = 10, 12, 14, 16$ and 18 is $117(108)$, $309(305)$, $827(816)$, $2160(2084)$ and $5376(5238)$ for the $\mathbb{Z}_2$-even(odd) sectors, respectively.

[17] The choice $E_L = 3E_T$ is done so that the local expansion is a good approximation for intermediate states with $E_j \geqslant E_L$. Also, for this E_L one has that $\Delta H_{2+}^{\phi^6} = \Delta H_{2+}^{\phi^8} = 0$.

given by [7]:

$$\Lambda/m^2 \;\; = \;\; -\frac{21\xi(3)}{16\pi^3}\,\bar{g}^2 + 0.04164(85)\,\bar{g}^3 + \dots\,, \tag{5.83}$$

$$m_{ph}^2 \;\; = \;\; m^2\Big[1 - \frac{3}{2}\,\bar{g}^2 + 2.86460(20)\,\bar{g}^3 + \cdots\Big], \tag{5.84}$$

where $\bar{g} \equiv g/m$ and m_{ph} is the physical mass. In Fig. 5.5 we show the result for the vacuum energy and m_{ph}. As explained before, only those entries with $E_{r,s}$ energies below a cutoff E_W are renormalized. We do the plot for different values of $E_W = E_T/2, E_T/5$ and we find that the vacuum energy and the physical mass do not depend much on this cutoff. For the left plot the difference between $E_W = E_T/2$ and $E_W = E_T/5$ is inappreciable. [18] We find that the spectrum is much flatter as a function of E_T for renormalized eigenvalues than the ones computed with H_T. Since the exact spectrum is independent of the truncation energy E_T, a flatter curve in E_T indicates a closer value to exact energy levels. However, it could still happen that adding ΔH_3 corrections shifted the spectrum by a small amount, as it happens for the ϕ^2 perturbation seen in Figs. 5.3 and 5.4 for the range $16 \lesssim E_T \leqslant 20$. In the plots we have superimposed constant dashed black lines that are obtained from the perturbative calculations in Eq. (5.83) and Eq. (5.84). We find that the eigenvalues computed with ΔH_2 are much closer to the perturbative calculation than the ones done with H_T. The difference between the perturbative result and the one from $\mathcal{E}^{VV}$ is of $\mathcal{O}(10^{-4})$ and can be attributed to higher order corrections in the perturbative expansion. Another source of uncertainty comes from higher order ΔH_n corrections not included.

In Fig. 5.6 we show plots with different energy levels as a function of the truncation energy E_T for $g = 1, 2, 3$. To compare with previous work, these plots have been done with the same choice of parameters and normalizations as in Figs. (9)-(10) of Ref. [7]. In all the plots the dotted lines are computed using the truncated Hamiltonian while the solid and dashed lines are computed using ΔH_2 with $E_W = E_T/2$ and $E_W = E_T/3$, respectively. The diamonds and the circles correspond to states in the $\mathbb{Z}_2$-even and $\mathbb{Z}_2$-odd sectors of the theory. We find that in all the plots, for high enough values of E_T, the solid lines for the ΔH_2 are flatter than the truncated ones. The difference between the dotted and dashed lines is bigger for the plot for $g = 3$ than the one for $g = 1$. This can be understood because one expects more overlap from higher H_0 excited states with the vacuum for higher coupling. The difference between the solid and dashed lines becomes smaller as E_T is increased. This can be understood because as E_T is increased bigger parts of $(H_T)_{rs}$ are being renormalized, and eventually the difference between using $E_W = E_T/2$ and $E_T/3$ becomes negligible. An intrinsic error of our calculation of the eigenvalues is the difference between the values obtained for different choices of E_W. This error could be reduced with a more careful estimate of the expansion parameter $\alpha_{r,s}$, which would be very interesting for the future development of the method. In fact, it seems that

---

[18]In fact, for this case we have checked that setting $E_W = E_T$ gives a result on top of the lines of $E_W = E_T/2$. This is because at weak coupling there is not much overlap between the lowest lying eigenstates of H and the high H_0 eigenstates.
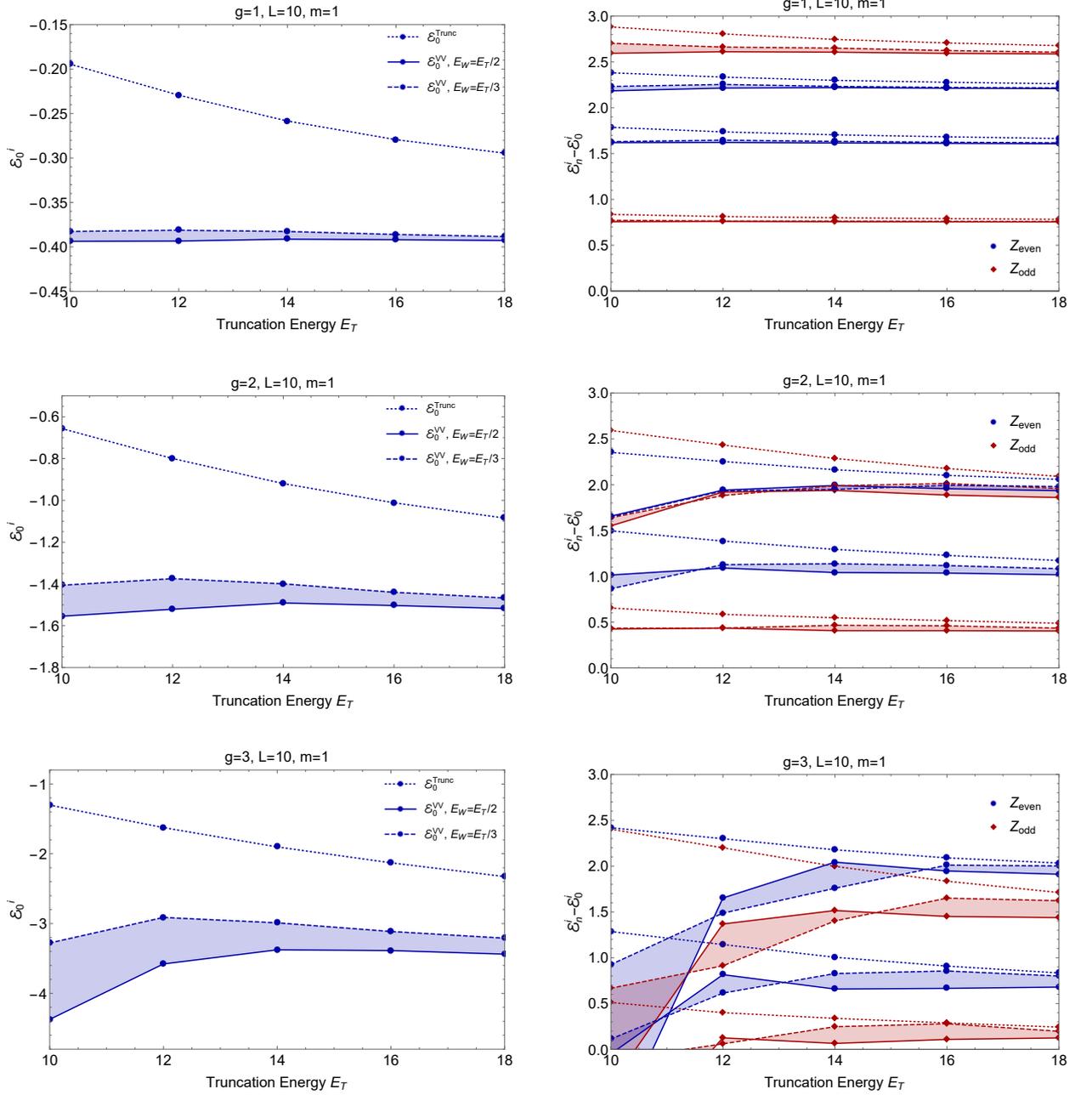
Figure 5.6: **Left:** *The vacuum energy $\mathcal{E}_0^i$ as a function of E_T for $g = 1$, 2 and 3 in descending order.* **Right:** *Energy difference between the first excited states and the vacuum energy as a function of the coupling E_T for $g = 1$, 2 and 3. In all the plots of the figure the blue curves correspond to the $\mathbb{Z}_2$-even sector while the red ones to the $\mathbb{Z}_2$-odd. The dotted curves are computed with the truncated Hamiltonian, while the solid and dashed lines are computed adding ΔH_2 with cutoffs $E_W = E_T/2$ and $E_W = E_T/3$.*
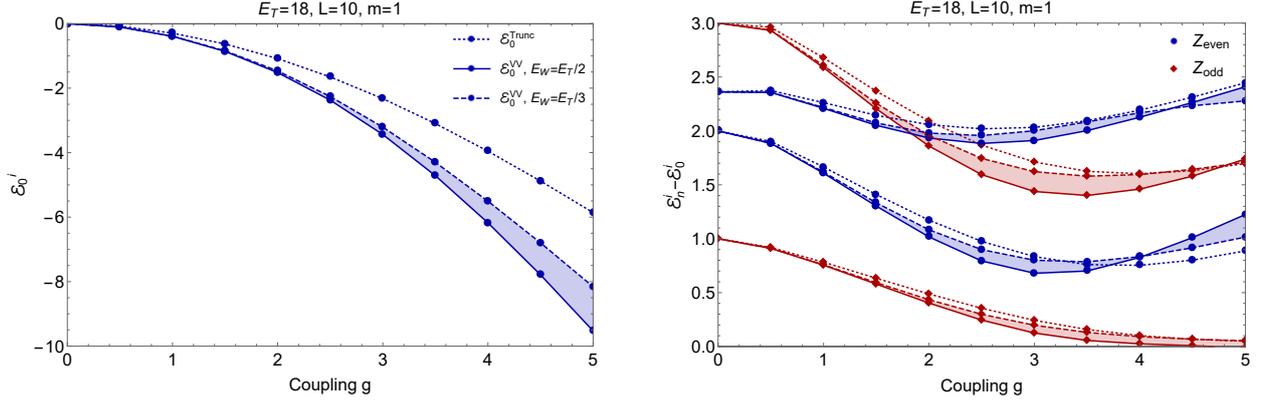
Figure 5.7: **Left:** *The vacuum energy $\mathcal{E}_0$ as a function of the coupling g.* **Right:** *Energy difference between the first excited states and the vacuum energy as a function of the coupling constant g. In all the plots of the figure the blue curves correspond to the $\mathbb{Z}_2$-even sector while the red ones to the $\mathbb{Z}_2$-odd. The dotted curves are computed with the truncated Hamiltonian for a truncation energy $E_T = 18$, while the solid and dashed lines are computed adding ΔH_2 with cutoffs $E_W = E_T/2$ and $E_W = E_T/3$.*

for $E_T \lesssim 12(14)$ for $g = 2(3)$ the cutoff E_W is too high (and might include non-perturbative corrections like the one in Eq. (5.82)) as the eigenvalues deviate a lot from the computation done with H_T. Another small source of uncertainty in our calculation comes from not having included higher order ΔH_n corrections; in the next section we explain the calculation of ΔH_3.

In Fig. 5.7 we show two plots of the vacuum and first excited states as a function of the coupling constant g for $E_T = 18$ (cf. Fig. 4 of Ref. [7]). There is an intrinsic uncertainty in our procedure in the choice of E_W, and as we discussed above it could be lowered by increasing the size of the truncation E_T or ideally by refining the determination of E_W. Notice that the renormalization of the truncated Hamiltonian matters as the solid lines have a significant difference with respect to the truncated (as seen in Fig. 5.6 the solid lines show a better convergence as a function of E_T). For $g \gtrsim 3.5$ the first $\mathbb{Z}_2$-odd excited state seems to become degenerate with the vacuum which is a signal of the spontaneous breaking of the $\mathbb{Z}_2$ symmetry. This plot can be used to determine the critical coupling, see Ref. [7].

5.5.4 Three point correction and further comments

As explained in the previous section we have performed the numerical study of the ϕ^4 theory without taking into account the three point correction ΔH_3. This would be an interesting point for the future and therefore we give a small preview of the type of expressions one obtains when computing the three point correction. As done throughout the paper, to get the expression for ΔH_3 we start by first computing

$$\Delta \widehat{H}_3(\mathcal{E})_{rs} = -\lim_{\epsilon \to 0} \int_0^\infty dt_1 dt_2 \, e^{i(\mathcal{E}-E_r+i\epsilon)(t_1+t_2)} \mathcal{T}\left\{V(T_1)V(T_2)V(T_3)\right\}_{rs} , \qquad (5.85)$$

where $T_k = \sum_{n=1}^{3-k} t_n$. Then we find ΔH_3 by keeping only those terms that have all poles at $\mathcal{E} > E_T$. Then, we see that the three point correction can be split into

$$\Delta H_3 = \Delta H_3^{\mathbb{1}} + \Delta H_3^{\phi^2} + \Delta H_3^{\phi^4} + \Delta H_3^{\phi^6} + \Delta H_3^{\phi^8} + \Delta H_3^{\phi^{10}} + \Delta H_3^{\phi^{12}} , \qquad (5.86)$$

where the subindices denote the number of fields in each term. The correction $\Delta H_3^{\mathbb{1}}$ is given by

$$\Delta H_3^{\mathbb{1}}(\mathcal{E}) = \frac{s_{222}\, g^3}{(2L)^6} \sum_{k_i, p_i, l_i} \frac{L^2 \delta_{p_1+p_2+k_1+k_2,0}^{l_1+l_2+k_1+k_2,0}}{\omega_{k_1}\omega_{k_2}\omega_{p_1}\omega_{p_2}\omega_{l_1}\omega_{l_2}} \frac{\theta(\Sigma_{i=1}^2[\omega_{p_i}+\omega_{k_i}]-E_T)}{\mathcal{E}-\Sigma_{i=1}^2[\omega_{p_i}+\omega_{k_i}]} \frac{\theta(\Sigma_{i=1}^2[\omega_{l_i}+\omega_{k_i}]-E_T)}{\mathcal{E}-\Sigma_{i=1}^2[\omega_{l_i}+\omega_{k_i}]} . \tag{5.87}$$

where the symmetry factor is defined in Eq. (5.39). The rest of the terms $\Delta H_3^{\phi^2}, \cdots, \Delta H_3^{\phi^{12}}$ can be computed in a similar fashion as explained in previous sections, but we do not present them here since we did not include them in the numerical analysis.

Another interesting thing to study in the future is the local expansion of ΔH_3 and higher orders in ΔH_n. Here we present some of the terms for the ΔH_3 case. As done for ΔH_2, when the local expansion applies the calculation is simplified. We use the diagrammatic representation explained in Appendix 5.6 for the expressions at $\mathcal{O}(t^0, z^0)$ of the local renormalization. As an example the leading local coefficients that renormalize the operators V_2, V_4 and V_6 are

$$\Delta H_{3+}^{\phi^2} \simeq \left(\text{} + \text{} + \text{} + \text{} + \cdots \right) V_2 \qquad (5.88)$$

where for example,

$$\text{} = \frac{s_{131}\, g^3}{(2L)^5} \sum_{k,l,p_i} \frac{L^2 \delta_{p_1+p_2+p_3+k,0}^{l+k,0}}{\omega_k \omega_{p_1}\omega_{p_2}\omega_{p_3}} \frac{\theta(\omega_l+\omega_k-E_L)}{\mathcal{E}-\omega_l-\omega_k} \frac{\theta(\omega_k+\Sigma_{i=1}^3\omega_{p_i}-E_L)}{\mathcal{E}-\omega_k-\Sigma_{i=1}^3 p_i} . \qquad (5.89)$$

For the renormalization of the quartic we get

$$\Delta H_{3+}^{\phi^4} \simeq \left(\text{} + \text{} + \text{} + \cdots \right) V_4 \qquad (5.90)$$

where for example,

$$\text{} = \frac{s_{220}\, g^3}{(2L)^4} \sum_{l_1 l_2 p_1 p_2} \frac{L^2 \delta_{l_1+l_2,0}^{p_1+p_2,0}}{\omega_{l_1}\omega_{l_2}\omega_{p_1}\omega_{p_2}} \frac{\theta(\omega_{l_1}+\omega_{l_2}-E_L)}{\mathcal{E}-\omega_{l_1}-\omega_{l_2}} \frac{\theta(\omega_{p_1}+\omega_{p_2}-E_L)}{\mathcal{E}-\omega_{p_1}-\omega_{p_2}} . \qquad (5.91)$$

For V_6

$$\Delta H_{3+}^{\phi^6} \simeq (\text{} + \cdots) V_6 \qquad (5.92)$$

where

$$\text{} = \frac{s_{111}\, g^3}{(2L)^3} \sum_k \frac{L^2}{m\,\omega_k^2} \left(\frac{1}{\mathcal{E}-2\omega_k} \right)^2 \theta(2\omega_k - E_L) . \qquad (5.93)$$

As final remark, notice that the expression in Eq. (5.91) is the square of the coefficient of V_4 (in $\Delta H_{2+}^{\phi^4}$) up to a numerical factor (see Eq. (5.59))

$$\left(\times\!\!\bigcirc\!\!\times \right)^2 = 6g \, \times\!\!\bigcirc\!\!\bigcirc\!\!\times \, . \tag{5.94}$$

It would be very interesting to investigate whether certain classes of diagrams in the $\Delta H_+ = \sum_n \Delta H_{n+}$ expansion can be resumed. This would reduce the error in the computed spectrum and its dependence on the arbitrary truncation energy E_T. For instance, it could be that the resummation comes only from the leading pieces of the different diagrams. [19]

5.5.5 Summary of the method and comparison with Ref. [7]

In this section we summarize our approach to the renormalized Hamiltonian truncation method and briefly comment on the main differences with Ref. [7].

The aim of the renormalized Hamiltonian truncation method is to find the lowest eigenvalues $\mathcal{E}$ of H. This is done by diagonalizing $H_{eff} \equiv H_T + \Delta H$, where H_T is the truncated Hamiltonian and ΔH encodes the contributions from the H_0 eigenstates with $E > E_T$. Computing ΔH is difficult but the problem is simplified if one expands ΔH in powers of V_{hh}/H_{hh}. One expects that the first terms of the series $\Delta H = \sum_n \Delta H_n$ are a good approximation to ΔH if the expansion parameter is small. These terms can be computed as explained in Sec. 5.2, by first finding $\Delta \hat{H}_n$ and keeping only the contributions from the states with $E > E_T$. Then, we notice that for some entries with E_r, E_s close to E_T, the series $(\Delta H)_{rs} = \sum_n (\Delta H_n)_{rs}$ is not perturbative (for the chosen parameters g, E_T). We deal with this problem by setting to zero all those entries with E_r or $E_s > E_W$ where E_W is chosen appropriately, see Sec. 5.5.3.

In order to speed up the numerics and gain analytic insight, we perform several approximations to the exact expression of ΔH_2. First we introduce a scale E_L so that $\Delta H_2 = \Delta H_{2-} + \Delta H_{2+}$ where ΔH_{2+} only receives contributions of the states with $E \geqslant E_L$ while ΔH_{2-} only receives contributions of states with $E_T < E < E_L$. The scale E_L is chosen such that ΔH_{2+} can be well approximated by the first terms of a local expansion. In our case, we only keep the leading terms $\Delta H_{2+} = \sum_{n=0}^{n=2} c_{2n} \int dx \, \phi^{2n}(x,t)$ and we find that the coefficients c_i can be written in terms of phase space functions. Lastly, the coefficients c_i are approximated by taking the continuum limit and then expanding them in powers of m/E_L. On the other hand ΔH_{2-} is kept exact because its numerical implementation is less costly and it does not admit an approximation by truncating a local expansion. The whole procedure has been described in Sec. 5.5 and used to do the plots of Sec. 5.5.3.

Comparison with Ref. [7]

Refs. [7,8] introduced a renormalized Hamiltonian truncation method by diagonalizing $H_{eff} = H_T + \Delta H$ and expanding ΔH in a series. As explained, we have used this as our starting

---

[19]This is the case in standard perturbation theory. For example the Renormalization Group Equations in $d = 4$ resum the leading logs coming from different diagrams.

point. In Ref. [7] though an approximation to ΔH_2 is calculated using a different approach than in this paper. To get ΔH_2, Ref. [7] starts by defining the following operator $M(E)$

$$M(E)_{rs}\, dE \equiv \sum_{E_j \leqslant E \leqslant E_j + dE} V_{rj} V_{js} \qquad \text{such that} \qquad \Delta H_2 = \int_{E_T}^{\infty} dE\, \frac{M(E)}{\mathcal{E} - E}, \qquad (5.95)$$

and then noticing that $M(E)$ is related to the matrix element

$$C(\tau)_{rs} \equiv \langle r\, |V(\tau/2)\, V(-\tau/2)|\, s \rangle = \int_0^{\infty} dE\, e^{-[E - (E_r + E_s)/2]\tau}\, M(E)_{rs} \qquad (5.96)$$

by a Laplace transform. In Ref. [7], the $E \to \infty$ behavior of $M(E)$ is found by doing the inverse Laplace transform of the non-analytic parts of $C(\tau)$ in the limit $\tau \to 0$. This is done in the continuum limit, which is a good approximation. The obtained result for $M(E)$ in this limit is taken to compute ΔH_2. Ref. [7] differentiates two renormalization procedures, one where the term $(E_r + E_s)/2$ in Eq. (5.96) is approximated to zero (called local), and one where it is taken into account (called sub-leading). In the later case $M(E)$ is given by $M(E - E_{rs})$, and therefore for entries with $E_{rs} \sim E_T$ taking the limit $E - E_{rs} \gg m$ is not justified when $E \sim E_T$. The way in which this problem is dealt with is by neglecting all the contributions of $M(E - E_{rs})$ for $E \leqslant E_{rs} + 5m$; in other words, a $\theta(E - E_{rs} - 5m)$ is multiplied to the integrand in Eq. (5.95). [20]

   With this, we can already find the main differences between the two approaches. In our case we calculate the exact expression of ΔH_2 which, if needed, can be approximated. Instead, Ref. [7] finds the contributions of ΔH_2 that are leading in the limit where $E \to \infty$ (which neglects the tree and disconnected contributions). From our approach we can recover the local result of Ref. [7] if we set $E_L = E_W = E_T$, neglect the tree and disconnected contributions, take the continuum limit, perform a local expansion to ΔH_{2+}, and make an expansion in $m/E \ll 1$. The choice $E_L = E_T$ implies $\Delta H_2 = \Delta H_{2+}$ and $\Delta H_{2-} = 0$, while $E_W = E_T$ means that no entries $(\Delta H_2)_{rs}$ are set to zero. In a similar way we can recover the sub-leading result taking into account the E_{rs} terms, while introducing by hand a $\theta(E - E_{rs} - 5m)$ in the integrals of the coefficients.

   Even though the two approaches are quite different, our method and their sub-leading renormalization can still give similar results due to the following. For large enough E_T, the low entries of $(\Delta H_2)_{rs}$ only receive contributions from loop-generated operators [21], and can be well approximated by a local (up to the E_{rs} dependence) expansion even if $E_L = E_T$. On the other hand, for high energy entries of $(\Delta H_2)_{rs}$ the tree and disconnected operators are non-zero, and none of the operators can be approximated by a truncated local expansion if $E_L = E_T$. However, in many cases these high energy entries become non perturbative and we set them to zero when E_r or $E_s > E_W$. Therefore we find that if E_W is used, it can be a good approximation for large enough E_T to neglect the tree and disconnected terms all together

---

[20]They find that $M(E)$ starts to be well approximated by the first terms in the m/E expansion when $E \geqslant 5m$.

[21]This can be easily seen from the exact calculations or using the diagrams in Appendix 5.6.

and set $E_L = E_T$ while performing a local expansion. With this we connect with Ref. [7] where the scale E_W is not used to get rid of the non-perturbative contributions. Instead the tree and disconnected terms are neglected, all the entries of $(\Delta H_2)_{rs}$ are approximated by the loop-generated local (up to E_{rs}) operators only and the $\theta(E - E_{rs} - 5m)$ is introduced in Eq. (5.95). As explained, neglecting the tree and disconnected terms is justified, while the introduction of $\theta(E - E_{rs} - 5m)$ and truncating the local expansion in practice largely reduce the values of the high energy entries with respect to the exact result. All of these effectively act as our scale E_W. Therefore we see that in many cases our approach and the one in Ref. [7] can give similar results.

Even though the numerical results are similar, our approach introduces new tools and insights that we think improve the renormalized Hamiltonian truncation method and can help to develop it further.

5.6 Conclusion and outlook

In this paper we have developed further the Hamiltonian truncation method. In particular we have explained a way to compute the corrections to the truncated Hamiltonian at any order in the large E_T expansion of $\Delta H = \sum_n \Delta H_n$. We have applied these ideas to scalar field theory in two dimensions and studied the spectrum of the theory as a function of the truncation energy and the coupling constant.

There are various open directions that are very interesting and deserve further investigation. Firstly, it would be a great improvement to the method to find a more precise estimate of the expansion parameter of the series. This estimate should be easy to implement numerically and lead to a precise definition of the cutoff E_W. In this work we have been pragmatic in this respect, and investigated the behaviour of the spectrum as this cutoff is modified. It might be that only removing the contribution of certain type of matrix elements (like the ones corresponding to high occupation number and zero momentum) the series is greatly improved.

We have not pushed the numerical aspects of the method very far and all the computations have been done with `Mathematica`. With more efficient programming languages it would be interesting to further study and check that as the truncation energy E_T is increased the uncertainty in the precise choice of E_W is reduced.

Another point that should be addressed is the dependence of the spectrum on L as higher ΔH_n corrections are added; also it could be relevant to inspect if there are diagrams that dominate for large $Lm \gg 1$.

Another very interesting path to develop further is to apply renormalization group techniques to resum the fixed order calculations of ΔH. Since the exact eigenvalues do not depend on the truncation energy E_T, it may be possible resum the calculation of ΔH_n. Our analytic expressions for the ΔH_n corrections permit a precise study of the possible resummation of the leading corrections at each order in the perturbation theory of the large E_T expansion. One could start by studying the resummation of the leading local corrections, and for that

the phase space formulation that we have introduced is useful as there are simple recursion relations for the differential phase space.

Another fascinating avenue to pursue is the applicability of the method to other theories with higher spin fields and to increase the number of dimensions. In this regard, we notice that the derivation of Eqs. (5.66)-(5.68) seems to be formally valid in any space-time dimension d. Recall that the c_i's are the coefficients of the local operators added to H_T to take into account the effect of the highest energetic H_0 eigenstates not included in the light Hilbert space $\mathcal{H}_l$. As d is increased beyond $d = 2$ the UV divergencies appear due to the increasingly rapid growth of the phase space functions $\Phi_i(E)$. One can then regulate the c_i coefficients with a cutoff Λ. For instance, consider the coefficient c_4 of the ϕ^4 operator

$$c_4^\Lambda(\mathcal{E}) = s_2 \, g_0^2 \int_{E_L}^\Lambda \frac{dE}{2\pi} \frac{1}{\mathcal{E} - E} \, \Phi_2(E) \,, \tag{5.97}$$

in $d = 4$. Then, requiring that the energy levels are independent of the regulator one finds the following β-function

$$\beta(g) = -\Lambda \frac{\partial c_4^\Lambda}{\partial \Lambda} + \mathcal{O}(g^3) = \frac{s_2 g^2}{2\pi} \Phi_2(\Lambda) + \mathcal{O}(g^3, \mathcal{E}) \,, \tag{5.98}$$

where the $\mathcal{E}$ corrections can be neglected in the limit of large $\Lambda \gg \mathcal{E}$. Redefining $g \equiv \lambda/4!$ one recovers the known result for the $\lambda\phi^4$ theory $\beta(\lambda) = \frac{3}{16\pi^2}\lambda^2 + \mathcal{O}(\lambda^3)$, where we have neglected the mass corrections that for $\Lambda \gg m$ decouple as $\Phi_2(\Lambda) = 1/(8\pi) + \mathcal{O}(m^2/\Lambda^2)$. A possible way to make contact between the calculation in the renormalized Hamiltonian method and the standard calculation of the beta function is by noticing that the coefficient of the divergent part of the amplitude is proportional to the coefficient of its finite imaginary part which in turn (by the optical theorem) is proportional to the two-particle phase space. It would be very interesting to further study RG flows from the perspective of the renormalized Hamiltonian truncation method approach.

We think that the Hamiltonian truncation method is a very promising approach to study strong dynamics, and that there are still open important questions to be addressed.

Appendix A: Diagramatic representation

There is a simple and powerful diagrammatic representation that permits to easily find the expression for ΔH_n. This can be used to either compute the full operator ΔH_n or the leading $\mathcal{O}(t^0, z^0)$ coefficients in the local expansion of ΔH_{n+} defined in Sec. 5.4. This representation is valid for any ϕ^α theory, but here we give examples only for the ϕ^4 case for concreteness.

Local coefficients

Imagine that we want to find the local coefficients $\mathcal{O}(t^0, z^0)$ for $\Delta H_{3+}^{\phi^2}$. To find them one puts 3 vertices ordered horizontally [22] and draws all possible diagrams that have only 2 external lines, four lines meeting at each vertex and don't have any lines starting and ending at the same vertex. Next, we assign a momentum for each internal line and draw a vertical line between every pair of vertices. One such diagrams is
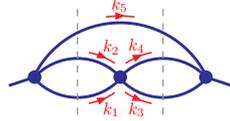
$$
\text{(5.6.99)}
$$

The expression corresponding to a given diagram with n vertices and N propagators is given by

$$
s g^n \sum_{k's} \frac{1}{\prod_{i=1}^N (2L\omega_{k_i})} \prod_{p=1}^{n-1} L\, \delta_p \frac{\theta\left(\sum_{k_j \in \{s_p\}} \omega_{k_j} - E_L\right)}{\mathcal{E} - \sum_{k_j \in \{s_p\}} \omega_{k_j}}, \tag{5.6.100}
$$

where $k_j = 2\pi n_j / L$ with $n_j \in \mathbb{Z}$. Each of the $n-1$ sets of momenta $\{s_p\}$ consist in the momenta of the internal lines that are cut by each vertical line. In (5.6.99) these would be $s_1 = \{k_1, k_2, k_5\}$ and $s_2 = \{k_3, k_4, k_5\}$. The symbol δ_p stands for a Kronecker delta that imposes that the total momentum crossing a cut is zero; s is a symmetry factor that counts all the ways that the lines of the vertices can be connected to form the diagram. Applying this recipe to the diagram in (5.6.99) one has
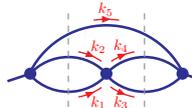
$$
= s_4^{221} g^3 \sum_{k's} \frac{L^2 \delta_{k_1+k_2+k_5,0}^{k_3+k_4+k_5,0}}{\prod_{i=1}^5 (2L\omega_{k_i})} \frac{\theta(\omega_{k_1} + \omega_{k_2} + \omega_{k_5} - E_L)}{\mathcal{E} - \omega_{k_1} - \omega_{k_2} - \omega_{k_5}} \frac{\theta(\omega_{k_3} + \omega_{k_4} + \omega_{k_5} - E_L)}{\mathcal{E} - \omega_{k_3} - \omega_{k_4} - \omega_{k_5}}. \tag{5.6.101}
$$

where the symmetry factor s_p^{mnv} is given in Eq. (5.39). Another example of a contribution to $\Delta H_{3+}^{\phi^2}$ would be
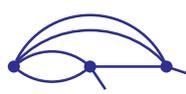
$$
= s_4^{212} g^3 \sum_{k's} \frac{L^2 \delta_{k_3+k_4+k_5,0}^{k_1+k_2+k_3+k_4,0}}{\prod_{i=1}^5 (2L\omega_{k_i})} \frac{\theta(\Sigma_{s=1}^5 \omega_{k_s} - E_L)}{\mathcal{E} - \omega_{k_1} - \omega_{k_2} - \omega_{k_3} - \omega_{k_4}} \frac{\theta(\Sigma_{s=1}^4 \omega_{k_s} - E_L)}{\mathcal{E} - \omega_{k_3} - \omega_{k_4} - \omega_{k_5}}. \tag{5.6.102}
$$

Notice that the ordering of the vertices matters since the diagrams of (5.6.101) and (5.6.102) have the same topology but give different results.

With this prescription one easily recovers Eqs. (5.55), (5.57), and (5.59) corresponding to the ΔH_{2+} coefficients in the ϕ^4 theory

$$
c_0 = \qquad , \qquad c_2 = \qquad , \qquad c_4 = \qquad . \tag{5.6.103}
$$

---

[22] The vertices are ordered in a line because the $V(T_s)$'s in Eq. (5.8) are time-ordered in the whole integration domain. This is in contrast with the standard Feynman diagrams in the calculation of an n-point function, where each space-time integral is over the whole real domain.

Notice that to include the contributions E_{rs} mentioned at the end of Sec. 5.5.2 the same diagrammatic representation applies but one must then substitute $\mathcal{E} \to \mathcal{E} - E_{rs}$ in Eq. (5.6.100) making the coefficients depend on the matrix entry.

Exact $\Delta \hat{H}_n$ opertors

A similar diagrammatic representation can be used to calculate the exact $\Delta \hat{H}_n$ operator from which one can easily get ΔH_n. The prescription to follow is very similar to the one for the local case, where one starts drawing the same diagrams and putting vertical lines between every pair of vertices. The only difference is that now one extends the external lines to left and right in all possible combinations for each diagram drawn and also assigns a momentum to the external lines. For the diagram in (5.6.99) this means
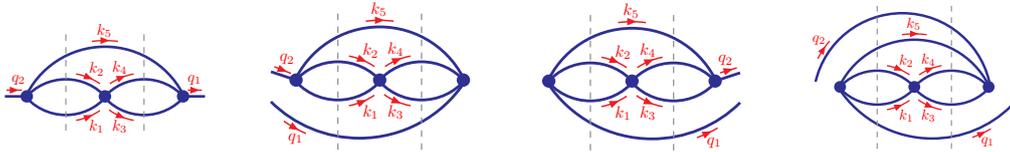

$$(5.6.104)$$

Now, the operator corresponding to a given diagram with n vertices, N propagators, A external lines starting left and B external lines starting right is

$$\kappa s g^n \sum_{k's,q's} \frac{1}{\prod_{i=1}^N (2L\omega_{k_i})} \prod_{p=1}^{n-1} \frac{\theta\left(\omega_{rs} + \sum_{Q_j \in \{s_p\}} \omega_{Q_j} - E_L\right)}{\mathcal{E} - \omega_{rs} - \sum_{Q_j \in \{s_p\}} \omega_{Q_j}} \prod_{\alpha=1}^n L\delta_\alpha \prod_{r=A+1}^{A+B} \frac{a_{q_r}^\dagger}{\sqrt{2L\omega_{q_r}}} \prod_{l=1}^A \frac{a_{q_l}}{\sqrt{2L\omega_{q_l}}},$$
$$(5.6.105)$$

where the sums over $k's$, $q's$ sum over all possible momenta for a given k_i, q_i. Then, each of the $n-1$ sets of momenta $\{s_p\}$ consists in the momenta of the lines that are cut by each vertical line. For the first diagram from the left in (5.6.105) these would be $s_1 = \{k_1, k_2, k_5\}$ and $s_2 = \{k_3, k_4, k_5\}$, and for the second one $s_1 = \{q_1, k_1, k_2, k_5\}$ and $s_2 = \{q_1, k_3, k_4, k_5\}$. The symbol δ_α stands for a Kronecker delta that imposes momentum conservation at each vertex α. The symbol ω_{rs} depends on the energy of the states $\langle E_r |$, $| E_s \rangle$ on which a and $a^\dagger$ act i.e. it is different for each entry $\left(a_{-q_r}^\dagger a_{q_l}\right)_{rs}$, and is given by $w_{rs} \equiv E_{rs} - \frac{1}{2}\sum_{i=1}^{A+B} \omega_{q_i}$ where $E_{rs} = (E_r + E_s)/2$. As before s is a symmetry factor that counts all the ways that the lines of the vertices can be connected to form the diagram. Lastly κ counts all the equivalent ways that the external lines coming out from the same vertex can be ordered left and right, for the diagrams in (5.6.105) is is always one, since there is only one external line per vertex. Applying this recipe to the first and second diagrams in (5.6.105) one has
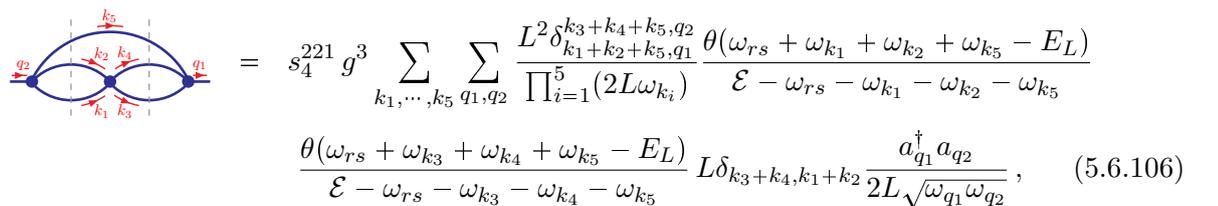
$$
\begin{aligned}
\text{} \quad = \quad & s_4^{221} g^3 \sum_{k_1,\cdots,k_5} \sum_{q_1,q_2} \frac{L^2 \delta_{k_1+k_2+k_5,q_1}^{k_3+k_4+k_5,q_2}}{\prod_{i=1}^5 (2L\omega_{k_i})} \frac{\theta(\omega_{rs} + \omega_{k_1} + \omega_{k_2} + \omega_{k_5} - E_L)}{\mathcal{E} - \omega_{rs} - \omega_{k_1} - \omega_{k_2} - \omega_{k_5}} \\
& \frac{\theta(\omega_{rs} + \omega_{k_3} + \omega_{k_4} + \omega_{k_5} - E_L)}{\mathcal{E} - \omega_{rs} - \omega_{k_3} - \omega_{k_4} - \omega_{k_5}} L\delta_{k_3+k_4,k_1+k_2} \frac{a_{q_1}^\dagger a_{q_2}}{2L\sqrt{\omega_{q_1}\omega_{q_2}}}, \quad (5.6.106)
\end{aligned}
$$
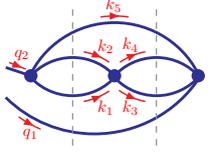
$$= s_4^{221} \, g^3 \sum_{k_1,\cdots,k_5} \sum_{q_1,q_2} \frac{L^2 \delta_{k_1+k_2+k_5+q_1,0}^{k_3+k_4+k_5+q_1,0}}{\prod_{i=1}^{5}(2L\omega_{k_i})} \frac{\theta(\omega_{rs} + \omega_{k_1} + \omega_{k_2} + \omega_{k_5} + \omega_{q_1} - E_L)}{\mathcal{E} - \omega_{rs} - \omega_{k_1} - \omega_{k_2} - \omega_{k_5} - \omega_{q_1}}$$

$$\frac{\theta(\omega_{rs} + \omega_{k_3} + \omega_{k_4} + \omega_{k_5} + \omega_{q_1} - E_L)}{\mathcal{E} - \omega_{rs} - \omega_{k_3} - \omega_{k_4} - \omega_{k_5} - \omega_{q_1}} \, L\delta_{q_1+q_2,0} \frac{a_{-q_1}^\dagger a_{q_2}}{2L\sqrt{\omega_{q_1}\omega_{q_2}}} \,, \tag{5.6.107}$$

where $\omega_{rs} = E_{rs} - (\omega_{q_1} + \omega_{q_2})/2$ and the symmetry factor s_p^{mnv} is given in Eq. (5.39).

With this set of rules one can easily get the expression for $\Delta\hat{H}_2$ and $\Delta\hat{H}_3$ for the ϕ^2 and ϕ^4 theories. Then one finds ΔH_2 and ΔH_3 by keeping only the contributions with all poles $\mathcal{E} > E_T$.

Appendix B: ΔH for the ϕ^2 perturbation

Two-point correction

In this section we give the full expressions of the $\Delta\hat{H}_2$ corrections for the scalar theory with potential $V = g_2 \int dx \phi^2$. Recall that the symmetry factor is given by $s_p = \binom{2}{p}^2 p!$. We will use the prescription $E_{rs} = (E_r + E_s)/2$ where E_r and E_s are H_0 eigenvalues.

$$\Delta\hat{H}_2^{\mathbb{1}}(\mathcal{E})_{rs} = g_2^2 s_2 \frac{1}{2^2} \sum_k \frac{1}{\omega_k^2} \frac{1}{\mathcal{E} - E_{rs} - 2\omega_k} \delta_{rs} \tag{5.6.108}$$

$$\Delta\hat{H}_2^{\phi^2}(\mathcal{E})_{rs} = g_2^2 s_1 \frac{1}{2^2} \sum_q \frac{1}{\omega_q^2} \left[\left(a_q a_{-q} \frac{1}{\mathcal{E} - E_{rs} - \omega_q} + \text{h.c.} \right) \right.$$

$$+ \left. a_q^\dagger a_q \left(\frac{1}{\mathcal{E} - E_{rs} - 2\omega_q} + \frac{1}{\mathcal{E} - E_{rs}} \right) \right] \tag{5.6.109}$$

$$\Delta\hat{H}_2^{\phi^4}(\mathcal{E})_{rs} = g_2^2 s_0 \frac{1}{2^2} \sum_{q_1,q_2} \frac{1}{\omega_{q_1}\omega_{q_2}} \left[a_{q_1} a_{q_2} a_{-q_1} a_{-q_2} \frac{1}{\mathcal{E} - E_{rs} - \omega_{q_1} + \omega_{q_2}} + \text{h.c.} \right.$$

$$+ 2 \, a_{q_1}^\dagger a_{q_1} a_{q_2} a_{-q_2} \left(\frac{1}{\mathcal{E} - E_{rs} + \omega_{q_2}} + \frac{1}{\mathcal{E} - E_{rs} - \omega_{q_2}} \right) + \text{h.c.}$$

$$+ a_{q_1}^\dagger a_{-q_1}^\dagger a_{q_2} a_{-q_2} \left(\frac{1}{\mathcal{E} - E_{rs} + \omega_{q_1} + \omega_{q_2}} + \frac{1}{\mathcal{E} - E_{rs} - \omega_{q_1} - \omega_{q_2}} \right)$$

$$+ \left. 4 \, a_{q_1}^\dagger a_{q_2}^\dagger a_{q_1} a_{q_2} \frac{1}{\mathcal{E} - E_{rs}} \right]. \tag{5.6.110}$$

Three-point correction

In this section we give the full expressions of the ΔH_3 corrections for the scalar theory with potential $V = g_2 \int dx \phi^2$. Recall that the symmetry factor is given by

$$s_p^{mnv} = \frac{p!^3}{(p-m-n)!(p-m-v)!(p-n-v)!m!n!v!} \,. \tag{5.6.111}$$

We use the notation $\Delta H_3 = \Delta H_3^{\mathbb{1}} + \Delta H_3^{\phi^2} + \Delta H_3^{\phi^4} + \Delta H_3^{\phi^6}$, where

$$\Delta H_3^{\mathbb{1}}(\mathcal{E})_{rs} = \frac{g_2^3 s_2^{111}}{2^3} \sum_k \frac{1}{\omega_{k_1}\omega_{k_2}\omega_{k_3}} G_0(k_1, k_2, k_3, E_T) \,, \tag{5.6.112}$$

$$\Delta H_3^{\phi^2}(\mathcal{E})_{rs} = \frac{g_2^3}{2^3} \sum_{k,q} \frac{1}{\omega_{k_1}\omega_{k_2}} \frac{1}{\sqrt{\omega_{q_1}\omega_{q_2}}} \big[s_2^{200} G_{2,1}(k_1, k_2, q_1, q_2, E_T)$$
$$+ s_2^{110} G_{2,2}(k_1, k_2, q_1, q_2, E_T) \big] \,, \tag{5.6.113}$$

$$\Delta H_3^{\phi^4}(\mathcal{E})_{rs} = \frac{g_2^3 s_2^{100}}{2^3} \sum_{k,q} \frac{1}{\omega_k} \frac{1}{\sqrt{\omega_{q_1} \cdots \omega_{q_4}}} G_4(k, q_1, \ldots, q_4) \,, \tag{5.6.114}$$

$$\Delta H_3^{\phi^6}(\mathcal{E})_{rs} = \frac{g_2^3 s_2^{000}}{2^3} \sum_q \frac{1}{\sqrt{\omega_{q_1} \cdots \omega_{q_6}}} G_6(q_1, \ldots, q_6) \,, \tag{5.6.115}$$

where

$$G_0 = \delta_{k_1+k_2,0}\delta_{k_1+k_3,0} [f_0]^{12}[f_0]^{13} \,, \tag{5.6.116}$$

$$G_{2,1} = a_{q_1}a_{q_2} \, \delta_0 \delta_{k_1+k_2,0} [f_2]_{12}^{12}[f_2]^{12} + \text{h.c.} + 2a_{q_1}^\dagger a_{q_2} \, \delta_1 \delta_{k_1+k_2,0} [f_2]_1^{12}[f_2]_2^{12} \,, \tag{5.6.117}$$

$$G_{2,2} = a_{q_1}^\dagger a_{q_2} \, \delta_1 \delta_{k_1+q_1,0}\delta_{k_1+k_2,0} \left([f_2]_{12}^1[f_2]_1^{12} + [f_2]_{12}^1[f_2]_2^{12} + [f_2]_{12}^1[f_2]_{12}^2 \right) \,, \tag{5.6.118}$$

$$\begin{aligned} G_4 =\ & a_{q_1}^\dagger a_{q_2}a_{q_3}a_{q_4} \, \delta_1 \delta_{k+q_1,0}\delta_{q_3+q_4,0}[f_4]_{1234}^1[f_4]_{12}^1 + \text{h.c.} \\ &+ 2a_{q_1}^\dagger a_{q_2}^\dagger a_{q_3}a_{q_4} \, \delta_2 \delta_{q_1-q_3,0}\delta_{k+q_2,0}[f_4]_{124}^1[f_4]_{234}^1 \\ &+ a_{q_1}^\dagger a_{q_2}^\dagger a_{q_3}a_{q_4} \, \delta_2 \left(\delta_{q_1+q_2,0}\delta_{k+q_4,0}[f_4]_{1234}[f_4]_{124}^1 + \delta_{q_3+q_4,0}\delta_{k+q_1,0}[f_4]_{1234}[f_4]_{124}^1 \right) \end{aligned} \tag{5.6.119}$$

$$\begin{aligned} G_6 =\ & a_{q_1}^\dagger a_{q_2}^\dagger a_{q_3}a_{q_4}a_{q_5}a_{q_6} \, \delta_2 \delta_{q_1+q_2,0}\delta_{q_3+q_4,0}[f_6]_{123456}[f_6]_{1234} + \text{h.c.} \\ &+ 2a_{q_1}^\dagger a_{q_2}^\dagger a_{q_3}^\dagger a_{q_4}a_{q_5}a_{q_6} \, \delta_3 \delta_{q_1+q_2,0}\delta_{q_5+q_6,0}[f_6]_{12356}[f_6]_{12456} \,. \end{aligned} \tag{5.6.120}$$

We have defined $w_{rs}^p \equiv E_{rs} - \frac{1}{2}\sum_{i=1}^p \omega_{q_i}$, $\delta_d \equiv \delta_{\Sigma_{i=1}^d q_i, \Sigma_{j=d+1}^p q_j}$ (the Kronecker delta that imposes momentum conservation to the creation/annihilation operators) and

$$[f_p]_Q^K = \frac{\theta(\omega_{rs}^p + \Sigma_{i\in\{Q\}}\omega_{q_i} + \Sigma_{i\in\{K\}}\omega_{k_i} - E_T)}{\mathcal{E} - \omega_{rs}^p - \sum_{i\in\{Q\}}\omega_{q_i} - \sum_{i\in\{K\}}\omega_{k_i}} \,. \tag{5.6.121}$$

Appendix C: ΔH for the ϕ^4 theory

In this appendix we give the exact two-point correction and the first terms in the local expansion of the three-point correction. Getting the exact three-point correction would be

straightforward.

Two-point correction

In this appendix we give the full expressions of the ΔH_2 for the ϕ^4 theory. Using the notation $\Delta H_2 = \sum_{n=0}^{8} \Delta H_2^{\phi^n}$ we have

$$\Delta H_2^{\mathbb{1}}(\mathcal{E}, E_T) = \frac{s_4 g^2}{2^4 L^2} \sum_{k_1 k_2 k_3 k_4} \frac{1}{\omega_{k_1} \omega_{k_2} \omega_{k_3} \omega_{k_4}} F_0(k_1, k_2, k_3, k_4, E_T), \tag{5.6.122}$$

$$\Delta H_2^{\phi^2}(\mathcal{E}, E_T) = \frac{s_3 g^2}{2^4 L^2} \sum_{k_1, k_2, k_3} \sum_{q_1, q_2} \frac{1}{\omega_{k_1} \omega_{k_2} \omega_{k_3}} \frac{1}{\sqrt{\omega_{q_1} \omega_{q_2}}} F_2(k_1, k_2, k_3, q_1, q_2, E_T), \tag{5.6.123}$$

$$\Delta H_2^{\phi^4}(\mathcal{E}, E_T) = \frac{s_2 g^2}{2^4 L^2} \sum_{k_1, k_2} \sum_{q_1, q_2, q_3, q_4} \frac{1}{\omega_{k_1} \omega_{k_2}} \frac{1}{\sqrt{\omega_{q_1} \cdots \omega_{q_4}}} F_4(k_1, k_2, q_1, \ldots, q_4, E_T), \tag{5.6.124}$$

$$\Delta H_2^{\phi^6}(\mathcal{E}, E_T) = \frac{s_1 g^2}{2^4 L^2} \sum_{k} \sum_{q_1, \ldots, q_6} \frac{1}{\omega_k} \frac{1}{\sqrt{\omega_{q_1} \cdots \omega_{q_6}}} F_6(k, q_1, q_2, \ldots, q_6, E_T), \tag{5.6.125}$$

$$\Delta H_2^{\phi^8}(\mathcal{E}, E_T) = \frac{s_0 g^2}{2^4 L^2} \sum_{q_1, \ldots, q_8} \frac{1}{\sqrt{\omega_{q_1} \cdots \omega_{q_8}}} F_8(q_1, q_2, \ldots, q_8, E_T) \tag{5.6.126}$$

The F_i functions are given by

$$F_0 = \delta_{k_1+k_2+k_3+k_4, 0} [f_0]^{1234} \tag{5.6.127}$$

$$F_2 = a_{q_1}^\dagger a_{q_2} \delta_1 \delta_{k_1+k_2+k_3, q_1} \left([f_2]^{123} + [f_2]_{12}^{123} \right) + a_{q_1} a_{q_2} \delta_0 \delta_{k_1+k_2+k_3, q_1} [f_2]_2^{123} + \text{h.c.} \tag{5.6.128}$$

$$\begin{aligned} F_4 = {} & a_{q_1} a_{q_2} a_{q_3} a_{q_4} \delta_0 \delta_{k_1+k_2, q_1+q_2} [f_4]_{34}^{12} + \text{h.c.} \\ & + 2 a_{q_1}^\dagger a_{q_2} a_{q_3} a_{q_4} \delta_1 \left(\delta_{k_1+k_2, q_1-q_2} [f_4]_2^{12} + \delta_{k_1+k_2, -q_1+q_2} [f_4]_{134}^{12} \right) + \text{h.c.} \\ & + a_{q_1}^\dagger a_{q_2}^\dagger a_{q_3} a_{q_4} \delta_2 \left(\delta_{k_1+k_2, q_1+q_2} [f_4]^{12} + \delta_{k_1+k_2, -q_1-q_2} [f_4]_{1234}^{12} + 4 \delta_{k_1+k_2, q_1-q_3} [f_4]_{14}^{12} \right) \end{aligned} \tag{5.6.129}$$

$$\begin{aligned} F_6 = {} & a_{q_1}^\dagger a_{q_2} a_{q_3} a_{q_4} a_{q_5} a_{q_6} \delta_1 \delta_{k, q_2+q_3-q_1} 3 [f_6]_{1456}^1 + \text{h.c.} \\ & + a_{q_1}^\dagger a_{q_2}^\dagger a_{q_3} a_{q_4} a_{q_5} a_{q_6} \delta_2 \left(9 \delta_{k, q_3+q_4-q_1} [f_6]_{156}^1 + 3 \delta_{k, q_3-q_1-q_2} [f_6]_{12456}^1 \right) + \text{h.c.} \\ & + a_{q_1}^\dagger a_{q_2}^\dagger a_{q_3}^\dagger a_{q_4} a_{q_5} a_{q_6} \delta_3 \left(9 \delta_{k, q_4+q_5-q_1} [f_6]_{16}^1 + 9 \delta_{k, -q_4-q_5+q_1} [f_6]_{2345}^1 + \delta_{k+q_1+q_2+q_3, 0} [f_6]_{123456}^1 \right) \end{aligned} \tag{5.6.130}$$

$$\begin{aligned} F_8 = {} & a_{q_1}^\dagger a_{q_2}^\dagger a_{q_3} a_{q_4} a_{q_5} a_{q_6} a_{q_7} a_{q_8} \delta_2 \, 6 \delta_{q_1+q_2-q_3-q_4, 0} [f_8]_{125678} + \text{h.c.} \\ & + a_{q_1}^\dagger a_{q_2}^\dagger a_{q_3}^\dagger a_{q_4} a_{q_5} a_{q_6} a_{q_7} a_{q_8} \delta_3 \left(24 \delta_{q_1+q_2-q_4-q_5} [f_8]_{12678} + 4 \delta_{q_1+q_2+q_3-q_4} [f_8]_{1235678} \right) + \text{h.c.} \\ & + a_{q_1}^\dagger a_{q_2}^\dagger a_{q_3}^\dagger a_{q_4}^\dagger a_{q_5} a_{q_6} a_{q_7} a_{q_8} \delta_4 \left(16 \delta_{q_1-q_5-q_6-q_7, 0} \left([f_8]_{18} + [f_8]_{234567} \right) \right. \\ & \left. + 36 \delta_{q_1+q_2-q_5-q_6, 0} [f_8]_{1278} + \delta_{q_1+q_2+q_3+q_4, 0} [f_8]_{12345678} \right). \end{aligned} \tag{5.6.131}$$

We have defined $w_{rs}^p \equiv E_{rs} - \frac{1}{2}\sum_{i=1}^p \omega_{q_i}$, $\delta_d \equiv \delta_{\Sigma_{i=1}^d q_i, \Sigma_{j=d+1}^p q_j}$ (the Kronecker delta that imposes momentum conservation to the creation/annihilation operators) and

$$[f_p]_Q^K = \frac{\theta(\omega_{rs}^p + \Sigma_{i\in\{Q\}}\omega_{q_i} + \Sigma_{i\in\{K\}}\omega_{k_i} - E_T)}{\mathcal{E} - \omega_{rs}^p - \sum_{i\in\{Q\}}\omega_{q_i} - \sum_{i\in\{K\}}\omega_{k_i}} . \tag{5.6.132}$$

Bibliography

[1] M. Montull and F. Riva, JHEP **1211** (2012) 018 doi:10.1007/JHEP11(2012)018 [arXiv:1207.1716 [hep-ph]].

[2] M. Montull, F. Riva, E. Salvioni and R. Torre, Phys. Rev. D **88** (2013) 095006 doi:10.1103/PhysRevD.88.095006 [arXiv:1308.0559 [hep-ph]].

[3] R. S. Gupta, M. Montull and F. Riva, JHEP **1304** (2013) 132 doi:10.1007/JHEP04(2013)132 [arXiv:1212.5240 [hep-ph]].

[4] J. Elias-Miro, M. Montull and M. Riembau, JHEP **1604** (2016) 144 doi:10.1007/JHEP04(2016)144 [arXiv:1512.05746 [hep-th]].

[5] S. R. Coleman, J. Wess and B. Zumino, Phys. Rev. **177** (1969) 2239. doi:10.1103/PhysRev.177.2239

[6] C. G. Callan, Jr., S. R. Coleman, J. Wess and B. Zumino, Phys. Rev. **177** (1969) 2247. doi:10.1103/PhysRev.177.2247

[7] S. Rychkov and L. G. Vitale, Phys. Rev. D **91** (2015) 8, 085011 [arXiv:1412.3460 [hep-th]].

[8] M. Hogervorst, S. Rychkov and B. C. van Rees, Phys. Rev. D **91** (2015) 025005 [arXiv:1409.1581 [hep-th]].

[9] G. Drexlin, V. Hannen, S. Mertens and C. Weinheimer, Adv. High Energy Phys. **2013** (2013) 293986 doi:10.1155/2013/293986 [arXiv:1307.0101 [physics.ins-det]].

[10] A. Strumia and F. Vissani, hep-ph/0606054.

[11] K. A. Olive, astro-ph/0301505.

[12] D. Hooper, doi:10.1142/9789812838360 0014 arXiv:0901.4090 [hep-ph].

[13] D. Baumann, doi:10.1142/97898143271830010 arXiv:0907.5424 [hep-th].

[14] G. Degrassi, S. Di Vita, J. Elias-Miro, J. R. Espinosa, G. F. Giudice, G. Isidori and A. Strumia, JHEP **1208** (2012) 098 doi:10.1007/JHEP08(2012)098 [arXiv:1205.6497 [hep-ph]].

[15] P. W. Graham, D. E. Kaplan and S. Rajendran, Phys. Rev. Lett. **115** (2015) no.22, 221801 doi:10.1103/PhysRevLett.115.221801 [arXiv:1504.07551 [hep-ph]].

[16] G. F. Giudice, PoS EPS **-HEP2013** (2013) 163 [arXiv:1307.7879 [hep-ph]].

[17] G. Panico and A. Wulzer, Lect. Notes Phys. **913** (2016) pp.1 doi:10.1007/978-3-319-22617-0 [arXiv:1506.01961 [hep-ph]].

[18] G. Panico and A. Pomarol, JHEP **1607** (2016) 097 doi:10.1007/JHEP07(2016)097 [arXiv:1603.06609 [hep-ph]].

[19] S. Weinberg, Phys. Rev. D **13**, 974 (1976); L. Susskind, Phys. Rev. D **20**, 2619 (1979).

[20] C. Csaki, C. Grojean, H. Murayama, L. Pilo and J. Terning, Phys. Rev. D **69**, 055006 (2004) [hep-ph/0305237]; C. Csaki, C. Grojean, L. Pilo and J. Terning, Phys. Rev. Lett. **92**, 101802 (2004) [hep-ph/0308038].

[21] D. B. Kaplan and H. Georgi, Phys. Lett. B **136** (1984) 183; D. B. Kaplan, H. Georgi and S. Dimopoulos, Phys. Lett. B **136** (1984) 187; H. Georgi, D. B. Kaplan and P. Galison, Phys. Lett. B **143** (1984) 152; T. Banks, Nucl. Phys. B **243** (1984) 125; H. Georgi and D. B. Kaplan, Phys. Lett. B **145** (1984) 216; M. J. Dugan, H. Georgi and D. B. Kaplan, Nucl. Phys. B **254** (1985) 299; H. Georgi, Nucl. Phys. B **266** (1986) 274;

[22] L. Randall and R. Sundrum, Phys. Rev. Lett. **83**, 3370 (1999) [hep-ph/9905221].

[23] K. Agashe, A. Delgado, M. J. May and R. Sundrum, JHEP **0308**, 050 (2003) [hep-ph/0308036].

[24] H. Davoudiasl, J. L. Hewett and T. G. Rizzo, Phys. Lett. B **473**, 43 (2000) [hep-ph/9911262]; A. Pomarol, Phys. Lett. B **486**, 153 (2000) [hep-ph/9911294].

[25] N. Arkani-Hamed, A. G. Cohen, E. Katz, A. E. Nelson, T. Gregoire and J. G. Wacker, JHEP **0208** (2002) 021 [arXiv:hep-ph/0206020].

[26] N. Arkani-Hamed, A. G. Cohen, E. Katz and A. E. Nelson, JHEP **0207** (2002) 034 [arXiv:hep-ph/0206021].

[27] R. Contino, Y. Nomura and A. Pomarol, Nucl. Phys. B **671** (2003) 148 [arXiv:hep-ph/0306259].

[28] K. Agashe, R. Contino and A. Pomarol, Nucl. Phys. B **719**, 165 (2005) [hep-ph/0412089].

[29] Y. Hosotani, Phys. Lett. B **126**, 309 (1983).

[30] I. Antoniadis, K. Benakli and M. Quiros, New J. Phys. **3**, 20 (2001) [hep-th/0108005].

[31] N. S. Manton, Nucl. Phys. B **158**, 141 (1979); H. Hatanaka, T. Inami and C. S. Lim, Mod. Phys. Lett. A **13**, 2601 (1998) [hep-th/9805067]; G. von Gersdorff, N. Irges and M. Quiros, Nucl. Phys. B **635**, 127 (2002) [hep-th/0204223]; L. J. Hall, Y. Nomura and D. Tucker-Smith, Nucl. Phys. B **639**, 307 (2002) [hep-ph/0107331]; C. Csaki, C. Grojean and H. Murayama, Phys. Rev. D **67**, 085012 (2003) [hep-ph/0210133]; C. A. Scrucca, M. Serone and L. Silvestrini, Nucl. Phys. B **669**, 128 (2003) [hep-ph/0304220]; C. A. Scrucca, M. Serone, L. Silvestrini and A. Wulzer, JHEP **0402**, 049 (2004) [hep-th/0312267].

[32] G. F. Giudice, C. Grojean, A. Pomarol and R. Rattazzi, JHEP **0706** (2007) 045 [arXiv:hep-ph/0703164].

[33] R. Barbieri, B. Bellazzini, V. S. Rychkov and A. Varagnolo, Phys. Rev. D **76** (2007) 115008 [arXiv:0706.0432 [hep-ph]].

[34] R. Contino, arXiv:1005.4269 [hep-ph].

[35] M. Schmaltz and D. Tucker-Smith, Ann. Rev. Nucl. Part. Sci. **55** (2005) 229 [hep-ph/0502182].

[36] M. Perelstein, Prog. Part. Nucl. Phys. **58** (2007) 247 [hep-ph/0512128].

[37] C. Csaki, In *Shifman, M. (ed.) et al.: From fields to strings, vol. 2* 967-1060 [hep-ph/0404096].

[38] C. Csaki, J. Hubisz and P. Meade, hep-ph/0510275.

[39] T. Gherghetta, hep-ph/0601213.

[40] R. Sundrum, hep-th/0508134.

[41] R. Rattazzi, *Cargese 2003, Particle physics and cosmology* 461-517 [hep-ph/0607055].

[42] M. Serone, New J. Phys. **12** (2010) 075013 [arXiv:0909.5619 [hep-ph]].

[43] T. Gherghetta, arXiv:1008.2570 [hep-ph].

[44] E. Ponton, arXiv:1207.3827 [hep-ph].

[45] A. Salvio and A. Strumia, JHEP **1406** (2014) 080 doi:10.1007/JHEP06(2014)080 [arXiv:1403.4226 [hep-ph]].

[46] N. Arkani-Hamed, T. Cohen, R. T. D'Agnolo, A. Hook, H. D. Kim and D. Pinner, arXiv:1607.06821 [hep-ph].

[47] S. Weinberg, "The quantum theory of fields. Vol. 2: Modern applications,"

[48] Z. Maki, M. Nakagawa and S. Sakata, Prog. Theor. Phys. **28** (1962) 870. doi:10.1143/PTP.28.870

[49] K. A. Olive *et al.* [Particle Data Group Collaboration], Chin. Phys. C **38** (2014) 090001. doi:10.1088/1674-1137/38/9/090001

[50] M. D. Schwartz, ISBN-9781107034730.

[51] J. F. Donoghue, E. Golowich and B. R. Holstein, Camb. Monogr. Part. Phys. Nucl. Phys. Cosmol. **2** (1992) 1.

[52] J. M. Pendlebury *et al.*, Phys. Rev. D **92** (2015) no.9, 092003 doi:10.1103/PhysRevD.92.092003 [arXiv:1509.04411 [hep-ex]].

[53] J. Incandela, CMS talk at *Latest update in the search for the Higgs boson* at CERN, July 4, 2012;

[54] F. Gianotti, ATLAS talk at *Latest update in the search for the Higgs boson* at CERN, July 4, 2012.

[55] K. Agashe, R. Contino and A. Pomarol, Nucl. Phys. B **719** (2005) 165.

[56] R. Contino, L. Da Rold and A. Pomarol, Phys. Rev. D **75** (2007) 055014.

[57] A. Pomarol and F. Riva, arXiv:1205.6434 [hep-ph].

[58] B. Gripaios, A. Pomarol, F. Riva, J. Serra, JHEP **0904** (2009) 070.

[59] J. Mrazek, A. Pomarol, R. Rattazzi, M. Redi, J. Serra and A. Wulzer, Nucl. Phys. B **853** (2011) 1.

[60] J. R. Espinosa, C. Grojean and M. Muhlleitner, JHEP **1005** (2010) 065 [arXiv:1003.3251 [hep-ph]].

[61] D. Carmi, A. Falkowski, E. Kuflik and T. Volansky, arXiv:1202.3144 [hep-ph].

[62] A. Azatov, R. Contino and J. Galloway, JHEP **1204** (2012) 127 [arXiv:1202.3415 [hep-ph]].

[63] J. R. Espinosa, C. Grojean, M. Muhlleitner and M. Trott, JHEP **1205** (2012) 097.

[64] J. Ellis and T. You, arXiv:1204.0464 [hep-ph].

[65] https://twiki.cern.ch/twiki/bin/view/LHCPhysics/ CrossSections

[66] CMS Collaboration, CMS PAS HIG-12-015.

[67] CMS Collaboration, CMS PAS HIG-12-008.

[68] Tackmann K., talk at ICHEP 2012.

[69] ATLAS Collaboration, ATLAS-CONF-2012-019.

[70] [The CDF Collaboration], arXiv:1207.0449 [hep-ex].

[71] G. F. Giudice, C. Grojean, A. Pomarol and R. Rattazzi, JHEP **0706** (2007) 045 [hep-ph/0703164].

[72] M. Frigerio, A. Pomarol, F. Riva and A. Urbano, arXiv:1204.2808 [hep-ph].

[73] A. Falkowski, Phys. Rev. D **77**, 055018 (2008); I. Low and A. Vichi, Phys. Rev. D **84**, 045019 (2011);

[74] A. Azatov and J. Galloway, arXiv:1110.5646 [hep-ph].

[75] B. Bellazzini, C. Csaki, J. Hubisz, J. Serra and J. Terning, arXiv:1205.4032 [hep-ph].

[76] P. P. Giardino, K. Kannike, M. Raidal and A. Strumia, JHEP **1206**, 117 (2012).

[77] J. R. Espinosa, M. Muhlleitner, C. Grojean and M. Trott, arXiv:1205.6790 [hep-ph].

[78] K. Cheung and T. -C. Yuan, Phys. Rev. Lett. **108** (2012) 141602 [arXiv:1112.4146 [hep-ph]].

[79] L. Vecchi, Phys. Rev. D **82** (2010) 076009 [arXiv:1002.1721 [hep-ph]].

[80] I. Low, J. Lykken and G. Shaughnessy, arXiv:1207.1093 [hep-ph].

[81] R. Barbieri, L. J. Hall and V. S. Rychkov, Phys. Rev. D **74** (2006) 015007 [hep-ph/0603188].

[82] For a review, see J. F. Gunion, H. E. Haber, G. L. Kane and S. Dawson, Front. Phys. **80** (2000) 1, and A. Djouadi, Phys. Rept. **459** (2008) 1 [hep-ph/0503173].

[83] A. Arvanitaki and G. Villadoro, JHEP **1202** (2012) 144 [arXiv:1112.4835 [hep-ph]].

[84] A. Azatov, S. Chang, N. Craig and J. Galloway, arXiv:1206.1058 [hep-ph].

[85] M. Carena, S. Gori, N. R. Shah and C. E. M. Wagner, JHEP **1203** (2012) 014 [arXiv:1112.3336 [hep-ph]].

[86] K. Blum, R. T. D'Agnolo and J. Fan, arXiv:1206.5303 [hep-ph].

[87] B. Bellazzini, C. Petersson and R. Torre, arXiv:1207.0803 [hep-ph].

[88] P. P. Giardino, K. Kannike, M. Raidal and A. Strumia, arXiv:1207.1347 [hep-ph].

[89] T. Corbett, O. J. P. Eboli, J. Gonzalez-Fraile and M. C. Gonzalez-Garcia, arXiv:1207.1344 [hep-ph].

[90] J. Beringer et al.(PDG), PR **D86**, 010001 (2012) (http://pdg.lbl.gov)

[91] K. Agashe, R. Contino and A. Pomarol, Nucl. Phys. B **719**, 165 (2005) doi:10.1016/j.nuclphysb.2005.04.035 [hep-ph/0412089].

[92] R. Contino, L. Da Rold and A. Pomarol, Phys. Rev. D **75** (2007) 055014 doi:10.1103/PhysRevD.75.055014 [hep-ph/0612048].

[93] O. Matsedonskyi, G. Panico and A. Wulzer, JHEP **1301** (2013) 164 doi:10.1007/JHEP01(2013)164 [arXiv:1204.6333 [hep-ph]].

[94] M. Redi and A. Tesi, JHEP **1210** (2012) 166 doi:10.1007/JHEP10(2012)166 [arXiv:1205.0232 [hep-ph]].

[95] D. Marzocca, M. Serone and J. Shu, JHEP **1208** (2012) 013 doi:10.1007/JHEP08(2012)013 [arXiv:1205.0770 [hep-ph]].

[96] A. Pomarol and F. Riva, JHEP **1208** (2012) 135 doi:10.1007/JHEP08(2012)135 [arXiv:1205.6434 [hep-ph]].

[97] G. Panico, M. Redi, A. Tesi and A. Wulzer, JHEP **1303** (2013) 051 doi:10.1007/JHEP03(2013)051 [arXiv:1210.7114 [hep-ph]].

[98] D. Pappadopulo, A. Thamm and R. Torre, JHEP **1307** (2013) 058 doi:10.1007/JHEP07(2013)058 [arXiv:1303.3062 [hep-ph]].

[99] CMS Collaboration, "Search for $T_{5/3}$ top partners in same-sign dilepton final state"

[100] CMS Collaboration, "Inclusive search for a vector-like T quark by CMS"

[101] ATLAS Collaboration, "Combined coupling measurements of the Higgs-like boson with the ATLAS detector using up to 25 fb^{-1} of proton-proton collision data"

[102] CMS Collaboration, "Measurements of the properties of the new boson with a mass near 125 GeV"

[103] A. Falkowski, F. Riva and A. Urbano, JHEP **1311** (2013) 111 doi:10.1007/JHEP11(2013)111 [arXiv:1303.1812 [hep-ph]].

[104] P. P. Giardino, K. Kannike, I. Masina, M. Raidal and A. Strumia, JHEP **1405** (2014) 046 doi:10.1007/JHEP05(2014)046 [arXiv:1303.3570 [hep-ph]].

[105] G. F. Giudice, C. Grojean, A. Pomarol and R. Rattazzi, JHEP **0706** (2007) 045 doi:10.1088/1126-6708/2007/06/045 [hep-ph/0703164].

[106] I. Low, R. Rattazzi and A. Vichi, JHEP **1004** (2010) 126 doi:10.1007/JHEP04(2010)126 [arXiv:0907.5413 [hep-ph]].

[107] A. Falkowski, Phys. Rev. D **77** (2008) 055018 doi:10.1103/PhysRevD.77.055018 [arXiv:0711.0828 [hep-ph]].

[108] I. Low and A. Vichi, Phys. Rev. D **84** (2011) 045019 doi:10.1103/PhysRevD.84.045019 [arXiv:1010.2753 [hep-ph]].

[109] A. Azatov and J. Galloway, Phys. Rev. D **85** (2012) 055013 doi:10.1103/PhysRevD.85.055013 [arXiv:1110.5646 [hep-ph]].

[110] D. B. Kaplan, Nucl. Phys. B **365** (1991) 259. doi:10.1016/S0550-3213(05)80021-5

[111] M. Gillioz, R. Grober, C. Grojean, M. Muhlleitner and E. Salvioni, JHEP **1210** (2012) 004 doi:10.1007/JHEP10(2012)004 [arXiv:1206.7120 [hep-ph]].

[112] C. Csaki, A. Falkowski and A. Weiler, JHEP **0809** (2008) 008 doi:10.1088/1126-6708/2008/09/008 [arXiv:0804.1954 [hep-ph]].

[113] M. Redi and A. Weiler, JHEP **1111** (2011) 108 doi:10.1007/JHEP11(2011)108 [arXiv:1106.6357 [hep-ph]].

[114] B. Keren-Zur, P. Lodone, M. Nardecchia, D. Pappadopulo, R. Rattazzi and L. Vecchi, Nucl. Phys. B **867** (2013) 394 doi:10.1016/j.nuclphysb.2012.10.012 [arXiv:1205.5803 [hep-ph]].

[115] R. Barbieri, D. Buttazzo, F. Sala, D. M. Straub and A. Tesi, JHEP **1305** (2013) 069 doi:10.1007/JHEP05(2013)069 [arXiv:1211.5085 [hep-ph]].

[116] J. R. Ellis, M. K. Gaillard and D. V. Nanopoulos, Nucl. Phys. B **106** (1976) 292. doi:10.1016/0550-3213(76)90382-5

[117] M. A. Shifman, A. I. Vainshtein, M. B. Voloshin and V. I. Zakharov, Sov. J. Nucl. Phys. **30** (1979) 711 [Yad. Fiz. **30** (1979) 1368].

[118] C. Delaunay, C. Grojean and G. Perez, JHEP **1309** (2013) 090 doi:10.1007/JHEP09(2013)090 [arXiv:1303.5701 [hep-ph]].

[119] J. Mrazek, A. Pomarol, R. Rattazzi, M. Redi, J. Serra and A. Wulzer, Nucl. Phys. B **853** (2011) 1 doi:10.1016/j.nuclphysb.2011.07.008 [arXiv:1105.5403 [hep-ph]].

[120] K. Agashe, R. Contino, L. Da Rold and A. Pomarol, Phys. Lett. B **641** (2006) 62 doi:10.1016/j.physletb.2006.08.005 [hep-ph/0605341].

[121] K. Agashe and R. Contino, Phys. Rev. D **80** (2009) 075016 doi:10.1103/PhysRevD.80.075016 [arXiv:0906.1542 [hep-ph]].

[122] A. De Simone, O. Matsedonskyi, R. Rattazzi and A. Wulzer, JHEP **1304** (2013) 004 doi:10.1007/JHEP04(2013)004 [arXiv:1211.5663 [hep-ph]].

[123] O. Matsedonskyi, F. Riva and T. Vantalon, JHEP **1404** (2014) 059 doi:10.1007/JHEP04(2014)059 [arXiv:1401.3740 [hep-ph]].

[124] C. Grojean, O. Matsedonskyi and G. Panico, JHEP **1310** (2013) 160 doi:10.1007/JHEP10(2013)160 [arXiv:1306.4655 [hep-ph]].

[125] G. Panico and A. Wulzer, JHEP **1109** (2011) 135 doi:10.1007/JHEP09(2011)135 [arXiv:1106.2719 [hep-ph]].

[126] S. De Curtis, M. Redi and A. Tesi, JHEP **1204** (2012) 042 doi:10.1007/JHEP04(2012)042 [arXiv:1110.1613 [hep-ph]].

[127] S. Weinberg, Phys. Rev. Lett. **18** (1967) 507. doi:10.1103/PhysRevLett.18.507

[128] J. Barnard, T. Gherghetta, A. Medina and T. S. Ray, JHEP **1310** (2013) 055 doi:10.1007/JHEP10(2013)055 [arXiv:1307.4778 [hep-ph]].

[129] B. Gripaios, A. Pomarol, F. Riva and J. Serra, JHEP **0904** (2009) 070 doi:10.1088/1126-6708/2009/04/070 [arXiv:0902.1483 [hep-ph]].

[130] M. Chala, JHEP **1301** (2013) 122 doi:10.1007/JHEP01(2013)122 [arXiv:1210.6208 [hep-ph]].

[131] G. Aad *et al.* [ATLAS Collaboration], Phys. Lett. B **710**, 49 (2012) [arXiv:1202.1408]; update at ATLAS-CONF-2012-019 (7 March 2012); S. Chatrchyan *et al.* [CMS Collaboration], arXiv:1202.1488 [hep-ex]; update at CMS-PAS-HIG-12-008 (7 March 2012); J. Incandela (CMS) and F. Gianotti (ATLAS), talk at *Latest update in the search for the Higgs boson* at CERN, July 4, 2012.

[132] F. Riva, C. Biggio and A. Pomarol, arXiv:1211.4526 [hep-ph].

[133] R. Davies, J. March-Russell and M. McCullough, JHEP **1104** (2011) 108 [arXiv:1103.1647 [hep-ph]].

[134] D. S. M. Alves, P. J. Fox and N. J. Weiner, arXiv:1207.5499 [hep-ph].

[135] R. S. Gupta and J. D. Wells, Phys. Rev. D **81**, 055012 (2010) [arXiv:0912.0267 [hep-ph]].

[136] ATLAS Collaboration, ATLAS-CONF-2012-019.

[137] ATLAS Collaboration, ATLAS-CONF-2012-161.

[138] ATLAS Collaboration, ATLAS-CONF-2012-019.

[139] ATLAS Collaboration, ATLAS-CONF-2012-091.

[140] ATLAS Collaboration, ATLAS-CONF-2012-170.

[141] ATLAS Collaboration, ATLAS-CONF-2012-091.

[142] ATLAS Collaboration, ATLAS-CONF-2012-091.

[143] K. Blum and R. T. D'Agnolo, Phys. Lett. B **714** (2012) 66 [arXiv:1202.2364 [hep-ph]].

[144] K. Blum, R. T. D'Agnolo and J. Fan, arXiv:1206.5303 [hep-ph].

[145] A. Azatov, S. Chang, N. Craig and J. Galloway, Phys. Rev. D **86**, 075033 (2012) [arXiv:1206.1058 [hep-ph]].

[146] D. Carmi, A. Falkowski, E. Kuflik and T. Volanski, arXiv:1202.3144 [hep-ph]; A. Azatov, R. Contino and J. Galloway, JHEP **1204** (2012) 127 [hep-ph/1202.3415]. J.R. Espinosa, C. Grojean, M. Muhlleitner and M. Trott, arXiv:1202.3697 [hep-ph]; P. P. Giardino, K. Kannike, M. Raidal and A. Strumia, arXiv:1203.4254 [hep-ph]; T. Li, X. Wan, Y. Wang and S. Zhu, arXiv:1203.5083 [hep-ph]; M. Rauch, arXiv:1203.6826 [hep-ph]; J. Ellis and T. You, JHEP **1206** (2012) 140, [arXiv:1204.0464 [hep-ph]]; A. Azatov, R. Contino, D. Del Re, J. Galloway, M. Grassi and S. Rahatlou, arXiv:1204.4817 [hep-ph]; M. Klute, R. Lafaye, T. Plehn, M. Rauch and D. Zerwas, arXiv:1205.2699 [hep-ph]; J.R. Espinosa, M. Muhlleitner, C. Grojean and M. Trott, arXiv:1205.6790 [hep-ph]; D. Carmi, A. Falkowski, E. Kuflik and T. Volansky, arXiv:1206.4201 [hep-ph]; M. J. Dolan, C. Englert and M. Spannowsky, arXiv:1206.5001 [hep-ph]; J. Chang, K. Cheung, P. Tseng and T. Yuan, arXiv:1206.5853 [hep-ph]; S. Chang, C. A. Newby, N. Raj and C. Wanotayaroj, arXiv:1207.0493 [hep-ph]; I. Low, J. Lykken and G. Shaughnessy, arXiv:1207.1093 [hep-ph]; T. Corbett, O. J. P. Eboli, J. Gonzalez-Fraile and M. C. Gonzalez-Garcia, arXiv:1207.1344 [hep-ph]; P. P. Giardino, K. Kannike, M. Raidal and A. Strumia, arXiv:1207.1347 [hep-ph]; J. R. Espinosa, C. Grojean, M. Muhlleitner and M. Trott, arXiv:1207.1717 [hep-ph]; D. Carmi, A. Falkowski, E. Kuflik, T. Volansky and J. Zupan, arXiv:1207.1718 [hep-ph]; M. Montull and F. Riva, JHEP **1211** (2012) 018 [arXiv:1207.1716 [hep-ph]], S. Banerjee, S. Mukhopadhyay and B. Mukhopadhyaya, JHEP bf 10 (2012) 062, [arXiv:1207.3588 [hep-ph]]; F. Bonnet, T. Ota, M. Rauch and W. Winter, arXiv:1207.4599 [hep-ph]; T. Plehn and M. Rauch, arXiv:1207.6108 [hep-ph]; B. Batell, S. Gori and L. T. Wang, arXiv:1209.6832 [hep-ph], G. Cacciapaglia, A. Deandrea, G. D. La Rochelle and J-B. Flament, arXiv:1210.8120 [hep-ph], E. Masso and V. Sanz, arXiv:1211.1320 [hep-ph].

[147] A. Azatov and J. Galloway, arXiv:1212.1380 [hep-ph].

[148] A. Djouadi, Phys. Rept. **459**, 1 (2008) [hep-ph/0503173].

[149] A. Maloney, A. Pierce and J. G. Wacker, JHEP **0606**, 034 (2006) [hep-ph/0409127].

[150] M. S. Carena, J. R. Espinosa, M. Quiros and C. E. M. Wagner, Phys. Lett. B **355**, 209 (1995) [hep-ph/9504316].

[151] L. J. Hall, D. Pinner and J. T. Ruderman, JHEP **1204**, 131 (2012) [arXiv:1112.2703 [hep-ph]].

[152] A. Arbey, M. Battaglia, A. Djouadi and F. Mahmoudi, JHEP **1209** (2012) 107 [arXiv:1207.1348 [hep-ph]]; A. Arbey, M. Battaglia, A. Djouadi and F. Mahmoudi, arXiv:1211.4004 [hep-ph].

[153] P. Lodone, JHEP **1005**, 068 (2010) [arXiv:1004.1271 [hep-ph]].

[154] CMS Collaboration, CMS-PAS-HIG-12-050.

[155] H. E. Haber and R. Hempfling, Phys. Rev. D **48**, 4280 (1993) [hep-ph/9307201].

[156] W. Altmannshofer, M. Carena, N. Shah and F. Yu, ÊÊarXiv:1211.1976 [hep-ph]. ÊÊ

[157] P. Batra, A. Delgado, D. E. Kaplan and T. M. P. Tait, JHEP **0402**, 043 (2004) [hep-ph/0309149].

[158] N. Craig and A. Katz, arXiv:1212.2635 [hep-ph].

[159] M. Dine, N. Seiberg and S. Thomas, Phys. Rev. D **76**, 095004 (2007) [arXiv:0707.0005 [hep-ph]].

[160] R. Barbieri, L. J. Hall, A. Y. Papaioannou, D. Pappadopulo and V. S. Rychkov, JHEP **0803** (2008) 005 [arXiv:0712.2903 [hep-ph]].

[161] D. Bertolini and M. McCullough, arXiv:1207.4209 [hep-ph].

[162] J. R. Ellis, J. F. Gunion, H. E. Haber, L. Roszkowski and F. Zwirner, Phys. Rev. D **39** (1989) 844.

[163] R. Barbieri, L. J. Hall, Y. Nomura and V. S. Rychkov, Phys. Rev. D **75** (2007) 035007 [hep-ph/0607332].

[164] A. Arvanitaki and G. Villadoro, JHEP **1202** (2012) 144 [arXiv:1112.4835 [hep-ph]].

[165] S. Antusch, L. Calibbi, V. Maurer, M. Monaco and M. Spinrath, arXiv:1207.7236 [hep-ph].

[166] N. Arkani-Hamed, K. Blum, R. T. D'Agnolo and J. Fan, arXiv:1207.4482 [hep-ph].

[167] A. Djouadi, V. Driesen, W. Hollik and J. I. Illana, Eur. Phys. J. C **1** (1998) 149 [hep-ph/9612362].

[168] J. R. Espinosa, C. Grojean, V. Sanz and M. Trott, arXiv:1207.7355 [hep-ph].

[169] CMS Collaboration, CMS-NOTE-2012-006; see also M. E. Peskin, arXiv:1207.2516 [hep-ph].

[170] L. Linssen *et al.* [CLIC], arXiv:1202.5940 [physics.ins-det].

[171] A. Djouadi, arXiv:1208.3436 [hep-ph].

[172] M. Reece, arXiv:1208.1765 [hep-ph].

[173] M. Montull, Talk given at IV CPAN Days, 27.11.2012.

[174] R. T. D'Agnolo, E. Kuflik and M. Zanetti, arXiv:1212.1165 [hep-ph].

[175] G. Degrassi, P. Gambino and G. F. Giudice, JHEP **0012**, 009 (2000) [hep-ph/0009337].

[176] M. S. Carena, D. Garcia, U. Nierste and C. E. M. Wagner, Phys. Lett. B **499**, 141 (2001) [hep-ph/0010003].

[177] R. S. Gupta, H. Rzehak and J. D. Wells, Phys. Rev. D **86**, 095001 (2012) [arXiv:1206.3560 [hep-ph]].

[178] G. C. Branco, P. M. Ferreira, L. Lavoura, M. N. Rebelo, M. Sher and J. P. Silva, Phys. Rept. **516**, 1 (2012) [arXiv:1106.0034 [hep-ph]].

[179] CMS Collaboration, CMS PAS HIG-12-015.

[180] CMS Collaboration, CMS PAS HIG-12-020

[181] CMS Collaboration, CMS PAS HIG-12-008.

[182] Tackmann K., talk at ICHEP 2012.

[183] [The CDF Collaboration], arXiv:1207.0449 [hep-ex].

[184] S. Dawson, A. Djouadi and M. Spira, Phys. Rev. Lett. **77** (1996) 16 [hep-ph/9603423].

[185] A. Djouadi, Phys. Lett. B **435** (1998) 101 [hep-ph/9806315].

[186] M. Spira, A. Djouadi, D. Graudenz and P. M. Zerwas, Nucl. Phys. B **453** (1995) 17 [hep-ph/9504378].

[187] S. Dawson, A. Djouadi and M. Spira, Phys. Rev. Lett. **77** (1996) 16 [hep-ph/9603423].

[188] [The CDF Collaboration], arXiv:1207.0449 [hep-ex].

[189] CMS Collaboration, CMS-PAS-HIG-12-050.

[190] S. Rychkov and L. G. Vitale, arXiv:1512.00493 [hep-th].

[191] V. P. Yurov and A. B. Zamolodchikov, Int. J. Mod. Phys. A **5** (1990) 3221.

[192] S. J. Brodsky, H. C. Pauli and S. S. Pinsky, Phys. Rept. **301** (1998) 299 [hep-ph/9705477].

[193] D. Lee, N. Salwen, and D. Lee, "The Diagonalization of quantum field Hamiltonians," *Phys.Lett.* **B503** (2001) 223–235, arXiv:hep-th/0002251 [hep-th].

[194] D. Lee, N. Salwen, and M. Windoloski, "Introduction to stochastic error correction methods," *Phys.Lett.* **B502** (2001) 329–337, arXiv:hep-lat/0010039 [hep-lat].

[195] N. Salwen, *Non-perturbative methods in modal field theory.* arXiv:hep-lat/0212035 [hep-lat]. Ph.D. thesis, Harvard University, 2001.

[196] M. Windoloski, *A Non-perturbative Study of Three-Dimensional Quartic Scalar Field Theory Using Modal Field Theory.* Ph.D. thesis, University of Massachusetts Amherst, 2000.

[197] I. Brooks, E.D. and S. C. Frautschi, "Scalars Coupled to Fermions in (1+1)-dimensions," *Z.Phys.* **C23** (1984) 263.

[198] E. Katz, G. M. Tavares, and Y. Xu, "Solving 2D QCD with an adjoint fermion analytically," *JHEP* **1405** (2014) 143, arXiv:1308.4980 [hep-th].

[199] E. Katz, G. M. Tavares, and Y. Xu, "A solution of 2D QCD at Finite N using a conformal basis," arXiv:1405.6727 [hep-th].

[200] S. Chabysheva and J. Hiller, "Basis of symmetric polynomials for many-boson light-front wave functions," arXiv:1409.6333 [hep-ph].

[201] P. Giokas and G. Watts, "The renormalisation group for the truncated conformal space approach on the cylinder," arXiv:1106.2448 [hep-th].

[202] M. Lencses and G. Takacs, "Excited state TBA and renormalized TCSA in the scaling Potts model," *JHEP* **09** (2014) 052, arXiv:1405.3157 [hep-th].

[203] A. Coser, M. Beria, G. P. Brandino, R. M. Konik and G. Mussardo, J. Stat. Mech. **1412** (2014) P12010 arXiv:1409.1494 [hep-th].

[204] M. Lencses and G. Takacs, JHEP **1509** (2015) 146 arXiv:1506.06477 [hep-th].

[205] M. Luscher, Commun. Math. Phys. **104** (1986) 177.

[206] M. Luscher, Commun. Math. Phys. **105** (1986) 153.